UNIVERSITÀ
POLITECNICA
DELLE MARCHE

Department of Life and Environmental Sciences
PhD course in Life and Environmental Sciences
Curriculum in Marine Biology and Ecology

Microbiome, metabolic and phenotypic traits in the adaptability of marine sponges to Ocean Acidification

Candidate: **Valerio Mazzella**

Tutor: **Prof. Antonio Dell'Anno**

Co-tutors: **Dr. Laura Núñez-Pons**

Prof. Barbara Calcinai

XXXIII cycle
AA 2020-2021

I am a naturalist. My "mission" is to show that ecologists are affected by physics' envy and that they try to heavily mathematize their discipline, predicting the future with equations. […] Ecology is a historical discipline. Do historians predict the future? Equational ecology is just a make-up. By the way, equational history is called economics and it has a bad reputation nowadays.

Ferdinando Boero

Summary

1. INTRODUCTION

Human activities have caused an unprecedented increase of carbon dioxide (CO_2) in the atmosphere (ca. 410 ppmv in 2020). Almost 30% of this greenhouse gas has been absorbed by the oceans and is causing an imbalance in the carbonate chemistry of the seawater with subsequent lowering of the pH in the surface's ocean. This phenomenon is known as Ocean Acidification (OA). Briefly, as more CO_2 dissolves in the sea water, more bicarbonate and carbonic acid accumulate, in detriment of carbonate, interfering with any biotic calcification process (Fig. 1). Most scientists agree in predicting a drop in the pH values by the end of the century that could reach values around 7.7, a drop of almost 0.4-0.5 units compared with the actual surface's pH (Caldeira and Wickett, 2003; Doney et al. 2009; Gattuso and Hansson, 2011).

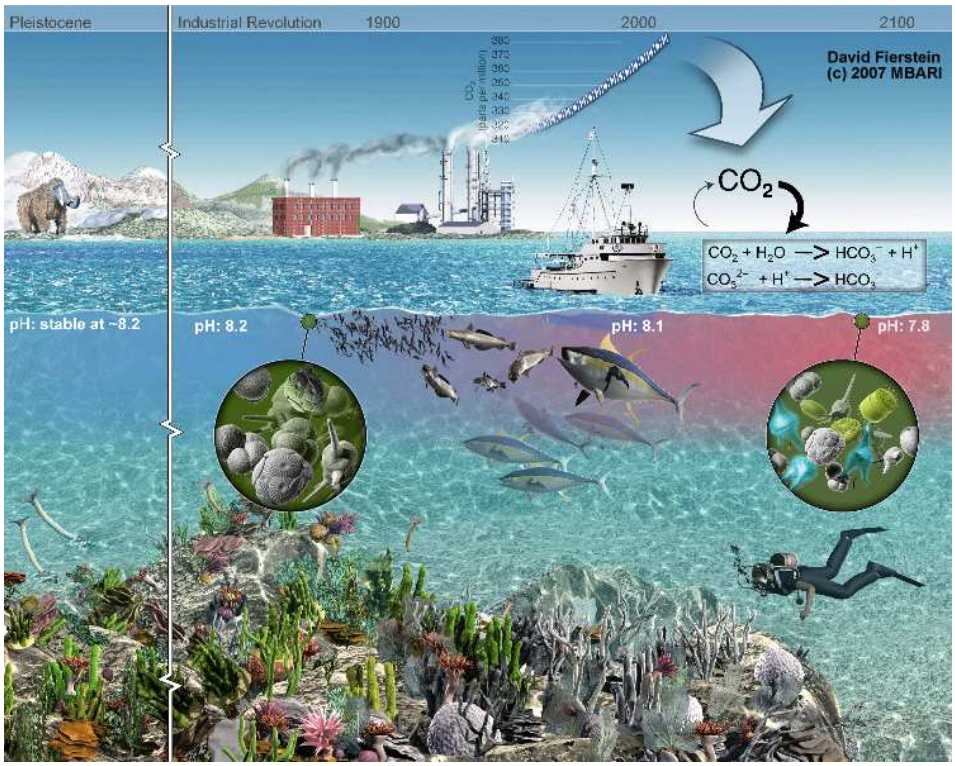

Figure 1 – Effects of ocean acidification (OA) on marine biota, (Monterey Bay Aquarium Research Institute - MBARI).

Several studies, most of which performed in controlled laboratory conditions, provide evidence, that marine organisms can be severely threatened by seawater acidification. Such an effect has been documented on relevant biological processes such as: reproduction, early development, metabolism and calcification. Regarding reproduction, impaired reproduction in echinoderms has been reported as a consequence of reduced fertilization processes (Albright et al. 2010; Sung et al. 2014; Uthicke et al. 2013). In mollusks reduced fertilization processes, delayed hatching and general negative effects are also reported (Kaplan et al. 2013; Scanes et al. 2014; Shi et al. 2017a). Crustaceans are affected in reproduction mainly by delayed hatching processes, while in cnidarians were found to occur different scenarios of which some negative and some highlighting no relevant effects of OA on reproduction processes, mostly based on species specificity (Fine and Tchernov, 2007; Gizzi et al. 2017; Gravinese, 2018; Hoadley et al. 2015; Jokiel et al. 2008; Zhang et al. 2011; Zheng et al. 2015). An overall picture on marine gametes has shown general negative trends of OA on marine gametes of several marine phyla (Foo and Byrne, 2017).

Concerning the early development, the response of marine organisms to OA seems to be more species specific. In mollusks controversial responses were found, some species experienced high mortality rates when exposed to OA scenarios, while others were not affected at all or experienced positive effects (Basso et al. 2015; Gazeau et al. 2010; Szalaj et al. 2017). Crustaceans, echinoderms and cnidarians seemed to be not notoriously affected in early development under increased pCO_2 scenarios except for experiments with very high pCO_2 levels and longtime exposures (Miller et al. 2016; Pansch et al. 2013; Pedersen et al. 2014). Regarding metabolism and physiology, the immune responses are among the most important processes tested under OA scenarios, resulting in a reduction of the immunomodulation for most of the organisms tested, belonging to the principal marine taxa (*e.g.* mollusks, echinoderms) (Castillo et al. 2017; Hernroth et al. 2011; Wang et al. 2016). Effects of OA on calcification processes are also widely documented in the literature. Most of the studies conducted in laboratory conditions, involving corals, mollusks and echinoderms demonstrate conspicuous reduction of calcification rates (Comeau et al. 2017; Horvath et al. 2016; Uthicke and Fabricius, 2012; Zheng et al. 2019). Overall, marine calcifiers (*e.g.* scleractinian corals, bryozoans, sea-urchins, crustose coralline algae) and shell-

building organisms (*e.g.* gastropod and bivalve mollusks) are severely threatened under OA due to the imbalance of the carbonate system in the seawater (Fabry, 2008; Kroeker et al. 2010) (Fig. 2). Nonetheless, little is known about the effect of lowered pH on the survival and physiology of non-calcifying organisms, such as soft corals, nudibranchs or sponges, that are ubiquitous and abundant all over the World's oceans and constitute an important and diversified component of the benthic marine ecosystems.

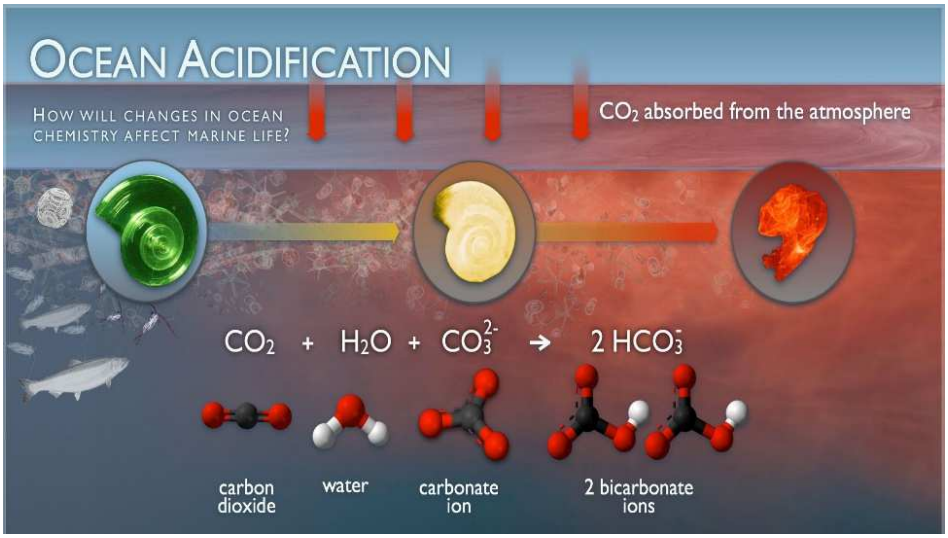

Figure 2 – Scheme of ocean acidification effects on marine calcifiers due to depletion of carbonate ions in the seawater.

The decline of calcifying organisms due to the progressive OA, could lead to the increasing of non-calcifying species that in these scenarios may emerge as "winners". Among them, marine sponges have been reported to thrive well, even in remarkable abundances under naturally low pH conditions (Goodwin et al. 2014; Morrow et al. 2015). Moreover, paleontological studies suggest that marine sponges can be more resistant to massive extinction events compared to other marine taxa. These findings suggest that in future scenarios coral reefs, highly impacted by OA, increased temperatures, eutrophication, turbidity and other disturbances might turn into sponge reefs, a process known as "spongification" (Bell et al. 2013). Furthermore, sponges might even profit from changing ocean conditions through increased productivity and reduced spatial competition against other taxa (Bell et al. 2013; Bell et al. 2018b). Other recent findings investigating relevant aspects of the sponge biology, ecology and

physiology from Bell and co-workers (Bell et al. 2018a) further suggest that marine sponges could represent "winner" taxa in future scenarios of increased atmospheric CO_2. Nonetheless, marine sponges have received less attention compared to other taxa (Fig. 3).

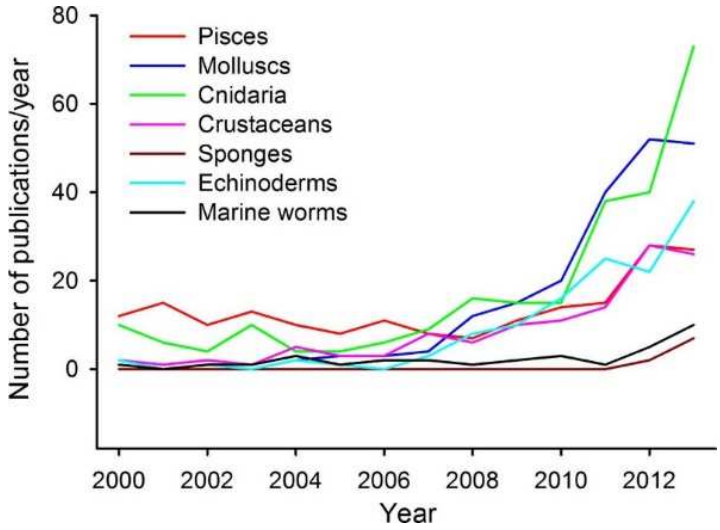

Figure 3 - Number of OA-related papers published each year from 2000 through 2013 for different phylogenetic animal groups. (from Heuer and Grosell, 2014).

Sponges are ubiquitous pluricellular organisms, found at all latitudes of the world's oceans throughout temperate, tropical and polar habitats and from the intertidal to the deep-sea (Bell, 2008). They are one of the most important components of the benthic fauna accounting for about 9375 accepted species (source: World Porifera Database, last accessed april 2021 - www.marinespecies.org/porifera). Sponges are diploblastic organisms with an intraepithelial mesenchyme called mesohyl, which is composed by collagen, amoeboid cells and skeletal elements. The body of these organisms lacks a true tissue organization and it is structured in a system of branched canals and choanocyte chambers (Fig. 4), that produce a water flow through the organism, allowing feeding, respiration, excretion and reproduction (Maldonado and Bergquist, 2002). Most of the sponges are filter feeder heterotrophs, with some exceptions that rely on partially (mixotrophic) or fully (phototropics) photosynthetic symbionts to obtain the energy or other few carnivorous species that feed on small invertebrates.

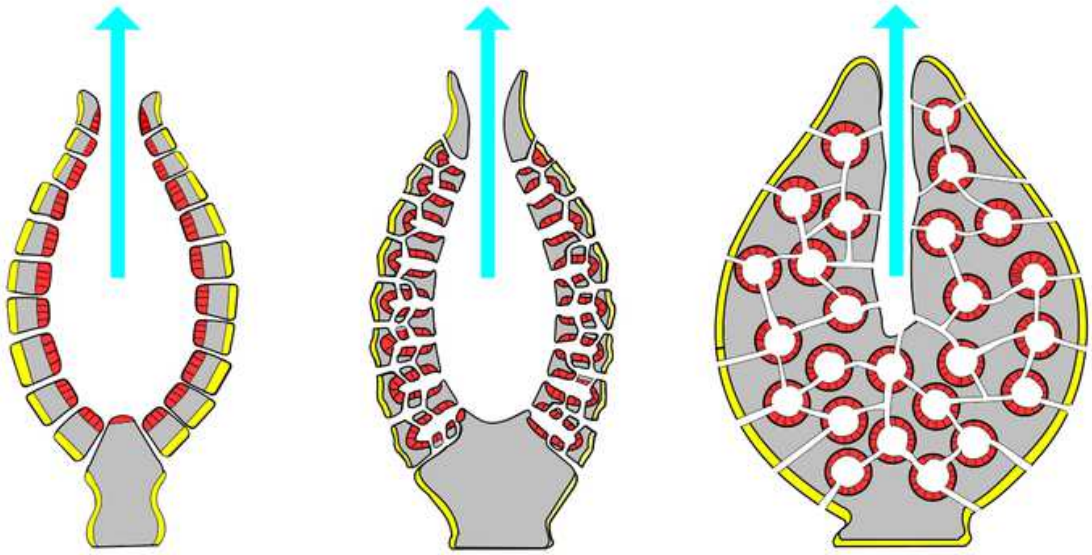

Figure 4 – Scheme of the internal anatomy of a sponge (from https://courses.lumenlearning.com/boundless-biology/chapter/phylum-porifera/).

There are contrasting reports on sponge coverage in natural gradients of lowered pH. Some researchers found low Porifera abundances in acidified areas (*e.g.* Fabricius et al. 2011), whereas others recorded a high presence (*e.g.* Morrow et al. 2015), and further surveys revealed mostly species-specific trends (Goodwin et al. 2014; Kroeker et al. 2013b). For instance, bio-eroding and sponges with photosynthetic symbionts seem to be favored by OA (Enochs et al. 2015; Morrow et al. 2015; Wisshak et al. 2014). Another case of apparent preference for acidified conditions is that of *Haliclona mediterranea* in Mediterranean CO_2 vents systems (Goodwin et al. 2014; Teixidó et al. 2018). This seems to be related with the capability of some sponges to deal with extreme conditions while reduced ecosystem complexity in absence of competitors or predators could further favor colonization (Kroeker et al. 2013a; Kroeker et al. 2013b). Certain sponges instead produce calcareous spicules (*e.g. Petrobiona massiliana*, *Clathrina clathrus*, *Paraleucilla magna*) and hence might be among the threatened taxa in future climate change scenarios (Bell et al. 2018a; Goodwin et al. 2014; Smith et al. 2013; Vicente et al. 2016).

The Phylum Porifera has been deeply studied as a model holobiont system to understand host-microbe's interactions. The concept "holobiont" considers the host plus its symbionts as a whole biological entity, abandoning the assumption of organisms as the minimal functional units (Dittami et al. 2019; Guerrero et al. 2013). Marine sponges, in fact, host dense microbial communities that in some cases can account for up to 40-50% of the weight of the animal, with different microbial taxa being species-specific (Hentschel et al. 2006; Webster and Taylor, 2012).

Microbial endosymbionts can supply nutrients and energy to their hosts while taking care of the waste products, as well as can produce secondary metabolites (Taylor et al. 2007), useful to avoid predators and fouling or compete for substrate space. Marine sponges moreover, represent key ecological players in nutrient re-cycling and bentho-pelagic coupling, *i.e.* the sponge loop (De Goeij et al. 2013) (Fig. 5). On the basis of the relative quantitative importance of microbial assemblages associated with sponges, two sponge typologies have been identified: the "low microbial abundance" (LMA) and "high microbial abundance" (HMA) sponges (Hentschel et al. 2003). The HMA sponge type, usually contains from ca. 10^8 to 10^{10} microbes/g sponge tissue, which can make up to 20%–35% of the sponge biomass (Hentschel et al. 2012); on the contrary, 10^5 to 10^6 microbes/g sponge tissue are found in LMA sponges (Hentschel et al. 2006).

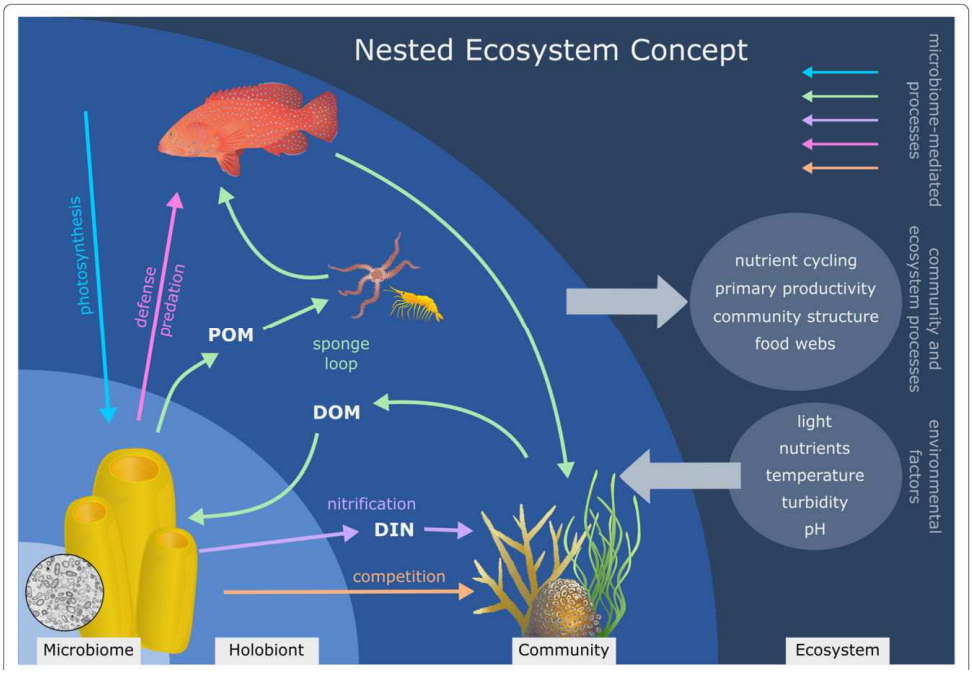

Figure 5 – Conceptual scheme of the sponge holobiont (from Pita et al. 2018).

Most of the laboratory experiments investigating the effects of OA on marine organisms, have been carried out often at short time scales and using CO_2 concentration scenarios which are unlikely to occur in the near future (McElhany and Shallin Busch, 2013; Riebesell et al. 2010). Despite these experiments have improved our understanding on the potential mechanistic biological responses to OA, they still do not provide robust information on the acclimatization and adaptation processes of organisms to long-term progressive OA exposures (González-Delgado and Hernández, 2018; McElhany and Shallin Busch, 2013; Riebesell et al. 2010). For these reasons, some scientists initiated research on lowered pH habitats naturally occurring in vent seep ecosystems. However, not all vents systems are suitable to test hypotheses on OA acclimatization. For instance, many underwater vents are also influenced by high temperatures (hydrothermal vents) or by the emission of gas mixtures, (*i.e.* Panarea or Vulcano's vents in southern Italy) that include H_2S emissions together with CO_2 (González-Delgado and Hernández, 2018). Suitable underwater seeps to assess OA effects, should be affected almost exclusively by CO_2 emissions, and have been reported in a few areas such as the Island of Ischia (Italy), Columbretes Islands (Spain), Faial in Azores (Portugal) and in Papua Nuova Guinea (Fig. 6). These underwater volcanic ecosystems are characterized by a constant bubbling of predominantly CO_2 emissions, which create a decrease in the pH similar to that predicted for the end of this century (Caldeira and Wickett, 2003, 2005). These sites, can thus represent natural laboratories for studying the effects of OA on organisms long-term adapted to acidified conditions, in an effort to forecast their fate under future global change scenarios (Hall-Spencer et al. 2008). Many questions have been raised about the reproducibility of natural conditions, such as natural variability, and the ecological interactions between different species (Foo et al. 2018; González-Delgado and Hernández, 2018; Williamson et al. 2020). Addressing these issues would ensure a more realistic prediction of the effects of acidification on marine ecosystems.

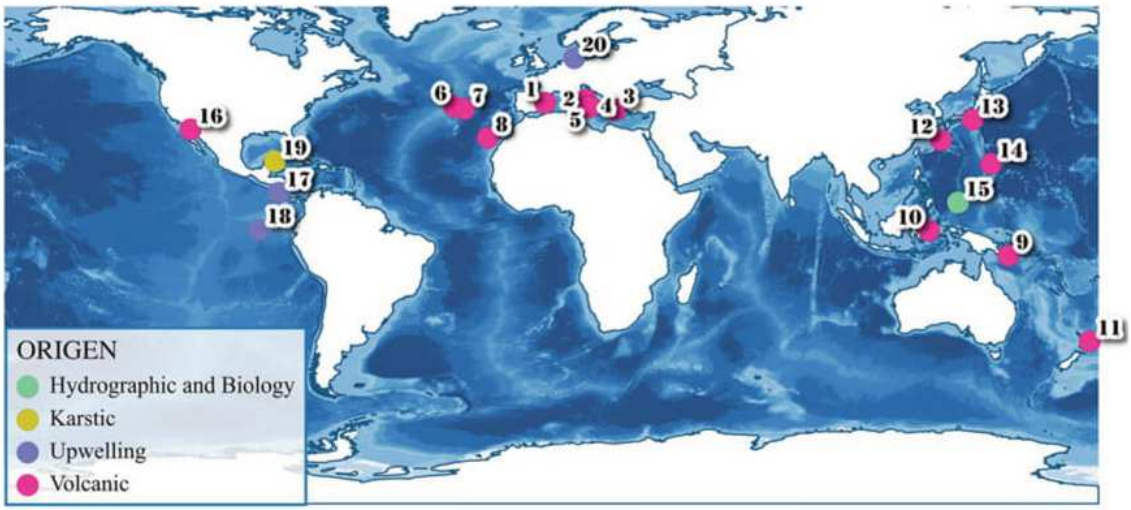

1	Columbretes Islands (Spain)	8	La Palma (Canary Islands)	15	Palau (Oceania)
2	Ischia (Italy)	9	Papua New Guinea	16	Wagner Basin (Northern Gulf of California)
3	Methana (Greece)	10	Indonesia	17	Bahia Culebra (Gulf of Papagayo)
4	Panarea (Italy)	11	White Island (New Zealand)	18	Eastern Tropical Pacific
5	Vulcano (Italy)	12	Iwatorishima (Japan)	19	Puerto Morelos (Mexico)
6	Faial (Azores)	13	Shikine Island (Japan)	20	Kiel Fjord (Baltic Sea)
7	San Miguel (Azores)	14	Maug (Mariana Islands)		

Figure 6 – Map of the most studied natural CO_2 vents all over the world (from González-Delgado and Hernández, 2018).

The effect of OA on marine invertebrate's associate microbiome is still poorly understood, but in the last decade an increasing interest has grown on this field (Lesser et al. 2016; Meron et al. 2013). This novel research topic investigates not only the response of marine organisms to OA, but the response of the entire "holobiont" to environmental stressors or climate changes (Dittami et al. 2019; Guerrero et al. 2013; Pita et al. 2018). Different studies have been recently performed both in laboratory conditions (Alma et al. 2020; O'Brien et al. 2016, 2018; Rastelli et al. 2020; Thomas et al. 2016; Webster et al. 2013, 2016), and under natural pH gradients (Biagi et al. 2020; Meron et al. 2012, 2013). However information on the possible effects of OA on sponge associated microbiomes is still scant and mostly based on laboratory experiments, leading to contrasting conclusions (Bennett et al. 2017; Lesser et al. 2016; Ribes et al. 2016).

To the best of our knowledge there are only two studies evaluating the effect of sponge's associated microbiome in natural OA laboratories *in situ* (Kandler et al. 2018; Morrow et al. 2015). Kandler and coauthors (2018) found an overall stability of the sponge's microbiome under natural pH gradient in Papua Nuova Guinea. Instead,

another experiment entailing both, corals and sponges in Papua seeps highlighted that the two sponge species considered were 40 fold more abundant under low pH conditions. Moreover, cyanobacterial taxa seemed to confer stress tolerance to the sponge hosts living in acidified areas (Morrow et al. 2015). From these works, it seems that sponge associate microbiomes under OA could have a species-specific trend. Nonetheless, knowledge on the effects of OA on sponge-microbiome and their metabolic and functional shifts need to be largely improved for a better assessment and prediction of the acclimatization potential of holobionts to predicted global climate change scenarios.

Despite marine sponges have also been investigated for their metabolomics signatures, with particular focus on the secondary metabolites profiling and bioactivity (*e.g.* Bondu et al. 2012; Guo et al. 1994), few information is provided concerning OA conditions. A study performed by Sogin and coauthors (2016) showed that both primary and lipid metabolism underwent changes in some corals species, during experimental treatments carried out in acidified conditions and higher temperature regimes. Bennett and coauthors (2018) performed a similar experiment on sponges highlighting different responses, mostly related to the species-specificity and the trophic behavior. One more experiment on this line was performed by Duckworth and co-workers (2012) that targeted nine secondary metabolites showing that increased pCO_2 had effect only for two metabolites, whose concentrations, however, were comparable to those found in natural conditions. Interesting outcomes, come from an investigation performed on the coral *Sarcophyton sp.* surveyed under natural OA conditions in Indonesia CO_2 seeps. Extracts from corals collected in the control site were highly cytotoxic (on human cell lines) compared with corals coming from the acidified site. Assuming cytotoxicity as indicator of allelochemical levels, lower cytotoxic/allelochemical metabolites production in the samples from acidified sites could be related to a lower competition for space. To date no investigations have been carried out on metabolomics or secondary metabolites from sponge living in natural acidified conditions.

On the island of Ischia, (Gulf of Naples, Italy), the widespread effect of secondary volcanism, generated a system of CO_2 underwater vents. Communities inhabiting these areas are diverse and dominated by *Posidonia oceanica* meadows, along with a

number of algae (Porzio et al. 2011), and invertebrates including sponges, anemones, polychaetes, molluscs, bryozoans and crustaceans (Foo et al. 2018). These vents represent a real natural laboratory that have been exploited in the last decade by researchers to study the effects of OA on marine organisms, and in particular the cascade's effects on benthic ecosystems functioning (Calosi et al. 2013; Foo et al. 2018; Gambi et al. 2020; Hall-Spencer et al. 2008; Kroeker et al. 2011; Teixidó et al. 2018, 2020). Regarding the Porifera, till now a unique study has been performed, assessing the effect of OA long term adaptation on the whole sponge communities, and the result confirmed that some sponge species can thrive at low pH conditions (Goodwin et al. 2014).

In the present thesis, the effect of OA on several phenotypical multi-scalar aspects of sponge holobionts living in the CO_2 vents system and in adjacent sites unaffected by CO_2 emissions around the island of Ischia was investigated. In particular, four of the most common and widespread Mediterranean sponge species were selected: *i.e*. *Petrosia ficiformis* (Poiret, 1789)*, Chondrosia reniformis* Nardo 1847*, Crambe crambe* (Schmidt, 1862) and *Chondrilla nucula* Schmidt, 1862 coming from three naturally acidified areas, and three control sites along the nearby seep influenced area. Sponges were surveyed in terms of population abundance and external growth, spicule morphologies and tissue characteristics by optical and transmission electron microscopy. Further, their associated microbiomes (both prokaryotes and fungi) were analyzed by high throughput sequencing approaches followed by bioinformatics pipelines to explore changes in microbial diversity and composition among sponge species, and between pH conditions and across sites within species. Finally, the metabolic signatures of two selected species were analyzed, and characteristic secondary metabolites were isolated from one of the sponge species along the natural acidified gradient.

2. AIM OF THE THESIS

The study of Porifera living in natural CO_2 brings up a great opportunity to shed light on the impact of OA on sponge holobionts and provide new insights on their acclimatization potential under future forecasted OA scenarios. In this thesis we investigated the microbiome diversity and the phenotype adaptation traits of sponges inhabiting the CO_2 vents system off the island of Ischia. To this aim, four of the most common and widespread Mediterranean marine sponge species, were selected: *i.e*. *Petrosia ficiformis* (Poiret, 1789), *Chondrosia reniformis* Nardo 1847, *Crambe crambe* (Schmidt, 1862) and *Chondrilla nucula* Schmidt, 1862 coming from three naturally acidified areas and three control sites along the nearby seep influencing area. To the best of our knowledge, this represents the first study investigating the phenotypic responses of sponge microbiome and metabolome of specimens naturally adapted to OA conditions in the Mediterranean Sea. The specific question we addressed in the present thesis include:

1) Are there any characteristic macroscopic traits of adaptation in Porifera living under a natural gradient of OA conditions?

2) Are the microbial compartments (Bacteria, Archaea, Fungi) of sponge holobionts affected by acidification in long term adapted specimens?

3) Is there a phenotypic acclimatization reflected in the metabolic profiles of sponges inhabiting in areas exposed to diverse regimes of pH?

4) Do the different species exhibit comparable strategies to thrive under lowered pH environments as a result of high CO_2 concentrations?

5) Is there any phenotypic pattern attributable to the acclimatization to OA conditions?

3. MATERIALS AND METHODS

3.1 Field surveys

An extensive field work has been carried out to identify sites for sponge collection around the CO_2 vents system area of the island of Ischia (Gulf of Naples, Italy) and in adjacent unaffected areas. During this survey, quantitative information of the sponge coverage has been obtained by placing ten 25*25 cm quadrats on the hard bottom substrate of each sampling site. Each photo quadrat was subset into small squares 5x5 cm (n = 25). Sponge cover percentage was quantified by counting the number of quadrats which are covered by each species, and reporting this value in percentage according to Teixidó et al. (2018). Photo quadrats were processed by means GIMP software (Chastain and Pfaffman, 2006).

3.2 Sampling sites and sponge collections

Sponge samples (n = 5) of the four target species – *Petrosia ficiformis*, *Chondrosia reniformis*, *Crambe crambe* and *Chondrilla nucula* were collected in spring 2018 by scuba diving at 2-5 m depth in different sites around the CO_2 vents system area of the island of Ischia, Gulf of Naples, Italy. The sampling strategy included three acidified sites: Castello Aragonese (CAC - pH = 7.21 north side), Grotta del Mago (GM - pH = 7.6 – 7.88) and Vullatura (VU - pH = 7.1 – 6.8); and three control sites: Castello Control (CCO - pH = 8.04), Grotta Control (GF - pH = 8.04) and Sant'Anna (SA - pH = 8.04) (Fig. 7). Not all species were present in all the sampling sites. *P. ficiformi*s and *C. reniformis* were collected in all of the three control sites and in two acidified sites (*i.e.* CAC, GM). Within the cave site GM, *P. ficiformis* exhibited two phenotypic morphologies, the "normal" purple lobulated form and a bleached white morph with reticular growth. *C. reniformis* was also found to be in two morphs within the site GM, with similar growth pattern but different color, one with "normal" brown/gray/black color and one bleached. We collected five samples of each morph of *P. ficiformis* and *C. reniformis* to perform a comparison.

C. nucula was found only in one acidified site (GM) and in two controls (SA, GF), whereas *C. crambe* was found in every sampling site, and was the only species present in VU site (Fig. 8). Sponge samples were maintained in the seawater from the same collection site, in closed zip-bags, stored in ice boxes and brought to the SZN laboratory in Ischia, immediately after collection. Seawater from each site was also collected in triplicate in large 10 L containers and brought to laboratory for processing.

3.3 Sample processing

Sponge samples were divided in subsamples for the corresponding downstream analyses as follows:

- For spicule morphometry a small piece of sponge (~ 0.5 cm^3) was collected by sterile lancet and stored in a 1.5 mL tube containing 4% formaldehyde solution. Samples for these analysis were stored at + 4°C until processing.
- For microscopy observations small slices of ~ 0.4 cm^2 were collected by means of a sterile lancet. Three slices per sample were collected. Specimens were stored in 2 mL tubes containing 0.5% glutaraldehyde solution. Samples for these analyses were stored at + 4°C until processing.
- For the analysis of microbiome associated to sponges, sponge sub-samples of ca. 0.5 cm^3 were cut using a sterile lancet, rinsed with sterile seawater and then frozen in liquid nitrogen and stored at -80 °C at SZN in Naples. For the analysis of microbial assemblages in the surrounding seawater, seawater samples (1 L) were filtered through 0.22 µm pore size filters (Millipore MF^{TM}-Membrane). The filters were then stored at -80 °C until processed.
- For metabolomics and chemical analyses sponge sub-samples (~50 cm^3) were collected and stored at -80 °C until processing.

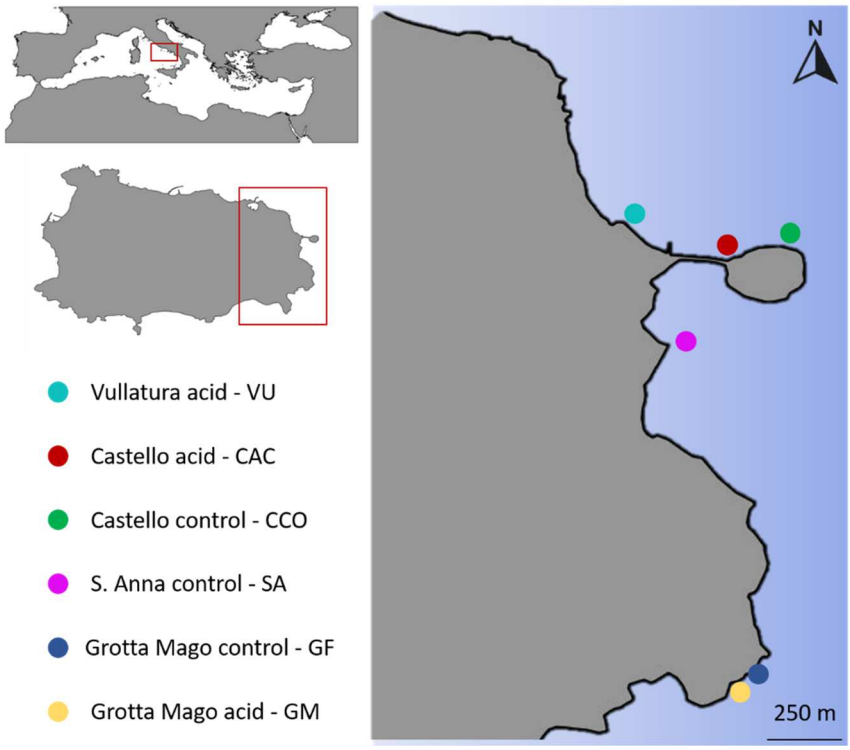

Figure 7 – Map of the CO_2 vents area off Ischia Island Naples, Italy) color icons indicate the acidified and control sampling sites where the sponges were collected.

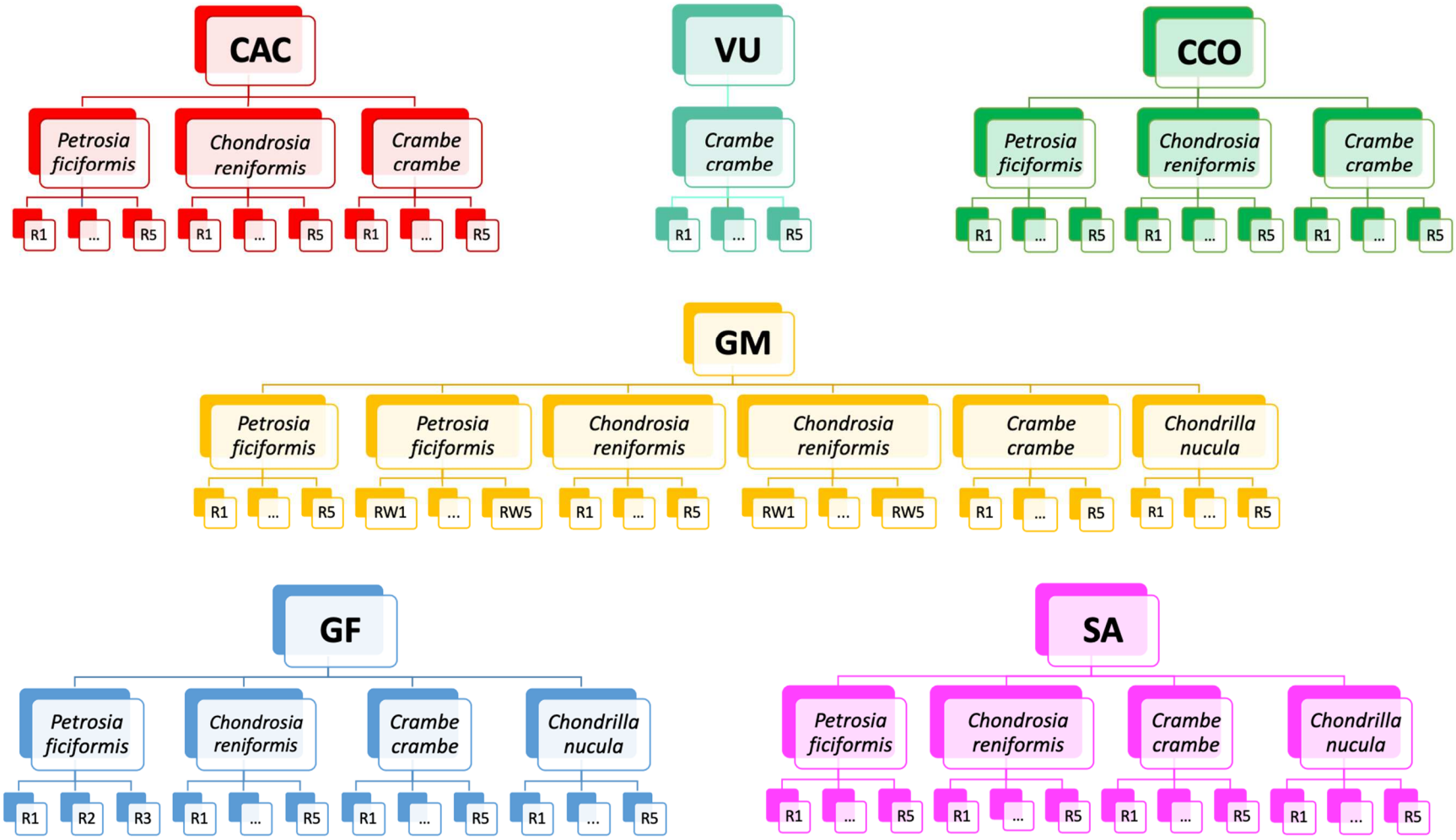

Figure 8 – Conceptual scheme of the sampling plan, with the sponge species we collected at every site. Five replicate specimens were sampled for every sponge species in every site when possible. *Note n = 3 for *Petrosia ficiformis* in GF. In site GM colored (n = 5) and bleached (n = 5) morph specimens for *Petrosia ficiformis* and *Chondrosia reniformis* were sampled.

3.4 pH and carbonate chemistry

In the different sampling sites, the pH has been determined by using a probe along with the collection of additional water samples for the determination of the carbonate system variables. Samples for total alkalinity (A_T) and for pH_T (total scale) were collected using standard operating protocols (Riebesell et al. 2010). A_T was determined using an auto-titrator (Mettler Toledo G20S). The HCl (0.1 M) titrant solution was calibrated against certified reference materials distributed by A.G. Dickson (CRM, Batches #177). Precision of the A_T measurements of CRMs was <2 μmol/kg from nominal values. Samples were processed for pH_T using an Ocean Optics spectrophotometer (USB2000) with 10 cm path length optical cells and with purified m-cresol purple (Fluidion). A_T and pH_T were used to determine the remaining carbonate system parameters at *in situ* temperature of each sampling site in the R package seacarb v3.2.12 (for further information, see Teixidó et al. 2020).

3.5 Spicule extraction and optical and transmission electron microscope observations

Sub-samples of sponges containing both ectosome and choanosome have been added with 2 mL of nitric acid (HNO_3) and then were gently heated until the disappearance of all the soft tissue. Spicules were washed in deionized water and then, after two additional washing steps with 70% ethanol, re-suspended in 1 mL of 100% ethanol (Hooper, 2003). For the observations of spicules by optical microscope, few drops of above-mentioned 100% ethanol solution containing spicules, were dropped by pipetting on a microscope slide and placed on a pre-heated laboratory heat plate, under the flume hood. Ethanol was then ignited with a lighter and dried, resulting in a spicules powder on the microscope slide. Few drops of EUKITT® laboratory resin were dropped on the glass slide and a cover glass slide was added to enclose the spicules. Optical microscope observations of spicules were carried out by means a Zeiss Axio Imager M1 Microscope. Fifty spicules per sample were randomly selected, photographed and measured. For *C. crambe* and *P. ficiformis* length of the most abundant spicular type (styles for *C. crambe*, oxeas for *P. ficiformis*) has been

measured while for *C. nucula* the diameter of spherasters has been determined. All measurements were further analyzed in the R environment.

To obtain details on sponge tissues, sponges have also been investigated by Transmission Electron Microscopy (TEM). Sub-samples of sponges were fixed in a solution of filtered seawater containing glutaraldehyde, to a final concentration of 2.5% and then stored at 4°C. For TEM observations, samples were washed three times with filtered seawater, incubated with 1% osmium tetroxide for 1 hour and then rinsed 4 times with filtered seawater. After the washing steps, four dehydration steps were performed for 30 minutes each with increasing acetone concentrations: 50%, 70%, 80% and 90%. Samples were then placed in 100% acetone for three times of 30 minutes each. Then, samples were embedded in Spurr resin with the following steps all performed on the shaker plate:

- Two hours 1/3 Spurr resin / Acetone
- Three hours 2/3 Spurr resin / Acetone
- Overnight 3/1 Spurr resin / Acetone
- Two hours 100% Spurr resin

Finally, the samples were left overnight in 100% Spurr resin at 60 °C for 24-48 h. Ultra-thin sections of the sponges samples obtained by using an ultra-microtome were observed by TEM.

3.6 DNA extraction, amplification and sequencing

DNA from frozen sponge samples and seawater filters (-80°C) was extracted using QIAGEN PowerSoil Pro Kit (2018), following manufacturer's instructions. The quantity and quality of the extracted DNA were assessed through a Thermo Scientific Nanodrop™ 1000.

Aliquots of the extracted DNA from sponges and seawaters were sent to Personal Genomics laboratories (www.personalgenomics.it) for amplicon library preparations and sequencing. For bacterial and archaeal diversity analysis, the V_3-V_4 hypervariable region of the 16S rRNA gene (*Escherichia coli* position: 341-805) was amplified using the bacterial and archaea universal primers: Bakt_341F 5′-CCTACGGGNGGCWGCAG-3′, Bakt_805R 5′-GACTACHVGGGTATCTAATCC-3′ following the Illumina protocol. Amplification reaction were prepared with: Metagenomic DNA (5ng/µL) 2.5 µL, Forward primer (1 µM) 5µL, Reverse Primer (1 µM) 5 µL, KAPA HiFi HotStart ReadyMix 12.5 µL, for a total volume of reaction of 25 µL. PCR were performed in a Veriti™ 96-Well Thermal Cycler following this thermocycling conditions: 95°C for 3 minutes followed by 25 cycles of 95°C for 30 seconds, 55°C for 30 seconds and 72°C for 30 seconds and a final elongation performed at 72°C for 5 minutes and a 4°C hold. After a purification with AMPure XP beads to eliminate free primers and primer dimer species sequencing was performed on a MiSeq sequencer (Illumina platform) with a Reagent Kit v3 (600-cycle) targeting ~400 – 450bp amplification products.

For fungal diversity analysis, the ITS1 region of the Internal Transcribed Spacer (ITS) was amplified using the universal fungal primers ITS1F (5′-CTTGGTCATTTAGAGGAAGTAA-3′) and ITS2R (5′-GCTGCGTTCTTCATCGATGC-3′) by Personal Genomics (www.personalgenomics.it) following the Illumina protocol with this reaction containing: 2.5 µL DNA (5ng/µL), 5µL Forward primer (1 µM), 5 µL Reverse Primer (1 µM), 12.5 µL KAPA HiFi HotStart ReadyMix, for a total volume of 25 µL. PCR were performed in a Veriti™ 96-Well Thermal Cycler following this conditions: 95°C for 3 minutes followed by 25 cycles of 95°C for 30 seconds, 55°C for 30 seconds and 72°C for 30 seconds and a final elongation performed at 72°C for 5 minutes followed by a 4°C hold. To avoid host ITS's co-amplification a PCR clamping approach was

conducted, in which 1 µL Peptide Nucleotide Acid (PNA, (10 mM) was added to the master mix (according to methods from Núñez-Pons, unpublished data). After purification with AMPure XP beads to remove potential primers and primer-dimer fragments, sequencing was performed using a MiSeq Illumina sequencer with Reagent Kit v3 (600-cycle) resulting in about 200-500 bp amplification products.

3.7 Sample processing for metabolomics and chemical analyses

For each sponge specimen ca. 500 mg of freeze-dried samples was crushed, added with 4.5 mL MeOH and sonicated for 30 seconds. After sonication, 15 mL of Methyl tert-butyl ether (MTBE) were added and left at room temperature for 1 h under gently shaking. Subsequently, 3.75 mL of LC/MS grade water were added and shacked for 10 minutes to induce phase separation via centrifugation at 1000 g for 10 min at 4 °C. The upper organic phase was transferred into a glass balloon, dried using a rotary evaporator, recovered in an aliquot of MeOH, and then transferred into a labeled glass vial. Each sample was preserved at -20 °C after solvent evaporation under N_2 stream (Cutignano et al. 2016). Thin layer chromatography (TLC) was performed on each sample to assess for extraction quality and chemical profiles, under three different elution conditions: $CHCl_3$/MeOH 9:1, EP/EE 6:4 and $CHCl_3$/MeOH/H2O 65:25:4.

3.8 Ultra high performance liquid chromatography - High resolution mass spectrometry (UHPLC/HRMS)

Dry extracts were dissolved in 4 mL of MeOH:$CHCl_3$ (1:1) and sonicated for 15 minutes. An aliquot was further diluted 40 times with MeOH:iPrOH (1:1) and 10 µL were injected in a Thermo Scientific Dionex UltiMate 3000 UHPLC coupled to a Thermo Scientific Q Exactive focus quadrupole-Orbitrap mass spectrometer, equipped with a heated electrospray ionization (HESI) source (Thermo, CA, USA). Chromatographic separations were performed through a Kinetex^R Biphenyl (2.6 µm, 100 A, 100 × 2.1 mm) column (Phenomenex, USA) using water (5 mM ammonium formate, 0.1% formic acid) and methanol (5 mM ammonium formate, 0.1% formic acid) as mobile phases. LC multistep gradient flux was kept constant at 0.3 mL min^{-1} starting with 40% organic mobile phase, increasing until 80% in 2 minutes and

reaching 100% at minute 15. It was maintained for 7 minutes and it returned to initial conditions over a 5 minutes' delay. Column was kept at 35˚C and samples were also maintained at constant temperature (4˚C) in the auto sampler. Samples were analyzed on positive and negative mode in the full scan – data dependent MS2 (Full MS-ddMS2) discovery acquisition mode. For the Full MS resolution was set at 70,000 (tolerance of 5 ppm), with a scan range of 150 to 18000 *m/z*; and for ddMS2 resolution was diminished to 17,500 with switching normalized collision energies of 10, 20 and 40 eV. One microscan per cycle was allowed in the Full MS, with an AGC target 1×10^6 and a maximum IT of 100 ms. At the ddMS2 the isolation window was of 0.8 m/z, with and automatic gain control (AGC) target of 2×10^5, with a maximum intensity threshold of 75 milliseconds, over a three look counts. Dynamic exclusion was set as automatic and no other thresholds of apex trigger or exclusion were used. HESI source temperatures were set for the capillary at 320˚ C and for the auxiliary gas heater at 350˚ C, and spray voltage was set at 3.20 kV. Source gases fluxes were fixed at 60 arbitrary units (au) for the sheath gas, 35 au for the auxiliary gas and 1 au for the sweep gas. S-lenses RF level was set at 55.0. Calibration of the instrument was conducted both for negative and positive ionization modes prior to analysis using Pierce LTQ ESI Calibration Solutions (Thermo Scientific, Waltham, Massachusetts, United States). The instrument was controlled with the software Xcalibur 3.1 (Thermo). A calibration curve was prepared injecting standards of 21 native lipids, in five calibration solutions (Cal01 to Cal05) with increasing concentrations, injected before the samples.

3.9 Isolation and identification of polyacetylenes from *Petrosia ficiformis*

Chemical analyses on the secondary metabolites of samples from *P. ficiformis* allowed to isolate and elucidate a group of compounds with diverse polarities belonging to the polyacetylene family. For each sample, three g of freeze-dried sponges were used for the chemical extractions, allowing to obtain ~250-300 mg of crude extracts.

Chromatographic separations were performed on silica gel, charging ~40 mg of crude extract and applying these stepwise elution protocols: EP/EE 9:1, EP/EE 8:2, EP/EE 7:3, EP/EE 6:4 in order to collect the most non-polar polyacetylenes, which yielded a fractions of ~7.5 mg; while ~70 mg of crude extract were processed through the elution

steps $CHCl_3$/MeOH 8:2, $CHCl_3$/MeOH 7:3, $CHCl_3$/MeOH/H_2O 65:25:4 to separate the most polar polyacetylenes accounting for ~22 mg. To obtain a single compound separation, molecular fractions obtained from the manual chromatographic separation were processed through High Performance Liquid Chromatography (HPLC) on a JASCO system (PU-2089 Plus quaternary gradient pump equipped with a MD-2018 Plus photodiode array detector and Sedex 85 high-sensitivity LT-ELS detector) equipped with a C18 column (Supelco-Ascentis C18 column, 25 × 0.46 cm, 100% MeOH; flow 1 mL/min). This allowed to isolate pure fractions of single polyacetylene molecules. To calculate the exact mass, each of the fractions containing the pure compound from the HPLC were dissolved in MS grade MeOH (concentration: 5 µg/mL) and analyzed on Q-Exactive Hybrid Quadrupole-Orbitrap mass spectrometer (Thermo Scientific, San Jose, CA, USA) equipped with a HESI source.

^{1}H and ^{13}C NMR spectra were recorded on DRX 600 MHz Bruker spectrometers in CDCl3, with chemical shifts reported in ppm referenced to $CHCl_3$ (δH 7.26 for proton and δC 77.0 for carbon) as an internal standard at each step of isolation and purification of the molecules.

3.10 Metabolomics data analysis, statistics and plotting

Compound Discoverer v3.1 (Thermo) was used to process the LC-HRMS data in the non-targeted mode. Chromatographic feature outputs (peaks and MS) were then introduced into a suit of statistical pipelines, including univariate and multivariate analyses. LipidSearch v4.0 was used to identify and plot metabolomic features grouped as molecule class profiles associated with each sponge species.

Xcalibur v3.1 (Thermo) was used to perform a targeted analysis on the exact masses of polyacetylenes from samples belonging to the species *P. ficiformis*. From this analysis, a presence/absence table was obtained for downstream statistical analyses.

Metaboanalyst v4.0 (https://www.metaboanalyst.ca/) was used to perform univariate statistical analyses and data visualization from the datasets obtained through Compound Discoverer (Chong et al. 2018).

Quantitative insights into microbial ecology (QIIME2) v.2019.10 (Caporaso et al. 2010) was used to perform differential abundance analysis based on log ratio rankings, applying the plugin Songbird (Martino et al. 2019). While Welch's Test were used to

test the statistical significance of the log ratios of the metabolites selected by Songbird and visualized by Qurro (Fedarko et al. 2020). These differential metabolite features were selected as the most defining to separate groupings across sample type.

ChemDraw software was used to draw the molecular formulas according on NMR and HR-MS spectra (Brown, 2014). Permutational multivariate analysis of variance (PERMANOVA) was used to detect significant differences between the sample groups. While pairwise Adonis (https://github.com/pmartinezarbizu/pairwiseAdonis) was used to perform multilevel comparison using the Adonis function (PERMANOVA) from the R package "vegan". Networks were visualized and computed by Gephi v0.9.2 (Bastian et al. 2009).

3.11 Bioinformatic pipelines

3.11.1 Quality control and filtering of raw microbiome data

The quantitative insights into microbial ecology pipeline (QIIME2) v.2019.10 was used to perform most of the bioinformatics analyses (Caporaso et al. 2010). Demultiplexed paired end sequence reads were imported in the QIIME environment, then primers and adapters were removed using the q2-cutadapt plugin. Sequences were then denoised (q2-dada2) by means of DADA2 (Callahan et al. 2016), which is a tool for detecting and correcting Illumina amplicon sequence by filtering, identifying chimera sequences and merging paired-end reads. Merged paired-ends were processed and clustered as "Amplicon Sequence Variants" (ASVs) in a feature frequency table (ASV table). Taxonomy was assigned using a pre-trained Naïve Bayes classifier (sklearn) (Bokulich et al. 2018) and the q2-feature-classifier plugin, based on pairwise identity (99%) of rRNA sequences. The classifier was pre-trained on the QIIME-compatible 16S SILVA (99% identity) reference database v.128 (Quast et al. 2013). The reference sequences were trimmed to span the query V_3-V_4 region (~411 bp) of the 16S rRNA gene using the extract-reads command of the plugin. The ASV feature tables were filtered considering a minimum of 10 reads counted throughout all the samples, and removing all features whose taxonomy contained untargeted assignments, such as "Chloroplast" or "Mitochondria". Alpha rarefaction tool (q2-

diversity) in qiime2 was used to build rarefaction curves setting the lowest number of reads sufficient to reach a plateau according to alpha-rarefaction plots. This guaranteed a full coverage of bacterial/archaeal diversity, while retaining the maximum number of samples for the analysis. The ITS1 region of the rDNA was extracted from all sequenced amplicons by means of ITSxpress (Rivers et al. 2018). Reverse reads, displaying with lower quality scores, were eliminated, to enhance the successful sequences after filtering (Pauvert et al. 2019). Forward reads were then processed in R by means of DADA2 package (Callahan et al. 2016) (see https://benjjneb.github.io/dada2). Quality-filtered reads were then used to estimate and correct sequencing errors, and remove de novo-detected chimeras within the DADA2 package. Taxonomy was assigned with the RDP Classifier algorithm against a custom database consisting of the UNITE database (v1.12.2017) and a custom set of outgroups. Any sequences matching non-fungal taxa were removed. The remaining ASVs that were taxonomically assigned as fungi were used in all downstream analyses within the phyloseq R package (McMurdie and Holmes, 2013). ASVs counts from each sample were transformed to relative abundance values to account for the compositional nature and sequence heterogeneity inherent in Illumina datasets (Gloor et al. 2017). More details for this analysis are reported at: https://github.com/gzahn/CO2_Sponge_Fungi.

3.11.2 α and β diversity analyses

Alpha-diversity analyses (within sample diversity) were computed using two metrics, Observed ASVs and Shannon Index (Lozupone and Knight, 2007); while concerning β-Diversity (between sample diversity), Bray Curtis and Jaccard metrics were applied, respectively accounting for difference in number of counts and presence/absence (Bloom, 1981; Ross et al. 1964). Alpha diversity analyses were run on rarefied ASV tables as well as beta diversity, plotted as PCoA ordinations, running core-metrics-phylogenetics command from q2-diversity plugin.

The problem of handling compositional data, such as relative microbial abundance is that the analysis of this data through classical methods (rarefaction and α and β diversity, taxa bar-plots) can lead to misleading and irreproducible results. In fact, compositional data sets are represented by relative abundances, or proportions, that

individually carry no information for the absolute abundance of a specific feature (Morton et al. 2017). For these reasons the analyses were complemented with DEICODE (https://library.qiime2.org/plugins/deicode/19), a pipeline that works on non-rarefied data throughout matrix completion and robust principal-component analysis (RPCA) for compositional data. DEICODE works with a non-supervised method (no co-variates included in a formula computing the model), whereas the distance matrix is calculated with no co-variates added in a formula, to calculate feature loadings (*e.g.* the coefficient of the linear combination between the variables and the factors of a principal component analysis). Log ratios of the most important features driving the differences in the ordination spaces were visualized with Qurro (Fedarko et al. 2020) (https://github.com/biocore/qurro).

This method brings the advantage of handling sparse dataset, scale invariance and unsupervised rankings, to analyze which taxa are driving the differences in the ordination space (Martino et al. 2019).

3.11.3 Differential abundance analysis

Differential abundance analysis aims at determining differences in taxonomic or functional composition between metagenomics samples.

Microbiome dataset are compositional dataset, that provide only relative abundance information. Determining differential abundance on microbiome data with classical methods, often brings to erroneous results and wrong statistical inferences that could lead on controversial interpretations and irreproducible results. For those reasons, to detect differential abundance of single ASVs, two new approaches, both accounting for compositional nature of microbiome data known as Gneiss and Songbird, have been used. These mathematical models have the advantage of being exploitable for all the compositional datasets such as microbiomes, metabolites, gene expressions or predictive functions.

3.11.4 Gneiss model

Gneiss is a plugin of qiime2 that performs differential abundance analysis on compositional data via multivariate response linear regression working on log transformed and non-normalized data. The algorithm, creates isometric log transformed balances of ASVs clustered by co-occurrence from a hierarchical tree calculated by Ward's algorithm (Dada et al. 2019; Morton et al. 2017).

The key concept of Gneiss are "balances". Each balance include all the bacterial taxa present under the internal node of a hierarchical or phylogenetic tree. In the simplest form a balance includes two taxa, one on the numerator and one on the denominator and it is calculated taking the logarithm of this ratio. To highlight which factor could determine a shift in microbial community assemblage Gneiss calculates changes in the R^2 of the linear model leaving one variable out of the model at each calculation. When the R^2 related to a certain covariate is > 0, this covariate is considered to be associated with changes in microbiome composition. To validate the model, Gneiss reports also a mean square error (model_MSE) for the model and a prediction accuracy MSE (pred_MSE) at each level of a ten-fold cross validation process. When the pred_MSE is lower than the model_MSE, the model is non-overfitted and then validated. The Gneiss models related to our study were validated based on the total R^2 explained by the linear regression plus the comparison of the model_MSE and pred_MSE of the ten-fold cross validation report. In the present study, all the four models computed by species recorded pred_MSE < than the model_MSE in all the ten cross validations.

3.11.5 Songbird model

Songbird (https://github.com/biocore/songbird) accounts for the compositional nature of microbial data, and uses a multinomial regression model to estimate differential ranks in relation to co-variates included in the formula (supervised). In this pipeline the log-fold change of features (*e.g.* microbes) within a dataset, produce a table of differentials. The term "differential", is related to the logarithm of the fold change in abundance of taxa (or every feature underlying compositionality), compared in two conditions or *versus* a given co-variate. Performing multinomial regressions on microbiome sequences data, provides coefficients that can be ranked in respect to a

given covariate to determine the taxa that are mostly contributing in changes between samples or sampling groups; this procedure is known as differential ranking. Differential rankings can be used in microbiome analysis considering the compositionality of this kind of data (Martino et al. 2019; Morton et al. 2019).

Differential ranking is obtained by sorting a column of differentials from lowest to highest and give information on the associations of features with a given co-variate. Similar as in Gneiss, Songbird has its own validation. To avoid over-fitting of the model, the initial step is to compare the query model with a "null" and "baseline" models (when more than one co-variates are considered). This is done by contrasting Q^2 between the corresponding validation models and the query; when the Q^2 value is greater than zero, this means that co-variates in the formula are informative to the model fit. Differential ranks were visualized by Qurro (Fedarko et al. 2020) (https://github.com/biocore/qurro), in which the log-ratios of the differentially abundant microbes (or features) can be selected and plotted in relation to a given co-variate. These log ratios can be in the end analyzed by a statistical test (*e.g.* Welch's Test) to proof for their statistical significance. Multinomial regression and related count regression models are commonly used in the context of microbiome analysis and Songbird has been demonstrated to be one of the most powerful tools in identifying the correct taxa (Calgaro et al. 2020).

3.12 Statistical analysis

Alpha diversity values (Observed ASVs, Shannon index,) obtained for the sponge species were compared among samples using Kruskal-Wallis test included in the QIIME pipeline (qiime feature-table alpha-group-significance). Pairwise Wilcoxon rank sum test (Rstats) was run on Rstudio, to perform multilevel comparison of the alpha-diversity values. Homogeneity of multivariate data was tested applying homogeneity of multivariate dispersion test (PERMDISP) included in the qiime2 package (qiime feature-table beta-group –significance). Permutational multivariate analysis of variance (PERMANOVA) was used to detect significant differences on beta diversity based on several resemblance matrices (Bray-Curtis, Jaccard, DEICODE). Pairwise Adonis (https://github.com/pmartinezarbizu/pairwiseAdonis) was used to perform multilevel comparison using the Adonis function

(PERMANOVA) from the R package “vegan”. Welch’s Test was used to test the statistical significance of the log ratios of the microbe consortia selected in Qurro. Similarity percentage analysis (SIMPER) (Clarke, 1993) was run on PRIMER 6 + software (Anderson et al. 2008) to calculate turnover diversity and to visualize the % similarity (or dissimilarity) within and between sampling groups, and to investigate intra and interspecific variability. Exclusive and shared ASVs were identified and counted manually using the CONTA.SE command in Microsoft Excel Software. R Studio (v1.2.5033) was used to compute all the analysis in R environment. Qiime2R package was used to import qiime2 artifacts into the R environment as R objects (https://github.com/jbisanz/qiime2R), to run further downstream analyses and build plots using: Phyloseq, Vegan and Ggplot2 R packages (McMurdie and Holmes, 2013; Oksanen et al. 2008; Wickham, 2016). Networks analysis were computed and visualized using the Gephi software v0.9.2 (Bastian et al. 2009). FAPROTAX v1.2.3 was used as a database for the predicted functions of the microbiomes.

4. RESULTS

4.1 Physical-chemical characteristics of seawaters in the selected sites

At all of the sampling sites, where sponges have been collected, salinity and temperature were characterized by values typically observed during the spring season in shallow waters of the South Tyrrhenian Sea. The pH values were characterized by a wide variability among sites influenced by CO_2 emissions and those unaffected. In particular, the lowest pH values were observed at the Vullatura (VU; pH ~7.01) and the Castello Acido sites (CAC; pH ~7.2) which were also characterized by the shallowest water depths. At the Grotta del Mago (GM) site, characterized by a water depth of ~8 m, a pH value of ~ 7.7 was observed.

Values of pH encountered at the Sant'Anna (SA) and Castello controllo (CCO) sites were ~ 8.0, in line with those typically of coastal areas of the Mediterranean Sea. Mean values of the seawater's physicochemical variables are summarized in the Table 1.

Table 1 - Measured and estimated seawater physicochemical parameters at the CO_2 vent sites and reference areas with ambient pH for salinity (S), temperature (T), total alkalinity (A_T), dissolved inorganic carbon (C_T), pH_T, pCO_2, calcite (Ωc) and aragonite (Ωa) saturation. Values are means, ± SD with 25th and 75th percentiles. Calculated concentrations of C_T, pCO_2, Ωc and Ωa are shown. 1: Parameters measured from discrete water samples; 2: parameters measured with in situ sensors; 3: parameters measured by Kroeker et al. (2011). Habitat: Infra: Infra-littoral reefs (0.5 -3 m); Cave: Cave (3 m); Photo: Photophilic reefs (10 m). pH conditions: V: Vent system; A: Ambient pH; EL: Extreme low pH.

Habitat	Local name	pH conditions	S	T (°C)	A_T (µmol kg^{-1})	C_T (µmol kg^{-1})	pHseacarb [H]	pCO_2 (µatm)	Ωc	Ωa
Infra	Castello North	V, EL pH	37.9[3] ± 0.4 n=3	23.4[3] ± 0.7 n=604	2559[3] ± 13 n=3	2579[3] ± 207 n=3	7.2[3] ± 0.4 n=604	6558[3] ± 21347 n=604	1.27[3] ± 0.82 n=604	0.84[3] ± 0.54 n=604
Infra	Castello North	A, A pH	37.9[3] ± 0.3 n=3	23.4[3] ± 0.7 n=604	2563[3] ± 3 n=3	1768[3] ± 96 (n=3)	8.0[3] ± 0.1 n=604	567[3] ± 100 n=604	4.75[3] ± 0.53 n=604	3.13[3] ± 0.35 n=604
Photo	Vullatura	V, L pH	37.9 ± 0 n=3	16.64[2] ± 0.6 (16.2, 17.1) n=538	2668[1] ± 2 n=3	2789 ± 284 (2558, 2952) n=538	7.01[2] (6.85, 7.71) n=538	6025 ± 6410 (1096, 8752) n=538	1.45 ± 1.29 (0.37, 2.43) n=538	0.93 ± 0.84 (0.24, 1.57) n=538
Photo	Sant' Anna	A, A pH	37.0 ± 0 n=3	26.4[2] ± 1 (25.9, 27.0), n=1691	2642[1] ± 17 (2629, 2659), n=17	2324 ± 21 (2310, 2338), n=1691	7.97[2] (7.94, 8.00), n=1691	556 ± 57 (513, 597), n=1691	5.53 ± 0.32 (5.31, 5.75), n=1691	3.67 ± 0.22 (3.53, 3.82), n=1691
Cave	Grotta Mago	V, L pH	37.8[1] ± 0 n=7	21.8[2] ± 2.1 (19.8, 23.8), n=1841	2541[1] ± 20 (2533, 2550), n=7	2352 ± 89 (2289, 2389), n=1841	7.74[2] (7.74, 7.93), n=1841	983 ± 868 (590, 978), n=1841	3.56 ± 1.05 (2.96, 4.39), n=1841	2.33 ± 0.69 (1.94, 2.88), n=1841

4.2 Sponge coverage at the different sampling sites

The coverage (expressed as percentage) of the sponge species at each sampling site is reported in Figure 9. *C. crambe* was the only species present at all the sampling sites, with the highest coverage percentage recorded in the acidified site CAC. This species, moreover, was the only one observed in the acidified site VU associated with the rhizomes of the seagrass *Posidonia oceanica*. In the acidified cave GM, all the sponge species considered in this study were present, with coverage percentage ranging from 0.4% to 0.8% for *C. crambe* and *C. nucula* respectively and from 7% to 10% for *P. ficiformis* and *C. reniformis* respectively. *P. ficiformis* was present (and collected) as two different coloured morphotypes, one dark purple with normal shape and one bleached with a reticular shape. *C. reniformis* was also present (and collected) massively as two coloured morphotypes, one dark greysh-brown and one bleached. *C. nucula* in the site GM had also a different external morphology and appeared to be in stressful conditions. Indeed, it was smaller, and bleached (pers. obs). In the control site SA, *C. nucula* was abundant with a coverage of ~20%.

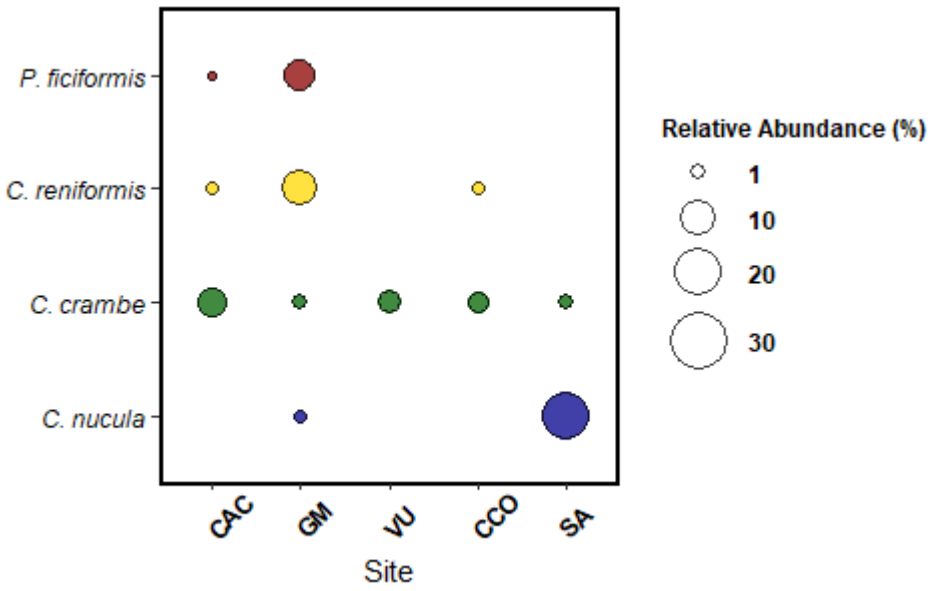

Figure 9 – Relative coverage percentages of the sponge species at each sampling site. *Crambe crambe* was the only species present in all the sampling sites. Within the sampling site GM all the sponge species of this study were found.

4.3 Microscopic observations of sponge spicules

Microscopic observations of the length of the silicon spicules were carried out on specimens of *C. crambe*, *P. ficiformis* and *C. nucula* collected at all the sampling sites (Fig. 10). Such analysis was not carried out for the sponge *C. reniformis*, since it lacks silicon spicules. *P. ficiformis* displayed the lowest values of the length of oxeas in the acidified site CAC, whereas the highest values were observed in the control site SA. However, differences in the length of the spicules for this sponge species across sampling sites was not statistically significant (ANOVA; $p > 0.05$). *C. crambe* and *C. nucula* were characterized by very similar values of the length of the styles and the diameter of the spherasters among the different sampling sites (ANOVA; $p > 0.05$). No relevant differences in the morphology of spicules collected in acidified sites *versus* control sites within the same sponge species were detected.

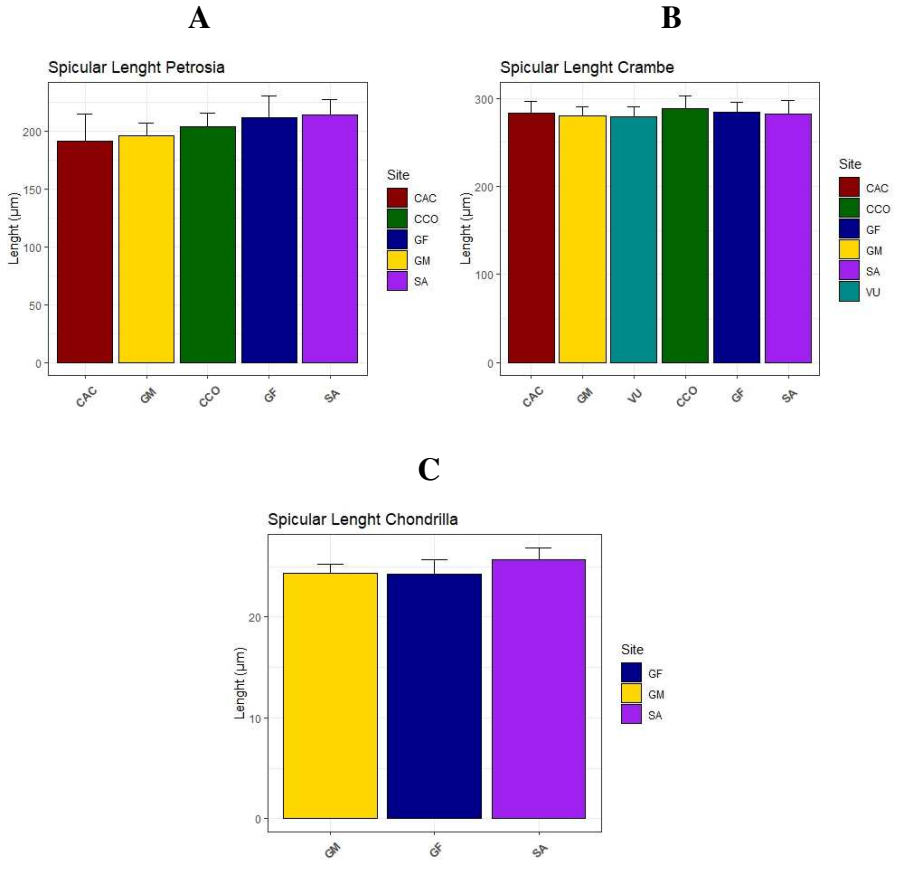

Figure 10 - Spicular measures plotted by sampling site. All the sponge species had very similar values across the different sampling sites, and the statistical analysis yielded non-significant results for all the species and sites considered in this study (ANOVA; $p > 0.05$) A) *Petrosia ficiformis*, B) *Crambe crambe*; C) *Chondrilla nucula.*

4.4 Transmission electron microscopy (TEM) analysis

To provide insights on the microbial assemblages associated with sponge tissue, ultrathin sections of the different sponge species were analyzed by transmission electron microscopy (TEM). *P. ficiformis, C. reniformis* and *C. nucula* were characterized by the presence of microbes enclosed in "bacteriocytes". Within these bacteriocytes was possible to identify the presence of different microbial components with a different morphology (Fig. 11). Abundant cyanobacterial cells were present within bacteriocytes of specimens of *C. nucula*, which conversely occurred in a lower abundance in specimens of *P. ficiformis*. Specimens of *C. crambe* lacked bacteriocytes, and all the microbes were free in the mesohyl of the sponge and morphologically similar. The comparison of specimens collected in acidified sites *versus* control sites did not show relevant morphological differences.

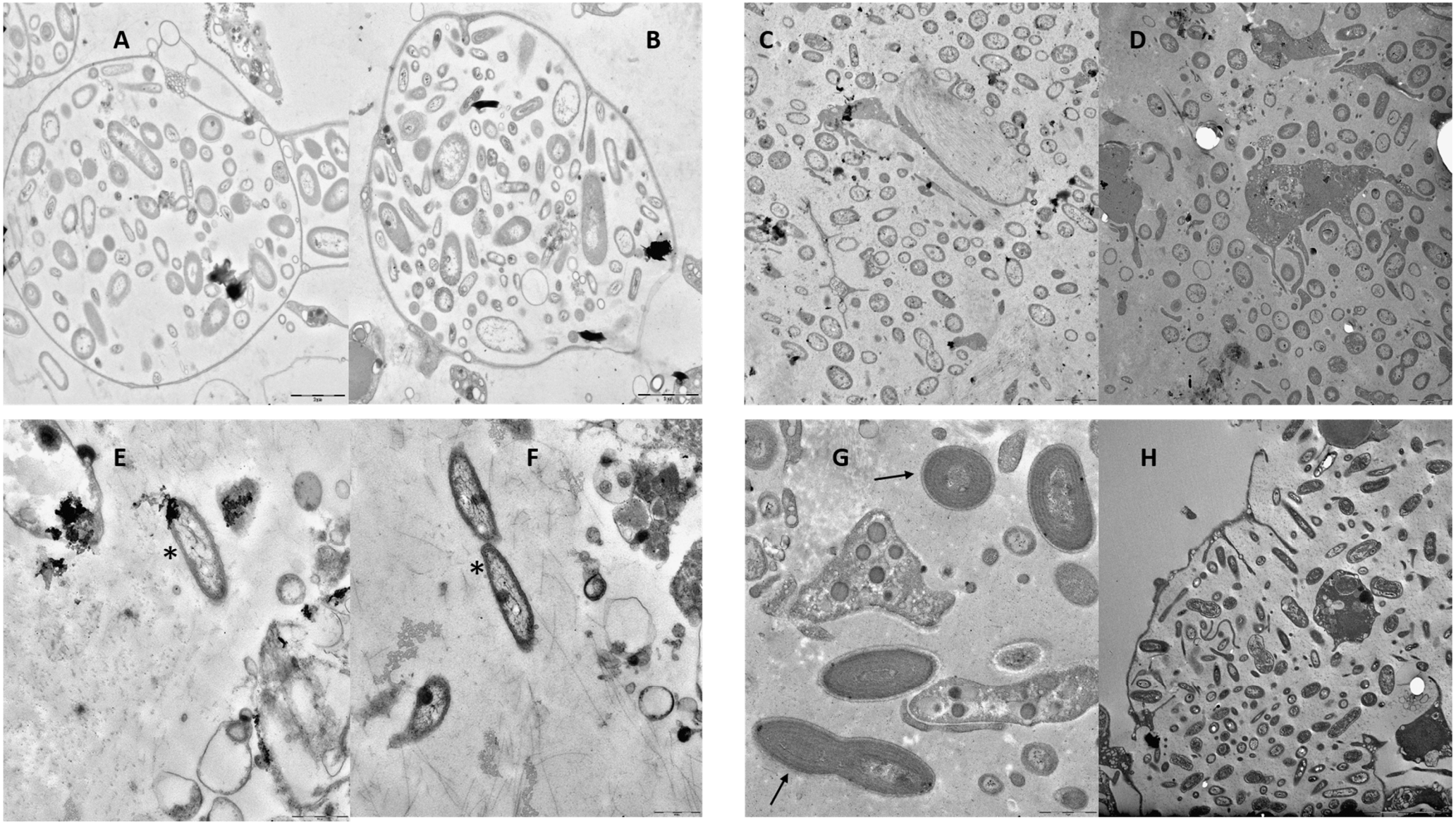

Figure 11 – Transmission electron microscopy (TEM) pictures of the four sponge species considered in this study. A-B) Bacteriocytes rich in microbial diversity captured in specimens of the sponge *Petrosia ficiformis*. C-D) Pictures of bacteriocytes from *Chondrosia reniformis*. E-F) Free bacteria in the mesohyl of *Crambe crambe* (black asterisks * indicate bacteria). G) Cyanobacteria in the bacteriocytes of the sponge *Chondrilla nucula.* (black arrows indicate a cyanobacterium on the top of the pictures, and two dividing cyanobacteria on the bottom of the picture). H) Overview of a bacteriocyte rich in bacterial diversity in the sponge *Chondrilla nucula.*

4.5 Interspecific comparison of microbiome associated with marine sponges – Bacteria and Archaea communities

4.5.1 α and β diversity analysis

Sequence data for the whole dataset was rarefied to 6881 reads per sample resulting in 791.315 reads distributed over 115 samples. Sequence reads ranged between a minimum of 10 and a maximum of 135.727 distributed over 1797 total ASVs (Fig S1; Table S1).

Alpha diversity values for the whole dataset (Fig. S2-S3) were highly variable, as the number of ASVs per sample ranged from 46 in the sponge *C. crambe* to 419 in a seawater sample. Similarly, values of the Shannon index were higher in seawater samples than in sponges, with *C. crambe*, displaying the lowest mean observed ASVs. Total ASVs per sponge species revealed that *P. ficiformis* (n=523) and *C. crambe* (n=511) were characterized by a higher number of total ASVs compared with *C. reniformis* (n=232) and *C. nucula* (n=130) (Fig. 12). The alpha diversity values, as ASVs or Shannon Index, were statistically different (Kruskal-Wallis, p-value < 0.05; Table S2) among the four sponge species and between sponge species and seawater. Beta diversity comparison based on Bray-Curtis (relative abundance) and Jaccard (presence/absence) dissimilarity indexes highlighted a clear separation among species in the ordination space of the PCoAs (Fig 12). Such differences of the microbial composition were statistically significant for every comparison (PERMANOVA, 9999 permutations, p-value < 0.05; Table S2), between sponge species respect to the surrounding seawater.

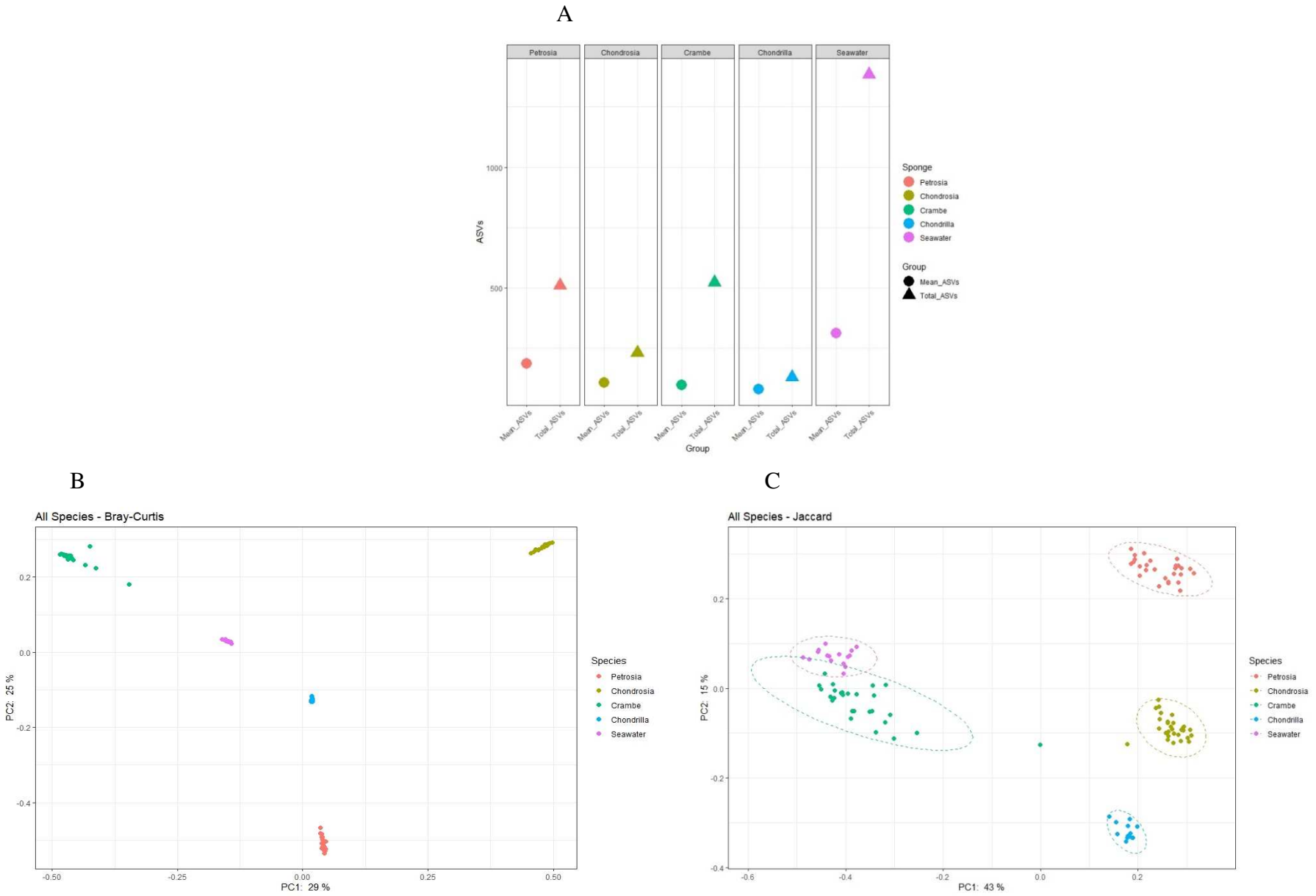

Figure 12 - Alpha and beta diversity plots of the bacterial communities associated to sponges belonging to the four sponge species and the surrounding seawater. A) Mean Observed ASVs and total ASVs. PCoA of beta diversity ordinations based on B) Bray-Curtis and C) Jaccard dissimilarity matrices (α-Diversity - Kruskal-Wallis, $p < 0.05$; β-Diversity PERMANOVA, $p < 0.05$, Table S2).

4.5.2 Composition of the microbiomes

The analysis of the microbiomes associated with the four sponge species investigated and of the microbial component in the seawater allowed identifying 29 Phyla, 63 Classes, 132 Orders, 188 Families and 254 Genera (Fig. 13). *Betaproteobacteriales*, *Flavobacteriales*, SAR11, SAR202 clade and *Synechococcales* were the most abundant bacterial orders. In *P. ficiformis* the five most abundant bacterial orders were *Caldilineales*, SAR202 clade, BD2-11, *Microtrichales* and TK17 accounting for 53%; in *C. reniformis* the five top bacterial orders were SAR202 clade, *Nitrosococcales*, Subgroup 6, SBR1031 and *Myxococcales* accounting for 47%; *C. crambe* had two principal bacterial orders, *Betaproteobacteriales* and *Synechococcales* that accounted 83% while in *C. nucula* the top five bacterial orders were *Synechococcales*, *Caldilineales*, UBA1053, TK17 and *Oceanospirillales*, accounting for 45%. *Flavobacteriales*, SAR11 clade, *Synechococcales*, *Rhodobacterales*, SAR86 clade, were the most abundant bacterial orders (accounting for 75%) present in the seawater. Cyanobacteria, was dominated by the order *Synechococcales* which was present in all the species with a relative abundance of 16% in *C. nucula* (Fig. 14), 10% in *C. crambe,* < 1% in *C. reniformis* and *P. ficiformis*, and ~10% in the seawater.

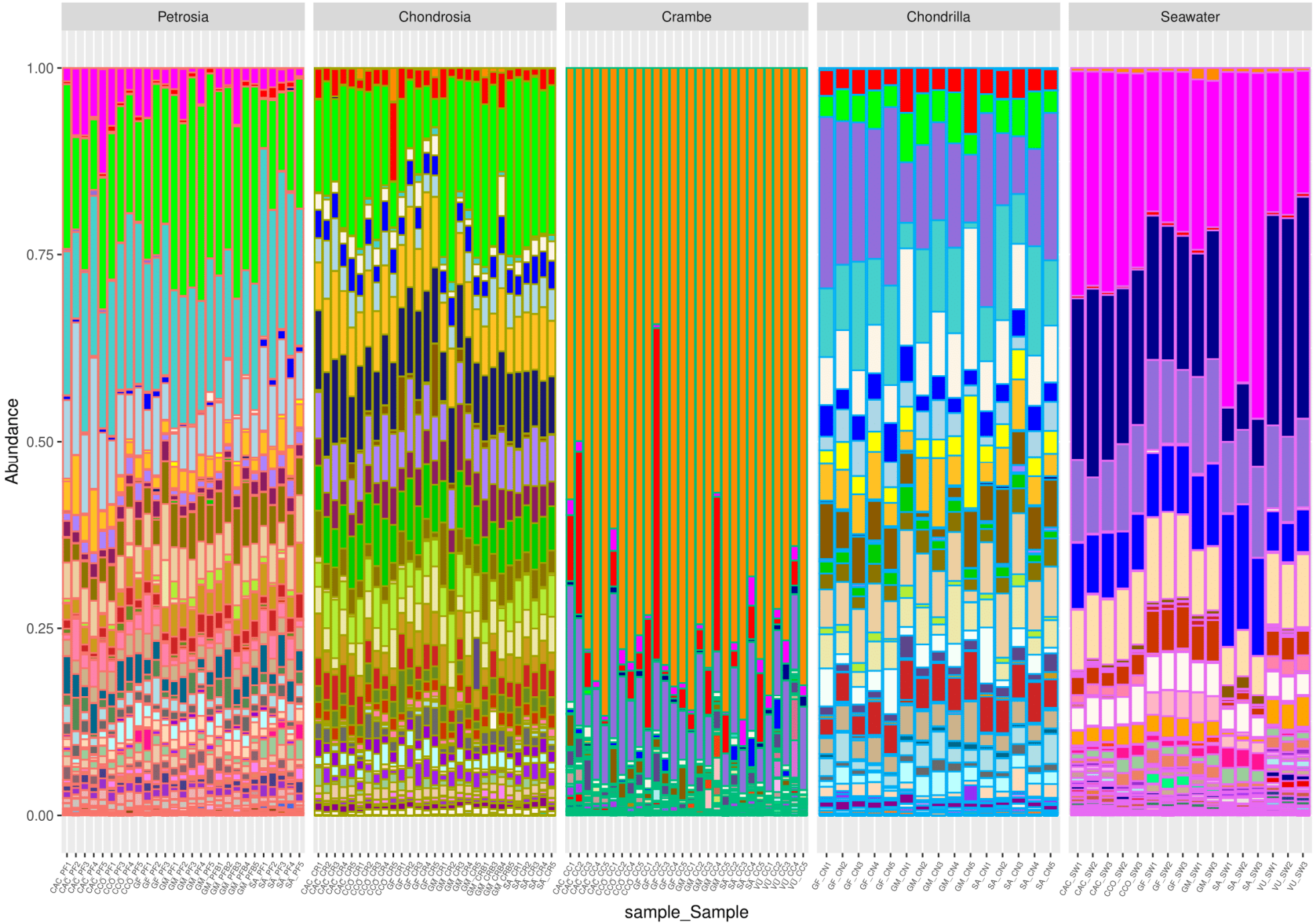
Petrosia
Chondrosia
Crambe
Chondrilla
Seawater
Abundance
1.00
0.75
0.50
0.25
0.00
sample_Sample

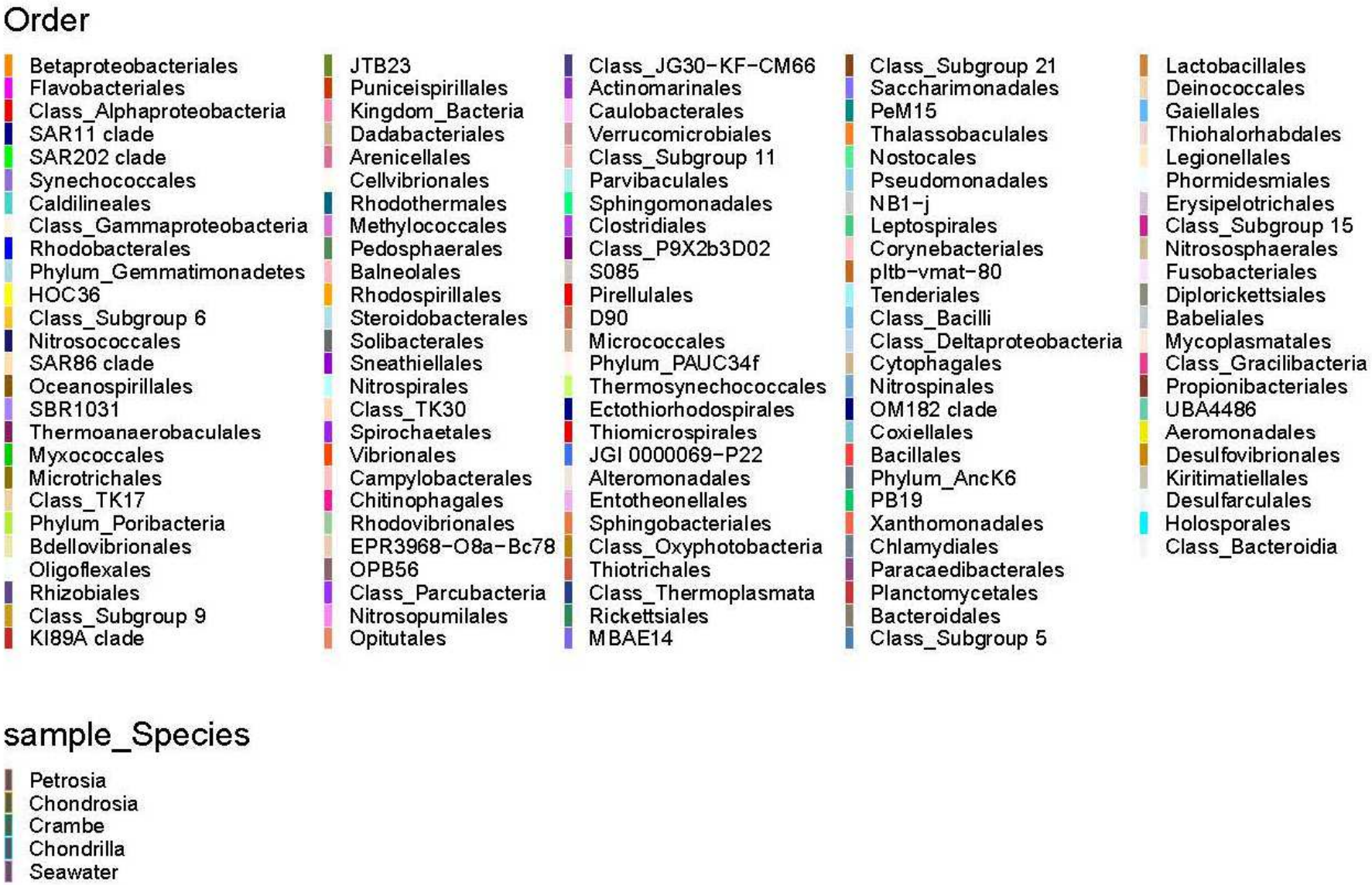

Figure 13 – Taxonomic composition of the microbiome associated with the four sponge species object of this study. All the sponge species had different microbiomes, different also from the seawater.

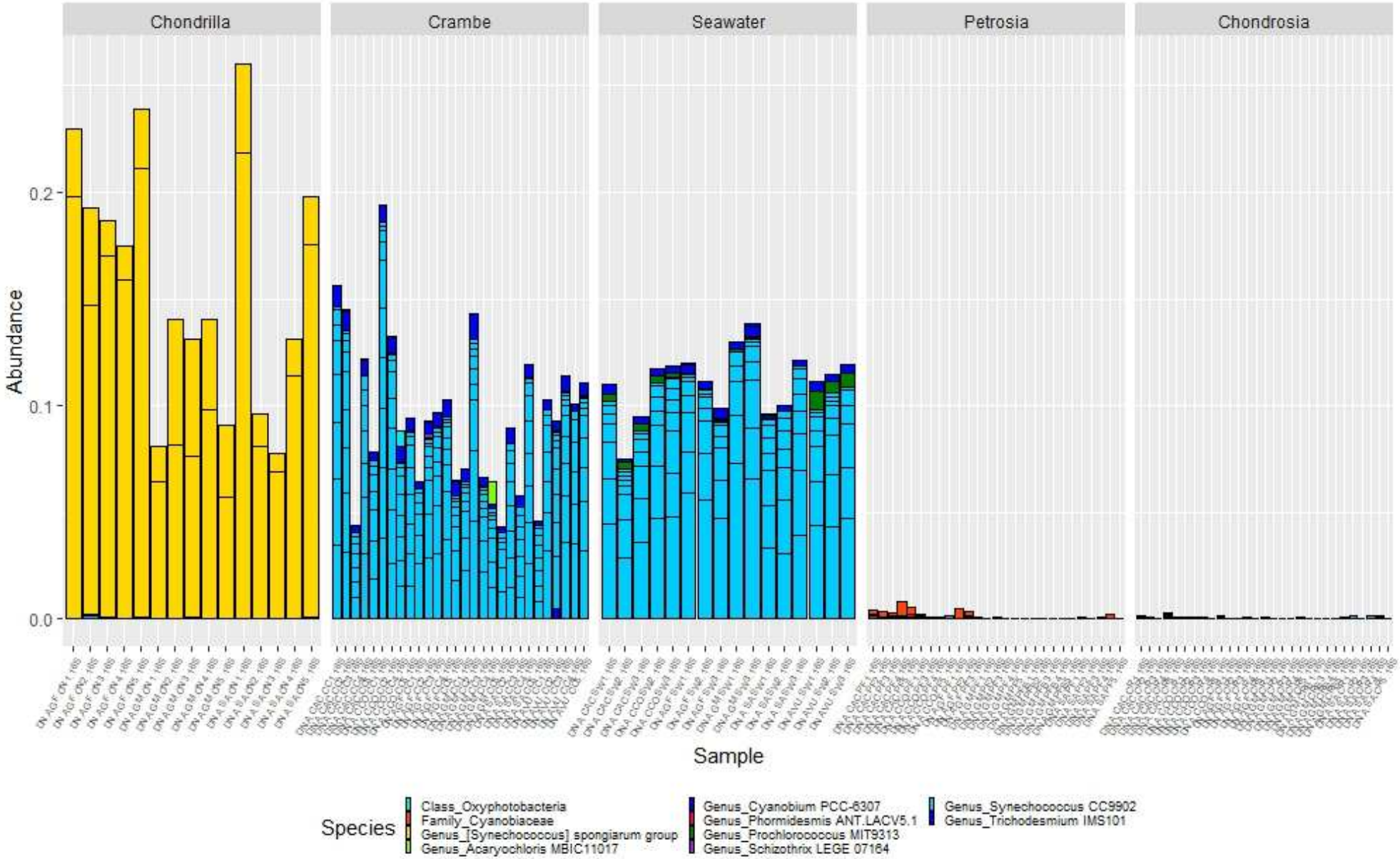

Figure 14 - Taxonomic composition of the Cyanobacteria associated with the four marine sponges, plotted at Genus level. *Chondrilla nucula* had the highest relative abundance of cyanobacteria associated, while *Petrosia ficiformis* the highest diversity. *Crambe crambe* had a cyanobacterial profile very similar to the one found in the surrounding seawater. *Chondrosia reniformis* revealed the lowest amount of cyanobacteria associated.

No ASVs were totally shared among the four sponge species (*i.e.* present in all of the sponge samples analyzed). *P. ficiformis* had 24 main ASVs belonging to 16 bacterial orders. The most abundant orders were *Caldilineales*, SAR202 clade, TK17 and *Microtrichales* accounting 65%, with *Caldilineales* as the dominant order (~30%), while the other bacterial orders equally accounted for ~ 35% (Fig.15). *C. reniformis* had 34 main ASVs belonging to 22 bacterial orders. The top abundant order was SAR 202 clade accounting for 25%, while other relevant orders were Subgroup 6, *Nitrosococcales*, SBR1031 accounting for 35%. *Crambe Crambe* had a microbiome mainly composed by eight ASVs affiliated to two bacterial orders, *Betaproteobacteriales* which account for 90% and *Synechococcales* accounting for 10%. *C. nucula* had instead 52 main ASVs affiliated to 40 bacterial orders; *Synechococcales* was the dominant main order accounting for 16%, whereas the other three relevant orders, *Caldilineales*, UBA10353 and TK17, accounted altogether for 42% (Fig. 15).

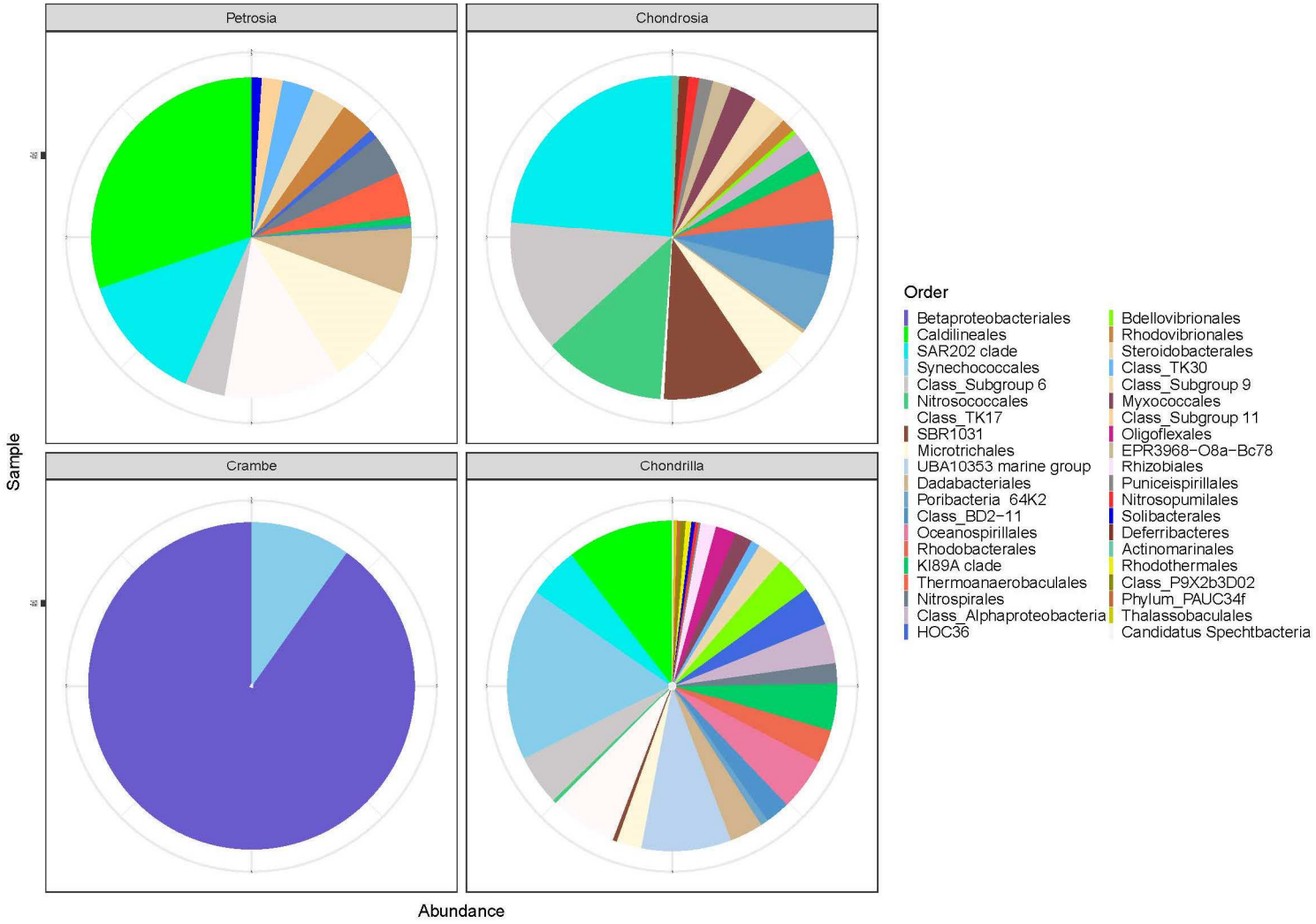

Figure 15 - Microbiome composition (100% shared AVSs within each sponge dataset) of the four sponge species investigated in the present study.

No totally shared ASVs were also found between the four sponge species and the seawater, with the majority of ASVs exclusive for each of the sponge species as shown by the network analysis (Fig. 16). The percentage of exclusive ASVs was 79, 65, 45 and 79% *in P. ficiformis, C. reniformis, C. crambe* and *C. nucula* respectively. *C. crambe* and Seawater shared 297 ASVs, while *P. ficiformis, C. reniformis and C. nucula* shared 97, 23 and 47 ASVs with the seawater (Fig. 17). *C. crambe* and *P. ficiformis* showed the highest number of exclusive ASVs (299, 487). In *C. crambe* one ASV dominated the microbial community from a total of 523 ASVs. *P. ficiformis* had 487 exclusive ASVs, while *C. reniformis*, *C. crambe* and *C. nucula* had 183, 299, and 110 exclusive ASVs. SIMPER analysis revealed a high dissimilarity among the composition of the microbiomes of the four sponge species investigated (at least 89%) as well as between prokaryotic assemblages of the sponges and those of the surrounding seawater (Table 2). Conversely, the similarity within each sponge species and among seawater samples was much higher (74.9% for *C. crambe*, 66.7% for *C. reniformis*, 52.9% for *P. ficiformis*, 71.4% for *C. nucula* and 60.9% for the seawater).

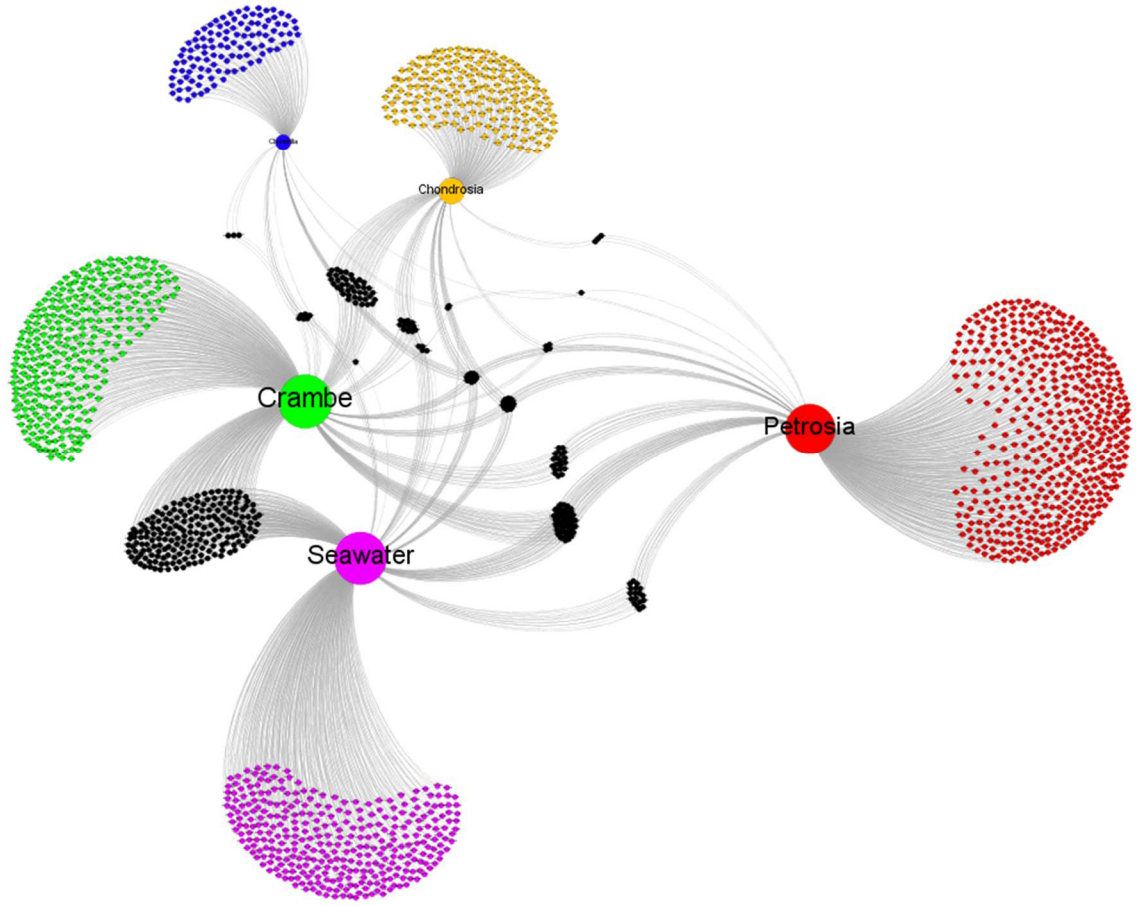

Figure 16 – Network showing interactions of bacterial ASVs between the four sponge species and the seawater. *Crambe crambe* shared a high number of ASVs with the surrounding seawater, while a few number of ASVs was shared with the other sponges. All species harbored a high number of exclusive AVSs, fact that reflected the divergences in the microbial compositions.

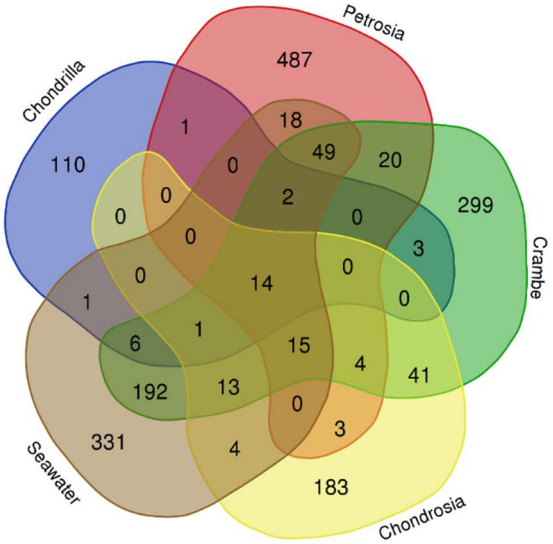

Figure 17 - Venn diagram showing exact numbers of shared and exclusive ASVs between the four sponge species and the surrounding seawater.

Table 2 – Results of the SIMPER analysis showing the dissimilarity in the microbial composition for every couple of sponge-sponge and sponge-seawater comparison.

Comparison		Dissimilarity %
Petrosia	**Chondrosia**	99.85
Petrosia	**Crambe**	99.8
Petrosia	**Chondrilla**	88.7
Petrosia	**Seawater**	91.5
Chondrosia	**Crambe**	95.42
Chondrosia	**Chondrilla**	88.89
Chondrosia	**Seawater**	92.2
Crambe	**Chondrilla**	94.52
Crambe	**Seawater**	90.65
Chondrilla	**Seawater**	94.52

4.5.3 Gneiss model output

A multivariate response linear regression model based on changes of proportion in the balances between microbial communities has been performed using the entire dereplicated dataset (119 samples) with all the factors included in this experimental design (Sponge species, Sampling site, Acidification) to assess which factor was more associated with a shift in microbial community composition. The model predicted 77% of the total variation in the bacterial community among sample groups ($R^2 = 0.7642$) with the sponge species accounting for 60% ($R^2 = 0.5853$) while sampling site explained only ca. 2.5% of the total variation ($R^2 = 0.0257$) (Table S5). The clustered ASVs, included in the principal balance "y0", were used to plot their log transformed abundance, across the factors Site and Acidification (Fig. 18). Log ratios of the relative abundance of the bacteria clustered in the balance "y0" revealed differences in the microbiome associated with each sponge species (Fig. 18). In particular, this model confirmed the outcome of the alpha and beta diversity, highlighting that all the sponge species had different microbiomes, that were also different from the microbial assemblages present in the seawater. Considering that the factor "sponge species" explained the highest fraction of the variation ($R^2 = 0.5853$) in bacterial communities, hiding possible differences due to other factors, further investigations were performed sub-setting the dataset by sponge species as presented in the following section.

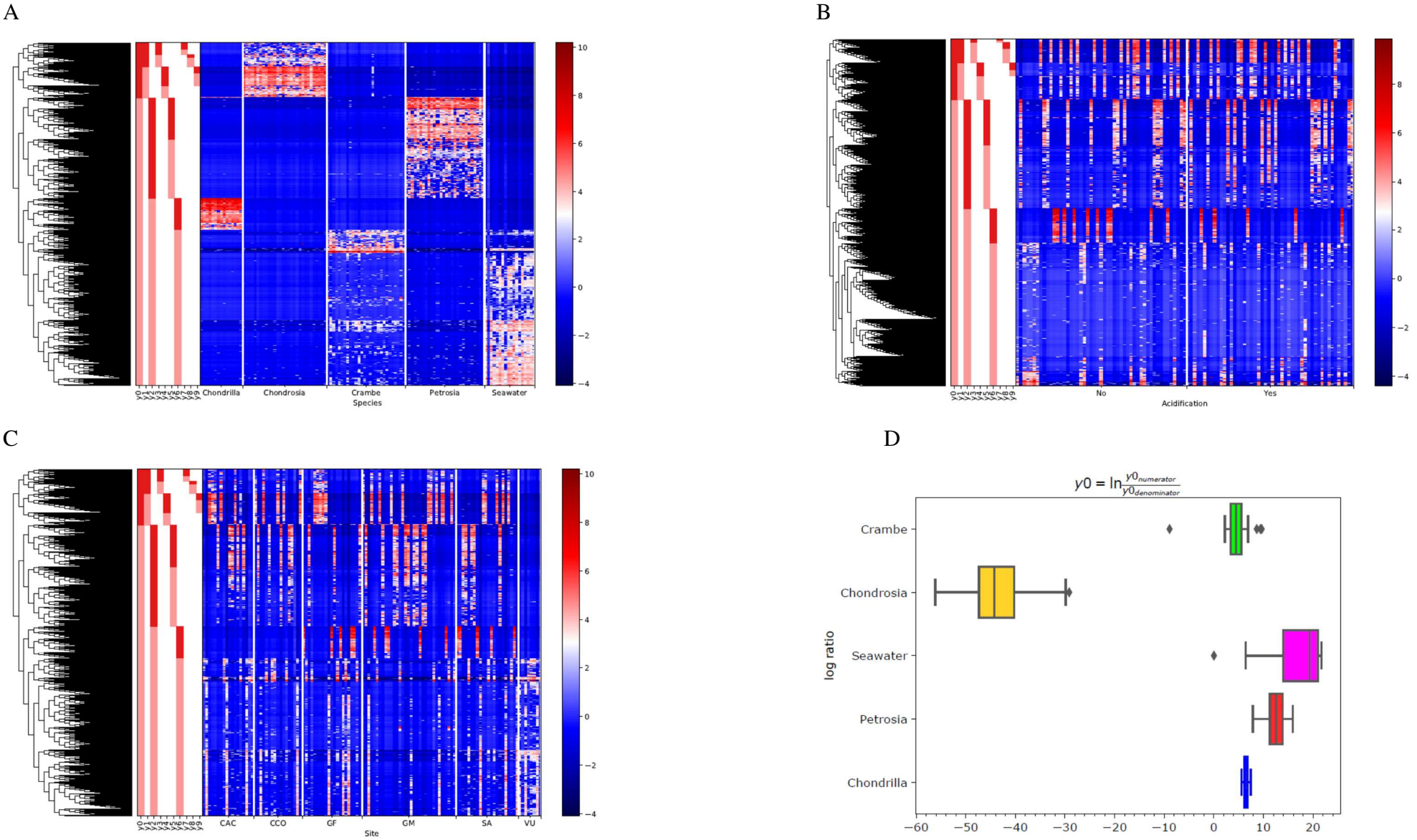

Figure 18 – Output heatmaps created by the linear regression model of gneiss. On the left of each heatmaps lies the hierarchical tree created by clustering the ASVs by co-occurrence, according to Ward's algorithm. Red bars indicate the balances created to compute the linear model; in particular dark red bars indicate the ASVs in the denominator, and light red bars indicate the ASVs in the numerator of each balance. The first balance "y0" was the one comprising a majority of ASVs, that could explain the difference in microbe composition, and was the balance used as baseline to interpret the outputs of the model. In this study, the co-variate Sponge species contributed most for the variation ($R^2 = 0.5853$) in microbial community composition. Heatmaps with the hierarchical clustering from Gneiss plotted by A) sponge species, B) sampling site and C) acidification status. D) Box plot of the log ratios of the microbes included in the balance "y0" visualized by sponge species.

4.5.4 Putative functions of the prokaryotic assemblages

The ASV table of the full dataset was converted into a putative functions table via cross-annotation against the Faprotax database. PCA ordination revealed three main clusters: one composed by specimens of *C. crambe,* one by *C. nucula* and another one by *C. reniformis* and *P. ficiformis* (Fig. 19). Overall differences in the putative functions pattern between the mentioned clusters were statistically significant according to PERMANOVA (9999 permutations; p-value < 0.05; Table S4).

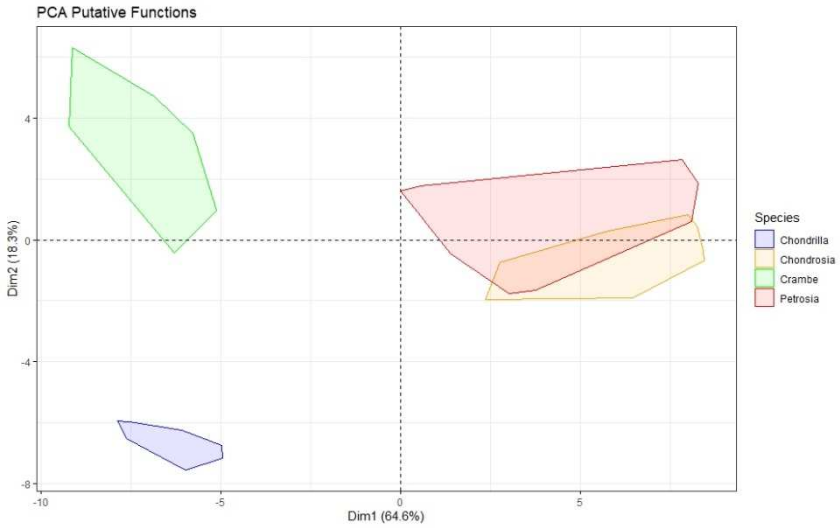

Figure 19 – PCA ordination showing different putative functions of the microbiomes associated with each sponge species.

The cluster composed by the sponges *P. ficiformis* and *C. reniformis* (Fig. 20) was dominated by functions related to chemo-heterotrophy and aerobic chemo-heterotrophy, accounting for 56 and 51% respectively. These functions only represented ~ 10% in the other two species. The other two clusters corresponding to *C. crambe* and *C. nucula* were mostly dominated by functions related to phototrophy, photo-autotrophy and cyanobacteria-related functions (accounting for > 75%). Other putative functions included nitrification, aerobic nitrite oxidation, fermentation and aerobic ammonia oxidation were more abundant in *P. ficiformis* and *C. reniformis*, accounting for 30 and 28% respectively, and < 10% in *C. nucula*.

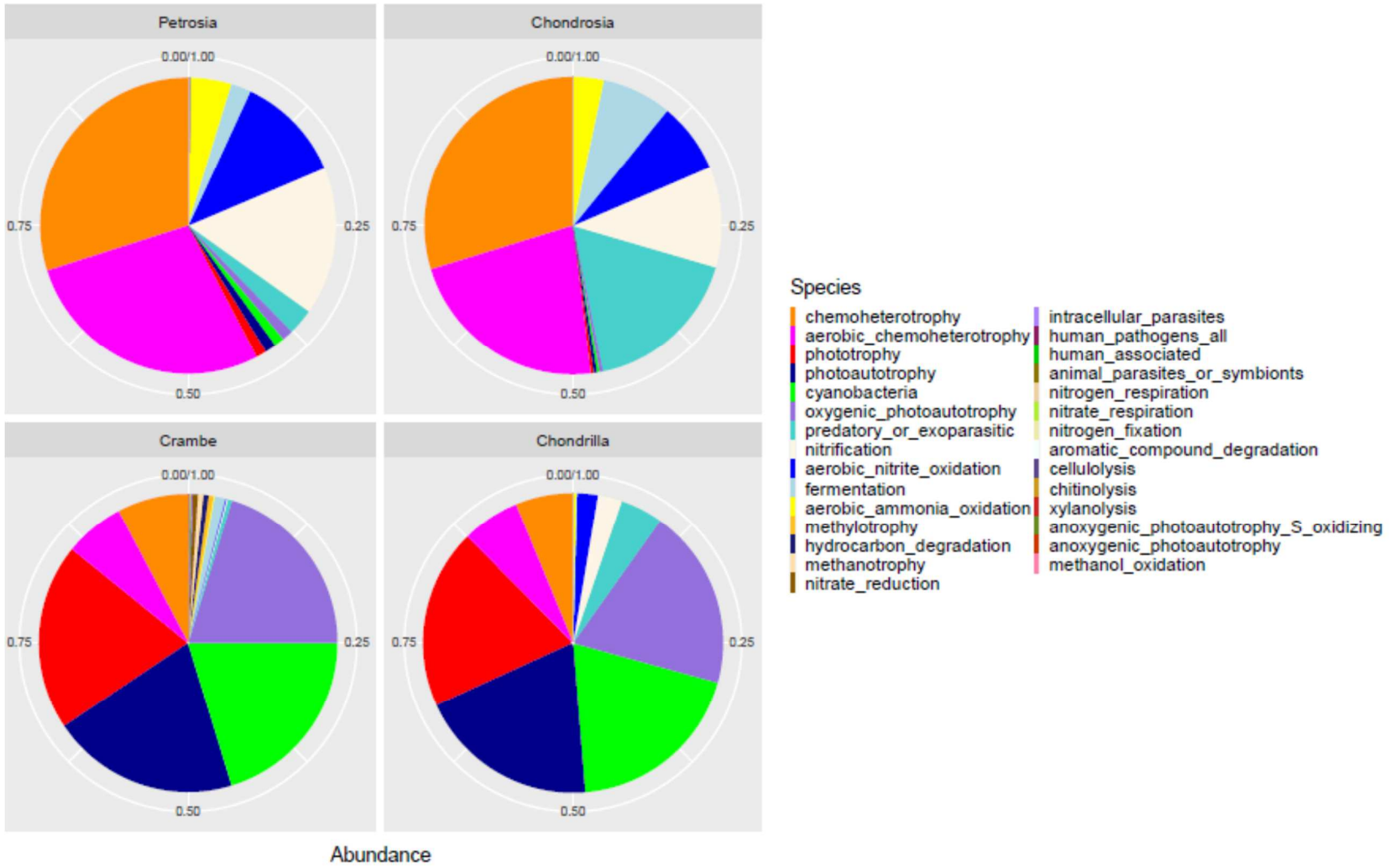

Figure 20 – Putative functions of the microbiome associated to our four sponge species. *Petrosia ficiformis* and *Chondrosia reniformis* were dominated by functions mostly related with heterotrophic metabolism, while *Crambe crambe* and *Chondrilla nucula* were mostly associated with autotrophic metabolism.

4.6 Diversity of fungal assemblages associated to sponges

4.6.1 α and β diversity analysis

The data of the mycobiomes associated with the four sponge species were not rarefied due to unequal sample size, resulting after sequence processing and filtering, and hence the analyses were performed on the unrarefied raw table. Observed fungal ASVs ranged from 5 (lowest value detected in *P. ficiformis)* to 120 (highest value recorded in the *C. nucula*), with a very variable number of AVSs per sample (Fig. 21). Similar results were obtained by considering the Shannon index. No significant differences either in the observed ASVs or in the Shannon index were found between the four sponge species and the seawater at every level of comparison (Kruskal-Wallis Test; p-value > 0.05; Table S3). Beta-Diversity comparisons based on Bray-Curtis and Jaccard dissimilarity indexes showed similar outcomes as those observed in the alpha-diversity analyses (Fig. 21). This analysis revealed a scattered sample distribution and the lack of a clear clustering among the mycobiomes of the different sponge species. No significant differences were found either in the Jaccard or in the Bray-Curtis dissimilarities comparisons (PERMANOVA 9999 permutations, p-value > 0.05; Table S3).

A

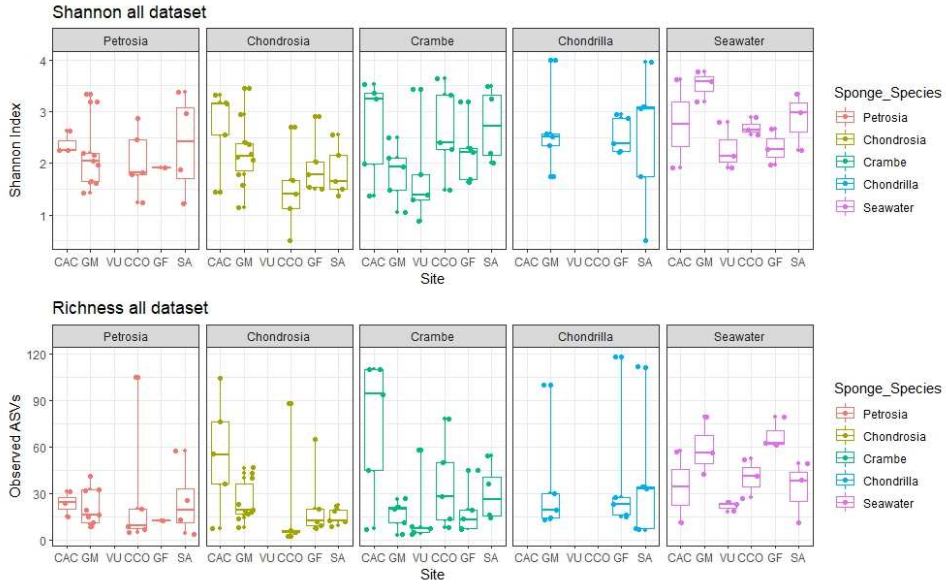

B

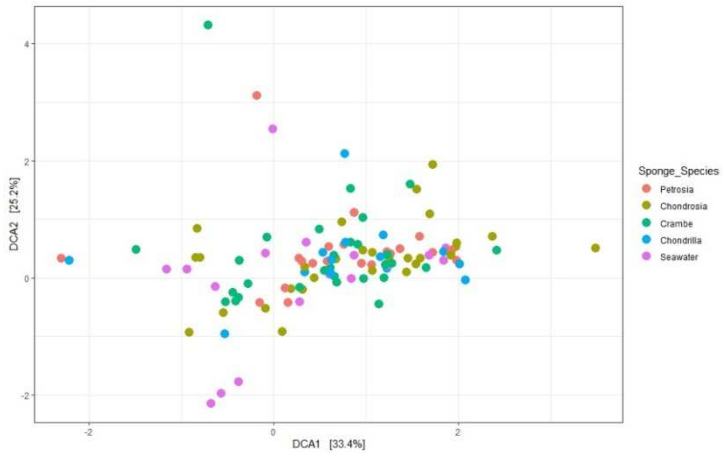

C

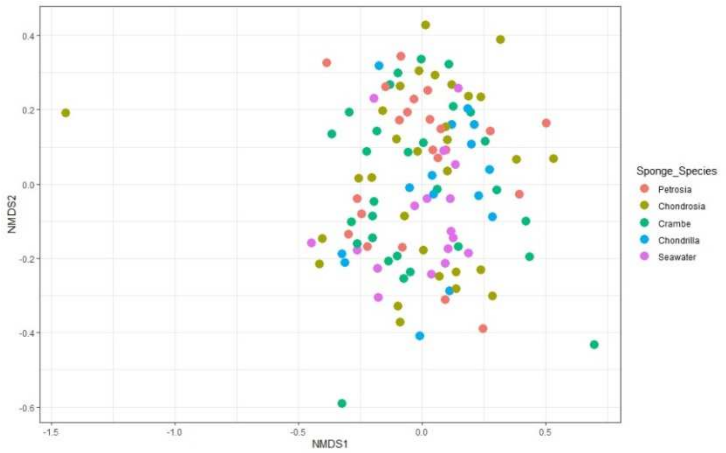

Figure 21 – Alpha and beta diversity plots of the mycobiome associated with the four sponge species. A) Shannon Index- Observed ASVs; B) DCA based on Jaccard distance; C) NMDS based on the Bray Curtis distance.

4.6.2 Mycobiome composition

A total number of 104.320 reads were obtained, ranging from 4 to 7581 read per sample and clustering in a total of 1182 fungal AVSs. Fungal ASVs taxonomical annotations allowed to identify 7 Phyla, 29 Classes, 83 Orders 173 families and 314 Genera. *Capnodiales*, *Pleosporales*, *Malasseziales*, *Hypocreales* and *Saccharomycetales* were the most abundant fungal Orders whose relative contribution varied widely among the sponge species investigated (Fig. 22). The most abundant fungal Genera within the entire dataset were *Aspergillus, Cladosporium, Malassezia,* and *Toxicladosporium.* No totally shared ASVs were found either considering the overall dataset, or sub-setting the dataset by sponge species. One specific fungal ASV assigned to the species *Malassezia restricta* was only found in the sponge *C. nucula*.

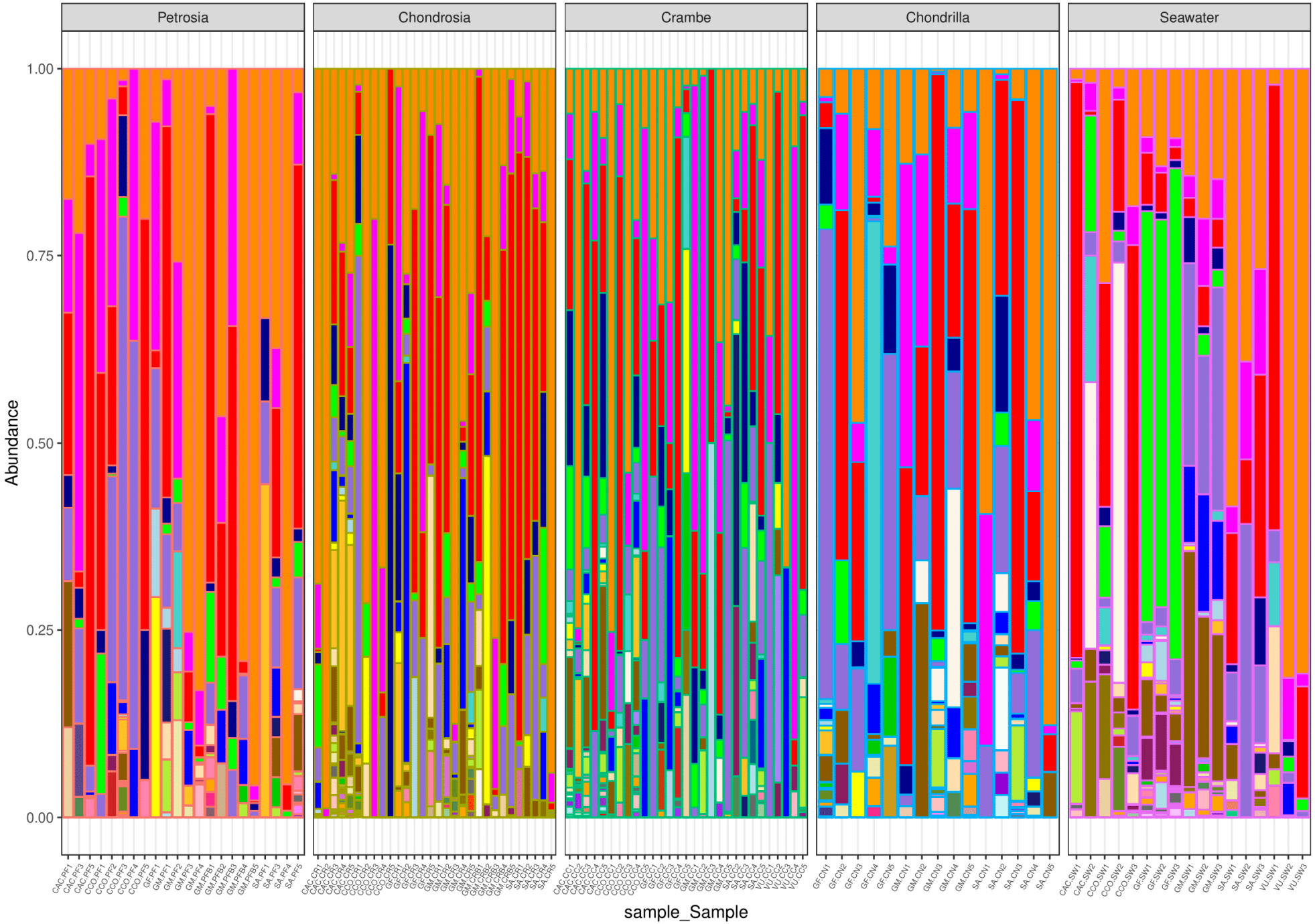
Petrosia
Chondrosia
Crambe
Chondrilla
Seawater
Abundance
1.00
0.75
0.50
0.25
0.00
sample_Sample

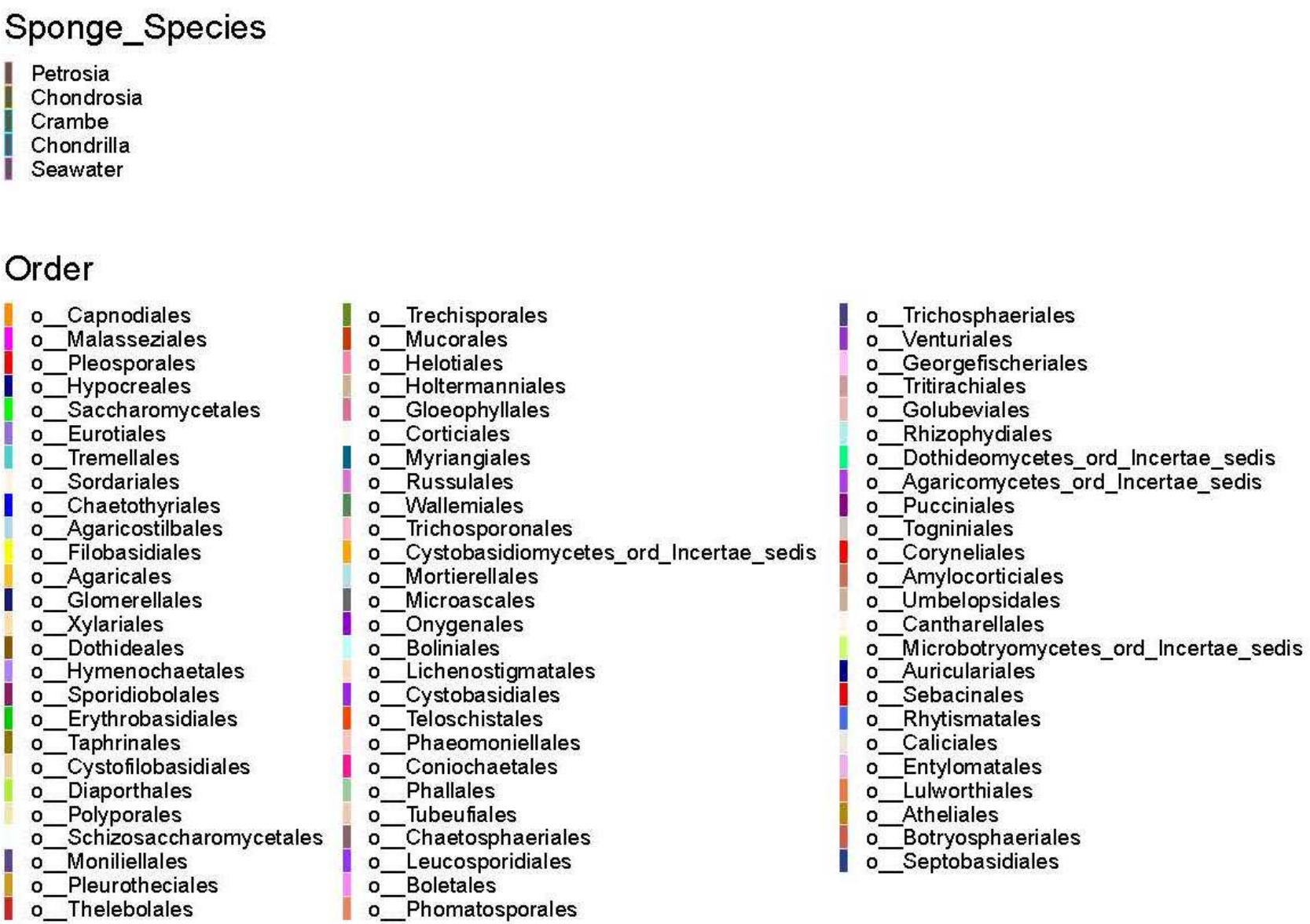

Figure 22 – Taxonomic composition of the mycobiome associated with the four marine sponge.

Totally shared fungal ASVs were also not observed between the four sponge species and the seawater and within samples from the same sponge species. Indeed, the majority of ASVs were exclusive as illustrated by the network analysis (Fig. 23).

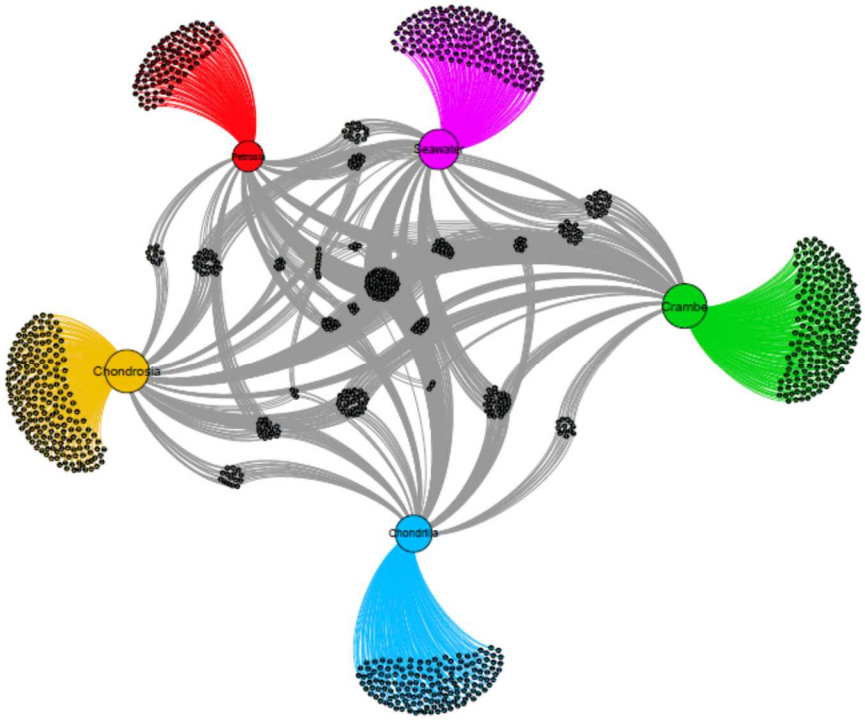

Figure 23 – Network showing the interactions of fungal ASVs between the four sponge species and the seawater. High interspecific variability is explained by the high number of exclusive ASVs associated with every sponge species.

P. ficiformis showed the lowest number of exclusive fungal ASVs (94), while *C. crambe, C. reniformis* and *C. nucula* showed 198, 197 and 152 exclusive ASVs respectively (Fig. 24). Without considering the replicates, 80 ASVs were shared between the four sponge species and the seawater.

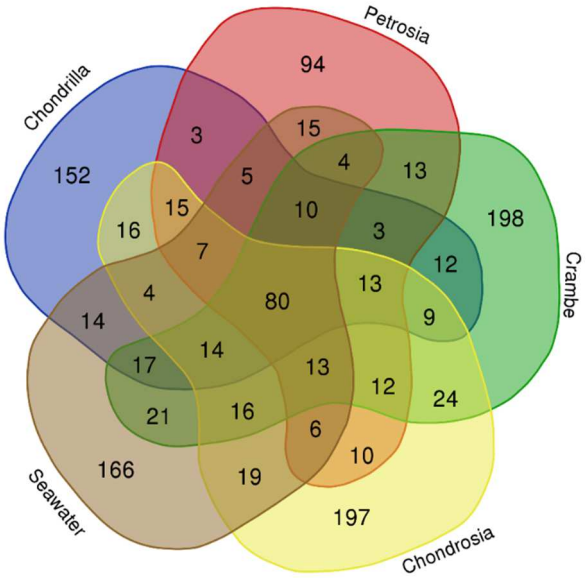

Figure 24 - Venn diagram showing exact numbers of shared and exclusive fungal ASVs between the four sponge species and the surrounding seawater

SIMPER analysis revealed a very high dissimilarity of the fungal assemblage composition among the different sponge species and between sponges and surrounding seawater (Table 3). SIMPER analysis highlighted also a very low similarity of the fungal assemblage composition among different replicate samples of the same sponge species. Indeed, the similarity within each sponge species was 4.7%, 4.5%, 5.3% and 5.4% for *P. ficiformis, C. reniformis, C. crambe and C. nucula*, respectively.

Table 3 – Report of SIMPER analysis showing the dissimilarity of the fungal assemblage composition for every couple of sponge-sponge and sponge-seawater comparison.

Comparison		Dissimilarity %
Crambe	**Chondrosia**	94.14
Crambe	**Petrosia**	94.85
Chondrosia	**Petrosia**	94.97
Crambe	**Seawater**	94.96
Chondrosia	**Seawater**	94.92
Petrosia	**Seawater**	94.94
Crambe	**Chondrilla**	94.33
Chondrosia	**Chondrilla**	95.07
Petrosia	**Chondrilla**	94.58
Seawater	**Chondrilla**	94.43

4.6.3 Gneiss model output

As for the microbiomes, a Gneiss linear regression model has also been performed on the entire fungal dataset (115 samples) to detect which factor was more associated with differences in fungal community composition. The model predicted less than 10% of the total variation in the fungal community among sample groups ($R^2 = 0.0979$) (Table S6). The clustered ASVs, included in the principal balance "y0", were used to plot their log transformed abundance, across the factors site and acidification (Fig. 25). Log ratios of the relative abundance of the fungal ASVs clustered in the balance "y0" revealed no differences in the mycobiome associated across the four sponge species (Fig. 25), either by sponge species or by sampling sites. This model corroborated the outcome of the alpha and beta diversity analysis. The model MSE was always higher compared to the predicted MSE, highlighting that the model was not over fitted.
Considering the low variance explained by the Gneiss model and the high inter and intraspecific variability of the mycobiomes associated with the sponge species investigated, we decided to do not perform further investigations on the associated fungal communities.

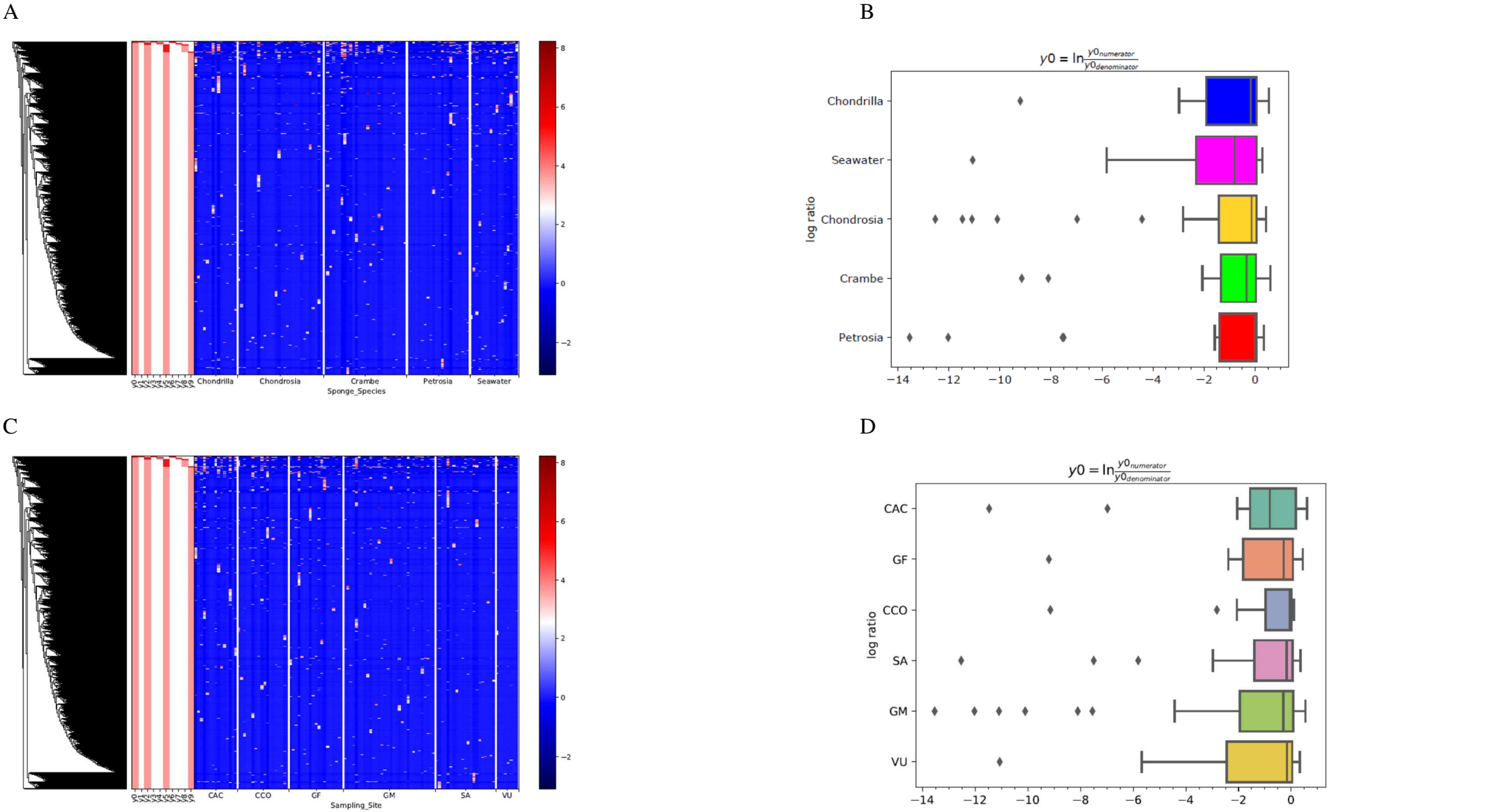

Figure 25 – Output heatmaps created by the linear regression model of gneiss. On the left of each heatmaps lies the hierarchical tree created clustering the ASVs by co-occurrence, according to Ward's algorithm. Red bars indicate the balances created to compute the linear model; dark red bars indicate the ASVs in the denominator, and light red bars indicate the ASVs in the numerator of each balance. The first balance "y0" was the one comprising a majority of ASVs, that could explain the difference in fungal composition, and was the balance used as baseline to interpret the outputs of the model. In this study, a low portion of variance was delimited by the gneiss model ($R^2 = 0.0979$). No particular differences were found in the mycobial community associated with our four sponge species either considering sponge species or sampling sites. Heatmaps explaining the differences by A) sponge species and B) sampling site. Log ratios of the fungal ASVs included in the balance "y0" plotted by C) sponge species and D) sampling site.

4.7 Comparison of bacterial and archaeal diversity associated to the same sponge species collected at different sites

The analysis on the interspecific comparison among the four sponge species reveled strong differences both in the alpha and beta diversity of the associated microbial communities. As Gneiss model's outcome revealed that the factor sponge species was responsible of more than 70% of the variation in the associated microbial communities hiding other possible driving factors, further analyses were performed by comparing the microbiomes of the same sponge species collected at different sites and in different acidification conditions. Such analysis has been also done to investigate the potential differential responses of the different sponge holobionts to OA.

4.7.1 *Petrosia ficiformis*

Petrosia ficiformis was collected in two acidified sites and three control sites, by selecting when possible, five individuals per site. In the GF site, three specimens were collected, while in the GM site two color morphotypes were sampled (n=5), dark purple with normal shape and bleached with a reticular shape.

4.7.2 α and β diversity analyses

Sequence data was rarefied to 6.528 (Fig. S4) reads per sample resulting in a total of 182.784 reads distributed in 28 samples and 511 features (Table S1). In *P. ficiformis* (Fig. 26) the observed ASVs ranged from a minimum of 128 to a maximum of 222 ASVs per sample, with the lowest and the highest values, observed in the two acidified sites CAC and GM respectively. The three control sites CCO, GF and SA had similar values between those records. The analysis of Shannon indexes provided similar results: GM exhibited the highest alpha diversity values, CAC the lowest and control sites were similar to each other, but diverse from the two acidified sites (Kruskal-Wallis, p-value $<$ 0.05; Fig. 26; Table S7). Differences in bacterial alpha diversity across sites and acidification conditions were only observed in *P. ficiformis* (Table S7). Beta diversity comparison based on Bray-Curtis and Jaccard dissimilarity indexes showed similar outcomes as those observed in alpha diversity. Sponges collected from

the two acidified sites were significantly different from each other, and also diverse from specimens living in the control sites (PERMANOVA 9999 permutations, F = 2.9861 p-value < 0.05; Table S7), which were similar to each other in terms of relative abundance and presence/absence. This clustering pattern highlighted the relevance of non-shared bacterial features rather than abundance in discriminating sponge groups by sites and acidification conditions. The two *P. ficiformis* morphotypes, coloured (GM) and bleached (GMW), collected at the site GM were characterized by similar values of alpha and beta prokaryotic diversity and no statistical differences according to the Wilcoxon rank sum test (p-value > 0.05) and PERMANOVA (9999 permutations; p-value > 0.05) were found (Table S7).

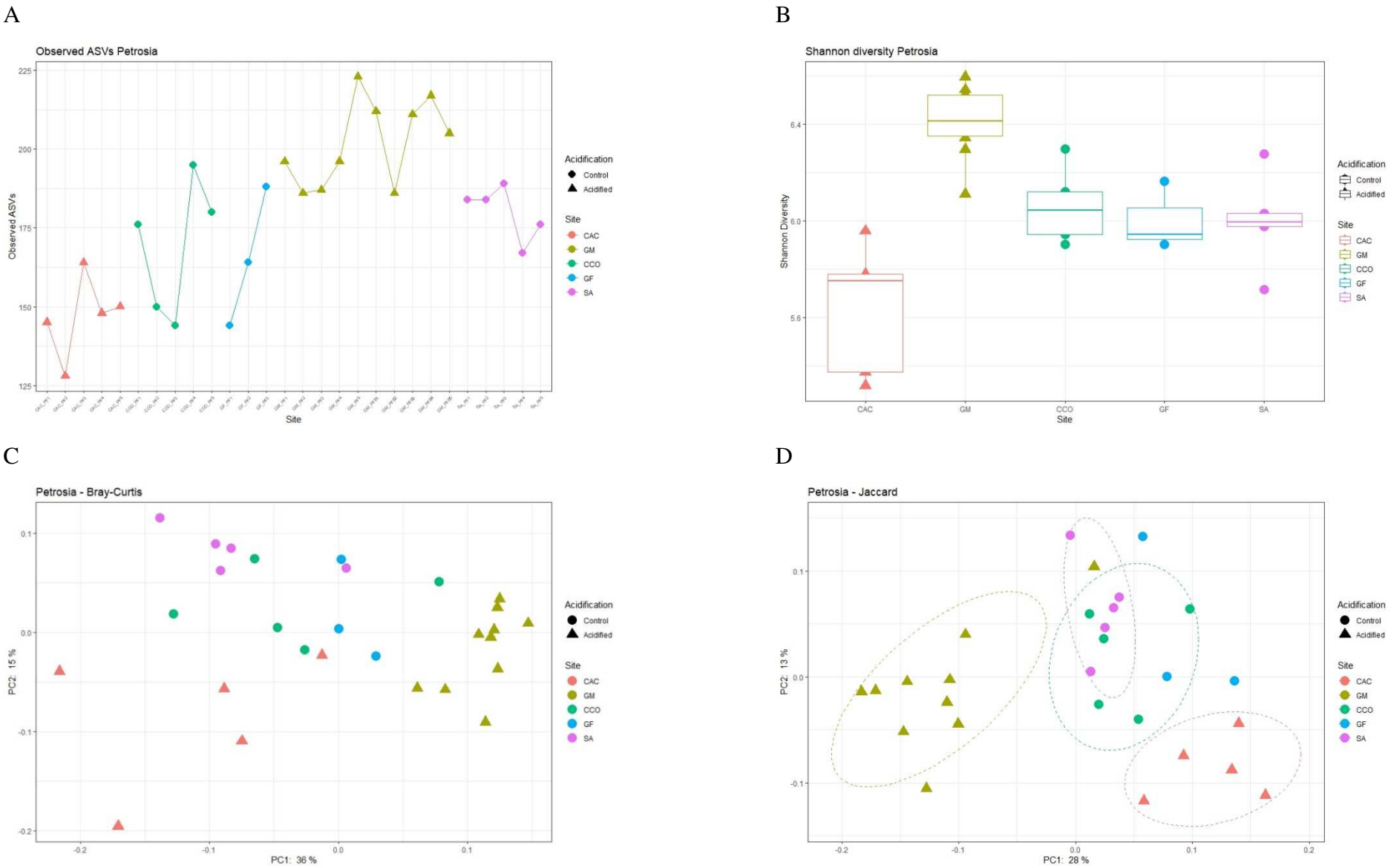

Figure 26 - Alpha and Beta diversity metrics of the bacterial communities associated to sponges belonging to the species *Petrosia ficiformis*: A) Observed ASVs, B) Shannon based box plot; PCoA beta diversity ordinations based on C) Bray-Curtis and D) Jaccard dissimilarity matrices (α-Diversity - Kruskal-Wallis, $p < 0.05$; β-Diversity PERMANOVA, $p < 0.05$, Table S7).

DEICODE RPCA analysis highlighted a difference in beta diversity between the sampling sites, which was statistically significant (PERMANOVA 9999 permutations, F = 21.305 p-value < 0.05). Three main clusters were produced by the DEICODE RPCA ordination. One composed by samples of the two morphotypes (coloured and bleached) clustering together, belonging to the acidified site GM on the right side of the ordination plot. Another cluster was composed by the acidified samples of the site CAC, while the third cluster was composed by the samples belonging to the three control sites CCO, GF and SA. The bacterial taxa that were the most significant drivers of distance in ordination space were identified (Fig. 27).

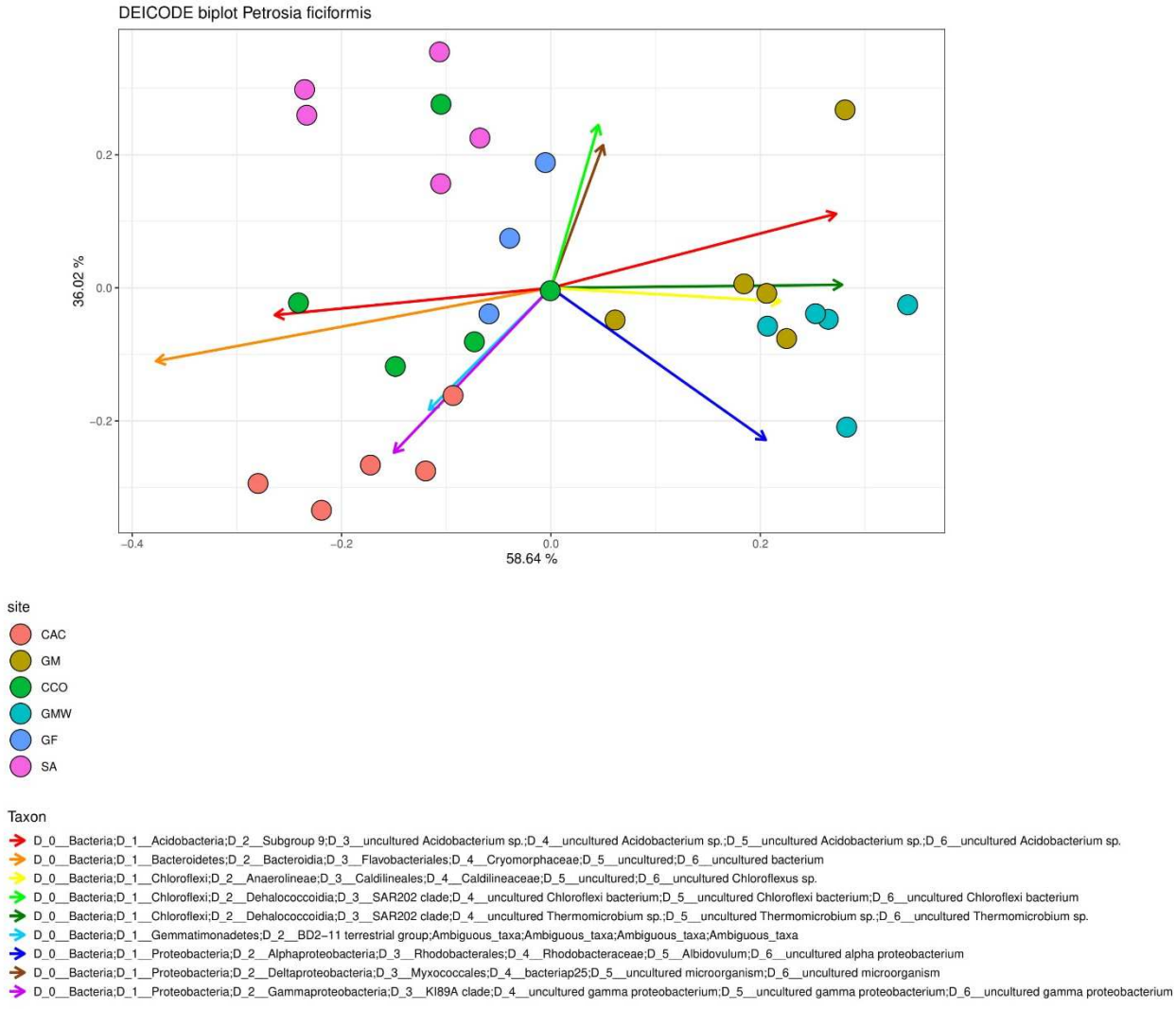

Figure 27 - Compositional biplot of beta diversity of bacterial communities associated to *Petrosia ficiformis* based on Aitchison distances. Sampling sites are depicted by colors and points represent individuals. Ten most relevant taxa driving differences in the ordination space are illustrated by the vectors labeled with the respective taxonomy.

Log ratio from DEICODE feature-loadings that best explained the separation of sample groups was composed by a consortium of two ASVs in the numerator belonging to the families *Cryomorphaceae* and *Caldilineaceae*, and one in the denominator belonging to genus *Albidovulum*. The acidified site GM yielded the highest log ratio, higher compared to the other acidified site CAC. Among the controls, CCO yielded the highest log ratio, close to the values recorded by CAC and different compared with the other two control sites SA and GF, which yielded the lowest log ratio (Fig. 28). The difference in the log ratios was not significant by sampling sites nor by acidification status according to the Welch's Test (p-value > 0.05).

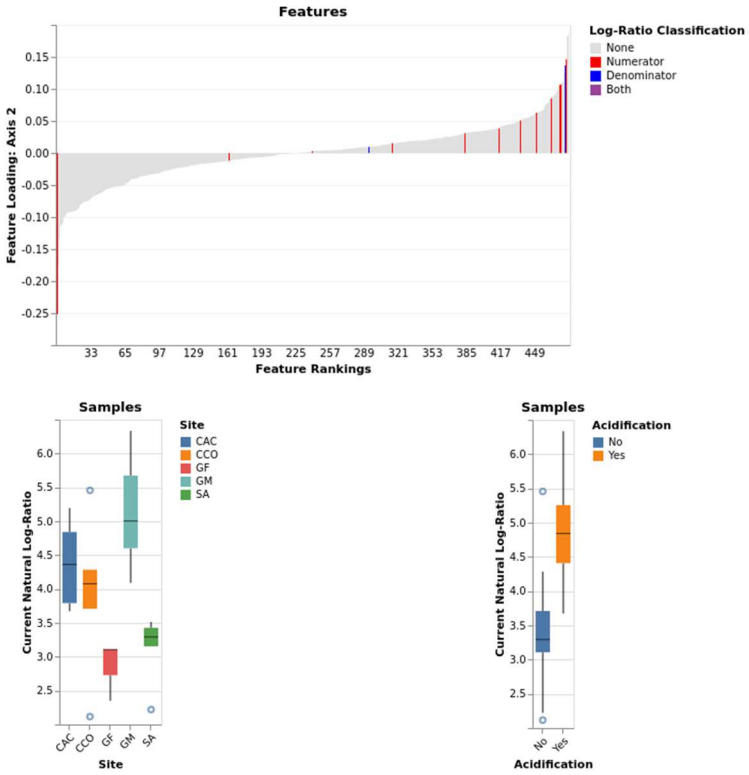

Figure 28 – The upper plot shows feature rankings, with the features selected to perform group separations by site and acidification status in the sponge *Petrosia ficiformis*. The lower left and lower right bar plots show the log ratio of the selected features by sampling sites and acidification status.

4.7.3 Microbiome composition of *Petrosia ficiformis* at control and acidified sites

A total number of 77 bacterial and one archaeal orders were identified within the microbiome of *P. ficiformis* sponge (Fig. 29). *Caldilineales*, SAR202 clade and Class BD2-11 were the three most relevant orders, whose presence ranged respectively between 16-21%, 12-25%, and 3-10% throughout the different sampling sites. *Flavobacteriales*, *Microtrichales*, Subgroup 6, TK17, *Rhodothermales*, *Dadabacteriales*, *Pedospheaerales* and *Thermoanaerobaculales* all together accounted for 31% of the bacterial community. Several orders were found to be exclusive from the acidified CAC and GM sites. *Phormidesmiales* and *Rhizobiales* were only found in CAC; whereas WGA-4E, WGA-A3, WGA-4C, *Planctomycetales*, *Poribacteria* 64K2, *Verrucomicrobiales*, *Sphingobacteriales* and S*phingomonadales* were only detected in GM, which was the site characterized by the highest number of exclusive ASVs. *Chitinophagales* was instead exclusive of the control sites CCO, GF, SA.

Coloured and bleached *P. ficiformis* specimens (Coloured: GM-PF1-GM-PF5; Bleached GMW-PF1-GMW-PF5) displayed similar associated microbial communities.

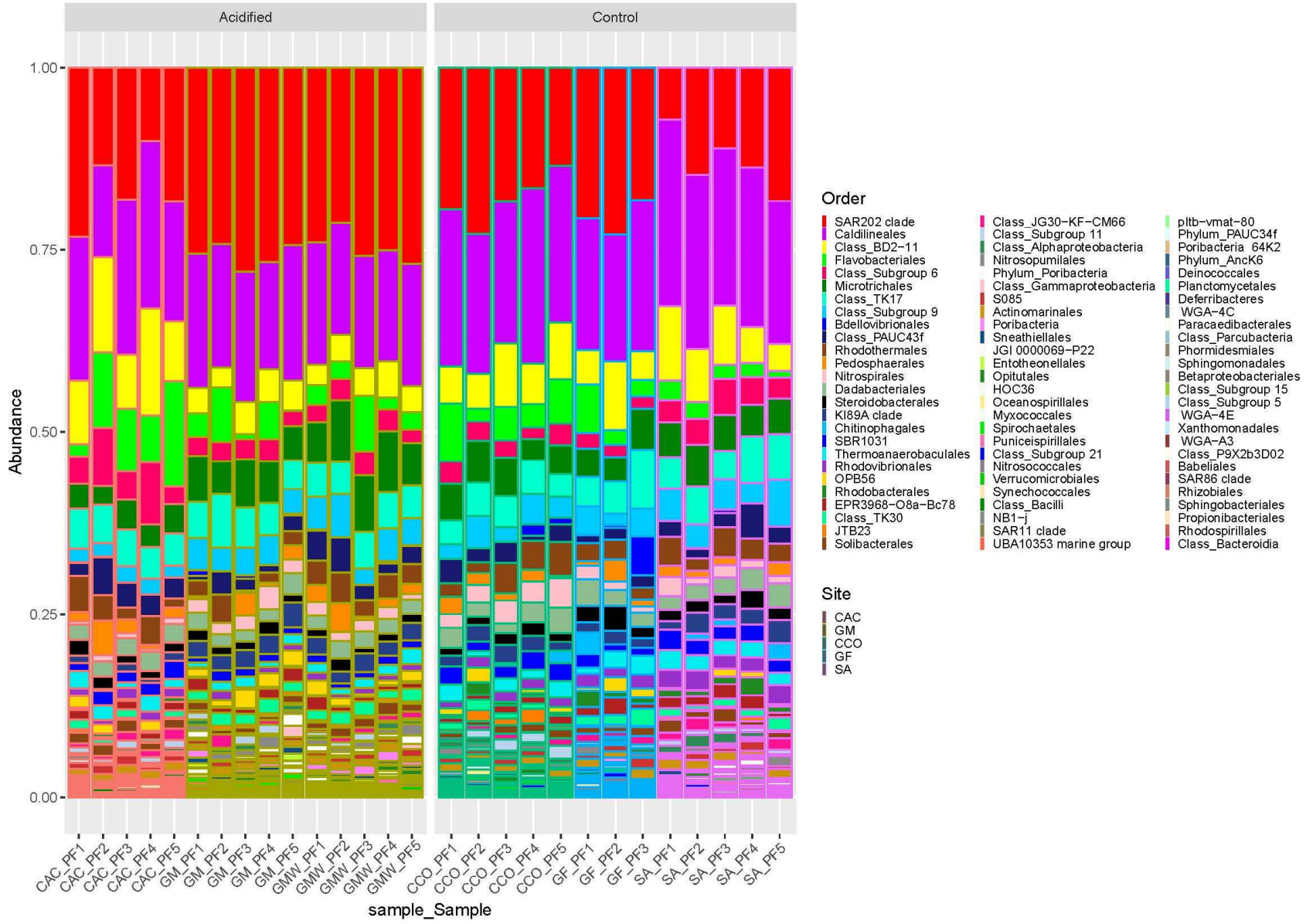

Figure 29 - Taxonomic composition of the microbiome associated with the sponge *Petrosia ficiformis* collapsed at the best annotated taxonomic rank: Order. Bars are visualized by individuals and grouped according to acidification conditions at the sites as acidified and control.

Core microbiomes (considered as those features shared 100% within a sample group, *i.e.* site and acidification condition) associated with *P. ficiformis* for every sampling site are reported in Figure 30. Regarding the acidified sites, SAR202 clade, *Flavobacteriales* and *Caldilineales* were found to be the most abundant bacterial core orders in CAC, accounting respectively for the 19, 11 and 10%. The three principal orders in sponges collected from the other acidified site GM were SAR202 clade, *Flavobacteriales* and *Caldilineales*, representing the 20, 5 and 25% respectively. *Poribacteria*, *Puniceispirillales*, and *Spirochaetales* were found in GM (accounting together 3%) but not in CAC. Instead PAUC34f, *Pedosphaerales*, SBR1031, *Rhodobacterales*, *Synechococcales*, *Opitutulales*, Subgroup 21, JTB23, OPB56, UBA10353 were only found in CAC acidified site with a total contribution of 8%. PAUC43f and JGI 0000069 -P22 were present in both acidified sites, but were core taxa only in CAC. In the three control sites CCO, GF and SA, core microbiomes showed higher similarities. The two most represented taxa SAR202 clade and *Caldilineales* accounted respectively for 34, 39, and 40%. *Flavobacteriales* were not represented as a core order in SA, while *Pedosphaerales* is only core in CCO. *Synechococcales*, AncK6, *Betaproteobacteriales*, JTB23, *Nitrosococcales* were only core microbiome in GF, while *Opitulales* were core only in SA. *Myxococcales* and *Spirochaetales* were not found in GF, yet were represented in sites CCO and SA.

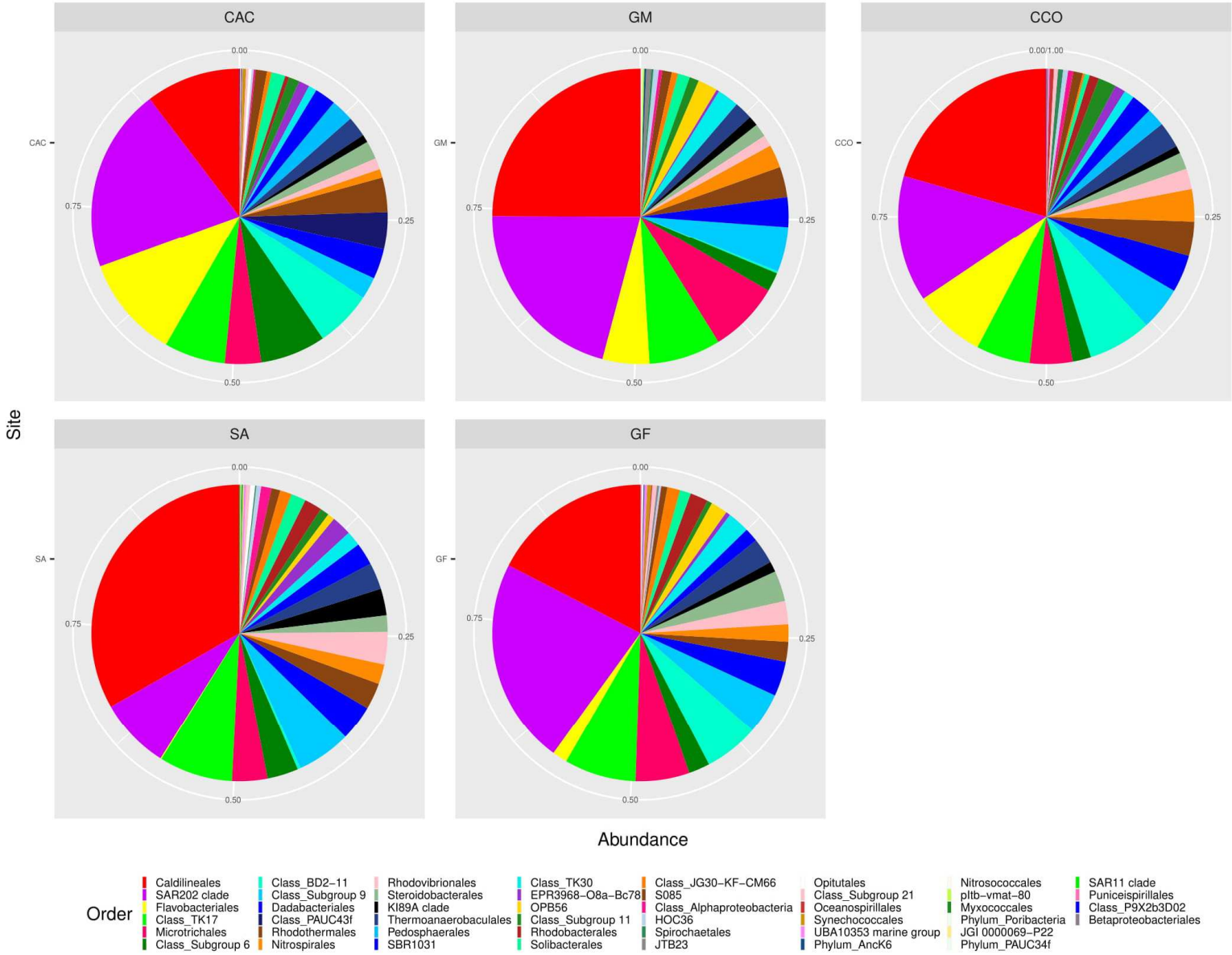

Figure 30 - Core microbiomes of *Petrosia ficiformis* calculated for every sampling site. CAC and GM are the acidified sampling sites, while CCO, SA, and GF the controls.

The core microbiome associated with sponges coming from acidified sites *versus* control sites showed that "control microbiomes" in *P. ficiformis* were dominated by 35 ASVs that belonged to 23 different bacterial orders (Fig. S6). Six bacterial orders were exclusive of control sites and accounted for 14% of the core microbiome, while the three most abundant orders (*Caldilineales*, SAR202 clade and TK17) accounted for 50% of the control's core microbiome. These taxa represent ~ 21% of the total bacterial community associated with *P. ficiformis*.

The core microbiome of the acidified sampling sites was represented by 39 ASVs affiliated to 21 bacterial orders (Fig. S5) of which four, were exclusive of this core community and accounted for 12%. SAR202 clade, *Caldilineales*, TK17 and *Microtrichales* accounted for > 50%. The acidified core community accounted for ~ 25% of the total microbial community associated with *P. ficiformis*.

To better appreciate the changes of the microbiome composition at the different sampling sites, the contribution of exclusive ASVs was visualized with a network analysis conducted at the ASV level (Fig. 31). The two acidified sites GM and CAC had a different number of exclusive ASVs (48 in GM and 19 in CAC), while a few ASVs were shared between the specimens of these two sites. This could further explain the differences observed in alpha and beta diversity. In the control sites, a lower number of exclusive ASVs and a higher number of ASVs shared between the sites were found.

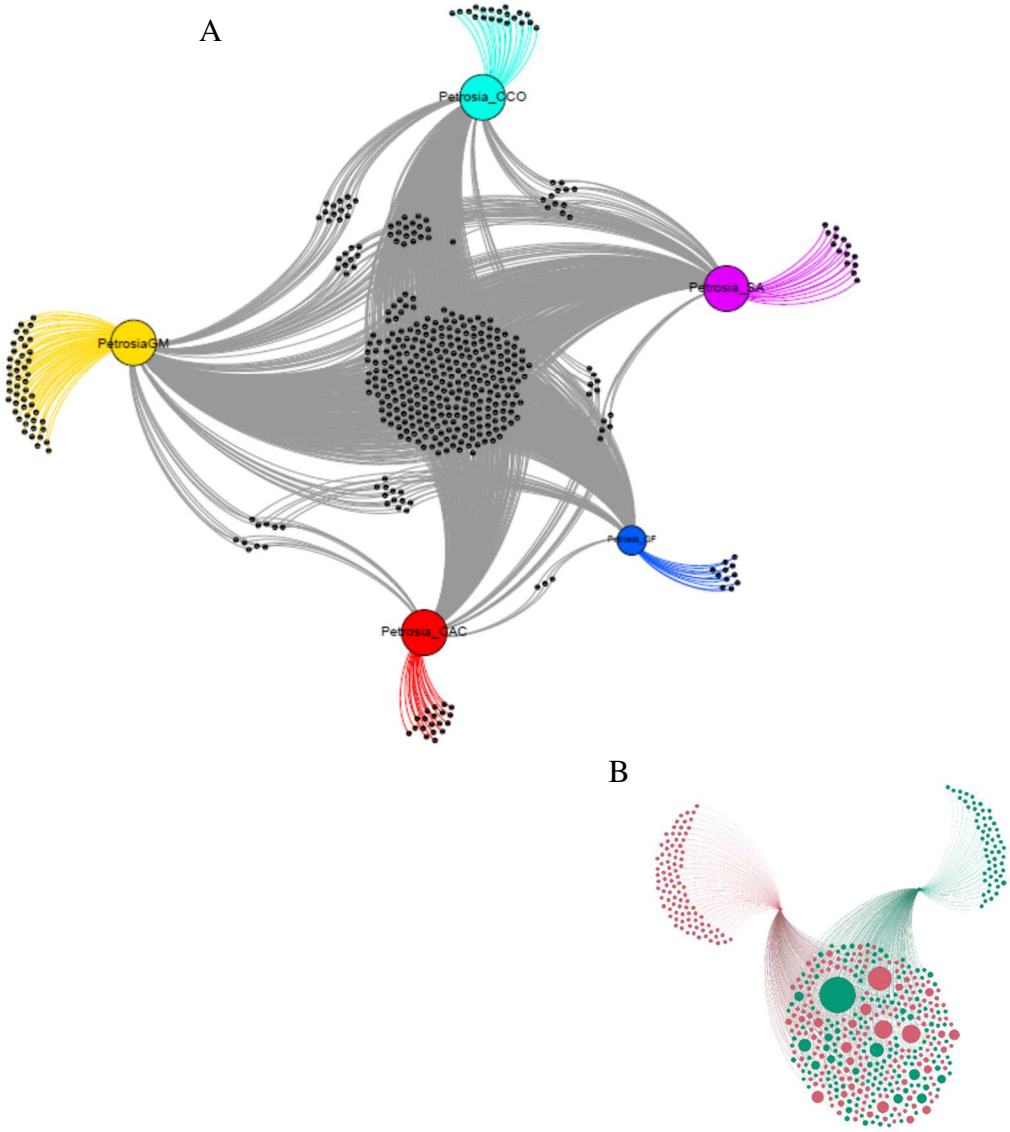

Figure 31 - A) Network based on the ASV table of the sponge species *Petrosia ficiformis* showing the relationships between the different sampling sites. B) Network grouped by Acidified and Control sites together to show the higher contribution of the exclusive ASVs in the acidified samples (red acidified – green controls).

SIMPER analysis highlighted that the similarity of the microbiome composition was ca. 50% both comparing controls vs. acidified sites and sites characterized by similar pH conditions (Table 4). Such similarity values were close to those observed among microbiomes of replicated sponge samples collected at the same site: 61.06% in CAC, 56% in CCO, 51% in GF, 60.55% in GM, 57.68% in SA.

Table 4 – Summary of the results of the SIMPER analysis performed comparing sampling sites, carried out on the ASV table of the microbiome associated with the sponge *Petrosia ficiformis*.

Comparison between different sampling sites		**Dissimilarity %**
Petrosia_CAC	**Petrosia_CCO**	47.82
Petrosia_CAC	**Petrosia_GF**	51.18
Petrosia_CCO	**Petrosia_GF**	47.74
Petrosia_CAC	**Petrosia_GM**	51.10
Petrosia_CCO	**Petrosia_GM**	46.98
Petrosia_GF	**Petrosia_GM**	49.18
Petrosia_CAC	**Petrosia_SA**	52.21
Petrosia_CCO	**Petrosia_SA**	46.78
Petrosia_GF	**Petrosia_SA**	48.04
Petrosia_GM	**Petrosia_SA**	48.74

4.7.4 Differential abundance

Differential abundance analyses were performed applying approaches that account for compositionality of data, and based on log-fold changes of feature's abundances. We used two different methods: Gneiss and Songbird (Morton et al. 2017, 2019).

Gneiss model output

To disentangle how the sampling sites were associated with a shift in microbial community composition we performed a multivariate linear regression model.

A total of 28 samples were introduced to build the linear model for the batch corresponding to *P. ficiformis*. The model explained 28% ($R^2 = 0.2828$) of the bacterial community variation among sample groups (factor included in the formula: sampling site). On what concerns the comparisons by sites, log ratios of the samples from GM were lower compared to the rest, indicating that the taxa in the denominator of the "y0" balance were more abundant in this site. Conversely the other acidified site CAC had higher log ratios compared with the other sites, indicating that in this case, the numerator taxa for balance "y0" were more prevalent. Again, the three control sites SA, GF, and CCO displayed similar log ratios among them, but different from the acidified sites (Fig. 32). Even if the analysis was performed at ASV level, differential taxa explaining shifts of microbial community in balance "y0" were annotated to the Order level, which was the highest accuracy for taxonomy assignments (see Fig. 32).

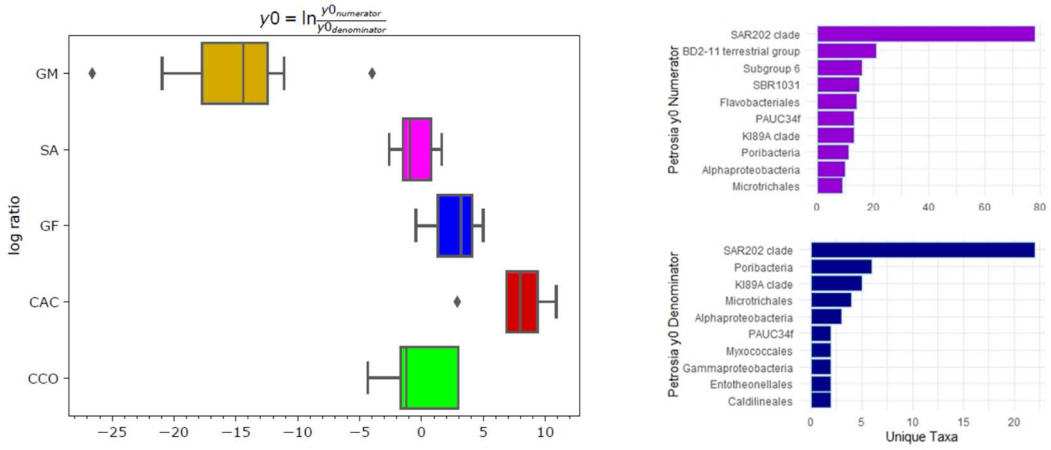

Figure 32 – Boxes of the log ratios in balance "y0" regarding the microbial communities associated with *Petrosia ficiformis* obtained from Gneiss linear model. Bar plots indicate the top 10 taxa of Numerator and Denominator of the "y0" balance, that mostly explain the differences between sampling sites. The two acidified sites CAC and GM reflect different log ratios for this cluster of bacteria between each other, and with respect to the controls SA, GF, and CCO, which show similar log ratio values among them.

A total of 70 ASVs collapsed in 28 Orders were included in the denominator of balance y0, plotted considering the factor "sampling site". The top five abundant were: SAR202 clade (n=22), *Poribacteria* (n=6), KI89A clade (n=5), *Microtrichales* (n=4) and *Alphaproteobacteria* (3). All the other 25 taxa were mostly composed by one ASV. The numerator of the balance was composed of 410 ASVs and the five most abundant orders were SAR202 clade (n=78), BD2-11 (n=21), Subgroup 6 (n=16), SBR1031 (n=15) and *Flavobacteriales* (n=14) accounting for a total of 144 ASVs. This analysis confirmed the outcomes from alpha and beta diversity.

Songbird model output

Songbird identifies the differential ASVs related to a certain covariate of interest, calculated based on rankings of log ratios values. Four ASVs in the numerator and six in the denominator were identified, according to positive coefficients in the numerator, and negative in the denominator, as most defining differential taxa with 83% of the samples retained. Such microbial taxa were found to explain significant differences in microbial composition between sites, with CAC and GM yielding higher log ratios with respect to CCO, SA, GF (Welch's Test, p-value < 0.05; Table S8); and also between acidified *versus* control conditions (Welch's Test, p-value < 0.05; Table S8). GM recorded higher log ratios that CAC, but this difference was not significant according to Welch's Test (p-value > 0.05; Table S8); GM had the highest log ratio, higher than CAC, and SA had the highest log ratio among the controls, but non-significantly different from the other two controls CCO and GF (Welch's Test, p-value > 0.05; Table S8) (Fig. 33).

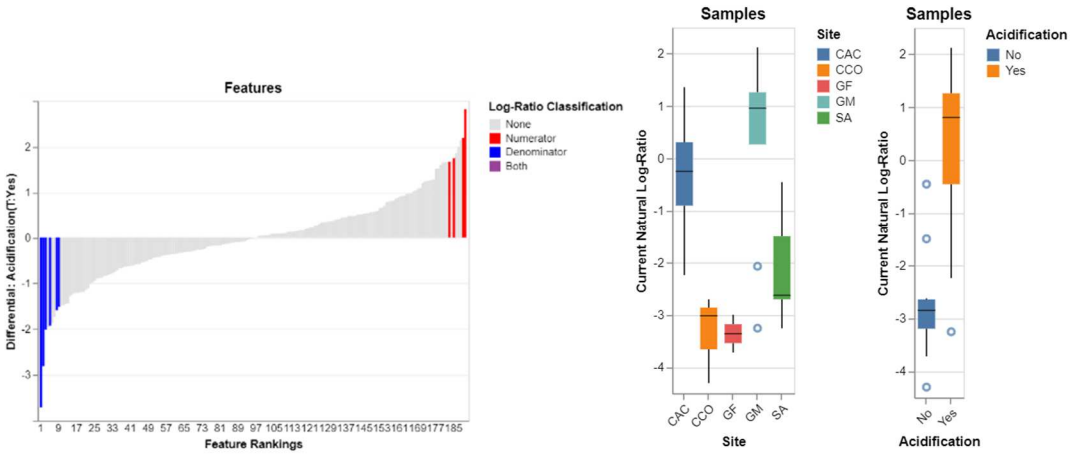

Figure 33 – Differential abundance analysis performed on Songbird for the Sponge *Petrosia ficiformis*. The left plot shows feature rankings with the features selected to perform the grouping separations. On the right, bar plots show the log ratios of the selected features by sampling sites and acidification status.

Differential taxa in the numerator and highly ranked to the acidification condition of sites GM and CAC included: *Thermomicrobium sp*, SAR11 clade, *Nitrosococcaceae* and *Microtrichaceae*. Conversely in the denominator, features negatively associated to acidification status of the sampling sites: KI89A clade, NB1-j, *Rhodothermaceae*, *Chloroflexus sp., Candidatus Nitrosopumilus, Spirochaeta sp.* These strains were positively ranked to the control sites CCO, GF and SA, and therefore to non-acidification status.

4.8 *Chondrosia reniformis*

Chondrosia reniformis was collected in two acidified sites and three controls, selecting five individuals per sampling site that resulted in a total of 30 samples. In the GM site we collected two color morphologies, one dark-greysh-brown and one bleached, both with an apparent normal growth, to perform a comparison.

4.8.1 α and β diversity analyses

Sequence data for *C. reniformis* was rarefied to 7.463 reads per sample resulting in a total of 223.890 reads distributed over 30 samples and 232 features (Fig. S7; Table S1). In *C. reniformis* the observed ASVs ranged from 74 to 123 per sample, with non-significant values across the different sampling sites (Kruskal-Wallis test, p-value > 0.05; Fig. 34; Table S9). The lowest value of the Shannon index was found at the CAC site while the highest at the GM site, but the difference was non-statistically significant.

Beta diversity comparison based on Bray-Curtis and Jaccard dissimilarity indexes showed similar outcomes as those observed on alpha diversity. Sparse distributions in the PCoA ordinations reflected no group clustering in the beta-diversity data. Microbiome composition of sponges coming from the two acidified sites were non-significantly different from specimens living in the control sites (Permanova 9999 permutations, F = 2.9861 p-value > 0.05; Fig. 34; Table S9). Moreover, values of alpha and beta diversity of the microbiome of the two *C. reniformis* morphs (coloured and bleached), collected in the site GM (named GM-CR and GMB-CR) were not significantly different (Wilcoxon rank sum test, p-value > 0.05 and PERMANOVA, 9999 permutations; p-value > 0.05; Table S9).

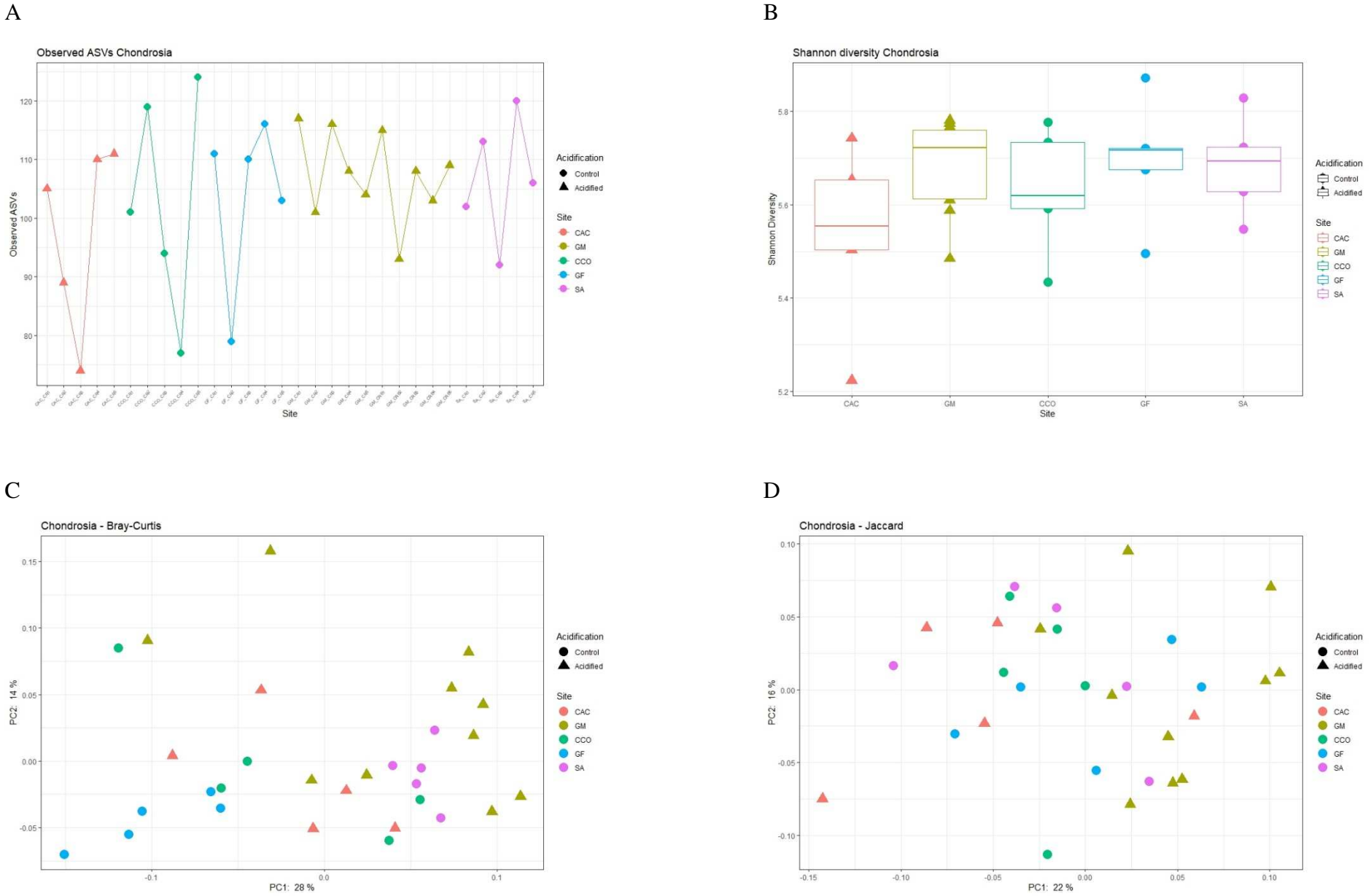

Figure 34 - Alpha and Beta diversity metrics of the bacterial communities associated to sponges belonging to the species *Chondrosia reniformis*: A) Observed ASVs, B) Shannon box plots; PCoA beta diversity ordinations based on C) Bray-Curtis and D) Jaccard dissimilarity matrices (α-Diversity - Kruskal-Wallis, p > 0.05; β-Diversity Permanova, p > 0.05, Table S9).

DEICODE RPCA analysis showed no clear clustering in the ordination space, but an overall difference in beta diversity between the sampling sites, which was statistically significant (Permanova 9999 permutations, F = 5.4677 p-value < 0.05). The ten bacterial taxa that were the most significant drivers of difference among sites were identified and illustrated by the vectors in the plot (Fig. 35).

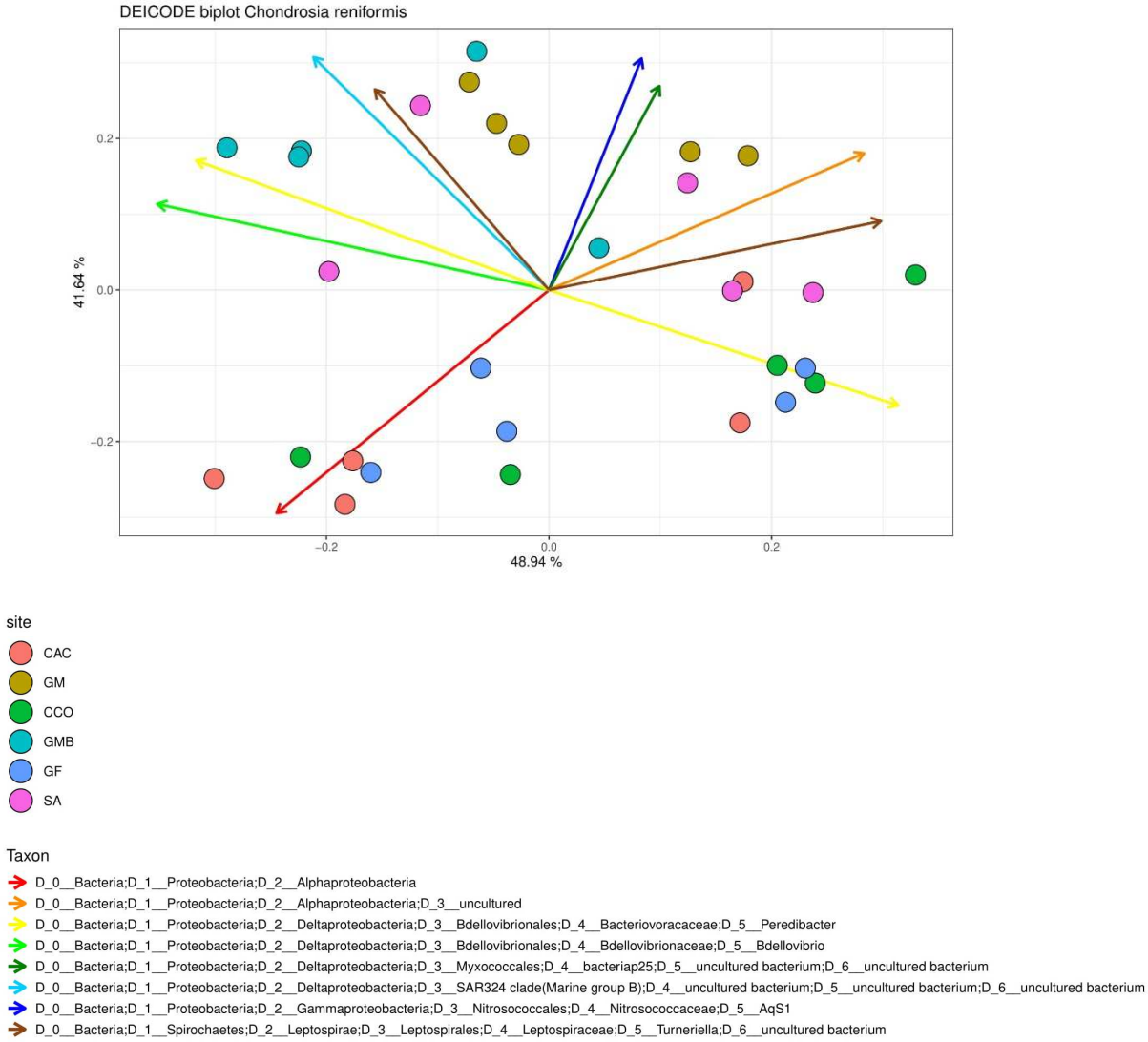

Figure 35 - Compositional DEICODE biplot of beta diversity of bacterial communities associated to *Chondrosia reniformis* based on Aitchison distances. Sampling sites are depicted by colors and points represent individuals. Ten most relevant taxa driving differences in the ordination space are identified by vectors labeled with the respective taxonomy.

Two ASVs in the numerator belonging respectively to the genera *Turneriella* and *Peredibacter* and one in the denominator belonging to the genus *Bdellovibrio* were selected in Qurro. Such bacterial consortium was found to explain the best separation between the sample groups. The acidified sites GM and CAC yielded the lowest log ratio, lower compared to the control sites CCO, GF, and SA, which yielded similar log ratios with respect to each other (Fig. 36). The difference in the log ratios of the selected bacterial consortium though, was non-statistically significant either by sampling sites or by acidification status according to the Welch's Test (p-value > 0.05).

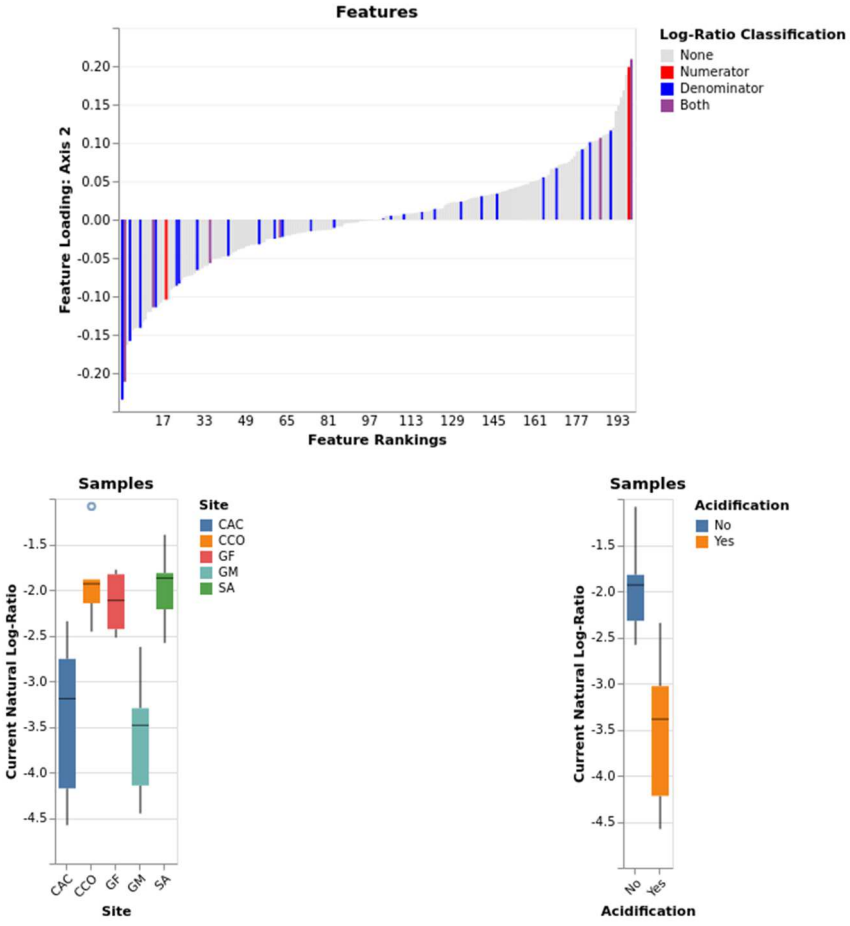

Figure 36 – The first plot shows feature rankings, with the features selected to perform group separations by site and acidification status in the sponge *Chondrosia reniformis*. The second and the third bar plots show the log ratio of the selected features by sampling sites and acidification status.

4.8.2 Microbiome composition of *Chondrosia reniformis* at control and acidified sites

A total number of 51 Bacteria and one Archaea orders composed the associated microbiome of *C. reniformis* sponge (Fig. 37). SAR202 clade, Nitrosococcales and Subgroup 6, were the most abundant orders which presence ranges respectively 9-21%, 8-10% and 7-10 % throughout the different sampling sites.

Myxococcales, SBR1031, BD2-11, *Microtrichales*, *Poribacteria* 64K2, KI89A clade, *Thermoanaerobaculales*, *Rhodobacterales*, and *Bdellovibrionales* accounted for 38 % of the bacterial community. *Rhizobiales* and *Cellvibrionales* were only found associated with samples collected in the acidified site GM, while bacteria belonging to the Order *Flavobacteriales* were only found in the control sites CCO, GF, and SA. Within the sampling site GM the two different morphs of *C. reniformis,* coloured and bleached, revealed similar associated microbial communities.

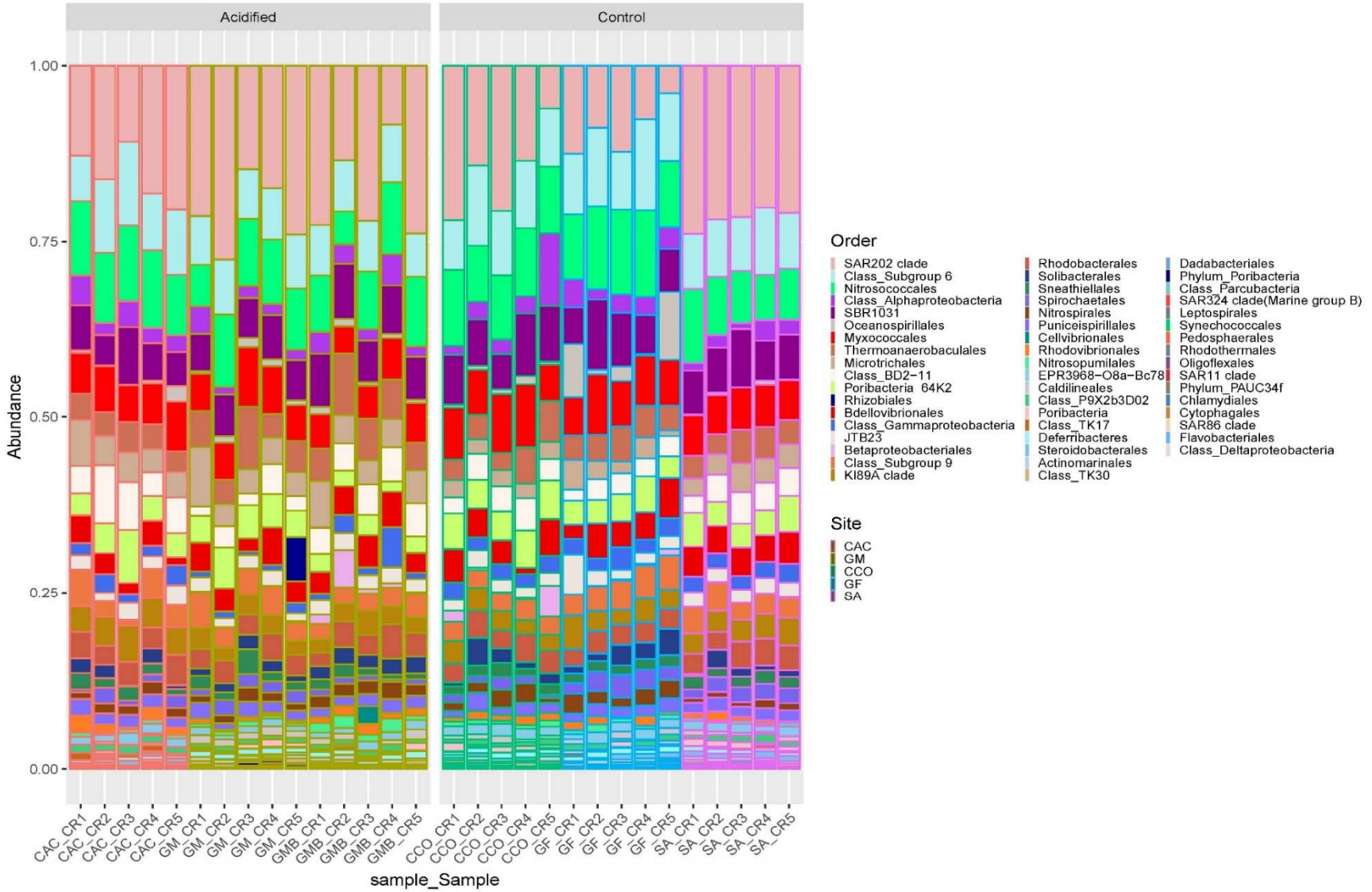

Figure 37 - Taxonomic composition of the microbiome associated with the sponge *Chondrosia reniformis* collapsed at the best annotated taxonomic rank: Order. Bars are visualized by individuals and grouped according to acidification conditions at the sites as acidified and control.

The core microbiomes (considered as those features shared 100% similarity within a sample group) associated with *C. reniformis* in each sampling site is reported in Figure 38. In the acidified sites CAC and GM, the most abundant taxa were SAR202 clade, *Nitrosococcales*, Subgroup 6 and SBR1031 accounting respectively for 50 and 45% of the total core. *Caldilineales*, TK30, *Nitrospirales*, *Oceanospirillales*, *Pedosphaerales*, PAUC34f, *Rhodothermales*, *Solibacterales*, *Spirochaetales* and *Thermoanaerobaculales* were only found in the acidified site GM, accounting for 7%. In the controls, the most abundant taxa were SAR202 clade, *Nitrosococcales*, *Myxococcales*, SBR1031 and Subgroup 6, with relative abundance ~ 50%.

The core microbiome associated to sponges coming from acidified sites *versus* controls sites showed that "control microbiomes" in *C. reniformis* were composed by 46 ASVs that were collapsed in 28 different bacterial orders (Fig. S9). Five bacterial orders were shared only among the controls (*Dadabacteriales*, *Oceanospirillales*, JTB23, *Solibacterales* and PAUC34f) accounting for 5.7%. The most abundant bacterial orders were SAR202 clade, *Nitrosococcales*, Subgroup 6, and SBR1031 representing together 51%.

The "acidified" core microbiome was represented by 40 ASVs clustered in 23 bacterial orders (Fig. S8). SAR202 clade, *Nitrosococcales*, Subgroup 6 and SBR1031 were the most abundant orders accounting 56%.

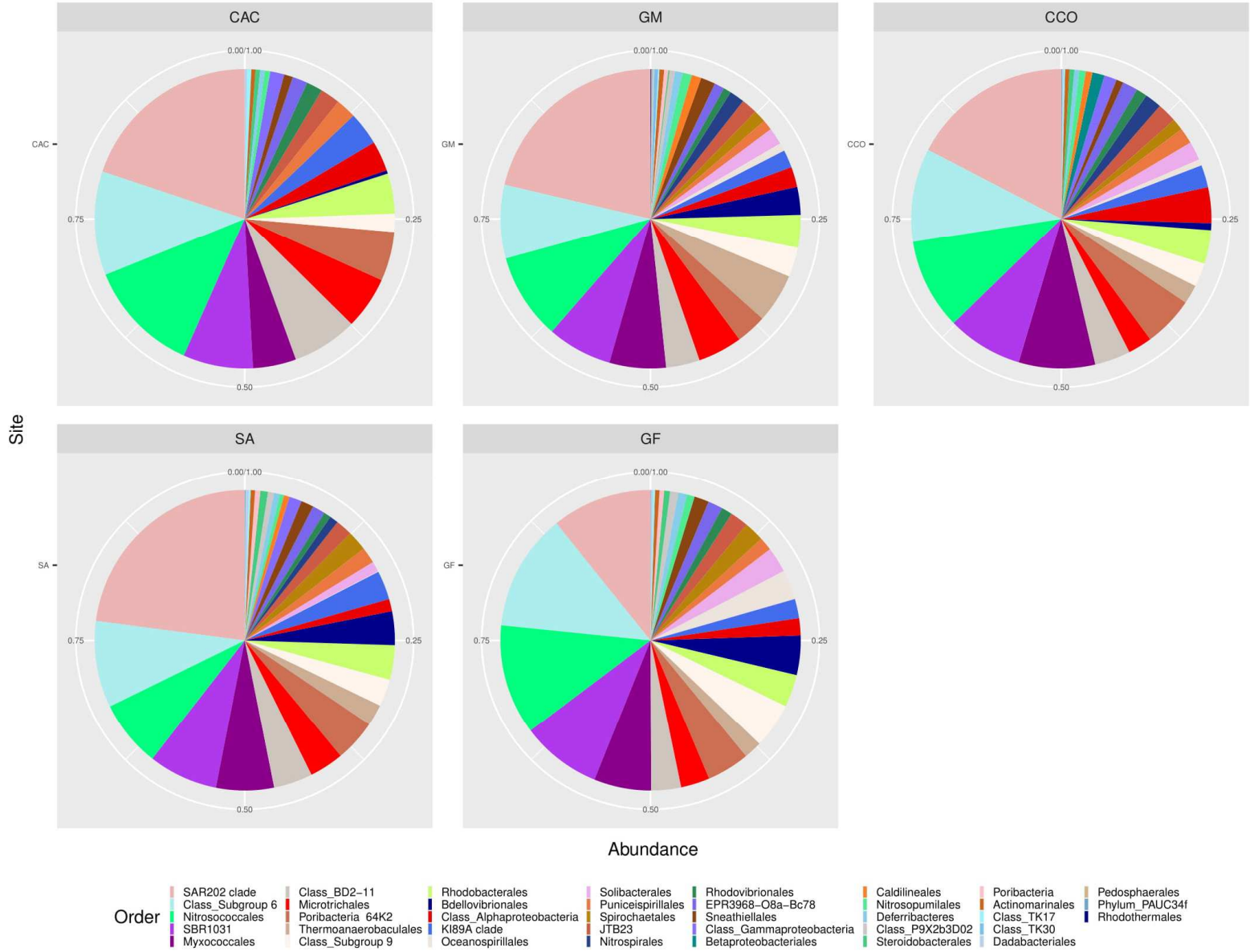

Figure 38 - Core microbiomes of *Chondrosia reniformis* calculated for every sampling site. CAC and GM are the acidified sampling sites, while CCO, SA, and GF the controls.

A low number of exclusive ASVs were found in all the sampling sites, with most of the ASVs being shared among the sites (Fig. 39).

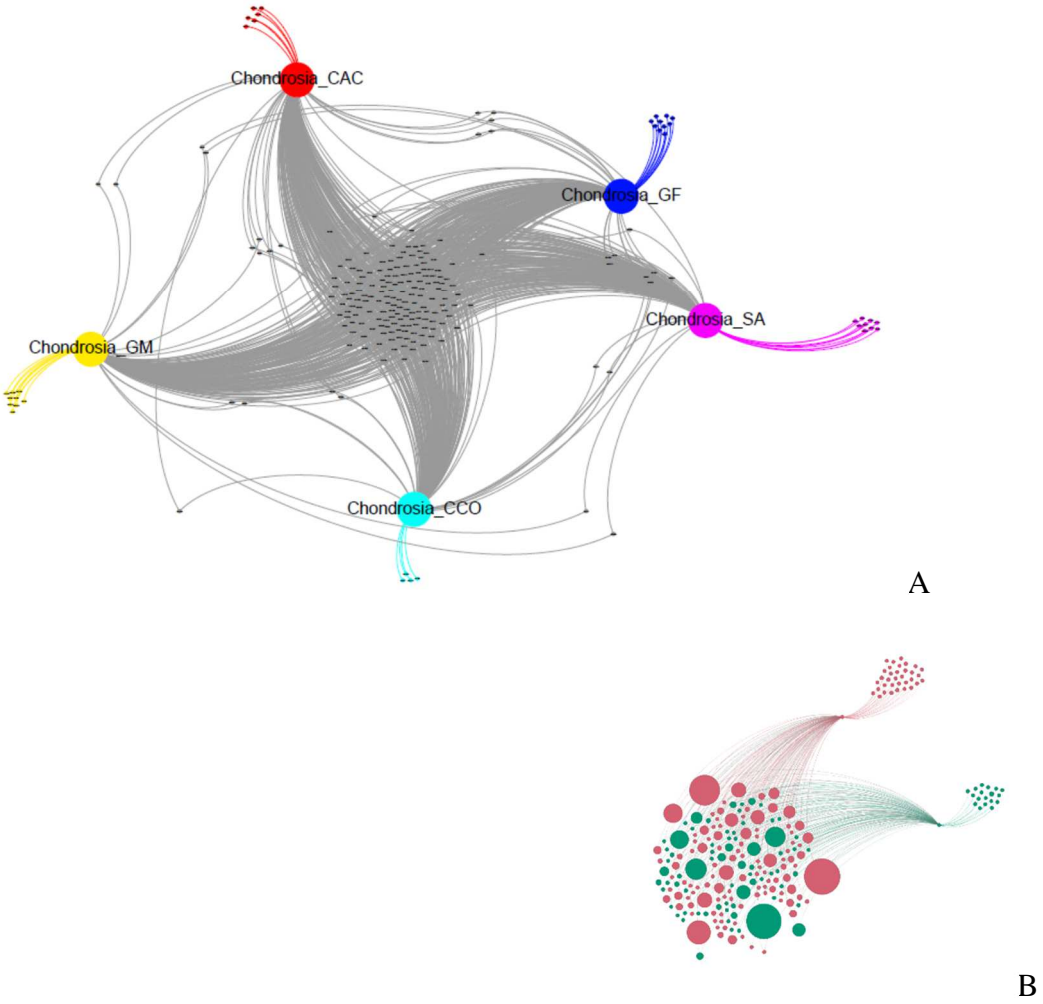

Figure 39 - A) Network based on the ASV table of the sponge species *Chondrosia reniformis* showing the relationships between the different sampling sites of this study. B) Network grouped by Acidified and Controls to show the slightly higher contribution of the exclusive ASVs in the acidified samples (red acidified – green controls).

SIMPER analysis revealed that the similarity of the microbiome composition was ca. 65-70% comparing controls vs. acidified sites and sites characterized by similar pH conditions (Table 5). The average similarity of samples within each sampling site was 66.2% in CAC, 70.5% in CCO, 66.7% in GF, 72.4% in GM and 76.4% in SA.

Table 5 – Summary of the results of a SIMPER analysis carried out on the ASV table of the microbiome associated with the sponge *Chondrosia reniformis*.

Comparison between different sampling sites		Dissimilarity %
Chondrosia_CAC	**Chondrosia_CCO**	33.34
Chondrosia_CAC	**Chondrosia_GF**	37.06
Chondrosia_CCO	**Chondrosia_GF**	32.92
Chondrosia_CAC	**Chondrosia_GM**	35.17
Chondrosia_CCO	**Chondrosia_GM**	33.03
Chondrosia_GF	**Chondrosia_GM**	36.93
Chondrosia_CAC	**Chondrosia_SA**	33.04
Chondrosia_CCO	**Chondrosia_SA**	30.42
Chondrosia_GF	**Chondrosia_SA**	34.90
Chondrosia_GM	**Chondrosia_SA**	29.86

4.8.3 Differential abundance

Gneiss model output

A total number of 30 samples of microbiomes associated to *C. reniformis* were considered as the data inputs in the Gneiss model. The model explained 26% (R^2 = 0.2624) of the variation in bacterial communities among sample groups (factor included in the formula: sampling site). On what regards the comparisons by sites, log ratios of the samples from GM were lower compared to the rest, indicating that the taxa in the denominator of the "y0" balance were more abundant in this site. Conversely the other acidified site CAC had higher log ratios, similar to the log ratios of the control sites CCO and GF, but different compared with the log ratio of control the site SA (Fig. 40).

A total of 44 ASVs collapsed in 21 Orders were included in the denominator of balance y0, plotted considering the factor "sampling site". The top five abundant were: *Bdellovibrionales* (n=18), *Nitrosococcales* (n=11), *Gammaproteobacteria* (n=10), *Alphaproteobacteria* (n= 8), KI89A clade (n=7). All the other 25 taxa were mostly composed by one ASV. The numerator of the balance was composed of 199 ASVs and the five most abundant orders were SAR202 clade (n=78), BD2-11 (n=21), Subgroup 6 (n=16), SBR1031 (n=15) and *Flavobacteriales* (n=14) accounting for a total of 144 ASVs.

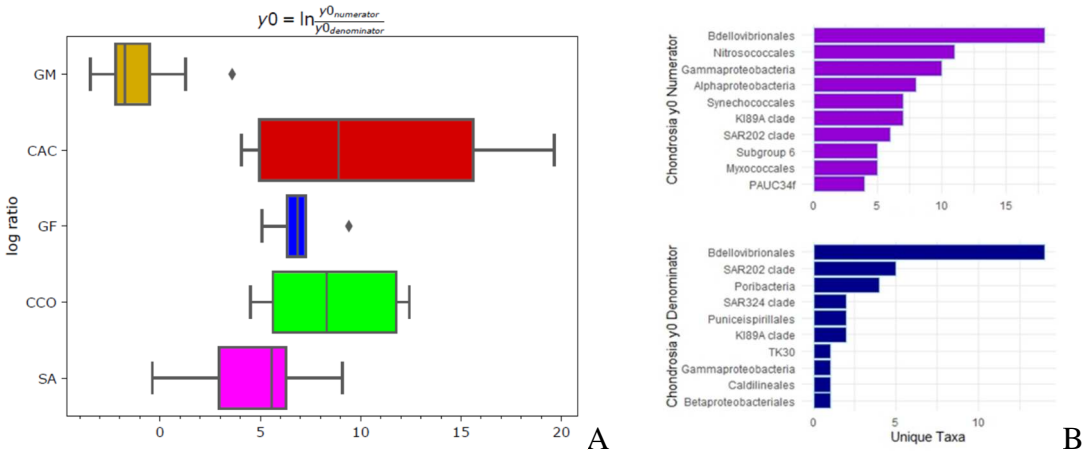

Figure 40 – A) Output of the Gneiss linear model for compositional data on the sponge *Chondrosia reniformis* showing the log ratios of the balance "y0" B) Unique taxa collapsed by Order representing the most abundant groups belonging to the numerator and denominator of the balance "y0".

Songbird model output

Three ASVs in the numerator and two the denominator were identified, according to positive coefficients in the numerator, and negative in the denominator, as most defining differential taxa, with 100% of the samples retained. Such microbial taxa did not explain significantly the differences in microbial composition of *C. reniformis* between sites (Welch's Test, p-value > 0.05; Table S10), and also between acidified *versus* control conditions (Welch's Test, p-value > 0.05; Table S10) (Fig. 41).

Differential taxa in the numerator and highly ranked to the acidification condition of sites GM and CAC included: Subgroup 10 (*Thermoanaerobaculaceae*), Sva0996 (*Michrothrichaceae*), and *Chloroflexus sp.,* conversely in the denominator, *Peredibacter sp.* and *Bdellovibrio sp.* that were associated to the control sites CCO, GF and SA and therefore non-acidification status.

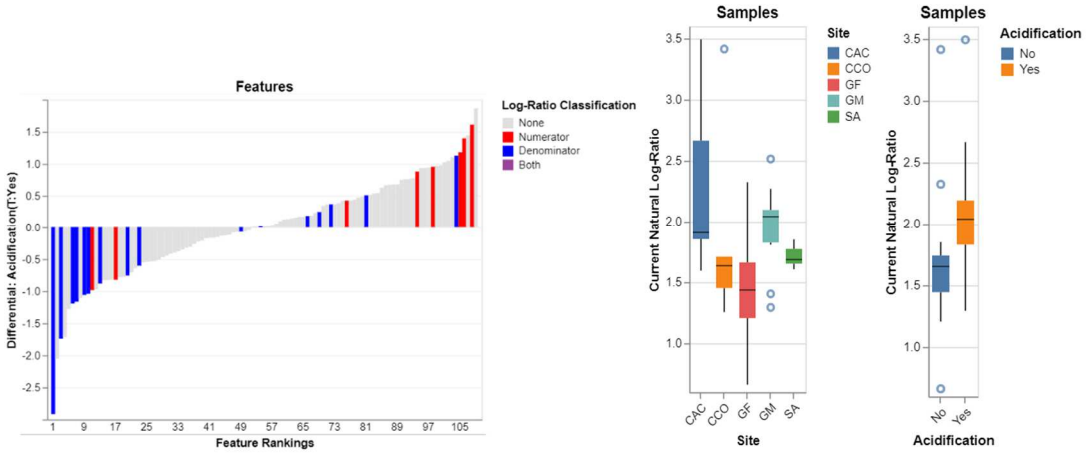

Figure 41 – Differential abundance analysis performed on Songbird for the Sponge *Chondrosia reniformis*. The left plot shows feature rankings with the features selected to perform the grouping separations. On the right, box plots show the log ratios of the selected features by sampling sites and acidification status.

4.9 *Crambe crambe*

Crambe crambe was collected in three acidified sites and three control sites, selecting five individuals per locations that resulted in 30 samples. This sponge was the only one present in the acidified site VU, and it was characterized by a massive growth, instead of the classical encrusting feature, on the rhizome of the seagrass *Posidonia oceanica*.

4.9.1 α and β diversity analyses

Sequence data for *C. crambe* was rarefied to 9.759 reads per sample resulting in a total of 273.252 reads distributed over 28 samples and 523 features (Fig S10; Table S1).
Observed ASVs ranged from 48 to 177 ASVs per sample, CAC acidified site reported the lowest value and SA the highest, with notable variabilities among replicates (Fig. 42). Shannon indexes reflected similar result throughout all sampling sites, but here CCO displayed the highest value (Fig. 42). The alpha-diversity values were not significant different between the sampling sites (Kruskall-Wallis test, p-value > 0.05; Table S11).
The analysis of the beta diversity, based on Bray-Curtis distances, revealed the lack of significant differences across sites (PERMANOVA 9999 permutations, F=1.634, p-value > 0.05; Fig. 42; Table S11). Conversely, significant difference in the microbiome compositions were found using Jaccard distance matrices, (PERMANOVA 9999 permutations, F = 1.9535, p-value < 0.05; Table S11).

A

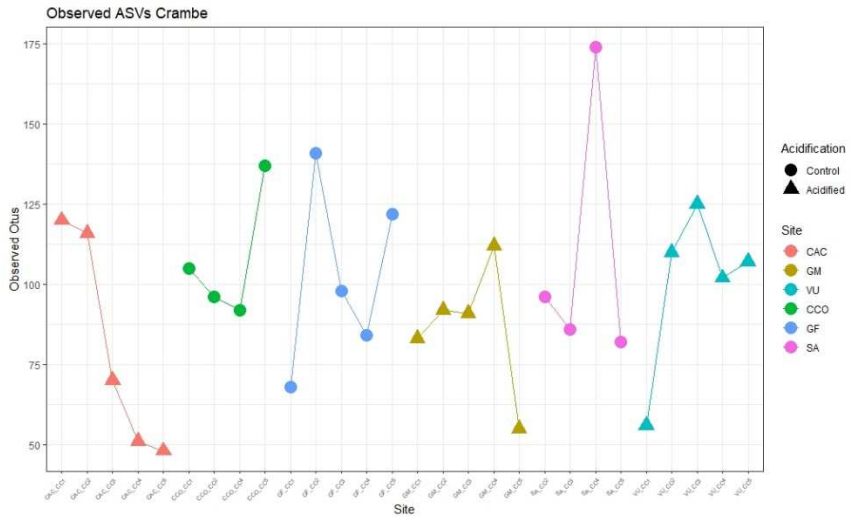

B

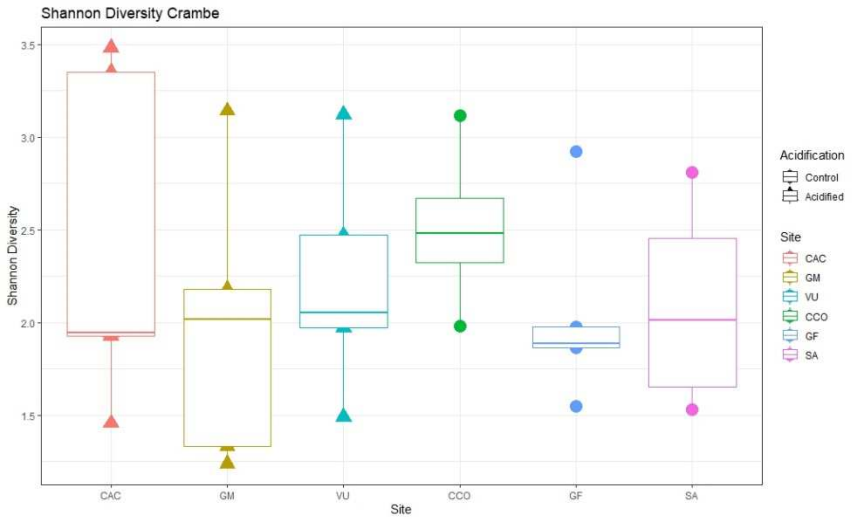

C

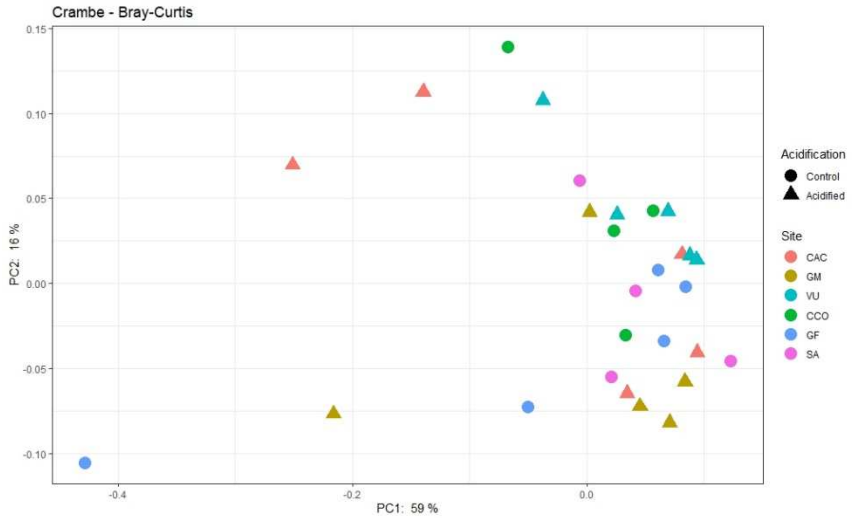

D

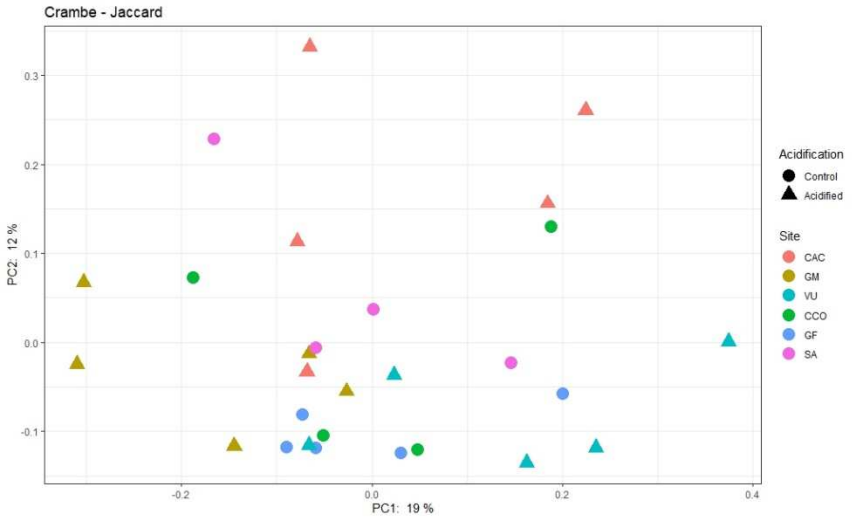

Figure 42 - Alpha and Beta diversity metrics of the bacterial communities associated to sponges belonging to the species *Crambe crambe*: A) Observed ASVs, B) Shannon Index box plot; PCoA beta diversity ordinations based on C) Bray-Curtis and D) Jaccard dissimilarity matrices (α-Diversity - Kruskal-Wallis, $p > 0.05$; β-Diversity PERMANOVA, $p < 0.05$, Table S11).

DEICODE RPCA analysis revealed no clear clustering of microbiome composition among sampling sites (Fig. 43).

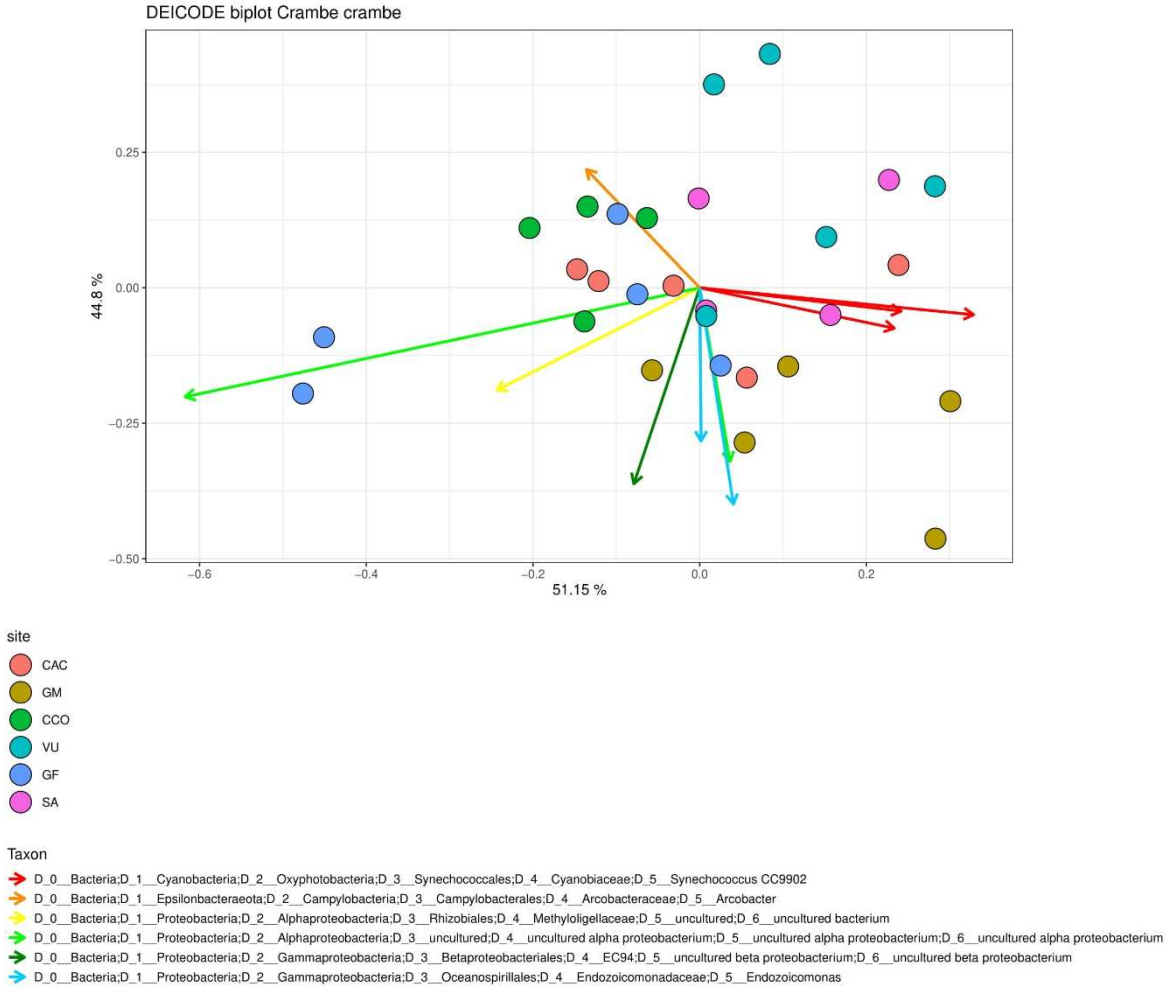

Figure 43 – Compositional RPCA biplot of the sponge *Crambe crambe*, generated using DEICODE for beta diversity comparisons across sampling sites, based on Aitchison distances. Data points represent individuals. Top differential features (*i.e.* taxa driving differences in ordination space) are illustrated by the vectors labeled with the respective taxonomy.

One ASVs in the numerator belonging respectively to the genera *Synechococcus* and one in the denominator belonging to the genus *Endozoicomonas* were selected for providing the best separation between the sample groups. The acidified sites CAC and VU yielded the highest log ratios, higher compared to the acidified site GM and control site SA which resulted in similar log ratios. Control sites GF and CCO displayed the lowest log-ratios (Fig. 44). The difference in the log ratios of the selected bacterial

taxa was not significant, neither by sampling sites or by acidification status according to Welch's Tests (p-value > 0.05).

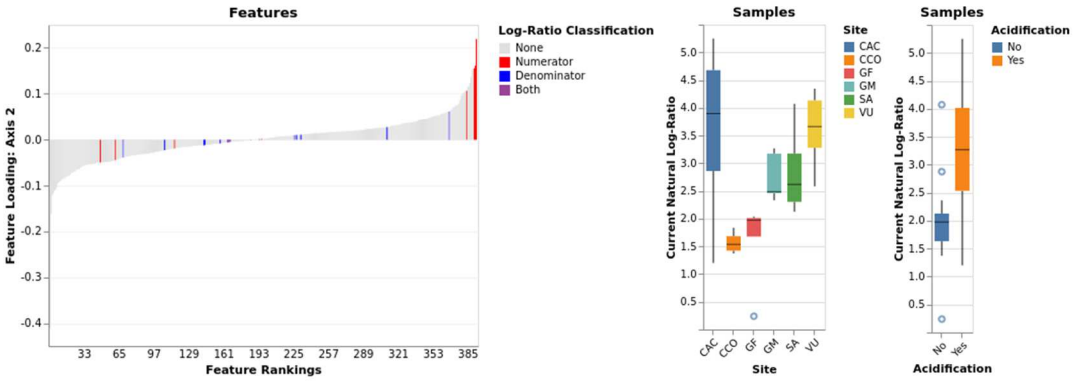

Figure 44 – The first plot shows feature rankings, with the taxa selected to perform group separations by site and acidification status in the sponge *Crambe crambe*. The second and the third bar plots show the log ratio of the selected features plotted by sampling sites and acidification status.

4.9.2 Microbiome composition of *Crambe crambe* at control and acidified sites

A total number of 88 bacterial and 1 archaeal orders was found in the microbiome associated to *C. crambe* sponges. *Betaproteobacteriales* was the most abundant order, accounting for 70-78% of the whole microbiome throughout the different sampling sites. *Synechococcales* was the second most relevant order, accounting for 7-12%, with the lowest relative abundance recorded in GM and SA, and the highest in CCO. The remaining microbial orders accounted for 13-21%, with the lowest value found in VU, while the highest in GF (Fig. 45).

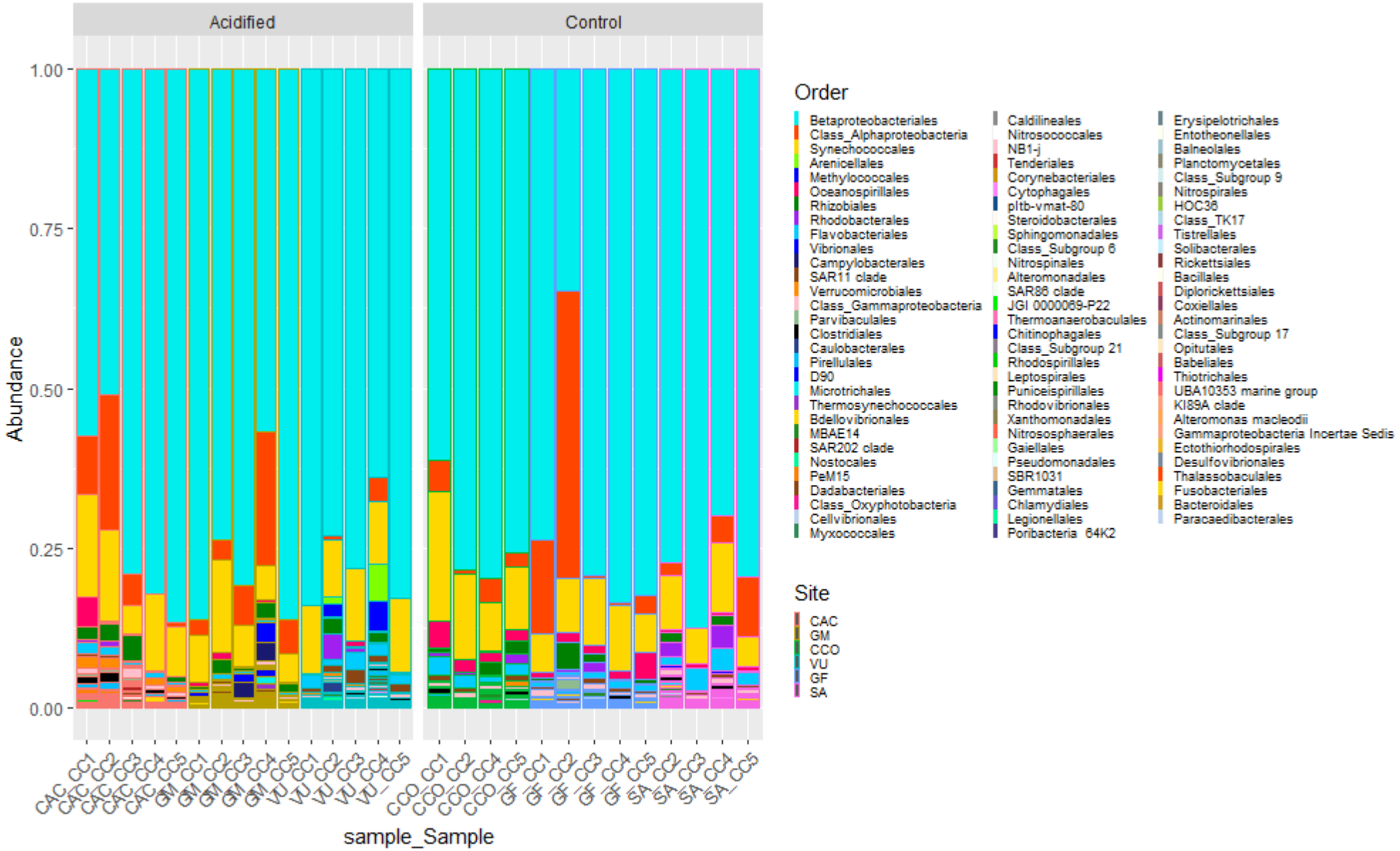

Figure 45 - Taxonomic composition of the microbiome associated with the marine sponge *Crambe crambe,* collapsed at the best annotated taxonomic rank: Order, visualized by individuals per site, and grouped according to acidification status as acidified and control.

The core microbiomes (100% shared features within a sample group) associated with *C. crambe* for every sampling site are reported in Fig. 46. *Betaproteobacteriales* and *Synechococcales* dominated all the core microbiomes (accounting together 78-86%). *Verrucomicrobiales*, *Clostridiales* and *Pirellulales* were recorded only at CAC site, while *Vibrionales* and *Campylobacterales* were found at GM site as core features, and *Rhodobacterales*, *Arenicellales*, *Methylococcales* and SAR11 clade at VU site. No relevant differences were found in the core composition of the three control sites CCO, GF and SA where "control microbiomes" (Fig. S12) were dominated by 13 ASVs that were collapsed in five different bacterial orders. *Betaproteobacteriales* represented alone 88% of the control core microbiome, followed by *Synechococcales* that accounted for 10%. The remaining 2% was equally distributed by the three bacterial orders: *Oceanospirillales*, *Flavobacteriales* and PeM15 that were exclusive of the control's core microbiome.

The core microbiome of the acidified sampling site was represented by 13 ASVs that were collapsed in two orders, *Betaprotaobacteriales* representing 90% and *Synechococcales* the remaining 10% (Fig. S11).

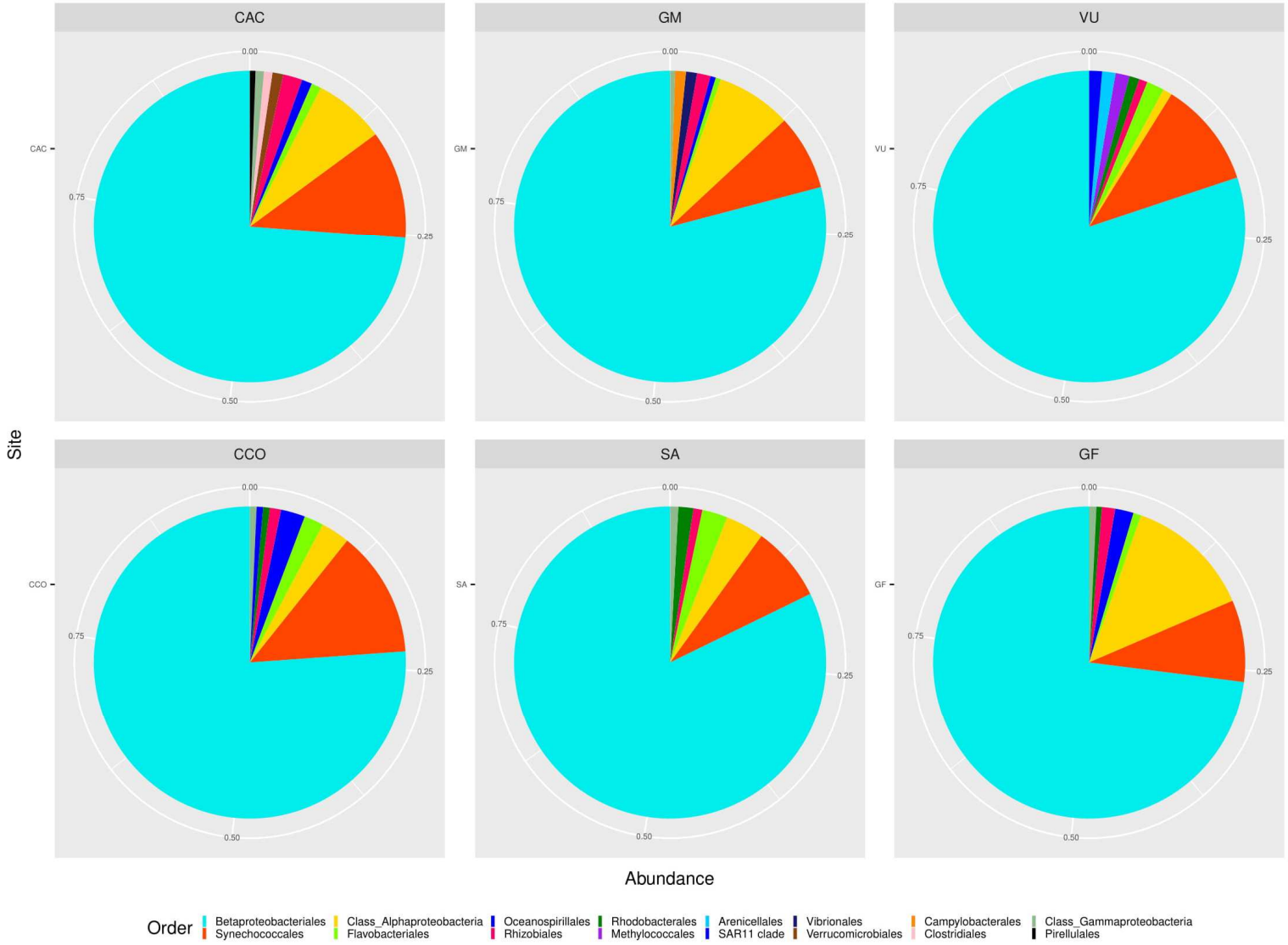

Figure 46 – Core microbiome of the sponge species *Crambe crambe* calculated by sampling site as number of AVSs shared by the 100% of the samples and collapsed to the Order taxonomic rank. CAC, GM, VU (acidified); CCO, SA, GF (controls).

The three acidified sites CAC, GM, and VU were characterized by a higher number of exclusive ASVs (30, 43, 53 respectively) as compared to the controls CCO, GF and SA (Fig. 47). Fifty-three ASVs were shared among all sites. Moreover, one ASV belonging to the order *Betaprotaobacteriales* was reported to be common to all specimens in acidified and control sites, as well as dominant in its relative abundance.

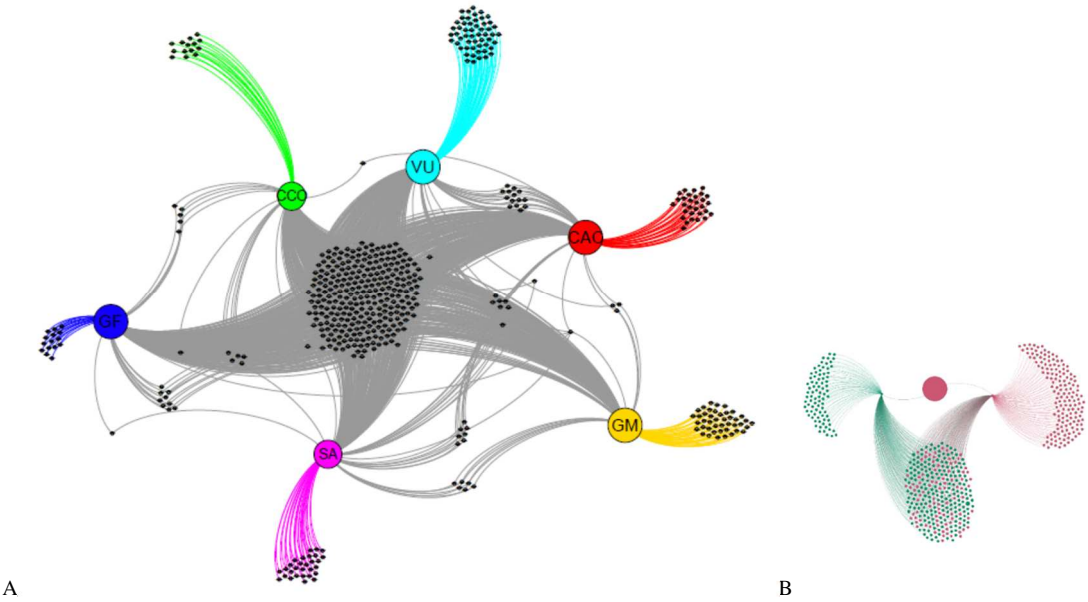

Figure 47 – A) Network based on the ASV table of the sponge species *Crambe crambe* showing the relationships between the different sampling sites of this study. B) Network collapsed by Acidified and Controls together show the higher contribution of the exclusive ASVs in the acidified samples (red acidified – green controls).

SIMPER analysis highlighted that the similarity of the microbiome composition was ca. 70-80% comparing controls vs. acidified sites and sites characterized by similar pH conditions (Table 6). Such similarity values were close to those observed among microbiomes of replicated sponge samples collected at the same sampling sites (71.9% in CAC, 79.0% in CCO, 70.2% in GF, 76.7% in GM, 82.7% in SA and 82.2% in VU).

Table 6 – Summary of the results of a SIMPER analysis carried out on the ASV table of the microbiome associated with the sponge *Crambe crambe.*

Comparison between different sampling sites		Dissimilarity %
Crambe_CAC	**Crambe_CCO**	33.34
Crambe_CAC	**Crambe_GF**	31.22
Crambe_CCO	**Crambe_GF**	27.37
Crambe_CAC	**Crambe_GM**	27.99
Crambe_CCO	**Crambe_GM**	25.47
Crambe_GF	**Crambe_GM**	25.84
Crambe_CAC	**Crambe_SA**	23.73
Crambe_CCO	**Crambe_SA**	19.81
Crambe_GF	**Crambe_SA**	24.85
Crambe_GM	**Crambe_SA**	21.68
Crambe_CAC	**Crambe_VU**	24.19
Crambe_CCO	**Crambe_VU**	20.79
Crambe_GF	**Crambe_VU**	28.18
Crambe_GM	**Crambe_VU**	25.69
Crambe_SA	**Crambe_VU**	21.69

4.9.3 Differential abundance

Gneiss model output

A total number of 28 samples were considered to build a model for the batch corresponding to *C. crambe*. The model explained 33% ($R^2 = 0.3275$) of the variation in bacterial communities across sample groups (factor included in the formula: sampling site). On what regards the comparisons by sampling sites, log ratios of the samples from GM were lower compared to the rest, indicating that the taxa in the denominator of the "y0" balance were more abundant in this site. Conversely all the other sampling sites yielded overlapping log ratios values comparing each other, indicating no differences in the abundance of the taxa enclosed in the balance "y0" within these sites (Fig. 48).

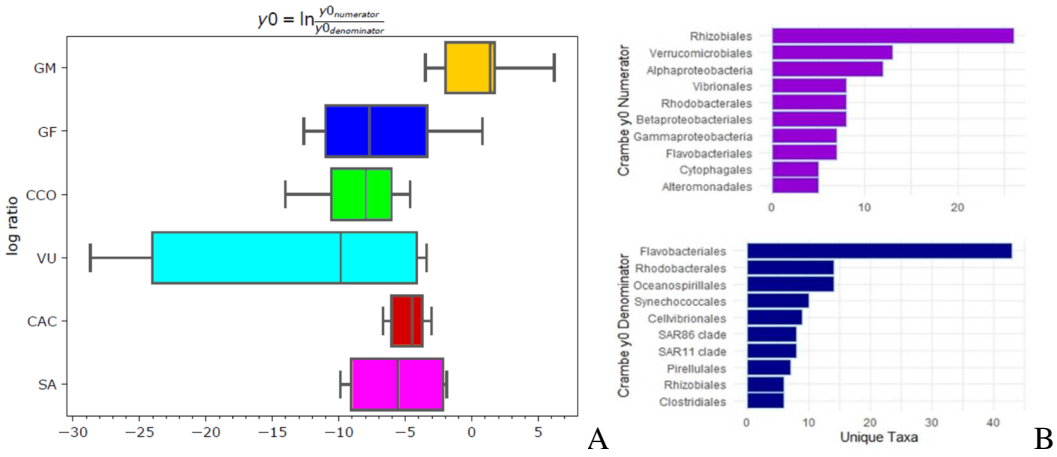

Figure 48 – Boxes of the log ratios in balance "y0" regarding the microbial communities associated with *Crambe crambe* obtained from Gneiss linear model. Bar plots indicate the top 10 taxa of Numerator and Denominator of the "y0" balance, that mostly explain the differences between sampling sites. The acidified site GM reflect different log ratios for this cluster of bacteria, while all the other sites showed similar log ratio values.

A total of 200 ASVs were included in the denominator of the balance "y0", plotted considering the factor "sampling site". The top five abundant orders were: *Flavobacteriales* (n=43), *Oceanospirillales* (n=14), *Rhodobacterales* (n=14), *Synechococcales* (n=10) and *Cellvibionales* (n=9). The numerator of the balance was composed of 192 ASVs and the five most abundant orders were: *Rhizobiales* (n=26), *Verrucomicrobiales* (n=13), *Alphaproteobacteria* (n=12), *Betaproteobacteriales* (n=8) and *Vibrionales* (n=8).

Songbird model output

Four ASVs in the numerator and six in the denominator were identified, according to positive coefficients in the numerator, and negative in the denominator, as most defining differential taxa with 100% of the samples retained. Such microbial consortium was found to explain significant differences in microbial composition between sites, with CAC, GM and VU yielding higher log ratios with respect to the control sites CCO, SA, GF (Welch's Test, p-value < 0.05; Table S12); and also between acidified *versus* control conditions (Welch's Tests, p-value < 0.05; Table S12). CAC recorded highest log ratios, higher than GM and VU, and this difference was significant according to Welch's Test (p-value < 0.05; Table S12); SA had the lowest log ratio among the controls, but non-significantly different from the other two controls CCO and GF (Welch's Test, p-value > 0.05; Table S12) (Fig. 49).

In the numerator, *Filomicrobium sp., Rubripirellula sp., Blastopirellula sp., Persicirhabdus sp.* were the differential features highly ranked to the acidified sites CAC, GM and VU; whereas *Endozoicomonas sp., Ruegeria sp., Flavobacteriaceae, Filomicrobium sp. and Formosa sp.* were ranked to the control sites CCO, GF and SA and therefore non-acidification status.

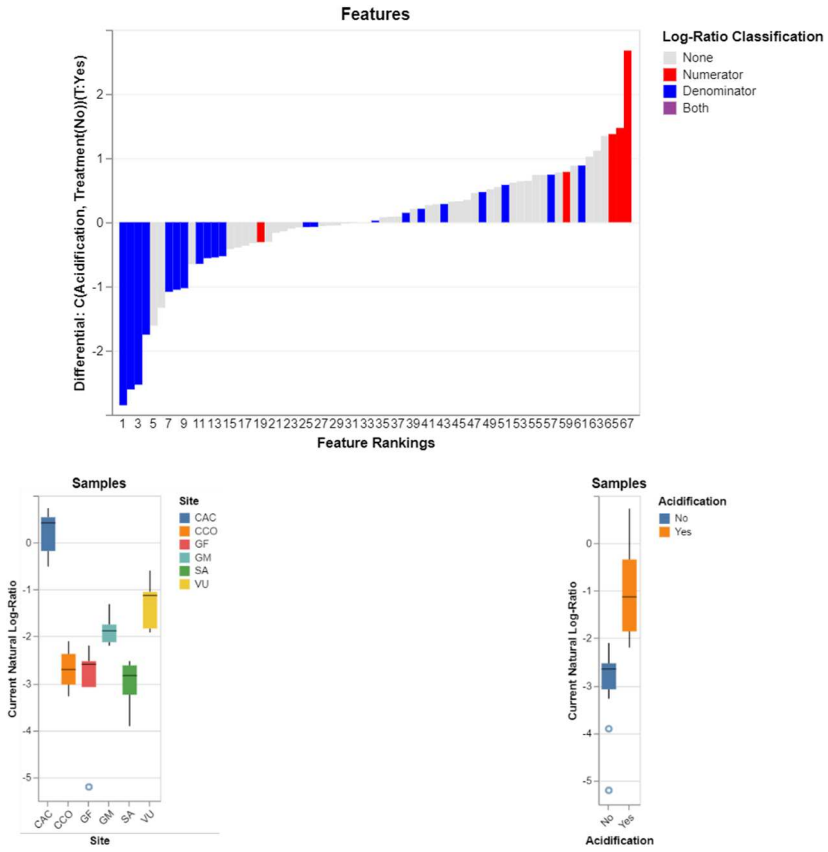

Figure 49 – In the first plot, feature rankings with the features selected to perform the differential abundance analysis for the sponge *Crambe crambe* are represented. In the second and third plots, log ratios of the selected features by sampling sites and acidification status are shown.

4.10 *Chondrilla nucula*

Chondrilla nucula had the lowest number of samples (n = 15). We sampled this sponge species in two control sites (GF, SA) and in one acidified site (GM).

4.10.1 α and β diversity analyses

Sequence data for *C. nucula* was rarefied to 16.804 reads per sample resulting in a total of 252.060 reads distributed over 15 samples and 130 features (Fig. S13; Table S1).

Observed ASVs ranged from 72 to 91 with the lowest value recorded in the site GM, and the highest in SA. The analysis of the Shannon indexes provided similar results between the three groups (Fig. 50). No statistical difference was recorded either with Observed ASVs or with Shannon Index across the sampling sites or the acidification status according to Kruskal-Wallis test (p-value > 0.05; Table S13).

Beta diversity comparison based on Bray-Curtis and Jaccard dissimilarity indexes showed different outcomes as those observed on alpha diversity. Sponge coming from the acidified site GM were significantly different from specimens living in the control sites according to both the Bray-Curtis (PERMANOVA 9999 permutations, F = 2.2425, p-value < 0.05; Fig X and Table S13) and Jaccard distance matrices (PERMANOVA 9999 permutations, F = 5.7398, p-value < 0.05; Fig. 50; Table S13).

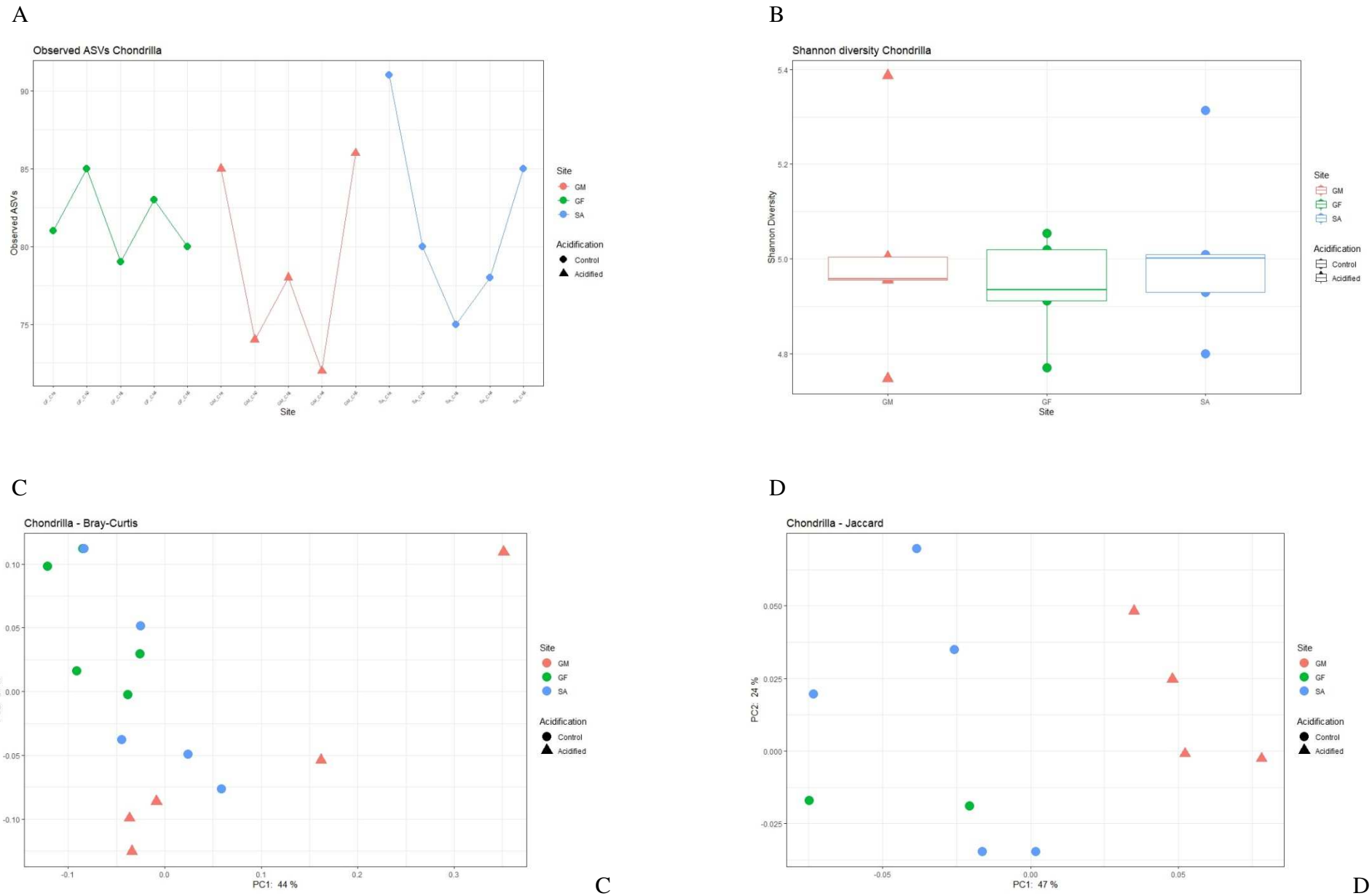

Figure 50 - Alpha and Beta diversity metrics of the bacterial communities associated to sponges belonging to the species *Chondrilla nucula*: A) Observed ASVs, B) Shannon Index box plot; PCoA beta diversity ordinations based on C) Bray-Curtis and D) Jaccard dissimilarity matrices (α-Diversity - Kruskal-Wallis, $p > 0.05$; β-Diversity PERMANOVA, $p < 0.05$; Table S13).

DEICODE RPCA analysis provided a clear clustering in beta diversity between the sampling sites, which were statistically significant (PERMANOVA 9999 permutations, F = 16.549 p-value < 0.05). Three different clusters corresponding to the sampling sites were formed in the ordination space. Ten most discriminatory ASVs taxa were plotted in the biplot (Fig. 51).

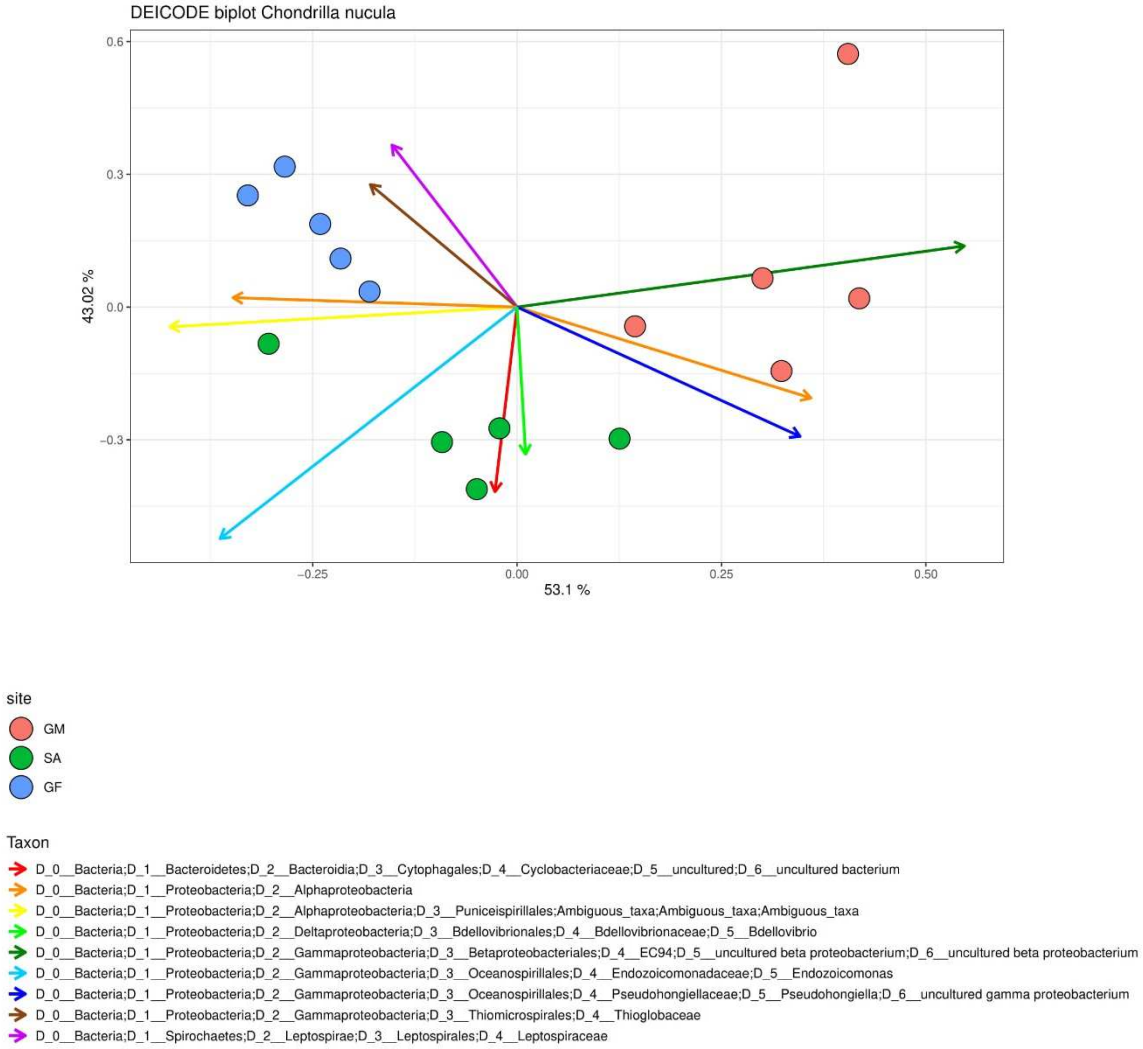

Figure 51 - Compositional biplot of the beta diversity of the sponge *Chondrilla nucula*, generated using DEICODE on Aitchison distances. Points represent individuals. Top differential features (*i.e.* taxa driving differences in ordination space) are illustrated by the vectors labeled with the respective taxonomy.

One ASVs in the numerator belonging to the genus *Bdellovibrio* and one in the denominator belonging to the genus *Endozoicomonas* were selected in Qurro. Such bacterial consortium was found to explain the best separation between the groups. The acidified site GM yielded the highest log ratio, higher than control sites GF and SA, which yielded similar log ratios (Fig. 52). The difference in the log ratios of the

selected bacterial taxa was non-statistically significant either by sampling sites or by acidification status according to the Welch's Test (p-value > 0.05).

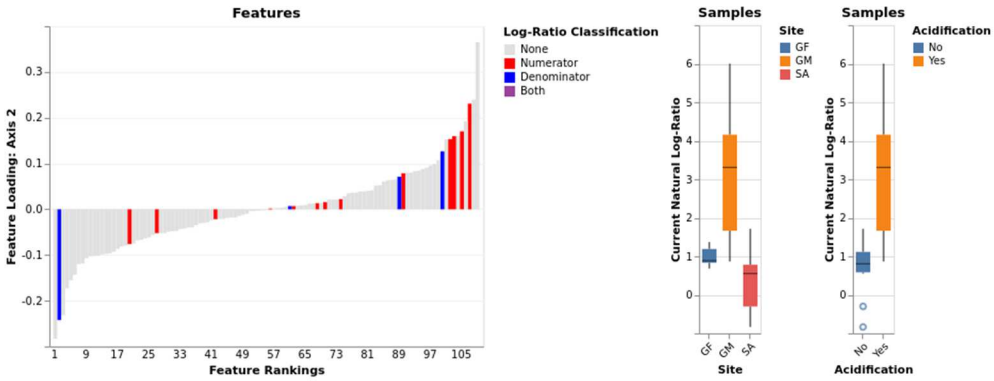

Figure 52 – The first plot shows feature rankings, with the taxa selected to perform group separations by site and acidification status in the sponge *Chondrilla nucula*. The second and the third bar plots show the log ratio of the selected features plotted by sampling sites and acidification status.

4.10.2 Microbiome composition of *Chondrilla nucula* at control and acidified sites

A total of 43 bacterial and one archaeal orders composed the associated microbiome of *C. nucula* (Fig. 53). *Synechococcales* was the most relevant order, ranging from 11 to 20% throughout the different sampling sites. UBA10353 and *Caldilineales* were other relevant orders found in association with *C. nucula*.

Flavobacteriales, and *Poribacteria* were only found associated with the samples collected in the control sites SA and GF, while no exclusive bacterial orders were found in association with the sponge collected in the acidified site GM.

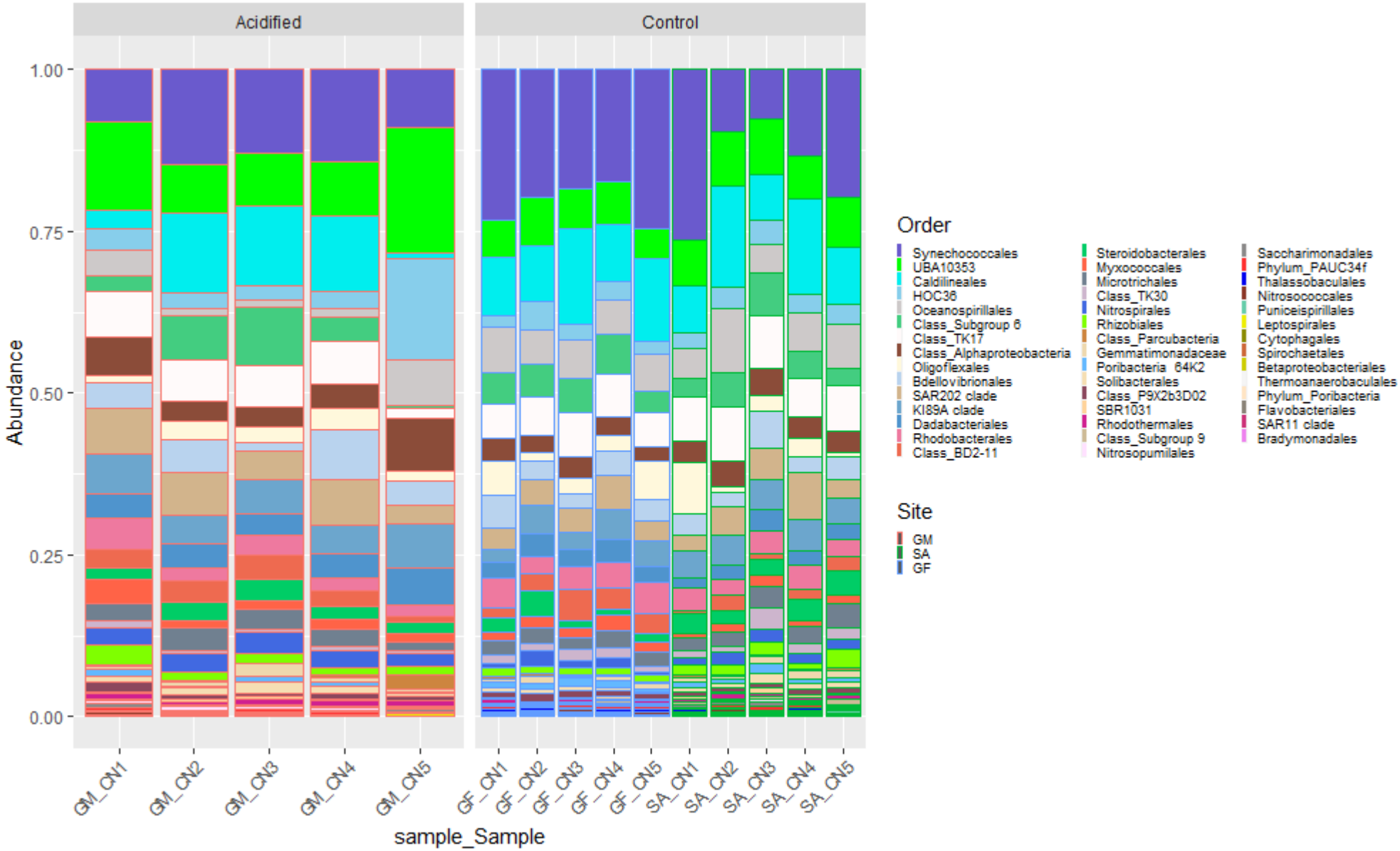

Figure 53 - Taxonomic composition of the microbiome associated with the sponge *Chondrilla nucula,* collapsed at the best annotated taxonomic rank: Order, visualized by individuals and grouped according to acidification conditions at the sites as acidified and control.

The core microbiomes (100% shared features) for every sampling site are reported in Figure 54. The taxon *Synechococcales* was the most abundant throughout the three sites GF, SA and GM, accounting for 12-21%. Other relevant taxa included *Caldilineales*, UBA10353 and TK17, accounting for ~ 40%. The core microbiome associated to control sponges was composed of 55 ASVs that were collapsed in 32 bacterial orders (Fig. S15). *Synechoccoccales*, *Caldilineales* UBA10353 and TK17 were the most abundant bacterial orders accounting for 44%. *Oligoflexales* and *Dadabacteriales* were exclusive orders of the control sites, accounting for 5%.

The core microbiome associated with the acidified sampling sites was represented by 60 ASVs that were collapsed in 35 bacterial orders (Fig. S14). *Synechoccoccales*, *Caldilineales* UBA10353 and TK17 were the most abundant orders accounting for ~ 37%. Subgroup 9, *Saccharimonadales* and *Gemmatimonadetes* were core orders only of the acidified samples accounting together for ~ 5%.

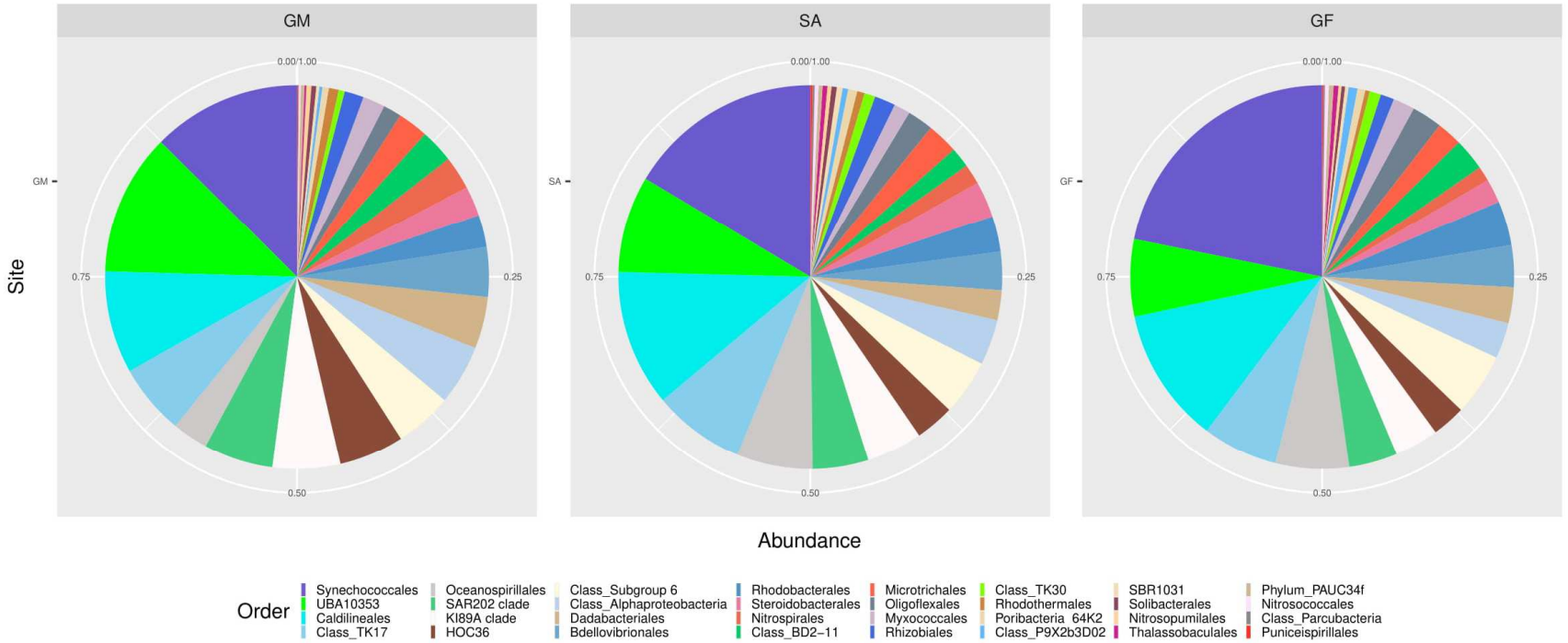

Figure 54 – Core microbiome of C*hondrilla nucula* calculated by sampling site as number of AVSs shared by the 100% of the samples and collapsed to the Order taxonomic rank. GM(acidified), SA, GF (controls).

The network analysis revealed a minor number of exclusive ASVs in the three sampling sites (12 exclusive ASVs in SA, 10 in GM and 6 in GF; Fig. 55). Instead, 84 ASVs over a total of 130 ASVs were shared among the three sites.

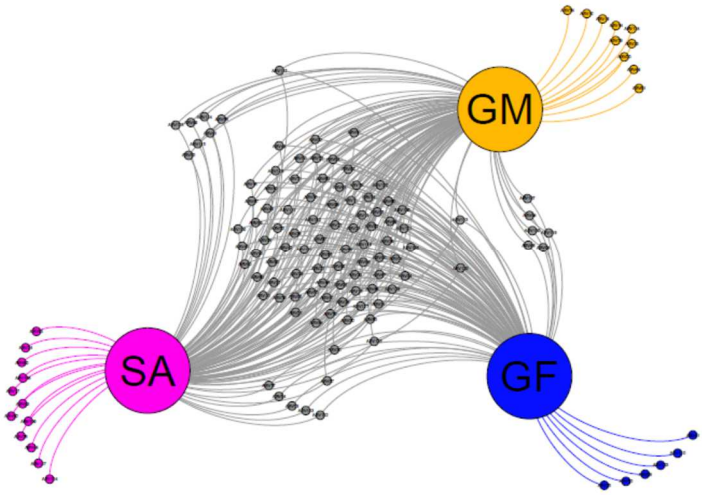

A

B

Figure 55 – A) Network based on the rarefied ASV table, showing the relationship between the microbes associated with *Chondrilla nucula* at different sampling sites. B) Network based on the same ASV table, collapsed by "acidification" status (red acidified, green controls).

SIMPER analysis highlighted that the similarity of the microbiome composition was ca. 67-75% comparing controls vs. acidified sites (Table 7). Such similarity values were close to those observed among microbiomes of replicated sponge samples collected at the same sampling sites (71.9% in CAC, 79.0% in CCO, 70.2% in GF, 76.7% in GM, 82.7% in SA and 82.2% in VU). The average similarity among microbiomes of replicated sponge samples collected at the same sampling sites was 81.1% in GF, 68.8% in GM and 76.0% in SA.

Table 7 – Summary of the results of a SIMPER analysis carried out on the ASV table of the microbiome associated with the sponge *Chondrilla nucula.*

Comparison between different sampling sites		Dissimilarity %
Chondrilla_GF	**Chondrilla_GM**	33.11
Chondrilla_GF	**Chondrilla_SA**	25.06
Chondrilla_GM	**Chondrilla_SA**	32.38

4.10.3 Differential abundance

Gneiss model output

All 15 samples from *C. nucula* were introduced to build the linear model which explained 29% ($R^2 = 0.2931$) of the variation in bacterial communities among sample groups (factor included in the formula: sampling site). On what regards the comparisons by sites, log ratios of the samples from GM were higher compared to the rest, indicating that the taxa in the denominator of the "y0" balance were more abundant in this site. Log ratio values in balance "y0" were similar and overlapping, highlighting no meaningful difference throughout the different sampling sites (Fig. 56).

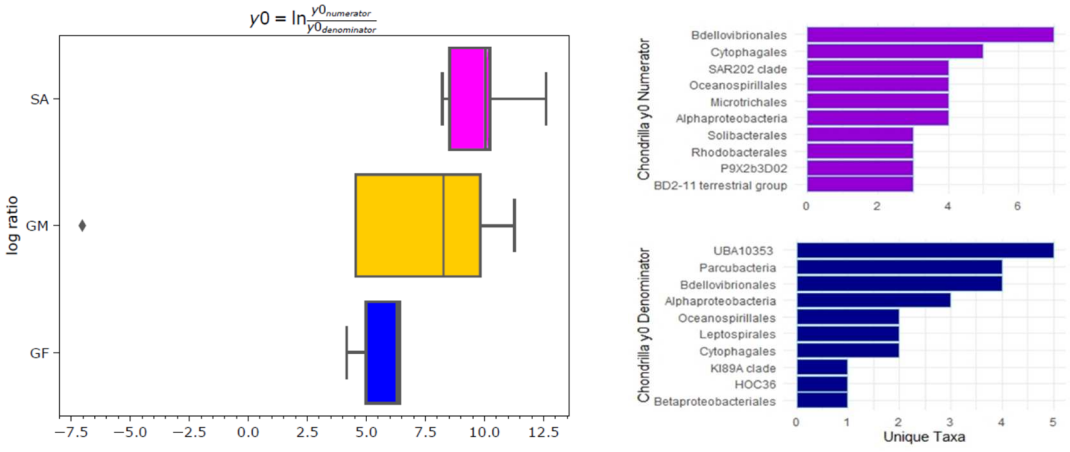

Figure 56 – Boxes of the log ratios in balance "y0" regarding the microbial communities associated with *Chondrilla nucula* obtained from Gneiss linear model. Bar plots indicate the top 10 taxa of Numerator and Denominator of the "y0" balance, that mostly explain the differences between sampling sites.

A total of 44 ASVs collapsed in 21 Orders were included in the denominator of balance y0, plotted considering the factor "sampling site". The top five order composing the

numerator of the balance were *Bdellovibionales* (n=7), *Cytophagales* (n=5), *Alphaproteobacteria* (n=4), *Microtrichales* (n=4), *Oceanospirillales* (n=4). The numerator of the balance was composed of 158 ASVs and the five most abundant orders were SAR202 clade (n=78), BD2-11 (n=21), Subgroup 6 (n=16), SBR1031 (n=15) and *Flavobacteriales* (n=14) accounting for a total of 144 ASVs.

Songbird model output

Three ASVs in the numerator and two in the denominator were identified, according to positive coefficients in the numerator, and negative in the denominator, as most defining differential taxa with 100% of the samples retained. The selected microbial taxa did not explain differences in microbial composition between sites. GM recorded higher log ratios with respect to SA and GF, but the differences were not significant (Welch's Test. P-value > 0.05; Table S14). Among the controls SA yielded a higher log ratio compared with GF. Differential taxa in the numerator and ranked to acidification condition of site GM included: SAR202 clade, PAUC26f, *Caldilineaceae*. In the denominator, *Poribacteria* and AqS1 (*Nitrosococcaceae*) that were more associated to the non-acidified control sites: GF and SA (Fig. 57).

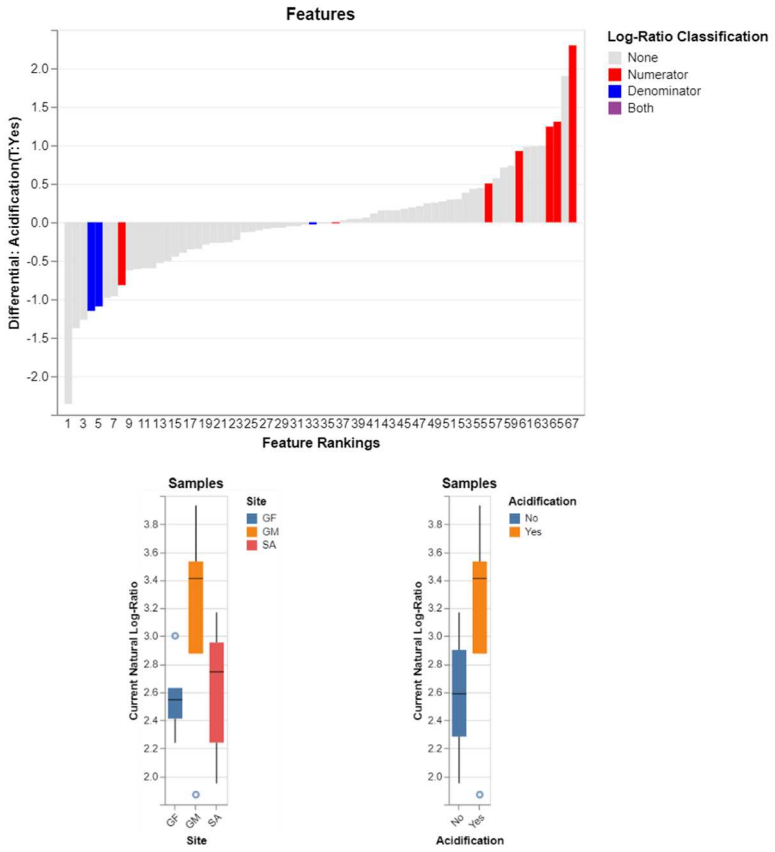

Figure 57 – In the first plot, feature rankings with the features selected to perform the differential abundance analysis are represented. In the second and in the third plot, log ratios of the selected features by sampling sites and acidification status are showed for the sponge *Chondrilla nucula.*

4.11 Metabolomics analyses

4.11.1 Comparison between the metabolomes of *Petrosia ficiformis* and *Crambe crambe*

To investigate the level of sharing features between the metabolomic profiles of the two sponge species, *P. ficiformis* and *C. crambe* a network analysis has been carried out. Such analysis allowed identifying important differences in the metabolomic profiles of the two sponge species, with many chemical features exclusive of each species (Fig. 58) and only some of them (blue dots) shared. SIMPER analysis showed that the dissimilarity of the metabolomic profiles between the two sponge species was 97%, while the similarity within each sponge species was 92% for *P. ficiformis* and 96% for *C. crambe*, indicating high interspecific variability *versus* low intraspecific variability.

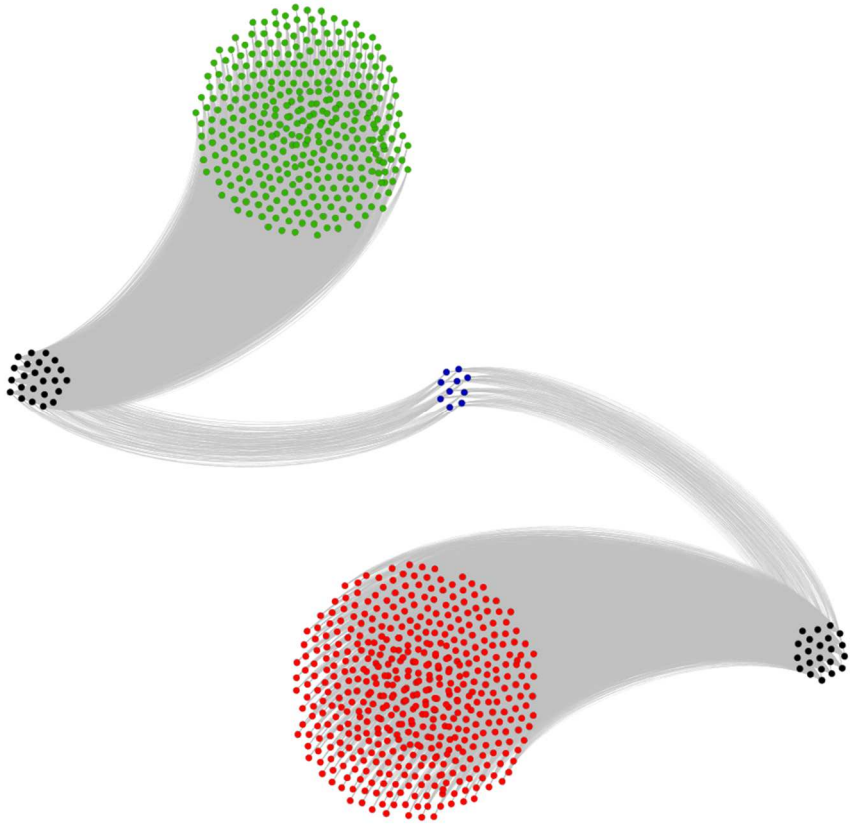

Figure 58 - Network representation of the chemical features associated with the two sponge species *Petrosia ficiformis* (red dots) and *Crambe crambe* (green dots). Ten blue features in the middle of the plot represent the shared molecules between the two species. Black dots by each of two corresponding specific coloured feature clouds represent the replicated samples from each species.

Additional analysis has been carried out also to investigate differences between the metabolomic profiles of the two sponge species collected from acidified and non-acidified sites. To do so, untargeted metabolomics analysis for *P. ficiformis* has been performed on 22 samples, yielding a total of 538 chemical features, after filtering out data with peak area lower than 100000. Such filtered metabolomics data were then used to visualize differences between samples coming from acidified and non-acidified sites by a Principal Component Analysis (Fig. 59). Metabolomic profiles of *P. ficiformis* collected from the acidified site GM clustered away from those obtained from specimens collected from the other acidified site CAC and from the two controls (GF and SA), and showed statistically significant differences (PERMANOVA 9999 permutations, F = 24.882, p-value < 0.05; Table S15). Within the site GM, coloured and bleached specimens of *P. ficiformis* formed a single group and showed no differences in the metabolomics composition (PERMANOVA 9999 permutations, p-value < 0.05; Table S15).

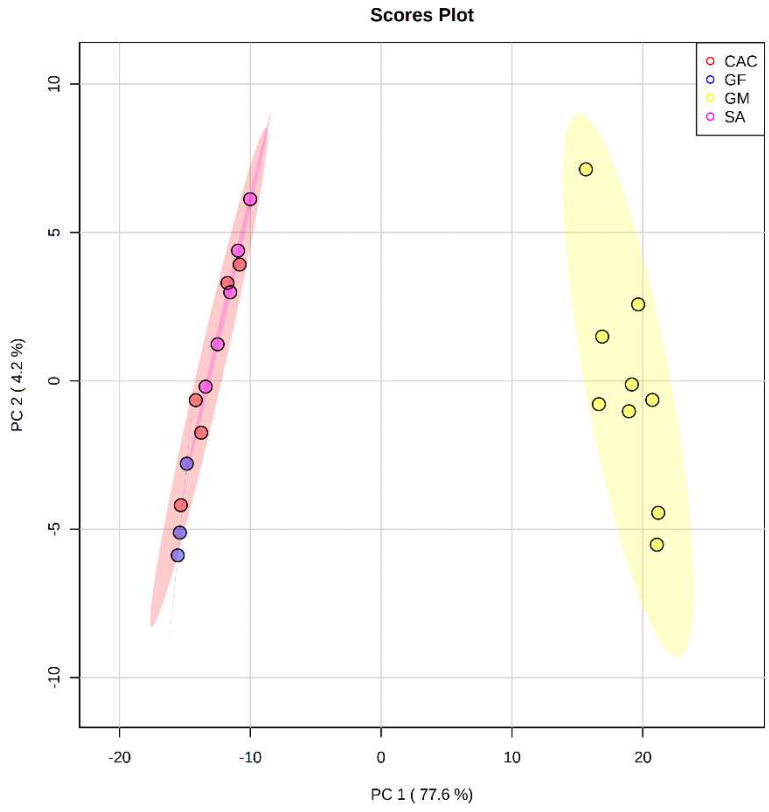

Figure 59 – PCA representing metabolomics feature data from *Petrosia ficiformis*. The acidified cave site GM (PERMANOVA; p-value < 0.05) clustered away from the controls and the other acidified site CAC, which grouped together with the controls (PERMANOVA; p-value > 0.05; Table S15).

The same approach has been used to analyze metabolomic profiles of *C. crambe.* In this case, untargeted metabolomics analysis has been performed on 24 samples resulting in a total of 364 chemical features after discarding all those features with a peak area lower than 100000. PCA analysis revealed the lack of a clear clustering between metabolomic profiles of *C. crambe* collected in acidified and non-acidified sites (Fig. 60). PERMANOVA analysis provided evidence of the lack of significant differences between the different sampling sites (PERMANOVA 9999 permutations, p-value > 0.05, Tables S15).

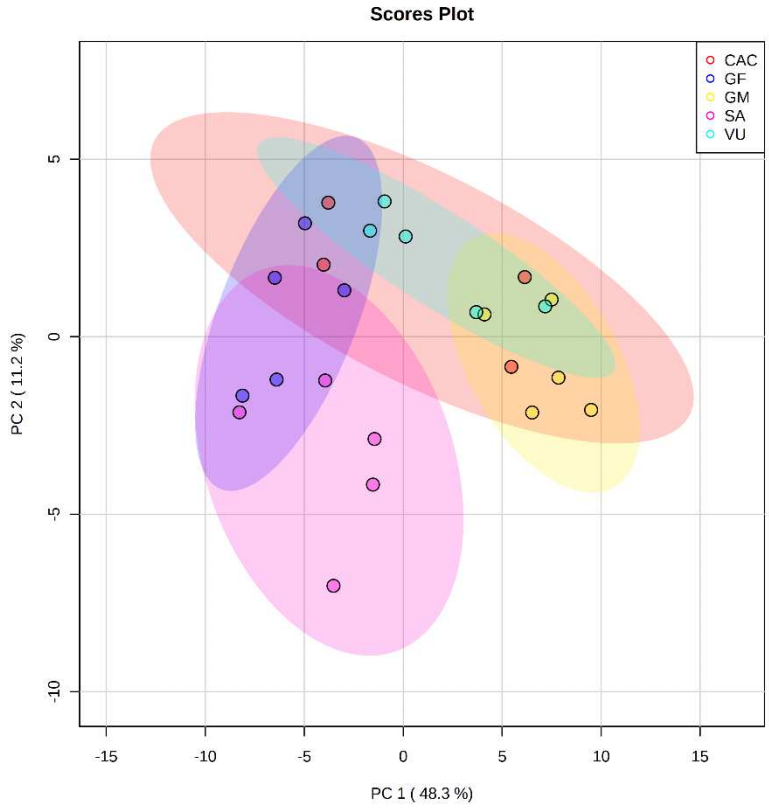

Figure 60 – PCA of the metabolomics data from *Crambe crambe* metabolomics. No clear clustering or statistical differences (PERMANOVA; p-value > 0.05; Table S15) were found among specimens living under diverse conditions of pH (control *versus* acidified).

4.11.2 Comparison between chemical profiles based on molecular classes of *Petrosia ficiformis* and *Crambe crambe*.

The metabolic/chemical profiles from both sponge species were analyzed on the basis of molecular classes, grouping compounds by functional affinity. The resulting molecular class profiles were then compared on the basis of presence/absence and on the basis of their relative abundances across sites and acidification conditions. Results showed that the metabolome of *P. ficiformis* was represented by 15 molecular classes, while in *C. crambe* seven compound families were identified (Fig. 61). The most abundant compounds in both sponge species were triglycerides (TG), phosphatidylcholines (PC), phosphatidylethanolamines (PE), diglycerides (DG) and Ceramides (Cer). *C. crambe* was characterized by the presence of the cholesterol esters (ChE), which were not detected in *P. ficiformis*. Conversely, the metabolome of *P. ficiformis* had eight exclusive molecular classes: hexosylceramides (Hex1Ce), methyl phosphatidylcholines (MePC), phosphatidylglycerols (PG), phosphatidylinositols PI, phosphatidylserines (PS), Sulfatide (ST), Stigmasterol Esters (StE), wax esters (WE), Zymosterol Ester (ZyE).

Relative abundance comparisons revealed differences across sampling sites in *P. ficiformis.* The most abundant classes, triglycerides (TG) and phosphatidylcholines (PC), showed higher relative abundances in GM, GMW and GF, as compared to CAC and SA. These differences were statistically significant in the main test and for the post-hoc comparisons GF-CAC, SA-GF and SA-GMW considering the class triglycerides (TG), while no statistical significance was found in the class phosphatidylcholines (PC) (TG: ANOVA, p-value < 0.05; PC: ANOVA, p-value > 0.05, Table S17) Within the acidified cave, samples of the two morphotypes GM and GMW had similar values for these molecular classes (ANOVA, p-value > 0.05, Table S17). Among the lower abundance molecular classes, diglycerides (DG), wax esters (WE) and monoglycerides (MG) displayed higher relative abundances in the acidified cave GM when compared to the other sampling sites (*i.e.* the other acidified site CAC and the controls GF and SA) (ANOVA, p-value < 0.05, Table S17). Sulfatides (ST) and phosphatidylinositols (PI) showed an opposite pattern, with lower relative abundances in the acidified cave GM compared with the other sampling sites (ANOVA, p-value < 0.05; Table S17).

In *C. crambe*, the most abundant molecular classes, such as phosphatidylcholines (PC), triglycerides (TG), ceramides (Cer) and phosphatidylethanolamines (PE), did not show significant differences among the acidified site GM, which was characterized by a lower relative abundance, and the other sampling sites. (ANOVA, p-values > 0.05; Table S18). Phosphatidylcholines (PC) showed higher relative abundance in the sites CAC, GF and SA compared with GM and VU, while triglycerides (TG) and phosphatidylethanolamines (PE) were more abundant in the control sites GF and SA, than in acidified sites CAC, GM and VU**.** Statistical analyses revealed significant differences only for the phosphatidylcholines (PC), between the sites GM-CAC and GM-GF (ANOVA, p-value < 0.05; Table S18).

A

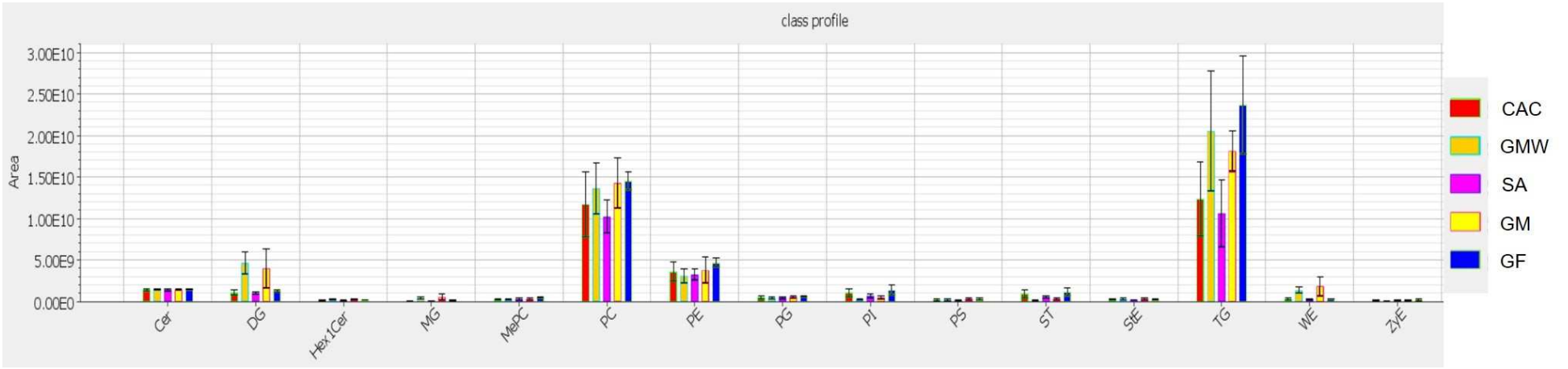

B

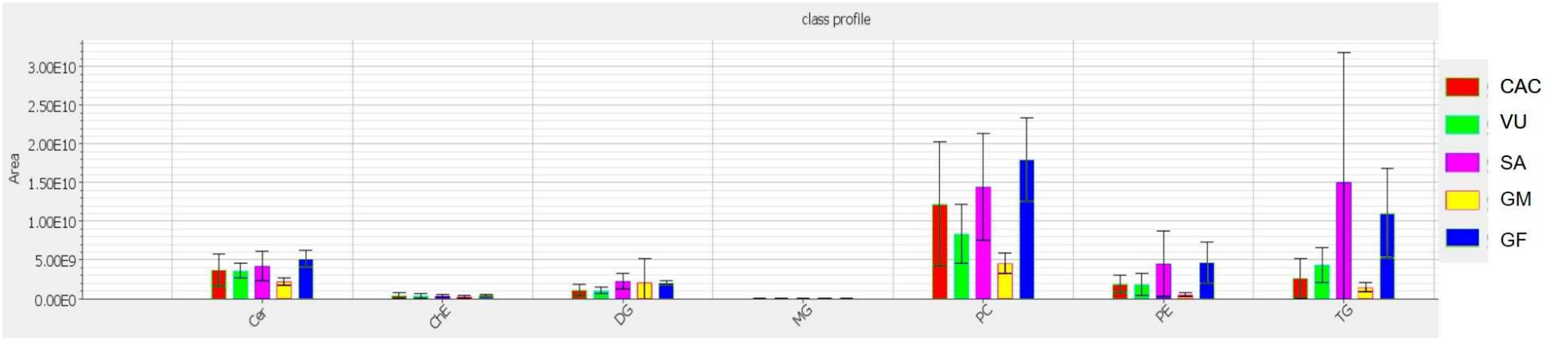

Figure 61 - Metabolic profiles by molecular classes associated with each sponge species (upper and lower plot) and sampling site (bar in colors). A) *Petrosia ficiformis* showed a metabolome composed by 15 chemical classes. B) *Crambe crambe* was charachterized by seven classes of molecules. Triglycerides (TG), Phosphatidylcholines (PC), Phosphatidylethanolamines (PE), Diglycerides (DG) and Ceramides (Cer), Cholesterol esters (ChE), Hexosylceramides (Hex1Ce), Methyl phosphatidylcholines (MePC), Phosphatidylglycerols (PG), Phosphatidylinositols (PI), Phosphatidylserines (PS), Sulfatide (ST), Stigmasterol esters (StE), Wax esters (WE), Zymosterol esters (ZyE), monoglycerides (MG); (Table S18).

4.11.3 Isolation and characterization of polyacetylenes from *Petrosia ficiformis*

Based on the outcome band visualization of the thin layer chromatography (TLC), performed after the chemical extraction, all *P. ficiformis* specimens displayed clear differences in the secondary metabolites composition across the different sampling sites. Instead, *C. crambe*, exhibited a secondary metabolites pattern strikingly similar and homogeneous throughout all the samples.

We found a differential presence of at least two groups of specific compounds belonging to the polyacetylene petroformynes family in *P. ficiformis*. Samples coming from the acidified cave GM, exclusively possessed a group of three non-polar compounds, that were absent in the other samples collected in the other sites. Instead, sponges collected from the other sites contained a group of five polar metabolites lacking in the specimen from the cave.

Further investigations on these specific molecule groups were conducted in three sponge samples (two controls: F3-I; F6-II and one from the acidified cave F5-IV), applying high resolution mass spectrometry (HR-MS) and nuclear magnetic resonance (NMR) to each isolated product. This analysis allowed the discrimination of ten different compounds in the polyacetylene class, eight of which mentioned above plus two additional petroformynes common to all sponges from all sites. The molecular formula, mass and sample of origin of each compound are reported in Table 8, whereas the chemical structures are reported in Fig. 62. The reported exact molecular masses (m/z) of each compound (Fig S17-S18), obtained from the HR-MS-NMR cross check, were then used to determine manually the presence of each compound throughout all the specimens in their corresponding HR-MS spectra.

Table 8 – Petroformyne secondary metabolites isolated from the sponge *Petrosia ficiformis*.

Molecular Formula	Molecular mass	Putative name	Isolation source
$C_{46}H_{68}NaO_4^+$	707.501	Petroformyne_5	F6-II/F3-I
$C_{42}H_{63}NaO_5^+$	670.45732	New_Petroformyne_3	F6-II
$C_{46}H_{66}NaO_3^+$	689.4904	Petroformyne_10	F6-II
$C_{46}H_{68}NaO_3^+$	691.5061	Petroformyne_1	F6-II/F3-I
$C_{42}H_{63}NaO_6^+$	686.452235	New_petrofomyne_2	F6-II
$C_{42}H_{63}NaO_4^+$	654.462405	New_petroformyne_1	F6-II
$C_{46}H_{66}NaO_2^+$	673.4955	Isopetroformyne_4	F5-IV
$C_{46}H_{68}NaO_2$	675.5112	23,24_diidro_petroformyne_4	F5-IV
$C_{46}H_{70}NaO_2$ (x2)	677.5268	Isopetroformyne_3	F5-IV
$C_{46}H_{72}NaO_2^+$	679.5425	23,24_diidro_petroformyne_3	F5-IV

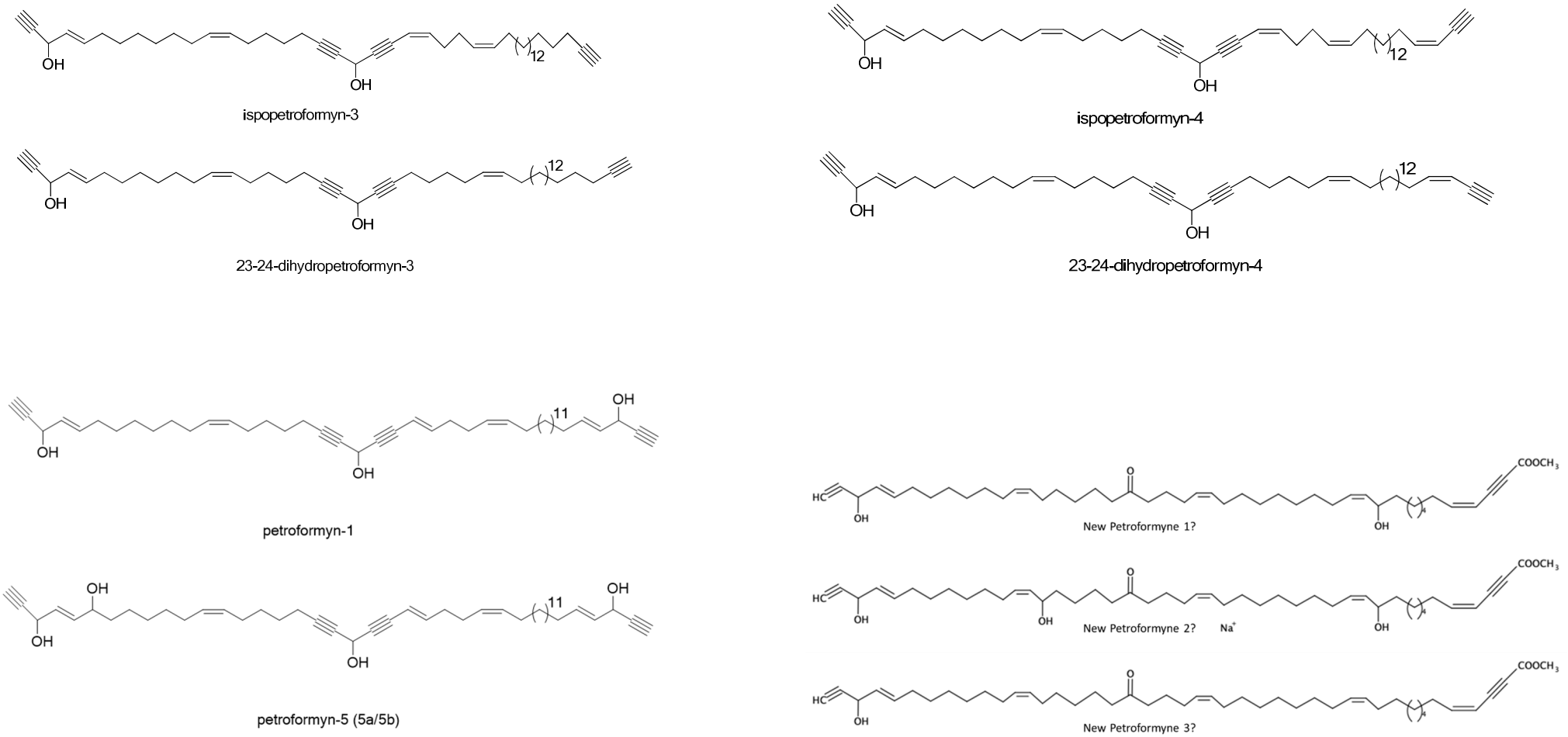

Figure 62 - Molecular structure of the polyacetylenes isolated from *Petrosia ficiformis*.

Exact masses (m/z) of the ten isolated polyacetylenes (Fig. S17-S18) were used for matching peaks across the metabolomics LC-MS spectra and create a presence/absence table for downstream analyses. According to the PCA on the polyacetylenes data, specimens from the acidified cave (GM) showed a clear difference compared with the two controls (GF and SA) and with the other acidified site CAC (Fig. 63). This difference was statistically significant according to PERMANOVA analysis output (9999 permutations, F=308.66, p-value < 0.05; Table S15).

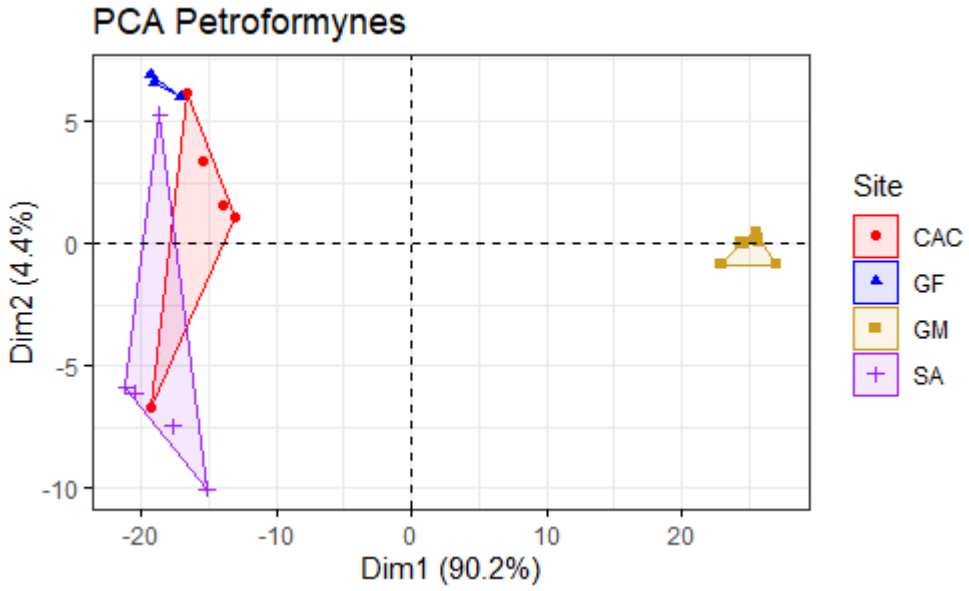

Figure 63 – PCA of the polyacetylenes composition associated with the sponge *Petrosia ficiformis* across the different sampling sites. Significant differences (PERMANOVA; p-value < 0.05) were in the samples coming from the acidified cave GM with respect to the rest.

A heat map showing the pattern of distribution of polyacetylenes across all *P. ficiformis* samples highlighted two different groupings (Fig 64). One group was composed by the samples coming from the acidified cave GM, containing the three non-polar polyacetylenes (molecular masses 675; 677; 679). The other cluster was composed by the samples belonging to the two controls (GF and SA) and the other acidified site CAC which were characterized by five exclusive polar polyacetylenes (molecular masses: 707; 691; 673; 670; 689). Two petroformyne products were found to be common to all sites. One was present in very low concentrations through all specimens (molecular mass 654), whereas the other one (molecular mass 686) was

dominant in all samples, with the exception of those collected in the acidified cave GM (Fig. 65).

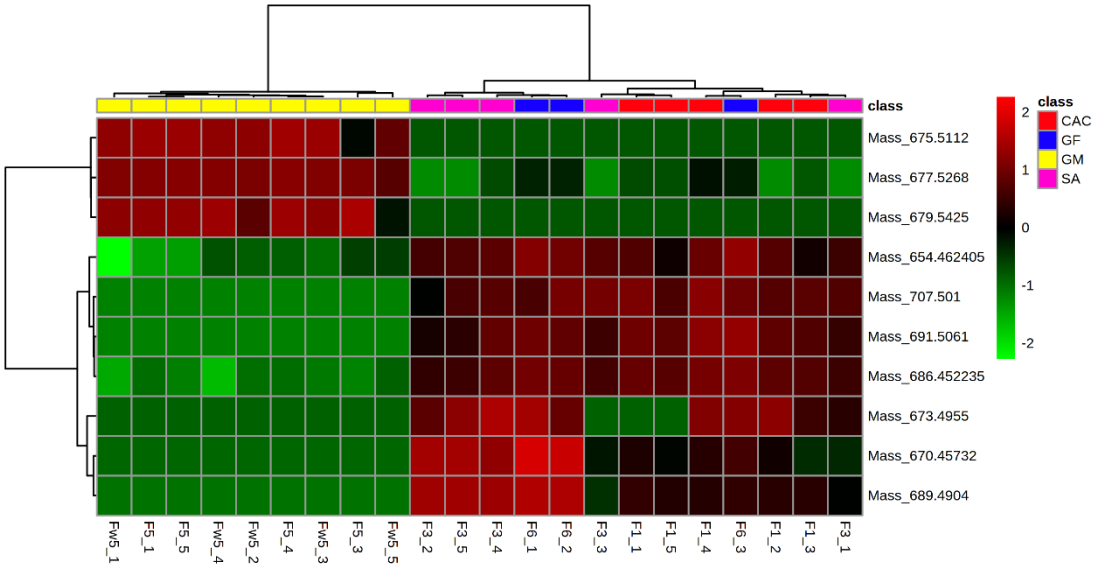

Figure 64 – Heat map showing all the samples from *Petrosia ficiformis* ordered by sampling site against the ten isolated petroformynes denoted by their molecular masses (m/z). Two clusters of samples are highlighted: One composed by the samples belonging to the acidified cave site GM and one by the other acidified site CAC and the two controls (GF and SA).

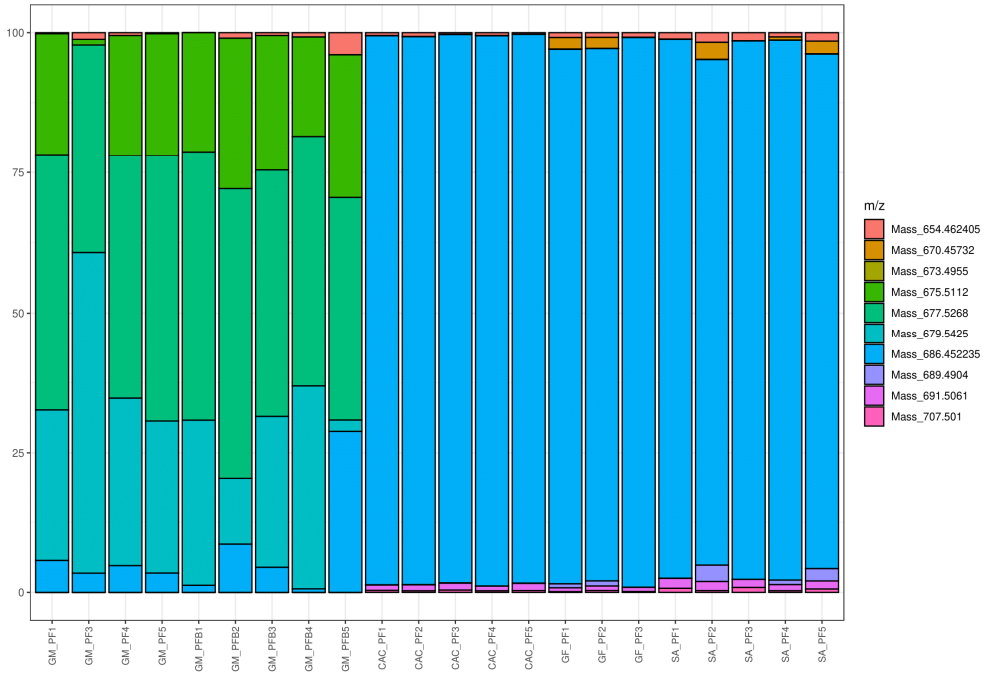

Figure 65 – Relative abundance of the petroformynes shown at single sample level. Sample from acidified cave GM revealed lower abundances of the compound with molecular mass 686 (~ 0.5 - 28%), which is dominant in all the other samples (~ 90%). A compound with molecular mass 654 is also present in all the samples with very low relative abundances (~ 0.2 – 4%). Three compounds with molecular masses 675 – 677 – 679 were exclusive of the acidified cave GM. These three molecules had a respective relative abundance of 20, 44 and 27% in the samples coming from the acidified cave GM. Five compounds with molecular masses 670, 673, 689, 691, 707 were exclusive of the controls (GF and SA) and the other acidified site (CAC).

4.11.4 Differential abundance analysis of metabolites associated with *Petrosia ficiformis* and *Crambe crambe*

Petrosia ficiformis

Differential abundance on metabolomics data across the covariate "acidification" was investigated. Six metabolites in the numerator and eight in the denominator were selected according to their coefficients of positive and negative ranking related to the acidification status, respectively. Metabolites were selected in relation to highest (numerator) and lowest (denominator) ranking coefficients, retaining 100% of the samples. Metabolites selected in the numerator included $C_{46}H_{68}O_3$; $C_{46}H_{64}O$; $C_{46}H_{64}O_2$; $C_{48}H_{77}NO_2$; $C_{27}H_{42}O_2$; $C_{46}H_{64}$; $C_{46}H_{73}NO_2$; $C_{46}H_{68}O$, positively ranked with the acidification status, while the denominator included $C_{46}H_{69}NO_3$; $C_{46}H_{62}O$; $C_{44}H_{70}O_7$; $C_{32}H_{66}O_5P_2$; $C_{47}H_{71}NO_3$; $C_{46}H_{62}O_2$, all negatively ranked with the acidification status. This metabolite combination was found to explain significant differences across different sampling sites. The acidified cave site GM yielded the highest log ratio compared with the other acidified site CAC and the control sites GF and SA, which yielded the lowest log ratios (Fig 66). Differences in the log-ratios of the selected metabolites were significant only for the site GM with respect to the others, according to the Welch's Test (p-value < 0.05; Table S16), in agreement with the outcome obtained from the PCA analysis.

A B

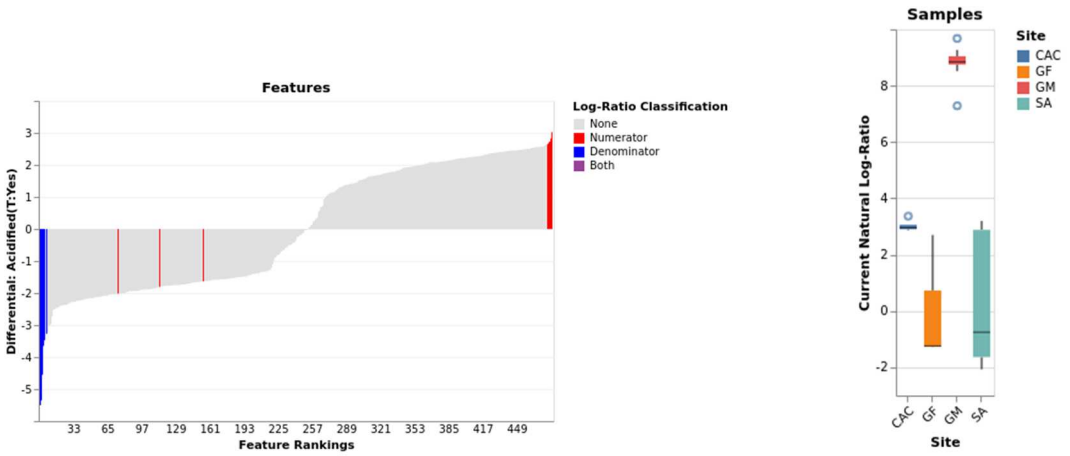

Figure 66 – A) Feature rankings of the metabolite features selected to perform the differential abundance analysis in *Petrosia ficiformis* B) Boxplots showing log ratios of the selected features across the different sampling sites.

Crambe crambe

Within the metabolome of the sponge *C. crambe* five metabolites in the numerator (positively ranked with the covariate "acidification") and five in the denominator (negatively ranked with the covariate "acidification") were selected to perform a differential abundance analysis, retaining 100% of the samples. Metabolites selected in the numerator included the following molecular formulas: $C_{17}H_{33}N_4O_2P$; $C_{15}H_{16}O$; $C_{30}H_{69}N_5O_7P_2$; $C_{22}H_{38}O_2$; $C_{23}H_{38}O_4$, positively ranked with the acidification status, while the denominator included $C_{37}H_{75}N_2O_6P$; $C_{35}H_{73}N_5O_6P_2$; $C_{49}H_{84}O_6$; $C_{37}H_{77}N_5O_6P_2$; $C_{34}H_{72}N_7O_6P$, which were negatively ranked with the acidification status.

The log ratio of this combination of metabolites showed differences across the different sampling sites. The two acidified sites CAC and VU yielded the highest log-ratios, higher with respect to the acidified cave site GM and with the controls GF and SA, which yielded the lowest log-ratios (Fig 67). The differences between the log-ratios of the different sampling sites were statistically significant only for CAC compared with SA (Welch's Test; p-value < 0.05; Table S16) and for VU compared with GF and SA (Welch's Test; p-value < 0.05; Table S16).

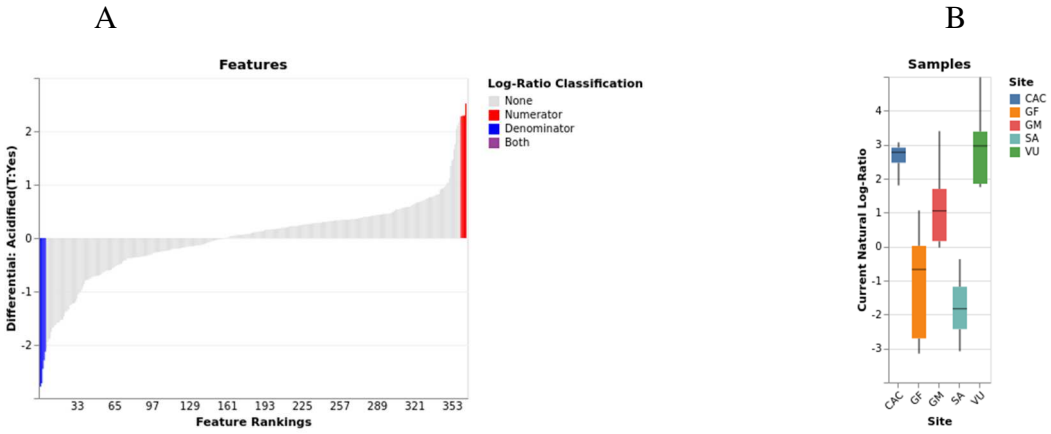

Figure 67 – A) Feature rankings of the metabolite features selected to perform the differential abundance analysis in *Crambe crambe* B) Boxplots showing log ratios of the selected features across the different sampling sites.

5. DISCUSSION

In this study we performed for the first time in the Mediterranean area, a multidisciplinary study on the effect of ocean acidification on the population abundance, morphological traits, microbiome and metabolome of Porifera collected along a natural gradient of pH conditions. In particular, this study was conducted at the CO_2 volcanic seeps off the island of Ischia, acting as a natural OA laboratory. Four sponge species were selected for being widespread in the Mediterranean Sea and also abundant across the vents system: *Petrosia ficiformis, Chondrosia reniformis, Crambe crambe Chondrilla nucula.*

Sponge were first investigated in terms of abundance and morphological traits, with focus on tracing possible changes in distribution and anatomical structures related to the pH gradient. A comparison of the microbiome (Bacteria and Archaea) and mycobiome (Fungi) was performed for all four species, providing new information about diversity, taxonomic composition and putative functions of sponge associated microbes, and in relation to OA adaptation. On two sponges, *Petrosia ficiformis* and *Crambe crambe*, metabolomics analyses were also conducted with the intention to compare their metabolic profiling, and contrast each metabolome across a gradient of natural acidification. Finally, the sponge *Petrosia ficiformis*, living in different pH environments was investigated for its secondary metabolites production, yielding several polyacetylenic compounds. Some of which new to science.

5.1 Sponge distribution along gradients influenced by CO_2 seeps

Results showed a different distribution of the four sponge species across sampling sites. *Crambe crambe* was present at all investigated sites, and was the only species encountered at the most acidified site "Vullatura" (VU), where pH value ranged from 7 down to 6.8. These data provide evidence that this species is highly tolerant to a wide range of pH. It is important to note that VU is charachterized by the presence of a *Posidonia oceanica* meadow, where the only available substrate for sponge growth are the phanerogam shoots. Since all four sponges have been reported as epiphytes on *P. oceanica* (Padiglia et al. 2018; Pansini and Pronzato, 1985), the distribution reported in the present study is likely majorly driven by pH. *Petrosia ficiformis* and *Chondrosia reniformis* were more abundant in the acidified sites CAC and GM (~7% and ~10%) as compared to the controls, indicating a potential adaptation of these sponge species to moderate acidification conditions. *Chondrilla nucula,* instead, was charachterized by a narrower distribution in relation to pH. It was recorded in all the control sites and at the cave GM, which has the highest pH (~ 7.74) among the acidified sites, suggesting a more limited endurance potential to OA. The acidified cave GM was the only sampling site where all the sponge species considered in this study were present representing a reservoir of "acidified sponge diversity", and an *unicum* in the Mediterranean area (pers. obs).

A general trend of sponge coverage reduction along a gradient pH decrease was reported by Fabricius and collaborators (2011) in CO_2 vents off Papua Nuova Guinea. Other studies, however, reported contrasting results, highlighting that sponge abundance under natural OA is species-specific, and is mostly related to other environmental conditions (Goodwin et al. 2014; Kroeker et al. 2013a; Morrow et al. 2015). For instance, again in Papua Nuova Guinea cold seeps, the sponges *Coelocarteria singaporensis* and *Cinachyra sp*. were 40 fold more abundant in the vent system compared with the control site, while the sponge *Stylissa massa* was seven fold less abundant (Morrow et al. 2015).

Goodwin and coauthors (2014) performed a study at Ischia volcanic vents, which included the acidified site Castello acidified, CAC. They showed that sponge distribution pattern was again species-specific. *Crambe crambe* was very abundant at the acidified site, while *Petrosia ficiformis*, *Chondrosia reniformis* and *Chondrilla*

nucula were restricted to the control site. Findings reported in the present study do not agree with such results, as we reported the presence of *Petrosia ficiformis* and *Chondrosia reniformis* at CAC, as also previously observed by Teixidó and co-workers (2018). *Chondrilla nucula,* instead, was previously described as well in GM by Gaino and coauthors (1977). The sponge *Haliclona mediterranea*, not analyzed in the present research, has a particular distribution, been reported at CAC and lacking at any control site (Goodwin et al. 2014; Teixidó et al. 2018; pers. obs.). This pattern could suggest that certain species may colonize extreme ecosystems with reduced complexity, profiting a lower pressure of competitors and/or predators (Kroeker et al. 2013a; Kroeker et al. 2013b).

The sponge species analyzed in this study showed very different auto-ecological features. *Petrosia ficiformis* and *Chondrosia reniformis* are reported to live both in light or sciophilus environments, while *Crambe crambe* and *Chondrilla nucula* prefer photic or poorly shaded environments (Arillo et al. 1993; Bavestrello et al. 1988; Gaino et al. 1977; Garrabou and Zabala, 2001; Wilkinson and Vacelet, 1979). Concerning the reproductive strategy, *Petrosia ficiformis*, *Chondrosia reniformis*, and *Chondrilla nucula* have similar reproductive strategy (*i.e.* spawners), although the reproduction occurs in different seasons (Gaino, 1980; Maldonado and Riesgo, 2008; Sidri et al. 2005). *Crambe crambe*, on the contrary, is a brooder that produces a floating larva released into the water column, which remain planktonic until settlement takes places (Uriz et al. 2001). It has been suggested that brooding strategies could favor adaptation of sponges to extreme environments such as those occurring in the Southern Ocean (Koutsouveli et al. 2018), as well as to afford tolerance to lowered pH in other taxa (*e.g.* polychaetes; Gambi et al. 2016; Lucey et al. 2015). It could be possible that brooding reproduction could be among the phenotypic traits that allow *C. crambe* live under wide acidification ranges.

Overall marine sponges are considered to be "winners" in a future climate change scenario, because there is increasing evidence that they are generally more tolerant to OA compared with other benthic taxa (Bell et al. 2013; Bell et al. 2018a; Bell et al. 2018b). This concept, however, can not be applied to all sponges since calcareous sponges being characterized by carbonate spicule skeletal framework likely will result as "losers" in a future scenario of increased pCO_2 (Smith et al. 2013).

A particular case are bio-eroding clionid sponges, which can increase their bio-eroding activity favored by OA, displacing corals and other calcifying competitors, and resulting in an accelerated erosion of reefs (Enochs et al. 2015; Wisshak et al. 2014). However the synergistic effect of OA with other environmental stressors such as temperature rise induced by the present climate change, may have more detrimental effects on sponges than that of OA alone (Bennett et al. 2018; Bennett et al. 2017; Duckworth et al. 2012; Webster et al. 2013).

Ribes and coauthors (2016) showed that the sponges *Chondrosia reniformis, Agelas oroides and Dysidea avara* under laboratory induced OA displayed different responses in terms of growth rates. Growth rates under OA were severely affected in *Chondrosia reniformis*, halved in *Agelas oroides* and unaffected in *Dysidea avara.* Instead the capability to host new microbial taxa under stressful conditions was null in *Chondrosia reniformis*, moderate in *Agelas oroides* and high in *Dysidea avara,* indicating that flexibility in symbiont acquisition could be a winning strategy to thrive under a future high pCO_2 scenario. Our results showed that *Petrosia ficiformis* and *Crambe crambe* were more flexible in modulating their microbiomes in the high CO_2 sites compared with *Chondrosia reniformis* and *Chondrilla nucula*, fact that could have conferred to these two species more tolerance to natural OA. Therefore, the capability to acquire (or even lost) microbial taxa under stressful or extreme environmental condition could be a key adaptive element to thrive in a future climate change scenario. *Chondrosia reniformis*, however, showed tolerance to OA in natural conditions (this study), even with a very stable microbiome highlighting that maintaining a robust core microbiome could be another strategy.

5.2 Morphological traits related to habitat adaptation

The general growth pattern of the target species investigated in the present study is diverse. *Petrosia ficiformis* and *Chondrosia reniformis* are characterized by massive three dimensional growth, *Chondrilla nucula* is also three dimensional yet less bulky; whereas *Crambe crambe* is an encrusting species with a by-dimensional growth and a very different organization (Bavestrello et al. 1988; Becerro et al. 1994; Uriz et al. 1995). Sponge specimens belonging to the same species but collected in different sampling sites showed further morphological differences. *Petrosia ficiformis* collected

in the acidified cave GM exhibited two different colour morphotypes. The different colour morphotypes were present as depigmented (white) bleached specimens characterized by thin and reticular structure; and as pigmented coloured specimens, which were massive and reddish-purple. Colour of *P. ficiformis* has been for years attributed, to cyanobacterial pigments –*e.g.* phycocyanin, phycoerythrin (Liaci and Sarà, 1964; Sarà, 1964; Sarà et al. 1998; Steindler et al. 2007; Vacelet and Donadey, 1977). Nonetheless, several of these studies provide contradictory evidence, reporting low abundance (~1%) of Cyanobacteria in either bleached and pigmented specimens (Burgsdorf et al. 2014; Sipkema et al. 2015). Ergo, the ultimate origin about the pigmentation of this sponges remains an open question. Findings from this study, in agreement with other surveys including dark and light adapted individuals suggest that the pigmentation could be related to photoprotection (see below). Previous findings highlighted strong differences in the morphology and growth dynamics of *P. ficiformis* inhabiting inside and outside marine caves. Bavestrello and Sarà (1992) investigating several marine caves reported *P. ficiformis* specimens charachterized by cylindrical or spherical shapes which lead to hypothesize a parasympatric speciation. Both morphotypes were different from conspecifics found outside the caves. Furthermore, violet and pink-white specimens coming from different Mediterranean areas and Atlantic Ocean again supported low gene flow and a strong genetic diversification (Burgsdorf et al. 2014; Riesgo et al. 2019). Investigation around potential genotypic splits and speciation in *P. ficiformis* remains open, while all the diverse phenotypes keep being assigned to the same species.

Within the cave GM, *C. reniformis* present as two different color morphs: the coloured morph was gray-brown, whereas the bleached morph was white, both with similar massive growth. This species has slow growth rates, attributed by some authors to a greater energy investment in massive collagenous rich body-plans, which seem to provide resilience towards environmental and ecological (Garrabou and Zabala, 2001). The darker ectosome of *C. reniformis* was ascribed to the presence of melanocyte cells, likely producing a melanin-like pigment with photo-protective properties (Bavestrello et al. 1998a; Nickel and Brümmer, 2003). This would explain the occurrence of bleached specimens in low irradiance habitats as in GM.

Bleached specimens of *Chondrilla nucula* were found within GM. This sponge was previously documented to colonize submarine caves, in a reduced size and bleached morphotype (Gaino et al. 1977); even if other authors assume that this species is strictly light dependent, due to trophic mutualistic associations with photosymbionts (Arillo et al. 1993).

Crambe crambe had a typical encrusting growth in all the sampling sites, except in the most acidified site Vullatura (VU), where it was collected as a massive-lobular morph on *Posidonia oceanica* rhizomes. Although this sponge is a widely studied species, previous investigations have not reported morphotypes as the one described here. *Crambe crambe* has been described as a slow growth species, but at the same time, it can be very efficient in colonizing new habitats (Galera et al. 2000; Garrabou and Zabala, 2001). The capability to efficiently compete for space, which allows fast colonization may be due chemical defense mechanisms developed by this sponge species (Becerro, 1997; Becerro et al. 1997). Our hypothesis about the massive growth of *C. crambe* at VU is that: on the one hand, the low pH may favour this species by displacing other potential competitors and having more access for exploiting resources; and on the other, the micro-habitat created on the rhizome of *P. oceanica* may concentrate higher amounts of organic matter available for the sponge to grow.

Different studies showed how sponges undergo morphological variability in responses to water flow and extreme current regimes (Bell and Barnes, 2000; Bell et al. 2002; Palumbi, 1986). Gaino and collaborators (1991) showed that the sponge *Clathrina clatrus*, underwent tissue rearrangement and morphological changes just in few hours, indicating morphological plasticity towards changes in the surrounding environment. Different morphotypes related to the growth in caves and crevices in the sponge *Aplysina aerophoba* have been also documented (Costa et al. 2020). All these findings indicate that environmental factors may influence the morphology of marine sponges, suggesting a huge plasticity of these animals to cope with different environmental constraints.

Our investigations on spicule characteristics highlighted the lack of significant differences in spicule size and morphology along the environmental pH gradient, nor across the different sites in the sponges *P. ficiformis, C. crambe* and *C. nucula*. Accordingly, previous studies reported no significant changes in spicule

characteristics of the sponge *C. crambe* under natural OA, while in the sponge *Mycale grandis* elevated pCO_2 under laboratory conditions seemed to reduce spicule size (Bell et al. 2018a; Goodwin et al. 2014; Vicente et al. 2016). Investigation in this field highlighted that morphological changes of spicules can be dependent upon the concentration of silicic acid (Uriz et al. 2003). Other studies suggest that low temperatures and high concentrations of organic matter coupled with high concentrations of silicates usually found in upwelling areas can be responsible for an increase of spicule size (Bavestrello et al. 1993; Uriz et al. 2003). Further manipulative experiments showed that different spicule types are produced in relation with different silicic acid concentrations (Maldonado et al. 1999). In this thesis *C. reniformis* was not analyzed in this perspective as it lacks spicules, although this species, can integrate exogenous siliceous and calcareous material into its collagenous ectosome, as a strategy to strengthen this layer (Bavestrello et al. 1998b). Such foreign materials, could be important to live in low carbonates environments and may explain the reduced growth under laboratory induced OA (Ribes et al. 2016). The ecological relevance of such exogenous intrusions being not analyzed in the present study needs to be addressed in future investigations.

Specimens coming from acidified *versus* control sites did not reveal relevant differences in ultrastructural traits, according to TEM observations. "Bacteriocytes", specialized cells containing morphologically different kinds of bacteria, were found in *P. ficiformis*, *C. reniformis*, and *C. nucula*. *C. crambe* lacked this feature and instead showed mostly free-living bacteria in the mesohyl.

Porifera lack intercellular junctions and this makes the interstitial fluid similar to that of the surrounding environment, making sponges unable to perform acid-base regulation, compared to other animals (Goodwin et al. 2014; Pörtner, 2008; Ruppert and Barnes, 1996). On the basis of this, it has been hypothesized that sponges can be vulnerable taxa to future acidified scenarios. This hypothesis, however, does not agree with several recent evidences, demonstrating that a number of demosponge species can thrive under low pH conditions (Bell et al. 2018a; Fabricius et al. 2011; Goodwin et al. 2014; Morrow et al. 2015; Ribes et al. 2016). The capacity of sponges to cope with extreme conditions, has been attributed to their structural plasticity (Bavestrello et al. 1996, 1998a; Bonasoro et al. 2001). Our findings reveal that there is no clear

direct effect of OA in any of the morphological aspect analyzed. The intraspecific morphotypes variability observed in our sponges likely resulted from a combined influence of other factors related to the particular sites GM (light, nutrient availability) and VU (reduced competition, microhabitat related nutrients).

5.3 Prokaryotic diversity in sponge microbiomes

The associated prokaryotic communities found in the sponges investigated in this study were different both in terms of richness and taxonomic composition, that were also diverse from the surrounding seawater. Most of the prokaryotic taxa were exclusive of each sponge, while a small number of ASVs were shared among sponge species, supporting high specie-specific diversities. The specificity of sponge microbiomes was further confirmed by the Gneiss Linear Model, highlighting that the factor "sponge species" explains 60% of microbial community variation. Independent from pH conditions, a stable core microbiome was found in each specimen of the same sponge species, resulting in a low intraspecific variability, with *P. ficiformis* showing the highest variability. Based on microbial abundance associated to sponges *P. ficiformis, C. reniformis, C. nucula* are considered "high microbial abundance" (HMA) species (Erwin et al. 2015; Moitinho-Silva et al. 2017), while *C. crambe* is considered a "low microbial abundance" (LMA) species (Croué et al. 2013; Gantt et al. 2017; Gloeckner et al. 2014; Moitinho-Silva et al. 2017). Our results revealed that such differences can be evident also in terms of the number of ASVs. Similar values of ASVs were found in *P. ficiformis* and *C. crambe*, which were two times higher than those found in *C. reniformis* and four times those in *C. nucula*. The high prokaryotic richness observed in *C. crambe* is somewhat surprising, as this species has been reported in different studies to possess very few (even one solely) associated bacteria (Croué et al. 2013; Gantt et al. 2017; Sipkema et al. 2015). Such bacteria based on morphological studies were apparently represented by a single morphological type (Maldonado, 2007; Vacelet and Donadey, 1977).

In this study, the microbiome of *C. crambe* was dominated by one ASV (accounting ~70-80% of the total sequences), belonging to the order *Betaproteobacteriales*. These results improve the taxonomic resolution of the main bacterial taxa associated to *C. crambe* and reinforce previous findings that reported the dominance of the phylum

Proteobacteria (80-90% of the microbiome; Björk et al. 2019; Gantt et al. 2017) in this sponge species. Being these taxa widespread in *C. crambe* independently from sampling sites, they may be the core symbiont bacteria which are acquired by this sponge species by vertical transmission (Sipkema et al. 2015).

Besides the dominant taxa, *C. crambe* was characterized by the presence of rare bacterial taxa (*i.e.* less abundant taxa), that were taxonomically variable among individuals collected in different sampling sites. A large number of ASVs in *C. crambe* were shared with the seawater (~200; more than doubled with respect to the other species), suggesting that these rare taxa can be also acquired from the surrounding environment.

In this study, we observed a relatively high number of reads affiliated to the phylum Cyanobacteria as previously reported by Sipkema and co-workers (2015), suggesting a no negligible role of photosynthetic symbionts in this sponge species. The *in silico* analysis of the putative functions of the microbiome associated to *C. crambe* revealed a wide array of metabolic functions similar in individuals collected in the different sites. Findings reported here highlighted that *C. crambe* possessed a high number of diversified and rare taxa that might be functionally redundant across sites: different taxa playing the same metabolic functions and benefiting the host, favoring its flexible adaptation to environmental gradients.

Petrosia ficiformis exhibited the richest and most diverse microbiome in prokaryotic associates. This species indeed showed a high intraspecific variability, which is the cause of the variable alpha diversity values. The dominant taxa belonged to the phyla *Chloroflexi* and *Gemmatimonadetes*, while *Cyanobacteria* displayed low relative abundances and were not a core Phylum. Previous investigations, based on morphological approaches, reported that this species hosted vacuoles rich in specialized symbiotic bacteria, and also an elevated number of cyanobacteria (Arillo et al. 1993; Sarà et al. 1998; Vacelet and Donadey, 1977). Other studies based on molecular analyses confirmed some of these outcomes, improving knowledge on the taxonomy of the microbes associated. Schmitt and co-workers (2012) revealed that microbiome associated with *P. ficiformis* was dominated mostly by the phyla *Chloroflexi* and *Proteobacteria*, with several other minor phyla involved. Burgsdorf and coauthors (2014) showed that *Chloroflexi* and *Gammaproteobacteria* dominated

the microbial composition of all the specimens of *P. ficiformis*, independently from the sampling site or the morphology. Within *Chloroflexi*, SAR202 clade and TK10 were dominant, while *Gammaproteobacteria* were mostly composed by KI89A, *Chromatiales* and *Xanthomonadales*. *Cyanobacteria*, displayed highly variable or low relative abundances, fact that was noticed also by other authors (Burgsdorf et al. 2014; Schmitt et al. 2012; Sipkema et al. 2015). Björk and collaborators (2017) showed that the core microbiome associated with *P. ficiformis* was mostly dominated by transient or opportunistic taxa. The apparent flexibility in microbial community associations might confer this species trophic plasticity and capability to colonize different habitats. Indeed, *P. ficiformis* has been described to acquire symbionts from the surrounding environment, and harbor diverse microbiomes according to biogeographical trends (Britstein et al. 2020; Burgsdorf et al. 2014; Díez-Vives et al. 2020).

Chondrosia reniformis analyzed in the present study was characterized by the most stable microbiome both in terms of composition and richness. The dominant phyla were *Chloroflexi*, *Acidobacteria* and *Proteobacteria*. *Cyanobacteria* were present in very low abundances. A previous morphological study on this sponge holobiont highlighted the presence of high abundant bacterial assemblages associated with this sponge (Sarà et al. 1998). However, only a few studies investigated the taxonomic composition of the microbiome. Björk and co-workers (2017) showed that prokaryotic assemblages associated to this sponge were mostly represented by commensal strains and were very stable over time with a dominance of *Chloroflexi*, *Proteobacteria* and *Gemmatimonadetes*.

Chondrilla nucula investigated here showed a quite stable microbiome. The core microbiome was composed by a high number of ASVs (52 ASVs, 40 bacterial orders), with a number of core taxa double when compared to the other sponges. *Chloroflexi, Proteobacteria and Cyanobacteria* were the most abundant phyla. This sponge species displayed the highest relative abundance of cyanobacteria (reaching ~ 25%). Most of the morphological studies performed in the past were focused on studying the cyanobacteria associates, which in this sponge seem to be key symbionts (Gaino et al. 1977; Liaci and Sarà, 1964; Sarà, 1964). Thiel and collaborators (2007) further showed that *C. nucula* hosted a stable and constant bacterial community that was similar across time and sampling locations. Our findings along with those available in the literature

support the hypothesis that in this sponge the microbiome is mostly inherited by vertical transmission (Maldonado, 2007; Maldonado et al. 2005).

Marine sponges, depending on the species and the environmental context, can acquire microbial associates by two major mechanisms: via horizontal acquisition from the surrounding seawater, or vertical transmission from parents to offspring. On this line, assemblages transmitted horizontally are in general more variable (*e.g.* depending on locations and external ecological conditions) and can occur in diverse species; whereas inherited symbiont populations are more stable across ecosystems (for affording ecological competence) and are often species-specific (Díez-Vives et al. 2020; Sipkema et al. 2015). *P ficiformis* displayed the richest and most diverse microbiome, but also the most variable out of the four species. This aligns with previous researches reflecting microbial changes with biogeography (Burgsdorf et al. 2014), fact that has been attributed to the capability of this sponges to retrieve microbes by horizontal transmission (Burgsdorf et al. 2014; Maldonado, 2007; Sipkema et al. 2015). Other species, such as *C. nucula* and *C. crambe* have been observed to harbor microbial assemblages since the first life stages, denotating substantial parental transfer of symbionts (Maldonado et al. 2005; Maldonado, 2007; Sipkema et al. 2015) In *C. crambe* though, large proportions of background bacterial taxa have been proposed to come from the environment, due to the great correspondence with the microbiota in the water column, supporting our findings above (Sipkema et al. 2015). No recent studies on this topic have been performed on the sponge *C. reniformis*, however this sponge was described in the past to transmit bacteria from the bacteriocytes enveloping the egg, into the offspring and juveniles after metamorphosis (reviewed in Sarà et al. 1998).

Predicted functions of the associated microbial communities from the target sponge species investigated in this study showed different functional profiles, coherent with the species-specificity of the microbiome. *P. ficiformis* and *C. reniformis* revealed functions mostly related to heterotrophic taxa (*e.g.* chemoheterotrophy, aerobic heterotrophy); whereas *C. crambe* and *C. nucula* were mostly linked to autotrophic functions, in correlation with the consistent presence of cyanobacteria. Microbes in sponges are capable of a number of processes, of which photosynthesis, methane oxidation, nitrification, nitrogen fixation, sulfate reduction, and dehalogenation are the

most important (Taylor et al. 2007). Functional traits seem to differ between HMA and LMA sponges, probably due to other co-existing factors, such as pumping rates or other environmental parameters (Lurgi et al. 2019). A study performed by Schläppy and co-workers (2010) though, showed that processes as nitrification and denitrification were found to occur together both in LMA and HMA species, suggesting that the co-occurrence of these processes in some sponges could be related to the microbiome capability to deal with aerobic and anaerobic conditions within the host. Overall, rather than a "taxonomic core" a "functional core" microbiome is likely crucial for holobionts survival, which may undergo functional microbiome redundancy, affording the key to thrive in harsh habitats (Burke et al. 2011). Indeed, a functional equivalence of associated microbial consortia has been previously investigated in sponges indicating that phylogenetically divergent microbiomes possess strong functional equivalences, highlighting an evolutionary convergence in complex symbiont communities (Fan et al. 2012). Moreover, other genomic constraints such as horizontal gene transfer, random nucleotide changes, mutations and mobile genetic elements can contribute to a phenotypic variation and development of adaptive traits in the sponge holobiont (Webster and Thomas, 2016). The impossibility to cultivate most of the microbes associated with marine sponges is a major burden in the knowledge on the functions performed by symbionts (Taylor et al. 2007). Despite these limitations, omics approaches combined with physiological experiments can contribute to a substantial knowledge improvement of microbiome functions, including nitrogen and carbon metabolism, sulfur oxidation and secondary metabolites production (Hentschel et al. 2012).

5.4 Sponge-Cyanobacteria associations

Cyanobacteria play a crucial role in some sponge holobionts by providing organic compounds and recycling inorganic nutrients, and the type of associations differ depending on the strains involved (Carpenter and Foster, 2002; Taylor et al. 2007; Webster and Taylor, 2012). The sponge species considered in this study showed differences both, in richness and in taxonomic compositions of Cyanobacteria. *C. nucula* showed the highest relative abundance of Cyanobacteria (~30%), largely dominated by *Synechococcus spongiarum*. This sponge is known to establish

symbioses with photosynthetic cyanobacteria, which are transferred to the offspring (Maldonado, 2007). These strict nutritional interactions require irradiated habitats, preventing the survival of sponge holobionts in dark conditions (Arillo et al. 1993; Usher et al. 2001; Thiel et al. 2007). However some specimens of *C. nucula* were previously found to colonize dark habitats (Gaino et al. 1977), highlighting that some individuals can adapt and survive also in dark conditions.

The cyanobacterial assemblages of *C. crambe* ranged from ~8 to 10% and were composed by ASVs belonging to the class *Oxyphotobacteria* and to the genus *Synechococcus*, that were also abundant in the seawater. *C. crambe* is also known to live in association with cyanobacteria, but up to now no metabolic or symbiotic interaction has been unveiled (Croué et al. 2013; Sipkema et al. 2015).

Several different taxa, mainly represented by members belonging to the family *Cyanobiaceae*, followed by members affiliated to the genera like *Synechoccoccus*, *Schizotrix*, *Phormidesmis* were found in *P. ficiformis*. Such taxa were found either in coloured and in white specimens, in agreement with previous studies (Burgsdorf et al. 2014; Sipkema et al. 2015). The colour of this sponge species has been previously associated with the presence of symbiotic Cyanobacteria, even when present in low abundances (~1% relative abundance); (Burgsdorf et al. 2014; Liaci and Sarà, 1964). Older studies highlighted associations of *Petrosia ficiformis* with *Aphanocapsa feldmannii*, now renamed as *Synechococcus feldmannii* (Burgsdorf et al. 2014; Liaci and Sarà, 1964; Sarà et al. 1998; Usher et al. 2004); as well as to the presence of cultivable cyanobacterial strains (Caroppo et al. 2012; Pagliara et al. 2020; Pagliara and Caroppo, 2011). Arillo and coauthors (1993) showed that *P. ficiformis* holobionts are able to activate heterotrophic metabolism in dark conditions. Transplants experiments from dark to light conditions resulted in the death of the sponge (Regoli et al. 2000), while aposymbiotic specimens growing in partially shaded environments were able to acquire color and photosynthetic symbionts (*i.e.* cyanobacterium *Candidatus Synechococcus feldmannii*) after several months (~ 7) of acclimatization (Britstein et al. 2020). From all the above, it seems like *P. ficiformis* forms loose interactions with cyanobacteria that can acquire from the environment. These associations are unlikely to have an intrinsic nutritional value, but instead seem to provide pigments and/or sunscreen compounds as means of photoprotection. Our

results though, suggest that the purple pigmentation attributed to *P. ficiformis* is not always correlated (as previously believed; *e.g.* Liaci and Sarà, 1964; Sarà, 1964; Sarà et al. 1998; Steindler et al. 2007; Vacelet and Donadey, 1977) to the massive presence of cyanobacteria, as co-occurring coloured and bleached sponges living in the cave system GM had similar microbial compositions. Moreover, specimens from the control site SA had very low relative abundance of cyanobacteria and had a purple-reddish color. Hence, we hypothesize that the photoprotective products supplied by cyanobacterial/microbial components might be coloured-less, as many microbial sunscreen compounds in the sea (Núñez-Pons et al. 2018).

In *C. reniformis* all the cyanobacteria were assigned to the strain *Synechococcus* CC9902 and accounted < 0.5%. *C. reniformis* is known to have a microbiome mostly composed by heterotrophic bacteria lacking cultivable cyanobacteria (Konstantinou and Voultsiadou, 2015; Sarà et al. 1998). In this study, negligible amounts of cyanobacteria were found associated to both coloured and bleached individuals. Actually, the pigments present in *C. reniformis* seem to derive from melanin-like compounds unrelated to photosynthetic microbial pigments (Bavestrello, Benatti, et al. 1998; Nickel and Brümmer, 2003).

The *in silico* analysis of the putative functions revealed a large prevalence of photoautotrophic-related functions in *C. nucula* and *C. crambe* whereas heterotrophic metabolism was predominant in *P. ficiformis* and *C. reniformis*. This agrees with the abundance and diversity results obtained in the present study and with the eco-physiological data previously reported (*e.g.* Arillo et al. 1993; Britstein et al. 2020; Gaino et al. 1977; Liaci and Sarà, 1964; Sarà et al. 1998; Sipkema et al. 2015). Most of the papers published up to date on sponge–Cyanobacteria associations however have provided poor taxonomic resolution ranks, often only at the Phylum level. Further investigations, thanks to 'omics platforms', are likely to provide finer taxonomies and functional information, to better understand these key associations and their ecological roles.

5.5 Mycobiomes associated with marine sponges

Marine fungi, and in particular those associated to metazoans are still a big mystery to unveil, when compared to prokaryotic symbionts (Amend et al. 2019). The study of fungi from host invertebrates has been usually performed through cultivation and subsequent identification of fungal strains (Bolaños et al. 2015; Marchese et al. 2020; Paz et al. 2010). These techniques provide a biased picture of the total fungal diversity (limited to those cultivable), and are usually aimed to find new strains for the discovery of secondary metabolites for biotechnological purposes (Baker et al. 2009; Marchese et al. 2020; Taylor et al. 2007). One limiting factor when studying fungal-invertebrates associations with metabarcoding techniques is the high prevalence of host co-amplification when using the ITS1 gene as marker, which is the most resolutive for Fungi (Yang et al. 2018). The amplification of untargeted host DNA can be highly variable across species, ranging from > 99% of the total reads (as in most sponges and corals), down to be undetectable (Amend et al. 2019). All these issues often humper fungal community analyses in Porifera holobionts. In this study a PCR-clamping protocol (Von Wintzingerode et al. 2000) has been applied to face this issue (based on Núñez-Pons, unpublished data). Another important challenge is the poor representation of marine fungal taxa in the public databases, which lead to an important fraction of AVSs being annotated as unidentified Fungi.

Results presented here indicated that mycobiomes associated with the target sponges did not display differences regarding richness, diversity or composition across the four species. This outcome was accompanied by an enormous intraspecific variability, which impeded any sample grouping, as well as the identification of any core mycobiome throughout the sample set. These findings contrast with those of prokaryotic associates, which showed clear species-specificity in bacteria and archaea communities. Here, fungal assemblages had stochastic distributions across species and sampling sites.

Most of the fungal taxa isolated from marine sponges belong to the genera *Aspergillus* and *Pennicillium,* which are distributed worldwide in terrestrial ecosystems. It remains still unveiled in most of the cases whether fungi are really associated with the source sponge, or even whether they are obligate marine species. These questions were previously addressed by Jones and coauthors (1980) which divided marine fungi in

two groups: primary marine fungi derived from marine ancestors; and marine fungi which are thought to have evolved from terrestrial ancestors. Höller and coauthors (2000) performed one of the first studies on fungi isolated from marine sponges. They isolated and identified morphologically a high number of fungal strains (n = 681) from a wide variety of marine sponges coming from different seas. The most common genera isolated were widespread known fungi like: *Aspergillus*, *Acremonium, Arthrinium, Coniothyrium, Fusarium*, *Mucor, Penicillium, Phoma, Trichoderma, Verticillium, Cladosporium.* Most of these strains were able to grow both in media with or without salt, suggesting that probably these strains are not obligate marine fungi, but may as well have a terrestrial origin. This study was carried out to discover new bioactive natural products (*e.g.* as anti-fungal, anti-bacterial and anti-algal compounds) and no information on the ecology or functions of these taxa was provided. Proksh and co-workers (2008) isolated 81 fungal strains, mostly belonging to the genera *Cladosporium, Penicillium, Petriella, Phialophora,* and *Engyodontium,* from the Mediterranean sponge *Suberites domuncula*. From these strains, 19 compounds were isolated and structurally elucidated for biological activity. Another isolation study was performed by Paz and coauthors (2010) who isolated and identified by means of molecular techniques, 85 fungal taxa from a Mediterranean sponge, *Psammocinia sp*.. Some of these fungal strains exhibited anti-fungal properties against cultivated fungal strains. In another study, Wang and coauthors (2009) studied the diversity of fungi associated with three Hawaiian sponges. They isolated and cultured more than 200 strains and suggested that fungi in marine environments can be divided in sponge-generalists (genera *Pennicillium, Aspergillus and Eupennicillium*) sponge-associates (genera *Ampelomyces, Tubercularia, Cladosporium*) and sponge-specialists (genera *Dydimella, Fusicoccum, Lacazia*). Insights on the unculturable mycobiome associated with the Hawaiian sponges *Suberites zeteki* and *Mycale armata* were provided by Gao and coauthors (2008). They tried several sets of primers targeting the internal transcribed spacer (ITS) and identified for the first time several taxonomic orders (*Malasseziales*, *Corticiales*, *Polyporales*, *Agaricales*, *Dothideomycetes and Chaetothyriomycetes incertae sedis*) highlighting a much higher fungal diversity in the marine sponges as compared with studies based on fungal isolation. Recent studies applying metabarcoding approaches on Mediterranean and North Sea sponges and

combined cultivation and metabarcoding in Australian species suggested that fungal associations, being highly variable, can be considered "accidental" (Naim et al. 2017; Nguyen and Thomas, 2018). Our results reinforce previous findings of a high similarity of sponge fungal communities with the surrounding seawater, suggesting a prevalent horizontal acquisition. There are some exceptions in the literature of yeasts reported to be transmitted vertically in *Chondrilla nucula* (Maldonado et al. 2005). A recent metagenomics study performed on two Antarctic sponges highlighted that among Eukarya, fungal sequences were highly represented and again shared with the surrounding seawater, leading to hypothesize that these fungi were probably non-symbiotic (Moreno-Pino et al. 2020).

In another recent study from Mediterranean area, Bovio and coauthors (2020) showed that the culturable mycobiota associated with three sponges (*i.e. Crambe crambe*, *Phorbas tenacior* and *Aplysina cavernicola*) was very different and hypothesized a role in the production of toxic secondary metabolites in *Crambe crambe*. Genomic investigation on fungi isolated from marine sponges by Zhou et al. (2011) detected polyketide synthase and non-ribosomal peptide synthase genes, suggesting a potential involvement in the biosynthesis of bioactive secondary metabolites with chemical defense role. The strains analyzed further displayed antimicrobial activity providing a direct evidence for the possible participation of these fungi in the antibiotic defense for sponge holobiont (Zhou et al. 2011). Another study confirmed that sponge isolated fungi containing polyketide synthase genes displayed moderate to strong in vitro cytotoxicity against human cell lines, confirming their bioactive potential (Yu et al. 2013).

In this study a high number of exclusive fungal ASVs were found in association with each sponge, suggesting that sponges could be a reservoir of fungal diversity in the marine environments. Sponge-fungi associations deserve more attention and a huge effort in order to provide new knowledge on this field, but marine mycology is a discipline in its infancy and many aspects remain undocumented (Jones, 2011). For these reasons further research applying molecular and culture-dependent approaches, combined with 'omics' are required to develop solid baseline knowledge for this Kingdom (*e.g.* www.marinefungi.org). This will allow to build databases that

complement taxonomy with metabolic profiles and potential functions, facilitating the study of host-mycobiome associations in the sea.

5.6 Microbiomes associated with sponge living in CO2 vents systems

Sponge microbiomes living under natural ocean acidification were for the first time studied in the Mediterranean Sea. The present study included HMA and LMA species and photosynthetic and non-photosynthetic sponges, and revealed that prokaryotic diversity patterns varied differently according to the holobiont species. Previous surveys carried out in CO_2 seep systems of Papua reported that sponge microbiomes were mostly stable across pH gradients, with slight species specific variation. Moreover, sponges hosting cyanobacteria symbionts apparently had an enhanced tolerance to lowered pH (Kandler et al. 2018; Morrow et al. 2015). Results reported in this study confirm a species-specific pattern of microbiomes dynamics along acidification gradients, but they do not allow identifying any clear relationship between the presence of cyanobacteria and adaptation to low pH conditions.

Among the four investigated species *Petrosia ficiformis* showed the most compelling results, exhibiting three diverse groupings of microbial clusters across sampling sites. Specimens from the three control sites (CCO, GF and SA) had overlapping microbiomes, diverse from those from the two acidified sites CAC and GM, which at the same time had significantly different microbial compositions with each other. In the acidified cave GM, coloured and bleached morphotypes had similar microbiomes, and displayed the highest diversity and number of exclusive ASVs. On this line, *P. ficiformis* was reported to modulate its microbiome according to the biogeography (Burgsdorf et al. 2014), and such plasticity seems to be attained via horizontal transmission (Britstein et al. 2020; Sipkema et al. 2015). Moreover, other studies highlighted that in this sponge species transient and/or opportunistic assemblages dominated the core microbiome, that are probably in competitive relationships among them (Björk et al. 2017). This ability to select microbes from the surrounding water column, and shape the microbiome under diverse conditions could, however, confer to this species the possibility to acclimatize or adapt to changing environmental conditions. A study performed by Ruiz and co-workers (2020) revealed interesting outcomes. These researchers found that the cave dwelling sponge *Plakina kanaky* had

a specialized microbiome that could be acquired both via vertical and horizontal mechanisms. Having the possibility perform both acquisition processes might improve the capability of the sponge holobiont to live in extreme environments such as the acidified cave, object of this study. *P. ficiformis* displayed in the other acidified site CAC the lowest richness compared with all the other sampling sites. Functional redundancy of microbial strains, mostly found in HMA sponges could be also the adaptive mechanism by which this sponge can be able to face low pH with a reduced microbial consortium (*e.g.* Ribes et al. 2016).

The bacterial taxa *Thermomicrobium sp.* (SAR202 clade), SAR116 clade, AqS1 (*Nitrosococcaceae*) and Sva0996 (*Microtrichaceae*) were correlated with acidification in *P. ficiformis*. Members of the SAR202 cluster are widespread in marine systems and may play an important role in biogeochemical cycles. (Mehrshad et al. 2018; Morris et al. 2004). Among these, members of the genus *Thermomicrobium* are thermophilic bacteria that in some cases can adapt not only to elevated temperature, but also to other extreme environmental conditions (Jackson et al. 1973). The symbiont *AqS1* is a sulfur-oxidizing gammaproteobacterium that was firstly isolated from the sponge *Amphimedon queenslandica*, capable of sulfur oxidation, carbon monoxide oxidation and inorganic phosphate assimilation (Gauthier et al. 2016). The strain Sva0996 has been reported as symbiont in sponges, but its functional and ecological role remain mostly unknown (Verhoeven et al. 2017), while as free living organism has been suggested to assimilate phytoplankton-derived dissolved protein (Li et al. 2020). Members of the SAR116 clade have been reported as free-living organisms that possess genes encoding for proteo-rhodopsin, and to be involved in phototrophic metabolism (Lee et al. 2019; Oh et al. 2010).

We reported that taxa associated to non-acidification conditions included KI89A clade, NB1-j. *Rhodothermaceae*, *Chloroflexus sp.*, *Candidatus Nitrosopumilus* and *Spirochaeta sp.*. The genus *Candidatus Nitrosopumilus* is a group of autotrophic ammonia oxidizing archaea previously found in sponges that play an important role in nitrogen cycling (Feng et al. 2016; Könneke et al. 2005). Instead genus *Chloroflexus* is composed by bacteria with very versatile trophic behavior, being able to use numerous organic carbon sources. *Spirochaeta* instead can be found in marine sediments, and have been also previously found in association with marine sponges,

even though no information are available on the specificity of these partnerships (Neulinger et al. 2010; Shivani et al. 2015).

Even though in different acidified environments we found an increase (GM) or decrease (CAC) of bacterial richness values, the taxa encountered in both acidified sites have been found as free-living organisms and, once acquired by the host, could confer a wide range of nutritional benefit to the sponge holobiont, increasing tolerance to low pH conditions and buffering the loss of other important strains. Moreover, *P. ficiformis* conversely to other sponges seems to not reproduce asexually, but may undergo inbreeding processes that lead to a defined population structures also in population located less than 50 Km apart (Riesgo et al. 2019). Bavestrello and coauthors (1992) showed genetic differences in two ecologically and morphologically distinct populations of *P. ficiformis* suggesting that these two forms might be considered as different species. Burgsdorf and co-workers (2014) also detected genetic differences between color morphs of this species, and showed that microbial symbionts were more similar in genetically different *P. ficiformis* coming from the same location than genetically similar from distant locations hypothesizing a biogeographic trend. Díez-Vives and coauthors (2020) confirmed a primary role of the genetic cluster in shaping the symbiont microbial structure in *Petrosia ficiformis.*

According to the distributional data, *Crambe crambe* seems to have the widest pH range. Its microbiome was dominated by a single ASVs (order: *Betaproteobacteriales*) that accounted for ~70-80% that likely derives from parental vertical transmission, as already reported in previous studies (Croué et al. 2013; Sipkema et al. 2015). Background, rare ASVs instead, are highly fluctuant and shared with the surrounding seawater. These results suggest that *C. crambe* may cope OA by maintaining a stable microbiome, but also by selecting free bacteria from the surrounding environment, which could confer specific benefits in terms of nutrient cycling under the particular conditions of the CO_2 vents. A previous study showed that the microbial compartment of *C. crambe* remained stable across polluted and non-polluted areas (Gantt et al. 2017). While Björk and co-workers (2017) found that this species had a steady core microbiome, likely as. This to some extent could represent an endurance tactic to deal with changing conditions, but also a minor flexible acquisition of new strains might be crucial to cope with extreme scenarios in this species.

Taxa ranked to specimens of *C. crambe* living in the acidified sites CAC, GM and VU included: *Filomicrobium sp*., *Rubripirellula sp*., *Blastopirellula sp*., *Persicirhabdus sp.*. *Rubripirellula* and *Blastopirellula* which are chemoheterotrophic bacteria previously found in sponges, and correlated with polyphosphate accumulation (Ou et al. 2020). *Filomicrobium* is a genus of aerobic and chemo-organotrophic bacteria (Schlesner, 2015). Instead members of the genus *Persicirhabdus* were previously found in sediments and seawater (Rahlff et al. 2019). Members of the genus *Ruegeria* have been previously isolated from the Mediterranean sponge *Suberites domuncula*. These taxa are involved mostly in the carbon metabolism from diverse organic sources, while some of their secondary metabolites (*e.g.* cyclopeptides) have antimicrobial properties, and could play a role in sponge-bacterial interactions (Mitova et al. 2004a; Mitova et al. 2004b; Wirth and Whitman, 2019).

Microbes such as *Endozoicomonas sp*., *Ruegeria sp*., *Flavobacteriaceae*, *Filomicrobium sp*. and *Formosa sp*. were found in sponges collected in the control sites CCO, GF and SA and therefore in non-acidification status. *Endozoicomonas* have been reported to be symbionts in coral and sponges, but also to have a free-living stage. Their function within sponge hosts appears to be related with the production of secondary metabolites for feeding deterrence, antibiotics and carbon and nitrogen metabolism (Neave et al. 2016). *Flavobacteriaceae* seem involved in the production of antibiotics and enzymes involved in the digestion of complex polymers (Gavriilidou et al. 2020). The dominant ASV found in *C. crambe* was assigned to the order *Betaproteobacteriales*, and this taxon has been hypothesized to be involved in the synthesis of ecologically relevant allelochemicals, pentaciclyc guanidine alkaloids *e.g.* crambescidines (Croué et al. 2013). These compounds display a wide array of strong cytotoxic activities (*e.g.* antibacterial, antiviral, antifungal, antiprotozoal), which may facilitate out-competition against exogenous microbes, upholding a consistent core microbiome (Shi et al. 2017b). We hypothesize that the microbial stability across natural OA gradients in *C. crambe* could be modulated via an active production of cytotoxic secondary metabolites by core dominant symbionts (*i.e.* microbes belonging to the taxon *Betaproteobacteriales*), as a strategy to promote survival. Additionally, background transient strains in the microbial community, and often overlooked in

previous studies (*e.g.* Sipkema et al. 2015), could provide new functional traits useful for the holobiont under changing conditions.

The most stable microbial assemblages across the natural gradient of pH were those associated with *Chondrosia reniformis*. Ribes and coauthors (2016) showed that the microbiome of *C. reniformis* remained stable under laboratory induced OA, while the growth of the sponge was severely affected. Another investigation performed by Björk and collaborators (2017) showed that the core microbiome of *C. reniformis* was always stable over time. Our surveys revealed no major modified growth patterns in relation with acidification, while the microbiome remained stable. As seen previously, certain biological parameters can be contrasting when studying these organisms in natural or laboratory conditions, as some environmental factors can be overseen in the last. As with *C. crambe* above, for certain sponge holobionts maintaining a robust core microbiome seems to be a winning strategy to thrive in extreme environments.

The bacterial community composition associated to *Chondrilla nucula* was different in GM with respect to the control sites (GF and SA). This sponge was, however, less abundant in the acidified sites, suggesting a lower tolerance to OA conditions. Small re-arrangements in the microbiome recorded in specimens from GM could confer this species some buffering effect to resist lowered pH values at the cave. Nonetheless, these small changes are unlikely to provide real tolerance, as reflected by the distribution and growth characteristics (Gaino et al. 1977) of this species in the acidified cave (GM). Cyanobacteria were proposed by Morrow and coauthors (2015) as to bestow some sort of OA tolerance to sponge holobionts, after observing higher abundances of this phylum in specimens living under low pH conditions. Results of the present study disagree with these assumptions, as cyanobacterial abundances did not vary significantly from acidified to control specimens, and slight variations could be caused by a different light regime. Moreover, *C. nucula* was absent in the other two acidified sites CAC and VU, characterized by a lower pH when compared to GM. Cyanobacteria associated with *C. nucula* all belonged to the species *Synechococcus spongiarum*, which is also one of the most common cyanobacteria species found in association with marine sponges (Erwin and Thacker, 2008; Steindler et al. 2005). Morrow and co-workers (2015) found that cyanobacteria belonging to the genus *Synechococcus* were more abundant in sponges growing under natural OA. However,

cyanobacteria symbionts of the genus *Synechoccoccus* associated to the sponge *Xestospongia muta* were considered to be mostly commensals without benefit for sponge holobionts (Tacker et al. 2005). On the contrary, cyanobacteria symbionts belonging to the species *Oscillatoria spongeliae* are likely to be essential for the sponge *Lamellodysidea chlorea* acting as mutualist symbionts (Thacker, 2005). Arillo and coauthors (1993) found that *C. nucula* underwent a progressive decline in dark conditions, while Gaino and collaborators (1977) described its presence in the same cave of this study (GM), as well as in other caves, as a white morphotype. Results from this investigation showed that *Synechococcus spongiarum* was found to be associated only with *C. nucula,* while *Synechococcus* CC9902, along with another ASV assigned to the class *Oxyphotobacteria* was found associated with *C. crambe*. Considering that the two sponge species have two different distributions across the acidified sites, we hypothesize that in *C. crambe* different cyanobacteria strains could confer a further adaptive benefits to the sponge holobiont, while in *C. nucula* this relationship seemed to not confer the same benefits as this sponge appeared to be the less tolerant to OA.

There are only a few studies addressing the effect of OA on sponges and their associated microbiome. Among these, most of the experiments have been performed under laboratory conditions, an approach that provide information on a rather small spatial and temporal scale, and often on scenarios far from those that could realistically happen (Foo et al. 2018; McElhany and Shallin Busch, 2013; Williamson et al. 2020). Bennett and coauthors (2017) showed that OA alone had weaker effects on sponges than increased temperatures. They performed an experiment that showed that phototrophic and heterotrophic sponges responded differently to OA. High CO_2 exacerbated temperature stress in heterotrophic sponge holobionts, while ameliorated the response of phototrophic sponge holobionts. Additionally, larval survival and settlement success of the sponge *Carteriospongia foliascens* was shown unaffected by increased temperature and OA treatments, and juvenile sponges exhibited greater tolerance than their adult counterparts. Ribes and co-workers (2016) showed that, under laboratory induced OA, the microbiome of three sponge species was stable, but different sponge species showed different capabilities to acquire new microbial strains from the surrounding environments. In particular, the microbiome of *Chondrosia reniformis* remained stable across the treatments, while *Dysidea avara* and *Agelas*

oroides were found to acquire several new ASVs across the treatments. *Dysidea avara* gained more ASVs in control conditions, whereas *Agelas oroides* acquired more in the acidified conditions. This fact suggests once more that some sponge holobionts have plasticity to acclimatize under stress conditions by modulating their microbiomes, and this trend is species-specific. Rastelli and coauthors (2020) showed that the sponge *Hemymicale columella*, when exposed to acidification lost calcifying bacteria, but this loss was lower when the exposition was performed in tanks shared with a living community of species mimicking natural coralligenous ecosystems. A background biodiversity of holobionts may indeed serve as reservoirs of 'beneficial' microbial taxa that could assist in mitigating the effect of OA on sponge microbiomes. Lesser and collaborators (2016) found that combined effects of warming and acidification destabilized the microbiome of the sponge *Xestospongia muta*; in particular affecting the symbiotic cyanobacteria, and interfering on the nutrient transfer to the sponge holobiont. Exposition to low pH revealed no apparent effects on the sponge *Carteriospongia foliascens* nor on its associated microbial communities. Nonetheless, differences in the microbiome, in terms of presence and abundance of certain suits of bacteria were detected in the offspring. These outcomes imply that some vertically transmitted AVSs could potentially contribute to environmental adaptation of sponge holobionts (Luter et al. 2020).

A very low number of studies report the effect of OA on sponge associated microbiomes with an in situ approach. Morrow and coauthors (2015), while working at the cold seeps system of Papua, observed that *Synechococcus* cyanobacteria in *Coelocarteria singaporensis* and *Cinachyra sp*. doubled their relative abundances under lower pH; whereas, cyanobacteria in *Stylissa massa* manifested minor changes. As mentioned in previous sections, some cyanobacteria strains may be able to buffer the negative effects of elevated pCO_2, by using it for their metabolism, at the same time providing energy and protection for the host. In a reciprocal sponge transplant at the same Papua vents, Kandler and coauthors (2018) found changes in the microbiome across sampling sites in the species *Coelocarteria singaporensis*, as opposed to the maintenance of a stable microbial community in *Stylissa cf. flabelliformis*.

Research on microbiome dynamics under OA has been conducted in other non-sponge holobionts. A study performed by Webster and coauthors (2013) showed that after six

weeks of exposure to high pCO_2 and despite no detection of visible signs of host stress, microbial communities associated with some coral reef calcifiers (*i.e.* coral, foraminifera, crustose coralline algae) had substantial perturbations. Other studies on *Porites* spp., considered to have more OA tolerance, revealed stability in microbial communities (O'Brien et al. 2018). Contrastingly, Morrow and collaborators (2015) showed that along natural gradients of lower pH the corals *Acropora millepora* and *Porites cylindrica* underwent deep divergences in their associated microbial communities. The Mediterranean scleractinian corals *Balanophyllia europea* and *Cladocora caespitosa* exhibited the lack of significant effects in their physiology nor on their associated microbial communities when transplanted onto acidified sites at Ischia seeps (Meron et al. 2012). Instead, soft corals living along those vents systems showed differences in the microbiomes related to the different pH conditions (Biagi et al. 2020; Meron et al. 2013). Overall, long term adaptation to OA seems to entail rearrangements in the microbiome for some holobionts, as well as stability for others, with the definitive aim to fulfill nutritional requirements and maintain health and homeostasis.

5.7 Metabolomics profiles of sponges inhabiting natural CO_2 vents

A comparison of the metabolomic signatures associated to the two sponge species, *Petrosia ficiformis*, and *Crambe crambe*, recovered along the volcanic CO_2 seep system off Ischia island, was conducted. Untargeted metabolomics on the most nonpolar chemical fraction, containing mostly lipids, revealed two different metabolic profiles. *Petrosia ficiformis* yielded a larger number of detectable metabolites, as compared with *Crambe crambe*. The differences were also reflected in the classes of compounds identified for the two species. Only ten metabolites were shared between the two species, highlighting very diverse metabolomes mostly composed by exclusive compounds. These differences were chiefly related to the species specificity of the sponge holobiont, as co-occurring specimens from either species across the acidification gradient, produced highly different metabolites interspecifically, but similar intraspecifically. Likewise, changes in the metabolome between sites followed very different patterns in the two species (see below).

Both species were found to possess as the most representative lipid molecular classes triglycerides (TG), phosphatidyl cholines (PC), phosphatidyl ethanolamines (PE), diglycerides (DG) and ceramides (Cer). Moreover, *C. crambe* was characterized by the presence of the cholesterol esters (ChE), which were not identified in *Petrosia ficiformis*. Conversely *P. ficiformis* had eight exclusive molecular classes, most belonging to the family of phospholipids (PL): *i.e*. hexosylceramides, Hex1Ce; methyl phosphatidylcholines, MePC; phosphatidylglycerols, PG; phosphatidylinositols, PI; phosphatidylserines, PS; sulfatides, ST; stigmasterol esters, StE; wax esters, WE; zymosterol Esters, ZyE.

Marine organisms produce a variety of lipids, some of them are constitutive or structural, while others are linked to diet, life cycle, and ecological interactions (Bergé and Barnathan, 2005). Among the coelenterate, large amounts of tetracosapolyenoic acids, were found in different orders of the Octacorallia, while gorgonians are known sources of methylene-interrupted poly unsaturated fatty acids (PUFA). Significant amounts of tetracosa-polyenoic acids were found in different echinoderms, such as Ophiuroidea and Crinoidea. Poly unsaturated fatty acids (PUFA) are also highly represented in tunicates. In bivalve molluscs peculiar PUFA such as eicosapentaenoic acid (EPA) and docosahexaenoic acid (DHA) were found to account for high amounts, while cephalopod molluscs contain high concentrations of PUFA, followed by SFA and MUFA, EPA and DHA (Bergé and Barnathan, 2005). Marine invertebrates, especially sponges, have proved to be a rich source of many unusual fatty acids (FA), but phospholipids are the main class of polar lipids found in marine sponges (Rod'kina, 2005). Among sponge phospholipids, several classes of molecules are very common, including: phosphatidyl choline (PC), phosphatidyl ethanolamine (PE), phosphatidyl serine (PS), phosphatidyl glycerin (PG), phosphatidyl inosite (PI), and diphosphatidyl glycerin (DPG). In some species in particular, aminophospholipids (PE and PC), can account up to 50% (Rod'kina, 2005). Findings reported in previous studies provided evidence that *P. ficiformis* was characterized by a lipid composition rich in phospholipids, dominated by phosphatidyl ethanolamines (PE; accounting for 28%), followed by phosphatidylcholine (PC, 21%), phosphatidylglycerols (PG, 14%), phosphatidylserine (PS, 12%), phosphatidylinositols (PI, 7%). Other compounds known to be constituents of a marine bacteria, such as 9-hexadecenoic, 15-methyl-9-

hexadecenoic and l-octadecenoic acid were also identified, suggesting a tight connection between microbes and sponge metabolomes (Ayanoglu et al. 1982). To the best of our knowledge, no studies have addressed lipidomics or metabolomics in *C. crambe*. The only chemical studies on this species have been carried out for assessing bioactive secondary metabolites (guanidine alkaloids), of which the biosynthesis and metabolic function are still debated (*e.g.* Becerro, 1997; Becerro et al. 1997; Berlinck et al. 1993; Bondu et al. 2012; Croué et al. 2013; Silva et al. 2019).

Metabolite profiles were further analyzed across conspecific specimens living under the natural gradient of lowered seawater pH, associated to Ischia volcanic CO_2 vents. Untargeted analysis of primary metabolites comparing *P. ficiformis* sponges across sites unveiled that specimens from the acidified cave (GM) displayed a divergent metabolome with respect to samples from all the other sites. Conversely samples of *P. ficiformis* from the acidified CAC and the two controls GF and SA yielded similar outcomes from each other. A consortium of metabolites was identified as drivers for sample grouping, separating GM from the rest. This is, certain metabolic features were highly ranked with the acidified cave GM and poorly ranked with the controls and CAC. Instead, other compounds exhibited the opposite ranking trends.

No significant differences in the overall primary metabolites pattern were found in *C. crambe* across acidified and control sites. However, a differential set of metabolite features appeared to be responsible of a certain separation between the acidified groups CAC and VU with respect to the controls SA and GF.

The two sponge species exhibited divergent secondary metabolite patterns, as has already been described in the literature (Becerro et al. 1997; Zhou et al. 2015). Specimens of *C. crambe* from acidified and non-acidified sites, did not show relevant differences in secondary metabolite composition according to TLC and NMR data. Therefore, no deeper analysis was performed at this point. *C. crambe* is known to produce a wide set of bioactive secondary metabolites, with ecological and biotechnological relevance (Becerro et al. 1997; Pérez-López et al. 2014). These include the crambines, which are guanidine alkaloids with ichthyotoxic activities (Berlinck et al. 1990, 1992, 1993; Bondu et al. 2012; Silva et al. 2019). Furthermore, a family of pentaciclyc guanidines, crambescidines are known to have cytotoxic and anti-viral properties. These metabolites play putative important defensive functions

against predation and spatial competition. Indeed, certain allelochemicals that afford toxicity in this sponge were proved to be strategically allocated towards the external "ectosome", in peculiar cells named "spherolous cells", playing roles in avoiding fouling organisms (Becerro, 1997; Uriz et al. 1996).

Spectroscopic analyses based on TLC and NMR, disclosed characteristic secondary metabolite profiling in *P. ficiformis* across sampling sites. After chemical fractionation and elucidation, a peculiar group of polyacetylene compounds belonging to the family of the petroformynes resulted to be the major drivers of this pattern. In particular, specimens coming from the acidified cave GM were found to possess a group of three non-polar polyacetylenes that were exclusive from this sample group and absent in all the other specimens. In lieu, sponges from the controls GF and SA and the other acidified site CAC were found to contain five polar polyacetylenes absent in GM. Two additional petroformynes were common to all samples, one in background concentrations, and the other as minor metabolite in GM, but dominant in the other sites. Sponges of the genus *Petrosia* are a distinctive source of hydroxylated polyecetylenic compounds, which are indeed considered generic molecular markers (Cimino et al. 1985, 1990; Guo et al. 1994, 1995, 1998). Within the overall known polyacetylenes, ca. one third has been isolated from *Petrosia* spp. sponges (Mejia et al. 2013). These molecules contain carbon chains (ranging from C44 to C47), decorated with a high number of hydroxyl, keto, acetylenic, and non-conjugated cis/transalkenes (Minto and Blacklock, 2008; Zhou et al. 2015). Other studies on *P. ficiformis* collected in different geographic areas highlighted that this sponge can produce different polyacetylenes with different chemical conformations (Guo et al. 1998; Minto and Blacklock, 2008). Cimino and coauthors (1981) also found different polyacetylenic compounds in specimens collected in a dark cave, as compared to those from sponges collected in irradiated conditions. In this study, two different morphotypes, white and purple were retrieved within the semi-submerged acidified cave GM, where light was not totally absent. Both morphological phenotypes of *P. ficiformis* were characterized by overlapping metabolomic signatures and similar production of polyacetylenic compounds. This fact highlights that external macroscopic dichotomies do not always lead to changes in intrinsic functional aspects of the phenotype. The family of the polyacetylenes compounds include molecules that

are bioactive as anti-microbial and anti-mycobial agents, as well as embryo-toxic against starfish eggs. In *P. ficiformis* polyacetylenes have yielded cytotoxicity against several human cell lines an against brine shrimps (Guo et al. 1994; Kim et al. 1998; Kim et al. 1999; Lee et al. 2013; Lim et al. 1999; Lim et al. 2001a; Lim et al. 2001b). Moreover, polyacetylenic compounds of *P. ficiformis* are accumulated by its predator, the nudibranch *Peltodoris atromaculata*, as means of chemical defense (Castiello et al. 1980).

In the sponge samples analyzed in the present study, polyacetylene fractions of the non-polar and most polar compounds represented ca. 20% and 30% respectively of the dry weight of the crude extract. Considering that synthesis and/or bioaccumulation of these compounds is likely to be metabolically expensive, the massive presence of petroformynes in sponge holobionts is likely to respond to an important functional requirement. Actually, although the ecological function of polyacetylenes in *P. ficiformis* is still unclear, a putative defensive role has been hypothesized (Cimino et al. 1985). Regarding the biosynthesis, these compounds seem to derive from fatty acids even if the real biosynthetic pathway is still unclear. Their chemical diversity, however, led to hypothesize that polyacetylenes can be produced by certain microorganisms associated with sponges (Minto and Blacklock, 2008; Zhou et al. 2015). The characteristic non-polar polyacetylenes found in sponges from the acidified cave GM, could in this sense be derivative dehydrated compounds from the more polar (oxidized) polyacetylenes found in the rest of the sites.

The exceptional selection for dehydrated petroformynes exclusively within GM samples seems to respond to further additional factors inside the cave besides the lowered pH, as sponges from CAC (also acidified) were characterized by the oxidized products. We hypothesize that the more non-polar dehydrated petroformynes forms should provide particular benefits to sponges living at GM, in relation to physiological and ecological traits, aligned to the environmental conditions found in the acidified cave. *Viceversa*, oxidized polyacetylene compounds are probably needed by sponge holobionts outside the cave to provide other type ecological roles, related to protection against different infective microorganisms, predators (*e.g.* mollusks, fish) or other potential competitors. Interestingly, some of these secondary metabolites found in our

sponges could be new to science, which is surprising because this species has been widely studied for its chemical ecology.

The diverse metabolic composition patters reported in our sponge samples could, at least in part, be linked to the microbiome compositions associated with each species. *C. crambe* exhibited similar lipid and secondary metabolites signatures across acidified and non-acidified conditions, and displayed also consistent microbial compositions across sites. On top of this, a consortium of bacteria showed to have differential abundances across the sampling sites, separating the acidified sites VU and CAC from the controls GF and SA, with a pattern that was analogous to that observed for the metabolomics data. This may suggest that minor background microbial taxa could be involved in providing coupled metabolic signatures. Primary (lipids) and secondary (polyacetylenes) metabolites profiling displayed coincident drifts in *P. ficiformis*, yielding similar signatures throughout the three control sites and the acidified site CAC, which were divergent from those at the acidified cave GM. Such pattern somewhat matched the trends found for the associated microbial communities. Sponges from the control sites shared similar microbiomes and similar metabolic signatures, which were both highly divergent from those coming from GM. In CAC instead, the sponges had different microbial compositions from the rest of the sites, yet similar metabolomes as the controls. *P. ficiformis* in the acidified cave GM, was characterized by a different lipid metabolic profile and diverse production of polyacetylenic compounds, and revealed also a different microbiome from the rest of the sites. This may suggest that different primary and secondary metabolites might be produced by different microbiomes. But furthermore, that different metabolites acting as microbiome modulators (*e.g.* polyacetylenes) could play a role in shaping the microbial communities associated with the holobiont. All the above seems to suggest that the species analyzed in the present work may have adopted diverse strategies to cope with ocean acidification. Moreover, this suggest that microbial associates are likely playing a role in modulating the metabolism of their holobiont, but there may be other drivers participating in such mechanism.

A scarce number of studies on sponge microbiome-metabolome interactions has been published up to date, in spite of the growing evidence interconnecting these two fields, for trophic and allelochemical means (*e.g.* Botté et al. 2019; Mohanty et al. 2020;

Villegas-Plazas et al. 2019). Botté and coauthors (2019) showed a shift in the metabolic pathways of the microbiomes associated to two sponges collected under natural seawater acidification. However, metabolic signatures were assessed by means of predicted functions related to the microbial composition. Villegas-Plazas and coauthors (2019), instead, reported a microbial shift in the Caribbean sponge *Xestospongia muta* mainly related to season and depth and only partially reflected in the metabolomic signatures. Mohanty and coauthors (2020) investigated microbiome-metabolome interactions in two congeneric sponge species. They found that the two sponges showed a similar microbiome (at Phylum level), and a similar overall metabolome, while secondary metabolite profile was different. Some specimens showed greater abundance and diversity of sarasinosides, and others were enriched of melophlins. These findings suggest that similar players (same microbiome) could display a different metabolic profile. Findings from the present study suggest that sponge holobionts can have different microbiome/metabolic interactions depending on the environmental conditions, on the specific species and the relative ecological niches. Most of the available literature information provided insights on the sponge microbiome or metabolome alone, lacking of an integrated and multidisciplinary approach. Coupled microbiome and metabolomics approaches for investigating marine sponge holobionts are still in infancy, deserving big deal of development throughout diverse species inhabiting different ecosystems. Advances in these lines are highly timely, considering the prediction that Porifera, for their bio-ecological features, will thrive in the future global climate change scenarios.

6. GENERAL CONCLUSIONS AND FUTURE PERSPECTIVES

This research based on the analysis of multiple multi-scalar phenotypic traits – *i.e.* from the species distribution, morphology and ultrastructure, to the associated microbiomes and metabolomes, provides new insights on the adaptation of sponge holobionts to natural OA conditions. Our discoveries broaden knowledge on the state of the art regarding microbiomes and metabolomes associated with sponge holobionts adapted to live in extreme conditions. The four Porifera species investigated displayed different microbiomes, and diversified patterns of acclimatization traits across a natural gradient of acidification, ranging, on average from pH 7.1 to 7.8 and oscillating down to 6.8. Prokaryotic communities seemed to be modulating the acclimatization processes to OA, in contrast with the fungal associates, which appeared stochastically. Changes in the microbiome related to low pH conditions were mainly found in *P. ficiformis* and in *C. crambe*. Slight differences were found in samples from GM in *C. nucula*, while *C. reniformis* showed the most stable microbiome. Metabolomics analyses on *P. ficiformis* and *C. crambe* revealed different metabolic profile patterns. *C. crambe* had consistent signatures of primary and secondary metabolites across sites, with minor features changing in the acidified sites. Instead, marked differences were found in the metabolome of *P. ficiformis* only for samples coming from the cave GM as compared with the other sites. This trend was congruent with that found for the characteristic secondary metabolite family of polyacetylenes (petroformynes), which revealed several potentially new molecules to science. No morphological adjustments in growth form or spicular morphometry were found to be directly related to acidification. Despite diverse morphotypes were found in specimens living in the acidified sites GM and VU, the low pH is not likely to be the ultimate driver, as CAC (also acidified) harbored "normal" morphotypes. In the semi-submerged acidified cave GM, the peculiar environmental conditions, in association with the acidification of the seawater appeared to be synergistically acting as selective forces in shaping traits regarding: growth morphology in *C. nucula*, *C. reniformis* and *P. ficiformis*, microbial

communities in *C. nucula* and *P. ficiformis*, and metabolic profiles in *P. ficiformis*. As a general conclusion from this research, we found a general tolerance of sponge holobionts to OA scenarios, with acclimatization processes that were species-specific. Sponge holobionts represent optimal models to investigate the potential effects of global climate change due to their wide plasticity, fact that makes this phylum be forecasted as winner players in future acidification scenarios. Despite these predictions, research on acclimatization to OA is still scarce on this taxon. The Mediterranean Sea hosts more than 600 sponge species (Manconi et al. 2013; Pronzato et al. 2013), but deep knowledge on life cycle, physiology, microbiome, and metabolomics has been provided for less than ten, mostly being components of near shore communities. Improving knowledge on the phenotypic traits that Porifera implement to acclimatize to environmental stress is a timely assignment to understand how benthic ecosystems will face the ongoing anthropogenic and climate-driven impacts and their ecological cascading effects. In this sense, natural laboratories, such as cold CO_2 vents offer a unique opportunity to study long-term organismal adaptations to future foreseen scenarios (Alteriis, 2014; Gambi et al. 2016; Foo et al. 2018), taking also into consideration other environmental factors (*e.g.* pollution, increased temperature, turbidity) that could be act synergistically (Bennett et al. 2017). More research involving reciprocal transplants experiments to track acclimatization changes, and/or isotopic studies to decipher variability in the trophic ecology are needed. In general, multi-disciplinary multi-scalar researches that involve macro-, micro- and molecular aspects of the holobionts, and applying cutting edge techniques in field monitoring, imaging and 'omics' seem to be optimal approaches for an holistic understanding of how marine benthic communities will handle the inexorable changes of our Planet.

7. BIBLIOGRAPHY

Albright, R., Mason, B., Miller, M., & Langdon, C. (2010). Ocean acidification compromises recruitment success of the threatened Caribbean coral Acropora palmata. *Proceedings of the National Academy of Sciences of the United States of America*. https://doi.org/10.1073/pnas.1007273107

Alma, L., Kram, K. E., Holtgrieve, G. W., Barbarino, A., Fiamengo, C. J., & Padilla-Gamiño, J. L. (2020). Ocean acidification and warming effects on the physiology, skeletal properties, and microbiome of the purple-hinge rock scallop. *Comparative Biochemistry and Physiology -Part A : Molecular and Integrative Physiology*. https://doi.org/10.1016/j.cbpa.2019.110579

Alteriis, D. (2014). *Emissioni sommerse di co 2 lungo le coste dell'isola d'ischia: 150*(Dc), 67–79.

Amend, A., Burgaud, G., Cunliffe, M., Edgcomb, V. P., Ettinger, C. L., Gutiérrez, M. H., Heitman, J., Hom, E. F. Y., Ianiri, G., Jones, A. C., Kagami, M., Picard, K. T., Quandt, C. A., Raghukumar, S., Riquelme, M., Stajich, J., Vargas-Muñiz, J., Walker, A. K., Yarden, O., & Gladfelter, A. S. (2019). Fungi in the marine environment: Open questions and unsolved problems. In *mBio*. https://doi.org/10.1128/mBio.01189-18

Anderson, M. J., Gorley, R. N., & Clarke, K. R. (2008). PERMANOVA+ for PRIMER: Guide to Software and Statistical Methods. In *Plymouth, UK*.

Arillo, A., Bavestrello, G., Burlando, B., & Sarà, M. (1993). Metabolic integration between symbiotic cyanobacteria and sponges: a possible mechanism. *Marine Biology*. https://doi.org/10.1007/BF00346438

Ayanoglu, E., Walkup, R. D., Sica, D., & Djerassi, C. (1982). Phospholipid studies of marine organisms: III. New phospholipid fatty acids from Petrosia ficiformis. *Lipids*. https://doi.org/10.1007/BF02535368

Baker, P. W., Kennedy, J., Dobson, A. D. W., & Marchesi, J. R. (2009). Phylogenetic diversity and antimicrobial activities of fungi associated with haliclona simulans isolated from irish coastal waters. *Marine Biotechnology*. https://doi.org/10.1007/s10126-008-9169-7

Basso, L., Hendriks, I. E., & Duarte, C. M. (2015). Juvenile Pen Shells (Pinna nobilis) Tolerate Acidification but Are Vulnerable to Warming. *Estuaries and Coasts*. https://doi.org/10.1007/s12237-015-9948-0

Bastian, M., Heymann, S., & Jacomy, M. (2009). Gephi: An Open Source Software for Exploring and Manipulating Networks. *Third International AAAI Conference on Weblogs and Social Media*. https://doi.org/10.1136/qshc.2004.010033

Bavestrello, G., Arillo, A., Calcinai, B., Cerrano, C., Lanza, S., Sara', M., Cattaneo-Vietti, R., & Gaino, E. (1998a). Siliceous particles incorporation in chondrosia reniformis (porifera, demospongiae). *Italian Journal of Zoology*. https://doi.org/10.1080/11250009809386771

Bavestrello, G., Benatti, U., Calcinai, B., Cattaneo-Vietti, R., Cerrano, C., Favre, A., Giovine, M., Lanza, S., Pronzato, R., & Sara, M. (1998b). Body polarity and mineral selectivity in the demosponge Chondrosia reniformis. *Biological Bulletin*. https://doi.org/10.2307/1542819

Bavestrello, G., Bonito, J., & Sarà, M. (1993). Influence of depth on the size of sponge spicules. *Scientia Marina*.

Bavestrello, G., Burlando, B., & Sara', M. (1988). The architecture of the canal systems of Petrosia ficiformis and Chondrosia reniformis studied by corrosion casts (Porifera, Demospongiae). *Zoomorphology*, *108*(3), 161–166. https://doi.org/10.1007/BF00363932

Bavestrello, G., Cerrano, C., Cattaneo-Vietti, R., Sara, M., Calabria, F., & Cortesogno, L. (1996). Selective incorporation of foreign material in chondrosia reniformis (porifera, demospongiae). *Italian Journal of Zoology*. https://doi.org/10.1080/11250009609356136

Bavestrello, G., & Sarà, M. (1992). Morphological and genetic differences in ecologically distinct populations of Petrosia (Porifera, Demospongiae). *Biological Journal of the Linnean Society*. https://doi.org/10.1111/j.1095-8312.1992.tb00655.x

Becerro, M. A., Uriz, M. J., & Turon, X. (1994). Trends in space occupation by the encrusting sponge Crambe crambe: variation in shape as a function of size and environment. *Marine Biology*. https://doi.org/10.1007/BF00346738

Becerro, Mikel A. (1997). Multiple functions for secondary metabolites in encrusting marine invertebrates. *Journal of Chemical Ecology*. https://doi.org/10.1023/B:JOEC.0000006420.04002.2e

Becerro, Mikel A., Uriz, M. J., & Turon, X. (1997). Chemically-mediated interactions in benthic organisms: The chemical ecology of Crambe crambe (Porifera, Poecilosclerida). *Hydrobiologia*. https://doi.org/10.1007/978-94-017-1907-0_9

Bell, J. J., & Barnes, D. K. A. (2000). The influences of bathymetry and flow regime upon the morphology of sublittoral sponge communities. *Journal of the Marine Biological Association of the United Kingdom*. https://doi.org/10.1017/S0025315400002538

Bell, James J. (2008). The functional roles of marine sponges. *Estuarine, Coastal and Shelf Science*, *79*(3), 341–353. https://doi.org/10.1016/j.ecss.2008.05.002

Bell, James J., Barnes, D. K. A., & Shaw, C. (2002). Branching dynamics of two species of arborescent demosponge: The effect of flow regime and bathymetry. *Journal of the Marine Biological Association of the United Kingdom*. https://doi.org/10.1017/S0025315402005465

Bell, James J., Bennett, H. M., Rovellini, A., & Webster, N. S. (2018a). Sponges to be winners under near-future climate scenarios. In *BioScience*. https://doi.org/10.1093/biosci/biy142

Bell, James J., Davy, S. K., Jones, T., Taylor, M. W., & Webster, N. S. (2013). Could some coral reefs become sponge reefs as our climate changes? *Global Change Biology*, *19*(9), 2613–2624. https://doi.org/10.1111/gcb.12212

Bell, James J., Rovellini, A., Davy, S. K., Taylor, M. W., Fulton, E. A., Dunn, M. R., Bennett, H. M., Kandler, N. M., Luter, H. M., & Webster, N. S. (2018b). Climate change alterations to ecosystem dominance: how might sponge-dominated reefs function? *Ecology*, *99*(9), 1920–1931. https://doi.org/10.1002/ecy.2446

Bennett, H., Bell, J. J., Davy, S. K., Webster, N. S., & Francis, D. S. (2018). Elucidating the sponge stress response; lipids and fatty acids can facilitate survival under future climate scenarios. *Global Change Biology*, *24*(7), 3130–3144. https://doi.org/10.1111/gcb.14116

Bennett, H. M., Altenrath, C., Woods, L., Davy, S. K., Webster, N. S., & Bell, J. J. (2017). Interactive effects of temperature and pCO2 on sponges: from the cradle to the grave. *Global Change Biology*, *23*(5), 2031–2046. https://doi.org/10.1111/gcb.13474

Bergé, J. P., & Barnathan, G. (2005). Fatty acids from lipids of marine organisms: Molecular biodiversity, roles as biomarkers, biologically active compounds, and economical aspects. In *Advances in Biochemical Engineering/Biotechnology*. https://doi.org/10.1007/b135782

Berlinck, R. G. S., Braekman, J. C., Daloze, D., Bruno, I., Riccio, R., Ferri, S., Spampinato, S., & Speroni, E. (1993). Polycyclic guanidine alkaloids from the marine sponge crambe crambe and Ca++ channel blocker activity of crambescidin 816. *Journal of Natural Products*. https://doi.org/10.1021/np50097a004

Berlinck, R. G. S., Braekman, J. C., Daloze, D., Bruno, I., Riccio, R., Rogeau, D., & Amade, P. (1992). Crambines C1 and C2: Two further ichthyotoxic guanidine alkaloids from the sponge crambe crambe. *Journal of Natural Products*, *55*(4), 528–532. https://doi.org/10.1021/np50082a026

Berlinck, R. G. S., Braekman, J. C., Daloze, D., Hallenga, K., Ottinger, R., Bruno, I., & Riccio, R. (1990). Two new guanidine alkaloids from the mediterranean sponge crambe crambe. *Tetrahedron Letters*. https://doi.org/10.1016/S0040-4039(00)97109-0

Biagi, E., Caroselli, E., Barone, M., Pezzimenti, M., Teixido, N., Soverini, M., Rampelli, S., Turroni, S., Gambi, M. C., Brigidi, P., Goffredo, S., & Candela, M. (2020a). Patterns in microbiome composition differ with ocean acidification in anatomic compartments of the Mediterranean coral Astroides calycularis living at CO2 vents. *Science of the Total Environment*. https://doi.org/10.1016/j.scitotenv.2020.138048

Björk, J., O'Hara, R., Ribes, M., Coma, R., & Montoya, J. (2017). The dynamic core microbiome: Structure, dynamics and stability. *BioRxiv*. https://doi.org/10.1101/137885

Björk, J. R., Díez-Vives, C., Astudillo-García, C., Archie, E. A., & Montoya, J. M. (2019). Vertical transmission of sponge microbiota is inconsistent and unfaithful. *Nature Ecology and Evolution*, *3*(8), 1172–1183. https://doi.org/10.1038/s41559-019-0935-x

Bloom, S. (1981). Similarity Indices in Community Studies: Potential Pitfalls. *Marine Ecology Progress Series*. https://doi.org/10.3354/meps005125

Bokulich, N. A., Kaehler, B. D., Rideout, J. R., Dillon, M., Bolyen, E., Knight, R., Huttley, G. A., & Gregory Caporaso, J. (2018). Optimizing taxonomic classification of marker-gene amplicon sequences with QIIME 2's q2-feature-classifier plugin. *Microbiome*. https://doi.org/10.1186/s40168-018-0470-z

Bolaños, J., De León, L. F., Ochoa, E., Darias, J., Raja, H. A., Shearer, C. A., Miller, A. N., Vanderheyden, P., Porras-Alfaro, A., & Caballero-George, C. (2015). Phylogenetic Diversity of Sponge-Associated Fungi from the Caribbean and the Pacific of Panama and Their In Vitro Effect on Angiotensin and Endothelin Receptors. *Marine Biotechnology*, *17*(5), 533–564. https://doi.org/10.1007/s10126-015-9634-z

Bonasoro, F., Wilkie, I. C., Bavestrello, G., Cerrano, C., & Carnevali, M. D. C. (2001). Dynamic structure of the mesohyl in the sponge Chondrosia reniformis (Porifera, Demospongiae). *Zoomorphology*, *121*(2), 109–121. https://doi.org/10.1007/PL00008497

Bondu, S., Genta-Jouve, G., Leiròs, M., Vale, C., Guigonis, J. M., Botana, L. M., & Thomas, O. P. (2012). Additional bioactive guanidine alkaloids from the Mediterranean sponge Crambe crambe. *RSC Advances*. https://doi.org/10.1039/c2ra00045h

Botté, E. S., Nielsen, S., Abdul Wahab, M. A., Webster, J., Robbins, S., Thomas, T., & Webster, N. S. (2019). Changes in the metabolic potential of the sponge microbiome under ocean acidification. *Nature Communications*, *10*(1), 1–10. https://doi.org/10.1038/s41467-019-12156-y

Bovio, E., Sfecci, E., Poli, A., Gnavi, G., Prigione, V., Lacour, T., Mehiri, M., & Varese, G. C. (2020). The culturable mycobiota associated with the Mediterranean sponges Aplysina cavernicola, Crambe crambe and Phorbas tenacior. *FEMS Microbiology Letters*. https://doi.org/10.1093/femsle/fnaa014

Britstein, M., Cerrano, C., Burgsdorf, I., Zoccarato, L., Kenny, N. J., Riesgo, A., Lalzar, M., & Steindler, L. (2020). Sponge microbiome stability during environmental acquisition of highly specific photosymbionts Running title : Sponge microbiome during photosymbiont acquisition This article is protected by copyright . All rights reserved . *Environmental Microbiology*. https://doi.org/10.1111/1462-2920.15165

Brown, T. (2014). ChemDraw. *The Science Teacher*.

Burgsdorf, I., Erwin, P. M., López-Legentil, S., Cerrano, C., Haber, M., Frenk, S., & Steindler, L. (2014). Biogeography rather than association with cyanobacteria structures symbiotic microbial communities in the marine sponge Petrosia ficiformis. *Frontiers in Microbiology*, *5*(OCT), 1–11. https://doi.org/10.3389/fmicb.2014.00529

Burke, C., Steinberg, P., Rusch, D., Kjelleberg, S., & Thomas, T. (2011). Bacterial community assembly based on functional genes rather than species. *Proceedings of the National Academy of Sciences of the United States of America*. https://doi.org/10.1073/pnas.1101591108

Caldeira, K., & Wickett, M. (2005). Ocean model predictions of chemistry changes from carbon dioxide emissions to the atmosphere and ocean. *Journal of Geophysical Research C: Oceans*. https://doi.org/10.1029/2004JC002671

Caldeira, K., & Wickett, M. E. (2003). Anthropogenic carbon and ocean pH. *Nature*. https://doi.org/10.1038/425365a

Calgaro, M., Romualdi, C., Waldron, L., Risso, D., & Vitulo, N. (2020). Assessment of statistical methods from single cell, bulk RNA-seq, and metagenomics applied to microbiome data. *Genome Biology*, *21*(1), 1–31. https://doi.org/10.1186/s13059-020-02104-1

Callahan, B. J., McMurdie, P. J., Rosen, M. J., Han, A. W., Johnson, A. J. A., & Holmes, S. P. (2016). DADA2: High-resolution sample inference from Illumina amplicon data. *Nature Methods*. https://doi.org/10.1038/nmeth.3869

Calosi, P., Rastrick, S. P. S., Lombardi, C., de Guzman, H. J., Davidson, L., Jahnke, M., Giangrande, A., Hardege, J. D., Schulze, A., Spicer, J. I., & Gambi, M. C. (2013). Adaptation and acclimatization to ocean acidification in marine ectotherms: An in situ transplant experiment with polychaetes at a shallow CO2 vent system. *Philosophical Transactions of the Royal Society B: Biological Sciences*. https://doi.org/10.1098/rstb.2012.0444

Caporaso, J. G., Kuczynski, J., Stombaugh, J., Bittinger, K., Bushman, F. D., Costello, E. K., Fierer, N., Pẽa, A. G., Goodrich, J. K., Gordon, J. I., Huttley, G. A., Kelley, S. T., Knights, D., Koenig, J. E., Ley, R. E., Lozupone, C. A., McDonald, D., Muegge, B. D., Pirrung, M., … Knight, R. (2010). QIIME allows analysis of high-throughput community sequencing data. In *Nature Methods*. https://doi.org/10.1038/nmeth.f.303

Caroppo, C., Albertano, P., Bruno, L., Montinari, M., Rizzi, M., Vigliotta, G., & Pagliara, P. (2012). Identification and characterization of a new Halomicronema species (Cyanobacteria) isolated from the Mediterranean marine sponge Petrosia ficiformis (Porifera). *Fottea*, *12*(2), 315–326. https://doi.org/10.5507/fot.2012.022

Carpenter, E. J., & Foster, R. A. (2002). Cyanobacteria in Symbiosis. *Cyanobacteria in Symbiosis*, *May*, 10–17. https://doi.org/10.1007/0-306-48005-0

Castiello, D., Cimino, G., De Rosa, S., De Stefano, S., & Sodano, G. (1980). High molecular weight polyacetylenes from the nudibranch Peltodoris actromaculata and the sponge Petrosia ficiformis. *Tetrahedron Letters*. https://doi.org/10.1016/S0040-4039(00)71129-4

Castillo, N., Saavedra, L. M., Vargas, C. A., Gallardo-Escárate, C., & Détrée, C. (2017). Ocean acidification and pathogen exposure modulate the immune response of the edible mussel Mytilus chilensis. *Fish and Shellfish Immunology*. https://doi.org/10.1016/j.fsi.2017.08.047

Chastain, S., & Pfaffman, J. (2006). GIMP: GNU Image Manipulation Program. In *Learning & Leading with Technology*.

Chong, J., Soufan, O., Li, C., Caraus, I., Li, S., Bourque, G., Wishart, D. S., & Xia, J. (2018). MetaboAnalyst 4.0: Towards more transparent and integrative metabolomics analysis. *Nucleic Acids Research*. https://doi.org/10.1093/nar/gky310

Cimino, G., Crispino, A., De Rosa, S., De Stefano, S., & Sodano, G. (1981). Polyacetylenes from the sponge Petrosia ficiformis found in dark caves. *Experientia*. https://doi.org/10.1007/BF01971756

Cimino, Guido, Giulio, A. De, Rosa, S. De, & Marzo, V. Di. (1990). Minor bio active polyacetylenes from petrosia ficiformis. *Journal of Natural Products*. https://doi.org/10.1021/np50068a012

Cimino, Guido, Giulio, A. De, Rosa, S. De, Stefano, S. De, & Sodano, G. (1985). Further high molecular weight polyacetylenes from the sponge petrosia ficiformis. *Journal of Natural Products*. https://doi.org/10.1021/np50037a004

Clarke, K.R. (1993). Non-parametric multivariate analyses of changes in community structure. *Australian Journal of Ecology*.

Comeau, S., Cornwall, C. E., & McCulloch, M. T. (2017). Decoupling between the response of coral calcifying fluid pH and calcification to ocean acidification. *Scientific Reports*. https://doi.org/10.1038/s41598-017-08003-z

Costa, G., Violi, B., Bavestrello, G., Pansini, M., & Bertolino, M. (2020). Aplysina aerophoba (Nardo, 1833) (Porifera, Demospongiae): an unexpected miniaturised growth form from the tidal zone of Mediterranean caves: morphology and DNA barcoding. In *European Zoological Journal*. https://doi.org/10.1080/24750263.2020.1720833

Croué, J., West, N. J., Escande, M. L., Intertaglia, L., Lebaron, P., & Suzuki, M. T. (2013a). A single betaproteobacterium dominates the microbial community of the crambescidine-containing sponge Crambe crambe. *Scientific Reports*. https://doi.org/10.1038/srep02583

Cutignano, A., Luongo, E., Nuzzo, G., Pagano, D., Manzo, E., Sardo, A., & Fontana, A. (2016). Profiling of complex lipids in marine microalgae by UHPLC/tandem mass spectrometry. *Algal Research*. https://doi.org/10.1016/j.algal.2016.05.016

Dada, N., Lol, J. C., Benedict, A. C., López, F., Sheth, M., Dzuris, N., Padilla, N., & Lenhart, A. (2019). Pyrethroid exposure alters internal and cuticle surface bacterial communities in Anopheles albimanus. *ISME Journal*. https://doi.org/10.1038/s41396-019-0445-5

De Goeij, J. M., Van Oevelen, D., Vermeij, M. J. A., Osinga, R., Middelburg, J. J., De Goeij, A. F. P. M., & Admiraal, W. (2013). Surviving in a marine desert: The sponge loop retains resources within coral reefs. *Science*. https://doi.org/10.1126/science.1241981

Díez-Vives, C., Taboada, S., Leiva, C., Busch, K., Hentschel, U., & Riesgo, A. (2020). On the way to specificity - Microbiome reflects sponge genetic cluster primarily in highly structured populations. *Molecular Ecology*. https://doi.org/10.1111/mec.15635

Dittami, S., Arboleda, E., Auguet, J.-C., Bigalke, A., Briand, E., Cárdenas, P., Cardini, U., Decelle, J., Engelen, A., Eveillard, D., Gachon, C., Griffiths, S., Harder, T., Kayal, E., Kazamia, E., Lallier, F., Medina, M., Marzinelli, E., Morganti, T., … Not, F. (2019). *A community perspective on the concept of marine holobionts: state-of-the-art, challenges, and future directions*. *March 2018*, 1–25. https://doi.org/10.7287/peerj.preprints.27519v1

Doney, S. C., Fabry, V. J., Feely, R. A., & Kleypas, J. A. (2009). Ocean acidification: The other CO2 problem. *Annual Review of Marine Science*, *1*, 169–192. https://doi.org/10.1146/annurev.marine.010908.163834

Duckworth, A. R., West, L., Vansach, T., Stubler, A., & Hardt, M. (2012). Effects of water temperature and pH on growth and metabolite biosynthesis of coral reef sponges. *Marine Ecology Progress Series*. https://doi.org/10.3354/meps09853

Enochs, I. C., Manzello, D. P., Carlton, R. D., Graham, D. M., Ruzicka, R., & Colella, M. A. (2015). Ocean acidification enhances the bioerosion of a common coral reef sponge: Implications for the persistence of the Florida Reef Tract. *Bulletin of Marine Science*. https://doi.org/10.5343/bms.2014.1045

Erwin, P. M., Coma, R., López-Sendino, P., Serrano, E., & Ribes, M. (2015). Stable symbionts across the HMA-LMA dichotomy: Low seasonal and interannual variation in sponge-associated bacteria from taxonomically diverse hosts. *FEMS Microbiology Ecology*, *91*(10). https://doi.org/10.1093/femsec/fiv115

Erwin, P. M., & Thacker, R. W. (2008). Cryptic diversity of the symbiotic cyanobacterium *Synechococcus spongiarum* among sponge hosts. *Molecular Ecology*, *17*(12), 2937–2947. https://doi.org/10.1111/j.1365-294X.2008.03808.x

Fabricius, K. E., Langdon, C., Uthicke, S., Humphrey, C., Noonan, S., De'ath, G., Okazaki, R., Muehllehner, N., Glas, M. S., & Lough, J. M. (2011). Losers and winners in coral reefs acclimatized to elevated carbon dioxide concentrations. *Nature Climate Change*. https://doi.org/10.1038/nclimate1122

Fabry, V. J. (2008). Ocean science: Marine calcifiers in a high-CO2 ocean. In *Science*. https://doi.org/10.1126/science.1157130

Fan, L., Reynolds, D., Liu, M., Stark, M., Kjelleberg, S., Webster, N. S., & Thomas, T. (2012). Functional equivalence and evolutionary convergence in complex communities of microbial sponge symbionts. *Proceedings of the National Academy of Sciences of the United States of America*. https://doi.org/10.1073/pnas.1203287109

Fedarko, M. W., Martino, C., Morton, J. T., González, A., Rahman, G., Marotz, C. A., Minich, J. J., Allen, E. E., & Knight, R. (2020). Visualizing 'omic feature rankings and log-ratios using Qurro. *NAR Genomics and Bioinformatics*. https://doi.org/10.1093/nargab/lqaa023

Feng, G., Sun, W., Zhang, F., Karthik, L., & Li, Z. (2016). Inhabitancy of active Nitrosopumilus-like ammonia-oxidizing archaea and Nitrospira nitrite-oxidizing bacteria in the sponge Theonella swinhoei. *Scientific Reports*. https://doi.org/10.1038/srep24966

Fine, M., & Tchernov, D. (2007). Scleractinian coral species survive and recover from decalcification. *Science*. https://doi.org/10.1126/science.1137094

Foo, S. A., & Byrne, M. (2017). Marine gametes in a changing ocean: Impacts of climate change stressors on fecundity and the egg. *Marine Environmental Research*. https://doi.org/10.1016/j.marenvres.2017.02.004

Foo, S., Byrne, M., Ricevuto, E., & Cristina Gambi, M. (2018). The carbon dioxide vents of Ischia, Italy, a natural system to assess impacts of ocean acidification on marine ecosystems: An overview of research and comparisons with other vent systems. *Oceanography and Marine Biology*, *56*, 237–310. https://doi.org/10.1201/9780429454455-4

Gaino, E., Pansini, M., Pronzato, R., & Cicogna, F. (1991). Morphological and Structural Variations in Clathrina clathrus (Porifera, Calcispongiae). In *Fossil and Recent Sponges*. https://doi.org/10.1007/978-3-642-75656-6_28

Gaino, Elda. (1980). *Indagine Ultrastrutturale Sugli Ovociti Maturi Di Chondrilla nucula Schmidt*. 11–22.

Gaino, Elda, Pansini, M., & Pronzato, R. (1977). Aspetti dell´associazione tra Chondrilla nucula Schmidt (Demospongiae) e microorganismi simbionti (Batteri e Cianoficee) in condizioni naturali e sperimentali. *Cahiers de Biologie Marine*, *18*(1), 303–310.

Galera, J., Turon, X., Uriz, M. J., & Becerro, M. A. (2000). Microstructure variation in sponges sharing growth form: The encrusting demosponges Dysidea avara and Crambe crambe. *Acta Zoologica*. https://doi.org/10.1046/j.1463-6395.2000.00041.x

Gambi, M.C. (2016). *Un ' isola laboratorio per lo studio dell ' acidificazione marina*.

Gambi, M. C., Musco, L., Giangrande, A., Badalamenti, F., Micheli, F., & Kroeker, K. J. (2016). Distribution and functional traits of polychaetes in a CO2 vent system: Winners and losers among closely related species. *Marine Ecology Progress Series*. https://doi.org/10.3354/meps11727

Gambi, Maria Cristina, Zoologica, S., Dohrn, A., Gaglioti, M., Zoologica, S., & Dohrn, A. (2020). *I sistemi di emissione di CO 2 dell ' isola d ' Ischia (Mar Tirreno) The CO 2 vent ' s systems off the island of Ischia (Tyrrhenian Sea). April*.

Gantt, S. E., López-Legentil, S., & Erwin, P. M. (2017). Stable microbial communities in the sponge Crambe crambe from inside and outside a polluted Mediterranean harbor. *FEMS Microbiology Letters*, *364*(11), 1–7. https://doi.org/10.1093/femsle/fnx105

Gao, Z., Li, B., Zheng, C., & Wang, G. (2008). Molecular detection of fungal communities in the hawaiian marine sponges Suberites zeteki and Mycale armata. *Applied and Environmental Microbiology*. https://doi.org/10.1128/AEM.01315-08

Gareth Jones, E. B. (2011). Fifty years of marine mycology. In *Fungal Diversity*. https://doi.org/10.1007/s13225-011-0119-8

Garrabou, J., & Zabala, M. (2001). Growth dynamics in four Mediterranean demosponges. *Estuarine, Coastal and Shelf Science*. https://doi.org/10.1006/ecss.2000.0699

Gattuso, J.-P., & Hansson, L. (2011). Ocean acidification: background and history. *Ocean Acidification*.

Gauthier, M. E. A., Watson, J. R., & Degnan, S. M. (2016). Draft genomes shed light on the dual bacterial symbiosis that dominates the microbiome of the coral reef sponge Amphimedon queenslandica. *Frontiers in Marine Science*. https://doi.org/10.3389/fmars.2016.00196

Gavriilidou, A., Gutleben, J., Versluis, D., Forgiarini, F., Van Passel, M. W. J., Ingham, C. J., Smidt, H., & Sipkema, D. (2020). Comparative genomic analysis of Flavobacteriaceae: Insights into carbohydrate metabolism, gliding motility and secondary metabolite biosynthesis. *BMC Genomics*. https://doi.org/10.1186/s12864-020-06971-7

Gazeau, F., Gattuso, J. P., Dawber, C., Pronker, A. E., Peene, F., Peene, J., Heip, C. H. R., & Middelburg, J. J. (2010). Effect of ocean acidification on the early life stages of the blue mussel Mytilus edulis. *Biogeosciences*. https://doi.org/10.5194/bg-7-2051-2010

Gizzi, F., De Mas, L., Airi, V., Caroselli, E., Prada, F., Falini, G., Dubinsky, Z., & Goffredo, S. (2017). Reproduction of an azooxanthellate coral is unaffected by ocean acidification. *Scientific Reports*. https://doi.org/10.1038/s41598-017-13393-1

Gloeckner, V., Wehrl, M., Moitinho-Silva, L., Gernert, C., Hentschel, U., Schupp, P., Pawlik, J. R., Lindquist, N. L., Erpenbeck, D., Wörheide, G., & Wörheide, G. (2014). The HMA-LMA dichotomy revisited: An electron microscopical survey of 56 sponge species. *Biological Bulletin*. https://doi.org/10.1086/BBLv227n1p78

Gloor, G. B., Macklaim, J. M., Pawlowsky-Glahn, V., & Egozcue, J. J. (2017). Microbiome datasets are compositional: And this is not optional. In *Frontiers in Microbiology*. https://doi.org/10.3389/fmicb.2017.02224

González-Delgado, S., & Hernández, J. C. (2018). The Importance of Natural Acidified Systems in the Study of Ocean Acidification: What Have We Learned? *Advances in Marine Biology*, *80*, 57–99. https://doi.org/10.1016/bs.amb.2018.08.001

Goodwin, C., Rodolfo-Metalpa, R., Picton, B., & Hall-Spencer, J. M. (2014b). Effects of ocean acidification on sponge communities. *Marine Ecology*, *35*(SUPPL1), 41–49. https://doi.org/10.1111/maec.12093

Gravinese, P. M. (2018). Ocean acidification impacts the embryonic development and hatching success of the Florida stone crab, Menippe mercenaria. *Journal of Experimental Marine Biology and Ecology*. https://doi.org/10.1016/j.jembe.2017.09.001

Guerrero, R., Margulis, L., & Berlanga, M. (2013). Symbiogenesis: The holobiont as a unit of evolution. *International Microbiology*. https://doi.org/10.2436/20.1501.01.188

Guo, Y., Gavagnin, M., Salierno, C., & Cimino, G. (1998). Further petroformynes from both Atlantic and Mediterranean populations of the sponge Petrosia ficiformis. *Journal of Natural Products*. https://doi.org/10.1021/np970424f

Guo, Y., Gavagnin, M., Trivellone, E., & Cimino, G. (1994). Absolute stereochemistry of petroformynes, high molecular polyacetylenes from the marine sponge Petrosia ficiformis. *Tetrahedron*. https://doi.org/10.1016/S0040-4020(01)89334-0

Guo, Y., Gavagnin, M., Trivellone, E., & Cimino, G. (1995). Further structural studies on the petroformynes. *Journal of Natural Products*. https://doi.org/10.1021/np50119a009

Hall-Spencer, J. M., Rodolfo-Metalpa, R., Martin, S., Ransome, E., Fine, M., Turner, S. M., Rowley, S. J., Tedesco, D., & Buia, M. C. (2008). Volcanic carbon dioxide vents show ecosystem effects of ocean acidification. *Nature*, *454*(7200), 96–99. https://doi.org/10.1038/nature07051

Hentschel, U., Fieseler, L., Wehrl, M., Gernert, C., Steinert, M., Hacker, J., & Horn, M. (2003). Microbial diversity of marine sponges. In *Progress in molecular and subcellular biology*. https://doi.org/10.1007/978-3-642-55519-0_3

Hentschel, Ute, Piel, J., Degnan, S. M., & Taylor, M. W. (2012). Genomic insights into the marine sponge microbiome. *Nature Reviews Microbiology*, *10*(9), 641–654. https://doi.org/10.1038/nrmicro2839

Hentschel, Ute, Usher, K. M., & Taylor, M. W. (2006). Marine sponges as microbial fermenters. *FEMS Microbiology Ecology*, *55*(2), 167–177. https://doi.org/10.1111/j.1574-6941.2005.00046.x

Hernroth, B., Baden, S., Thorndyke, M., & Dupont, S. (2011). Immune suppression of the echinoderm Asterias rubens (L.) following long-term ocean acidification. *Aquatic Toxicology*. https://doi.org/10.1016/j.aquatox.2011.03.001

Heuer, R. M., & Grosell, M. (2014). Physiological impacts of elevated carbon dioxide and ocean acidification on fish. *American Journal of Physiology - Regulatory Integrative and Comparative Physiology*. https://doi.org/10.1152/ajpregu.00064.2014

Hoadley, K. D., Rollison, D., Pettay, D. T., & Warner, M. E. (2015). Differential carbon utilization and asexual reproduction under elevated pCO2 conditions in the model anemone, Exaiptasia pallida, hosting different symbionts. *Limnology and Oceanography*. https://doi.org/10.1002/lno.10160

Höller, G., Wright, A. D., Matthée, G. F., Konig, G. M., Draeger, S., Aust, H. J., & Schulz, B. (2000). Fungi from marine sponges: Diversity, biological activity and secondary metabolites. *Mycological Research*. https://doi.org/10.1017/S0953756200003117

Hooper, J. N. a. (2003). 'Sponguide'. Guide To Sponge Collection and Identification. *Order A Journal On The Theory Of Ordered Sets And Its Applications*.

Horvath, K. M., Castillo, K. D., Armstrong, P., Westfield, I. T., Courtney, T., & Ries, J. B. (2016). Next-century ocean acidification and warming both reduce calcification rate, but only acidification alters skeletal morphology of reef-building coral Siderastrea siderea. *Scientific Reports*. https://doi.org/10.1038/srep29613

Jackson, T. J., Ramaley, R. F., & Meinschein, W. G. (1973). Thermomicrobium, a new genus of extremely thermophilic bacteria. *International Journal of Systematic Bacteriology*. https://doi.org/10.1099/00207713-23-1-28

Jokiel, P. L., Rodgers, K. S., Kuffner, I. B., Andersson, A. J., Cox, E. F., & Mackenzie, F. T. (2008). Ocean acidification and calcifying reef organisms: A mesocosm investigation. *Coral Reefs*. https://doi.org/10.1007/s00338-008-0380-9

Jones, E. B. G., Kohlmeyer, E., & Kohlmeyer, J. (1980). Marine Mycology: The Higher Fungi. *Mycologia*. https://doi.org/10.2307/3759549

Kandler, N. M., Abdul Wahab, M. A., Noonan, S. H. C., Bell, J. J., Davy, S. K., Webster, N. S., & Luter, H. M. (2018a). In situ responses of the sponge microbiome to ocean acidification. *FEMS Microbiology Ecology*, *94*(12). https://doi.org/10.1093/femsec/fiy205

Kandler, N. M., Abdul Wahab, M. A., Noonan, S. H. C., Bell, J. J., Davy, S. K., Webster, N. S., & Luter, H. M. (2018b). In situ responses of the sponge microbiome to ocean acidification. *FEMS Microbiology Ecology*, *94*(12), 1–12. https://doi.org/10.1093/femsec/fiy205

Kaplan, M. B., Mooney, T. A., McCorkle, D. C., & Cohen, A. L. (2013). Adverse Effects of Ocean Acidification on Early Development of Squid (Doryteuthis pealeii). *PLoS ONE*. https://doi.org/10.1371/journal.pone.0063714

Kayley M. Usher, John Kuo, J. F. & D. C. S. (2001). Vertical transmission of cyanobacterial symbionts in the marine sponge Chondrilla australiensis (Demospongiae). *Hydrobiologia*, *461*, 15–23. https://doi.org/10.1023/A:1012748727678

Kim, Jung S., Im, K. S., Jung, J. H., Kim, Y. L., Kim, J., Shim, C. J., & Lee, C. O. (1998). New bioactive polyacetylenes from the marine sponge Petrosia sp. *Tetrahedron*. https://doi.org/10.1016/S0040-4020(98)00066-0

Kim, Jung Sun, Lim, Y. J., Im, K. S., Jung, J. H., Shim, C. J., Lee, C. O., Hong, J., & Lee, H. (1999). Cytotoxic polyacetylenes from the marine sponge Petrosia sp. *Journal of Natural Products*. https://doi.org/10.1021/np9803427

Könneke, M., Bernhard, A. E., De La Torre, J. R., Walker, C. B., Waterbury, J. B., & Stahl, D. A. (2005). Isolation of an autotrophic ammonia-oxidizing marine archaeon. *Nature*. https://doi.org/10.1038/nature03911

Konstantinou, D., & Voultsiadou, E. (2015). *Sponge-associated cyanobacteria of the Eastern Mediterranean : preliminary results*. *May*.

Koutsouveli, V., Taboada, S., Moles, J., Cristobo, J., Ríos, P., Bertran, A., Solà, J., Avila, C., & Riesgo, A. (2018). Insights into the reproduction of some Antarctic dendroceratid, poecilosclerid, and haplosclerid demosponges. *PLoS ONE*. https://doi.org/10.1371/journal.pone.0192267

Kroeker, K. J., Gambi, M. C., & Micheli, F. (2013a). Community dynamics and ecosystem simplification in a high-CO2 ocean. *Proceedings of the National Academy of Sciences of the United States of America*. https://doi.org/10.1073/pnas.1216464110

Kroeker, K. J., Kordas, R. L., Crim, R. N., & Singh, G. G. (2010). Meta-analysis reveals negative yet variable effects of ocean acidification on marine organisms. In *Ecology Letters*. https://doi.org/10.1111/j.1461-0248.2010.01518.x

Kroeker, K. J., Micheli, F., & Gambi, M. C. (2013b). Ocean acidification causes ecosystem shifts via altered competitive interactions. *Nature Climate Change*. https://doi.org/10.1038/nclimate1680

Kroeker, K. J., Micheli, F., Gambi, M. C., & Martz, T. R. (2011). Divergent ecosystem responses within a benthic marine community to ocean acidification. *Proceedings of the National Academy of Sciences of the United States of America*. https://doi.org/10.1073/pnas.1107789108

Lee, J., Kwon, K. K., Lim, S. Il, Song, J., Choi, A. R., Yang, S. H., Jung, K. H., Lee, J. H., Kang, S. G., Oh, H. M., & Cho, J. C. (2019). Isolation, cultivation, and genome analysis of proteorhodopsin-containing SAR116-clade strain Candidatus Puniceispirillum marinum IMCC1322. *Journal of Microbiology*. https://doi.org/10.1007/s12275-019-9001-2

Lee, Y. J., Yoo, S. J., Kang, J. S., Yun, J., Shin, H. J., Lee, J. S., & Lee, H. S. (2013). Cytotoxic petrosiacetylenes from the marine sponge Petrosia sp. *Lipids*. https://doi.org/10.1007/s11745-012-3727-5

Lesser, M. P., Fiore, C., Slattery, M., & Zaneveld, J. (2016). Climate change stressors destabilize the microbiome of the Caribbean barrel sponge, Xestospongia muta. *Journal of Experimental Marine Biology and Ecology*, *475*, 11–18. https://doi.org/10.1016/j.jembe.2015.11.004

Li, J., Gu, L., Bai, S., Wang, J., Su, L., Wei, B., Zhang, L., & Fang, J. (2020). Characterization of particle-associated and free-living bacterial and archaeal communities along the water columns of the South China Sea. *Biogeosciences Discussions*. https://doi.org/10.5194/bg-2020-115

Li, Q., & Wang, G. (2009). Diversity of fungal isolates from three Hawaiian marine sponges. *Microbiological Research*. https://doi.org/10.1016/j.micres.2007.07.002

Liaci, L., & Sara, M. (1964). Associazione fra la cianoficea aphanocapsa feldmanni e alcune demospongie marine. *Bolletino Di Zoologia*, *31*(1), 55–65. https://doi.org/10.1080/11250006409436067

Lim, Y. J., Kim, J. S., Im, K. S., Jung, J. H., Lee, C. O., Hong, J., & Kim, D. K. (1999). New cytotoxic polyacetylenes from the marine sponge Petrosia. *Journal of Natural Products*. https://doi.org/10.1021/np9900371

Lim, Y. J., Lee, C. O., Hong, J., Kim, D. K., Im, K. S., & Jung, J. H. (2001a). Cytotoxic polyacetylenic alcohols from the marine sponge Petrosia species. *Journal of Natural Products*. https://doi.org/10.1021/np010247p

Lim, Y. J., Park, H. S., Im, K. S., Lee, C. O., Hong, J., Lee, M. Y., Kim, D. K., & Jung, J. H. (2001b). Additional cytotoxic polyacetylenes from the marine sponge Petrosia species. *Journal of Natural Products*. https://doi.org/10.1021/np000252d

Lozupone, C. A., & Knight, R. (2007). Global patterns in bacterial diversity. *Proceedings of the National Academy of Sciences of the United States of America*. https://doi.org/10.1073/pnas.0611525104

Lucey, N. M., Lombardi, C., Demarchi, L., Schulze, A., Gambi, M. C., & Calosi, P. (2015). To brood or not to brood: Are marine invertebrates that protect their offspring more resilient to ocean acidification? *Scientific Reports*. https://doi.org/10.1038/srep12009

Lurgi, M., Thomas, T., Wemheuer, B., Webster, N. S., & Montoya, J. M. (2019). Modularity and predicted functions of the global sponge-microbiome network. *Nature Communications*. https://doi.org/10.1038/s41467-019-08925-4

Luter, H. M., Andersen, M., Versteegen, E., Laffy, P., Uthicke, S., Bell, J. J., & Webster, N. S. (2020). Cross-generational effects of climate change on the microbiome of a photosynthetic sponge. *Environmental Microbiology*, *00*. https://doi.org/10.1111/1462-2920.15222

Maldonado, M. (2007). Intergenerational transmission of symbiotic bacteria in oviparous and viviparous demosponges, with emphasis on intracytoplasmically-compartmented bacterial types. *Journal of the Marine Biological Association of the United Kingdom*, *87*(6), 1701–1713. https://doi.org/10.1017/S0025315407058080

Maldonado, M., & Bergquist, P. R. (2002). Chapter 2: Phylum Porifera. *Atlas of Marine Invertebrate Larvae*, *May*, 21–50. https://doi.org/10.1177/0004867414557161

Maldonado, M., Carmona, M. C., Uriz, M. J., & Cruzado, A. (1999). Decline in Mesozoic reef-building sponges explained by silicon limitation. *Nature*. https://doi.org/10.1038/44560

Maldonado, M., Cortadellas, N., Trillas, M. I., Ecology, A., Estudios, C. De, Blanes, A. De, & Cala, A. (2005). Endosymbiotic Yeast Maternally Transmitted in a. *Smithsonian*, *209*(October), 94–106.

Maldonado, M., Cortadellas, N., Trillas, M. I., & Rützler, K. (2005). Endosymbiotic yeast maternally transmitted in a marine sponge. *Biological Bulletin*. https://doi.org/10.2307/3593127

Maldonado, M., & Riesgo, A. (2008). Reproduction in the phylum *Porifera*: a synoptic overview. *Treballs de La Societat Catalana de Biologia*, *59*(January), 29–49. https://doi.org/10.2436/20.1501.02.56

Manconi, R., Cadeddu, B., Ledda, F., & Pronzato, R. (2013). An overview of the Mediterranean cave-dwelling horny sponges (Porifera, Demospongiae). *ZooKeys*, *281*, 1–68. https://doi.org/10.3897/zookeys.281.4171

Marchese, P., Garzoli, L., Gnavi, G., O'Connell, E., Bouraoui, A., Mehiri, M., Murphy, J. M., & Varese, G. C. (2020). Diversity and bioactivity of fungi associated with the marine sea cucumber Holothuria poli: disclosing the strains potential for biomedical applications. *Journal of Applied Microbiology*. https://doi.org/10.1111/jam.14659

Martino, C., Morton, J. T., Marotz, C. A., Thompson, L. R., Tripathi, A., Knight, R., & Zengler, K. (2019). A Novel Sparse Compositional Technique Reveals Microbial Perturbations. *MSystems*. https://doi.org/10.1128/msystems.00016-19

McElhany, P., & Shallin Busch, D. (2013). Appropriate pCO2 treatments in ocean acidification experiments. In *Marine Biology*. https://doi.org/10.1007/s00227-012-2052-0

McMurdie, P. J., & Holmes, S. (2013). Phyloseq: An R Package for Reproducible Interactive Analysis and Graphics of Microbiome Census Data. *PLoS ONE*. https://doi.org/10.1371/journal.pone.0061217

Mehrshad, M., Rodriguez-Valera, F., Amoozegar, M. A., López-García, P., & Ghai, R. (2018). The enigmatic SAR202 cluster up close: Shedding light on a globally distributed dark ocean lineage involved in sulfur cycling. *ISME Journal*. https://doi.org/10.1038/s41396-017-0009-5

Mejia, E. J., Magranet, L. B., De Voogd, N. J., Tendyke, K., Qiu, D., Shen, Y. Y., Zhou, Z., & Crews, P. (2013). Structures and cytotoxic evaluation of new and known acyclic Ene-Ynes from an American Samoa Petrosia sp. Sponge. *Journal of Natural Products*. https://doi.org/10.1021/np3008446

Meron, D., Buia, M. C., Fine, M., & Banin, E. (2013). Changes in Microbial Communities Associated with the Sea Anemone Anemonia viridis in a Natural pH Gradient. *Microbial Ecology*, *65*(2), 269–276. https://doi.org/10.1007/s00248-012-0127-6

Meron, D., Rodolfo-Metalpa, R., Cunning, R., Baker, A. C., Fine, M., & Banin, E. (2012). Changes in coral microbial communities in response to a natural pH gradient. *ISME Journal*. https://doi.org/10.1038/ismej.2012.19

Miller, J. J., Maher, M., Bohaboy, E., Friedman, C. S., & McElhany, P. (2016). Exposure to low pH reduces survival and delays development in early life stages of Dungeness crab (Cancer magister). *Marine Biology*. https://doi.org/10.1007/s00227-016-2883-1

Minto, R. E., & Blacklock, B. J. (2008). Biosynthesis and function of polyacetylenes and allied natural products. *Progress in Lipid Research*, *47*(4), 233–306. https://doi.org/10.1016/j.plipres.2008.02.002

Mitova, M., Popov, S., & De Rosa, S. (2004a). Cyclic peptides from a Ruegeria strain of bacteria associated with the sponge Suberites domuncula. *Journal of Natural Products*. https://doi.org/10.1021/np049900+

Mitova, M., Tommonaro, G., Hentschel, U., Müller, W. E. G., & De Rosa, S. (2004b). Exocellular cyclic dipeptides from a Ruegeria strain associated with cell cultures of Suberites domuncula. *Marine Biotechnology*. https://doi.org/10.1007/s10126-003-0018-4

Mohanty, I., Podell, S., Biggs, J. S., Garg, N., Allen, E. E., & Agarwal, V. (2020). Multi-omic profiling of melophlus sponges reveals diverse metabolomic and microbiome architectures that are non-overlapping with ecological neighbors. *Marine Drugs*. https://doi.org/10.3390/md18020124

Moitinho-Silva, L., Steinert, G., Nielsen, S., Hardoim, C. C. P., Wu, Y. C., McCormack, G. P., López-Legentil, S., Marchant, R., Webster, N., Thomas, T., & Hentschel, U. (2017). Predicting the HMA-LMA status in marine sponges by machine learning. *Frontiers in Microbiology*, *8*(MAY). https://doi.org/10.3389/fmicb.2017.00752

Moreno-Pino, M., Cristi, A., Gillooly, J. F., & Trefault, N. (2020). Characterizing the microbiomes of Antarctic sponges: a functional metagenomic approach. *Scientific Reports*. https://doi.org/10.1038/s41598-020-57464-2

Morris, R. M., Rappé, M. S., Urbach, E., Connon, S. A., & Giovannoni, S. J. (2004). Prevalence of the Chloroflexi-related SAR202 bacterioplankton cluster throughout the mesopelagic zone and deep ocean. *Applied and Environmental Microbiology*. https://doi.org/10.1128/AEM.70.5.2836-2842.2004

Morrow, K. M., Bourne, D. G., Humphrey, C., Botté, E. S., Laffy, P., Zaneveld, J., Uthicke, S., Fabricius, K. E., & Webster, N. S. (2015). Natural volcanic CO2 seeps reveal future trajectories for host-microbial associations in corals and sponges. *ISME Journal*. https://doi.org/10.1038/ismej.2014.188

Morton, J. T., Marotz, C., Washburne, A., Silverman, J., Zaramela, L. S., Edlund, A., Zengler, K., & Knight, R. (2019). Establishing microbial composition measurement standards with reference frames. *Nature Communications*, *10*(1). https://doi.org/10.1038/s41467-019-10656-5

Morton, J. T., Sanders, J., Quinn, R. A., McDonald, D., Gonzalez, A., Vázquez-Baeza, Y., Navas-Molina, J. A., Song, S. J., Metcalf, J. L., Hyde, E. R., Lladser, M., Dorrestein, P. C., & Knight, R. (2017). Balance Trees Reveal Microbial Niche Differentiation. *MSystems*. https://doi.org/10.1128/msystems.00162-16

Naim, M. A., Smidt, H., & Sipkema, D. (2017). Fungi found in Mediterranean and North Sea sponges: How specific are they? *PeerJ*. https://doi.org/10.7717/peerj.3722

Neave, M. J., Apprill, A., Ferrier-Pagès, C., & Voolstra, C. R. (2016). Diversity and function of prevalent symbiotic marine bacteria in the genus Endozoicomonas. In *Applied Microbiology and Biotechnology*. https://doi.org/10.1007/s00253-016-7777-0

Neulinger, S. C., Stöhr, R., Thiel, V., Schmaljohann, R., & Imhoff, J. F. (2010). New phylogenetic lineages of the Spirochaetes phylum associated with Clathrina species (Porifera). *Journal of Microbiology*. https://doi.org/10.1007/s12275-010-0017-x

Nguyen, M. T. H. D., & Thomas, T. (2018). Diversity, host-specificity and stability of sponge-associated fungal communities of co-occurring sponges. *PeerJ*, *6*, e4965. https://doi.org/10.7717/peerj.4965

Nickel, M., & Brümmer, F. (2003). In vitro sponge fragment culture of Chondrosia reniformis (Nardo, 1847). *Journal of Biotechnology*, *100*(2), 147–159. https://doi.org/10.1016/S0168-1656(02)00256-0

Núñez-Pons, L., Avila, C., Romano, G., Verde, C., & Giordano, D. (2018). UV-protective compounds in marine organisms from the southern ocean. In *Marine Drugs*. https://doi.org/10.3390/md16090336

O'Brien, P. A., Morrow, K. M., Willis, B. L., & Bourne, D. G. (2016). Implications of ocean acidification for marine microorganisms from the free-living to the host-associated. *Frontiers in Marine Science*, *3*(APR). https://doi.org/10.3389/fmars.2016.00047

O'Brien, P. A., Smith, H. A., Fallon, S., Fabricius, K., Willis, B. L., Morrow, K. M., & Bourne, D. G. (2018). Elevated CO2 has little influence on the bacterial communities associated with the pH-tolerant coral, massive Porites spp. *Frontiers in Microbiology*, *9*(NOV), 1–12. https://doi.org/10.3389/fmicb.2018.02621

Oh, H. M., Kwon, K. K., Kang, I., Kang, S. G., Lee, J. H., Kim, S. J., & Cho, J. C. (2010). Complete genome sequence of "Candidatus puniceispirillum marinum" IMCC1322, a representative of the SAR116 clade in the Alphaproteobacteria. *Journal of Bacteriology*. https://doi.org/10.1128/JB.00347-10

Oksanen, J., Kindt, R., Legendre, P., O'Hara, B., Simpson, G. L., Solymos, P. M., Stevens, M. H. H., & & Wagner, H. (2008). The vegan package. *Community Ecology Package*.

Ou, H., Li, M., Wu, S., Jia, L., Hill, R. T., & Zhao, J. (2020). Characteristic microbiomes correlate with polyphosphate accumulation of marine sponges in South China sea areas. *Microorganisms*. https://doi.org/10.3390/microorganisms8010063

Padiglia, A., Cadeddu, B., Ledda, F. D., Bertolino, M., Costa, G., Pronzato, R., & Manconi, R. (2018). Biodiversity assessment in Western Mediterranean marine protected areas (MPAs): Porifera of Posidonia oceanica meadows (Asinara Island MPA) and marine caves (Capo Caccia–Isola Piana MPA) of Sardinia. *European Zoological Journal*. https://doi.org/10.1080/24750263.2018.1525440

Pagliara, P., Barca, A., Verri, T., & Caroppo, C. (2020). The marine sponge *Petrosia ficiformis* harbors different cyanobacteria strains with potential biotechnological application. *Journal of Marine Science and Engineering*, *8*(9). https://doi.org/10.3390/JMSE8090638

Pagliara, P., & Caroppo, C. (2011). Cytotoxic and antimitotic activities in aqueous extracts of eight cyanobacterial strains isolated from the marine sponge *Petrosia ficiformis*. *Toxicon*, *57*(6), 889–896. https://doi.org/10.1016/j.toxicon.2011.03.006

Palumbi, S. R. (1986). How body plans limit acclimation: responses of a demosponge to wave force. *Ecology*. https://doi.org/10.2307/1938520

Pansch, C., Schlegel, P., & Havenhand, J. (2013). Larval development of the barnacle Amphibalanus improvisus responds variably but robustly to near-future ocean acidification. *ICES Journal of Marine Science*. https://doi.org/10.1093/icesjms/fst092

Pansini, M., & Pronzato, R. (1985). Distribution and Ecology of Epiphytic Portfera in two Posidonia oceanica (L.) DELILE Meadows of the Ligurian and Tyrrhenian Sea. *Marine Ecology*. https://doi.org/10.1111/j.1439-0485.1985.tb00316.x

Pauvert, C., Buée, M., Laval, V., Edel-Hermann, V., Fauchery, L., Gautier, A., Lesur, I., Vallance, J., & Vacher, C. (2019). Bioinformatics matters: The accuracy of plant and soil fungal community data is highly dependent on the metabarcoding pipeline. *Fungal Ecology*. https://doi.org/10.1016/j.funeco.2019.03.005

Paz, Z., Komon-Zelazowska, M., Druzhinina, I. S., Aveskamp, M. M., Shnaiderman, A., Aluma, Y., Carmeli, S., Ilan, M., & Yarden, O. (2010). Diversity and potential antifungal properties of fungi associated with a Mediterranean sponge. *Fungal Diversity*. https://doi.org/10.1007/s13225-010-0020-x

Pedersen, S. A., Våge, V. T., Olsen, A. J., Hammer, K. M., & Altin, D. (2014). Effects of elevated carbon dioxide (CO2) concentrations on early developmental stages of the marine copepod Calanus finmarchicus gunnerus (Copepoda: Calanoidae). *Journal of Toxicology and Environmental Health - Part A: Current Issues*. https://doi.org/10.1080/15287394.2014.887421

Pérez-López, P., Ternon, E., González-García, S., Genta-Jouve, G., Feijoo, G., Thomas, O. P., & Moreira, M. T. (2014). Environmental solutions for the sustainable production of bioactive natural products from the marine sponge Crambe crambe. *Science of the Total Environment*, *475*, 71–82. https://doi.org/10.1016/j.scitotenv.2013.12.068

Pita, L., Rix, L., Slaby, B. M., Franke, A., & Hentschel, U. (2018). The sponge holobiont in a changing ocean: from microbes to ecosystems. *Microbiome*, *6*(1), 46. https://doi.org/10.1186/s40168-018-0428-1

Pörtner, H. O. (2008). Ecosystem effects of ocean acidification in times of ocean warming: A physiologist's view. *Marine Ecology Progress Series*, *373*(March), 203–217. https://doi.org/10.3354/meps07768

Porzio, L., Buia, M. C., & Hall-Spencer, J. M. (2011). Effects of ocean acidification on macroalgal communities. *Journal of Experimental Marine Biology and Ecology*. https://doi.org/10.1016/j.jembe.2011.02.011

Proksch, P., Ebel, R., Edrada, R., Riebe, F., Liu, H., Diesel, A., Bayer, M., Li, X., Han Lin, W., Grebenyuk, V., Müller, W. E. G., Draeger, S., Zuccaro, A., & Schulz, B. (2008). Sponge-associated fungi and their bioactive compounds: The Suberites case. *Botanica Marina*. https://doi.org/10.1515/BOT.2008.014

Pronzato, R., Ledda, F. D., & Manconi, R. (2013). Mediterranean horny sponges: How to drive a neverending story of exploitation toward a sustainable management and conservation. In *Endangered Species: Habitat, Protection and Ecological Significance*.

Quast, C., Pruesse, E., Yilmaz, P., Gerken, J., Schweer, T., Yarza, P., Peplies, J., & Glöckner, F. O. (2013). The SILVA ribosomal RNA gene database project: Improved data processing and web-based tools. *Nucleic Acids Research*. https://doi.org/10.1093/nar/gks1219

Rahlff, J., Herlemann, D., Giebel, H. A., Mustaffa, N. I. H., Wurl, O., & Stolle, C. (2019). Marine foams represent compressed sea-surface microlayer with distinctive bacterial communities. In *bioRxiv*. https://doi.org/10.1101/820696

Rastelli, E., Petani, B., Corinaldesi, C., Dell'Anno, A., Lo Martire, M., Cerrano, C., & Danovaro, R. (2020). A high biodiversity mitigates the impact of ocean acidification on hard-bottom ecosystems. *Scientific Reports*, *10*(1), 1–13. https://doi.org/10.1038/s41598-020-59886-4

Regoli, F., Cerrano, C., Chierici, E., Bompadre, S., & Bavestrello, G. (2000). Susceptibility to oxidative stress of the Mediterranean demosponge Petrosia ficiformis: Role of endosymbionts and solar irradiance. *Marine Biology*. https://doi.org/10.1007/s002270000369

Ribes, M., Calvo, E., Movilla, J., Logares, R., Coma, R., & Pelejero, C. (2016). Restructuring of the sponge microbiome favors tolerance to ocean acidification. *Environmental Microbiology Reports*, *8*(4), 536–544. https://doi.org/10.1111/1758-2229.12430

Riebesell, U., Fabry, V. J., & Hansson, L. (2010). Guide to best practices for ocean acidification research and data reporting. *European Commission*.

Riesgo, A., Taboada, S., Pérez-Portela, R., Melis, P., Xavier, J. R., Blasco, G., & López-Legentil, S. (2019). Genetic diversity, connectivity and gene flow along the distribution of the emblematic Atlanto-Mediterranean sponge Petrosia ficiformis (Haplosclerida, Demospongiae). *BMC Evolutionary Biology*. https://doi.org/10.1186/s12862-018-1343-6

Rivers, A. R., Weber, K. C., Gardner, T. G., Liu, S., & Armstrong, S. D. (2018). ITSxpress: Software to rapidly trim internally transcribed spacer sequences with quality scores for marker gene analysis [version 1; peer review: 2 approved]. *F1000Research*. https://doi.org/10.12688/F1000RESEARCH.15704.1

Rod'kina, S. A. (2005). Fatty acids and other lipids of marine sponges. In *Russian Journal of Marine Biology*. https://doi.org/10.1007/s11179-006-0015-3

Ross, H. H., Sokal, R. R., Sneath, P. H. A., & Freeman, W. H. (1964). Principles of Numerical Taxonomy. *Systematic Zoology*. https://doi.org/10.2307/2411834

Ruiz, C., Villegas-Plazas, M., Thomas, O. P., Junca, H., & Pérez, T. (2020). Specialized microbiome of the cave-dwelling sponge Plakina kanaky (Porifera, Homoscleromorpha). *FEMS Microbiology Ecology*. https://doi.org/10.1093/femsec/fiaa043

Ruppert, E. E., & Barnes, R. D. (1996). Zoología de los Invertebrados. In *McGraw-Hill Interamericana Editores S.A de C.V.*

Sarà, M. (1964). Associazioni di demospongie con zooxantelle e cianelle. *Bolletino Di Zoologia*. https://doi.org/10.1080/11250006409441070

Sarà, M., Bavestrello, G., Cattaneo-vietti, R., & Cerrano, C. (1998). Endosymbiosis in sponges: Relevance for epigenesis and evolution. *Symbiosis*, *25*(1–3), 57–70.

Scanes, E., Parker, L. M., O'Connor, W. A., & Ross, P. M. (2014). Mixed effects of elevated pCO2 on fertilisation, larval and juvenile development and adult responses in the mobile subtidal scallop Mimachlamys asperrima (Lamarck, 1819). *PLoS ONE*. https://doi.org/10.1371/journal.pone.0093649

Schläppy, M. L., Schöttner, S. I., Lavik, G., Kuypers, M. M. M., de Beer, D., & Hoffmann, F. (2010). Evidence of nitrification and denitrification in high and low microbial abundance sponges. *Marine Biology*, *157*(3), 593–602. https://doi.org/10.1007/s00227-009-1344-5

Schlesner, H. (2015). Filomicrobium . In *Bergey's Manual of Systematics of Archaea and Bacteria*. https://doi.org/10.1002/9781118960608.gbm00818

Schmitt, S., Hentschel, U., & Taylor, M. W. (2012). Deep sequencing reveals diversity and community structure of complex microbiota in five Mediterranean sponges. *Hydrobiologia*, *687*(1), 341–351. https://doi.org/10.1007/s10750-011-0799-9

Shi, W., Han, Y., Guo, C., Zhao, X., Liu, S., Su, W., Wang, Y., Zha, S., Chai, X., & Liu, G. (2017a). Ocean acidification hampers sperm-egg collisions, gamete fusion, and generation of Ca2+ oscillations of a broadcast spawning bivalve, Tegillarca granosa. *Marine Environmental Research*. https://doi.org/10.1016/j.marenvres.2017.07.016

Shi, Y., Moazami, Y., & Pierce, J. G. (2017b). Structure, synthesis and biological properties of the pentacyclic guanidinium alkaloids. In *Bioorganic and Medicinal Chemistry*. https://doi.org/10.1016/j.bmc.2017.03.015

Shivani, Y., Subhash, Y., Tushar, L., Sasikala, C., & Ramana, C. V. (2015). Spirochaeta lutea sp. nov., isolated from marine habitats and emended description of the genus Spirochaeta. *Systematic and Applied Microbiology*. https://doi.org/10.1016/j.syapm.2014.11.002

Sidri, M., Milanese, M., & Bümmer, F. (2005). First observations on egg release in the oviparous sponge Chondrilla nucula (Demospongiae, Chondrosida, Chondrillidae) in the Mediterranean Sea. *Invertebrate Biology*, *124*(2), 91–97. https://doi.org/10.1111/j.1744-7410.2005.00011.x

Silva, S. B. L., Oberhänsli, F., Tribalat, M. A., Genta-Jouve, G., Teyssié, J. L., Dechraoui-Bottein, M. Y., Gallard, J. F., Evanno, L., Poupon, E., & Thomas, O. P. (2019). Insights into the Biosynthesis of Cyclic Guanidine Alkaloids from Crambeidae Marine Sponges. *Angewandte Chemie - International Edition*. https://doi.org/10.1002/anie.201809539

Sipkema, D., de Caralt, S., Morillo, J. A., Al-Soud, W. A., Sørensen, S. J., Smidt, H., & Uriz, M. J. (2015). Similar sponge-associated bacteria can be acquired via both vertical and horizontal transmission. *Environmental Microbiology*, *17*(10), 3807–3821. https://doi.org/10.1111/1462-2920.12827

Smith, A. M., Berman, J., Key, M. M., & Winter, D. J. (2013). Not all sponges will thrive in a high-CO2 ocean: Review of the mineralogy of calcifying sponges. *Palaeogeography, Palaeoclimatology, Palaeoecology*. https://doi.org/10.1016/j.palaeo.2013.10.004

Sogin, E. M., Putnam, H. M., Anderson, P. E., & Gates, R. D. (2016). Metabolomic signatures of increases in temperature and ocean acidification from the reef-building coral, Pocillopora damicornis. *Metabolomics*. https://doi.org/10.1007/s11306-016-0987-8

Steindler, L., Huchon, D., Avni, A., & Ilan, M. (2005). 16S rRNA phylogeny of sponge-associated cyanobacteria. *Applied and Environmental Microbiology*, *71*(7), 4127–4131. https://doi.org/10.1128/AEM.71.7.4127-4131.2005

Steindler, L., Schuster, S., Ilan, M., Avni, A., Cerrano, C., & Beer, S. (2007). Differential gene expression in a marine sponge in relation to its symbiotic state. *Marine Biotechnology*, *9*(5), 543–549. https://doi.org/10.1007/s10126-007-9024-2

Sung, C. G., Kim, T. W., Park, Y. G., Kang, S. G., Inaba, K., Shiba, K., Choi, T. S., Moon, S. D., Litvin, S., Lee, K. T., & Lee, J. S. (2014). Species and gamete-specific fertilization success of two sea urchins under near future levels of pCO2. *Journal of Marine Systems*. https://doi.org/10.1016/j.jmarsys.2014.04.013

Szalaj, D., De Orte, M. R., Goulding, T. A., Medeiros, I. D., DelValls, T. A., & Cesar, A. (2017). The effects of ocean acidification and a carbon dioxide capture and storage leak on the early life stages of the marine mussel Perna perna (Linneaus, 1758) and metal bioavailability. *Environmental Science and Pollution Research*. https://doi.org/10.1007/s11356-016-7863-y

Taylor, M. W., Radax, R., Steger, D., & Wagner, M. (2007). Sponge-Associated Microorganisms: Evolution, Ecology, and Biotechnological Potential. *Microbiology and Molecular Biology Reviews*, *71*(2), 295–347. https://doi.org/10.1128/MMBR.00040-06

Taylor, Michael W., Hill, R. T., Piel, J., Thacker, R. W., & Hentschel, U. (2007). Soaking it up: The complex lives of marine sponges and their microbial associates. *ISME Journal*, *1*(3), 187–190. https://doi.org/10.1038/ismej.2007.32

Teixidó, N., Caroselli, E., Alliouane, S., Ceccarelli, C., Comeau, S., Gattuso, J. P., Fici, P., Micheli, F., Mirasole, A., Monismith, S. G., Munari, M., Palumbi, S. R., Sheets, E., Urbini, L., De Vittor, C., Goffredo, S., & Gambi, M. C. (2020). Ocean acidification causes variable trait-shifts in a coral species. *Global Change Biology*. https://doi.org/10.1111/gcb.15372

Teixidó, N., Gambi, M. C., Parravacini, V., Kroeker, K., Micheli, F., Villéger, S., & Ballesteros, E. (2018). Functional biodiversity loss along natural CO2 gradients. *Nature Communications*, *9*(1), 1–9. https://doi.org/10.1038/s41467-018-07592-1

Thacker, R. W. (2005). Impacts of shading on sponge-cyanobacteria symbioses: A comparison between host-specific and generalist associations. *Integrative and Comparative Biology*, *45*(2), 369–376. https://doi.org/10.1093/icb/45.2.369

Thiel, V., Leininger, S., Schmaljohann, R., Brümmer, F., & Imhoff, J. F. (2007a). Sponge-specific bacterial associations of the Mediterranean sponge Chondrilla nucula (Demospongiae, Tetractinomorpha). *Microbial Ecology*, *54*(1), 101–111. https://doi.org/10.1007/s00248-006-9177-y

Thomas, T., Moitinho-Silva, L., Lurgi, M., Björk, J. R., Easson, C., Astudillo-García, C., Olson, J. B., Erwin, P. M., López-Legentil, S., Luter, H., Chaves-Fonnegra, A., Costa, R., Schupp, P. J., Steindler, L., Erpenbeck, D., Gilbert, J., Knight, R., Ackermann, G., Victor Lopez, J., … Webster, N. S. (2016). Diversity, structure and convergent evolution of the global sponge microbiome. *Nature Communications*, *7*(May). https://doi.org/10.1038/ncomms11870

Uriz, M. J., Becerro, M. A., Tur, J. M., & Turon, X. (1996). Location of toxicity within the mediterranean sponge Crambe crambe (Demospongiae: Poecilosclerida). *Marine Biology*. https://doi.org/10.1007/BF00351039

Uriz, Maria J., Turon, X., & Becerro, M. A. (2003). *Silica Deposition in Demosponges*. https://doi.org/10.1007/978-3-642-55486-5_7

Uriz, María J., Turon, X., & Becerro, M. A. (2001). Morphology and ultrastructure of the swimming larvae of crambe crambe (Demospongiae, Poecilosclerida). *Invertebrate Biology*. https://doi.org/10.1111/j.1744-7410.2001.tb00039.x

Uriz, Maria J, Becerro, A., Galera, J., & Lozano, J. (1995). Patterns of resource allocation to somatic, defensive, and reproductive functions in the Mediterranean encrusting sponge Crambe crambe (Demospongiae, Poecilosclerida). *Marine Ecology Progress Series*, *124*, 159–170.

Usher, K., Toze, S., Fromont, J., Kuo, J., & Sutton, D. (2004). A new species of cyanobacterial symbiont from the marine sponge Chondrilla nucula. *Symbiosis*, *36*(2), 183–192.

Uthicke, S., & Fabricius, K. E. (2012). Productivity gains do not compensate for reduced calcification under near-future ocean acidification in the photosynthetic benthic foraminifer species Marginopora vertebralis. *Global Change Biology*. https://doi.org/10.1111/j.1365-2486.2012.02715.x

Uthicke, S., Pecorino, D., Albright, R., Negri, A. P., Cantin, N., Liddy, M., Dworjanyn, S., Kamya, P., Byrne, M., & Lamare, M. (2013). Impacts of ocean acidification on early life-history stages and settlement of the coral-eating sea star Acanthaster planci. *PLoS ONE*. https://doi.org/10.1371/journal.pone.0082938

Vacelet, J., & Donadey, C. (1977a). Electron microscope study of the association between some sponges and bacteria. *Journal of Experimental Marine Biology and Ecology*. https://doi.org/10.1016/0022-0981(77)90038-7

Verhoeven, J. T. P., Kavanagh, A. N., & Dufour, S. C. (2017). Microbiome analysis shows enrichment for specific bacteria in separate anatomical regions of the deep-sea carnivorous sponge Chondrocladia grandis. *FEMS Microbiology Ecology*. https://doi.org/10.1093/femsec/fiw214

Vicente, J., Silbiger, N. J., Beckley, B. A., Raczkowski, C. W., & Hill, R. T. (2016). Impact of high pCO2 and warmer temperatures on the process of silica biomineralization in the sponge mycale grandis. In *ICES Journal of Marine Science*. https://doi.org/10.1093/icesjms/fsv235

Villegas-Plazas, M., Wos-Oxley, M. L., Sanchez, J. A., Pieper, D. H., Thomas, O. P., & Junca, H. (2019). Variations in Microbial Diversity and Metabolite Profiles of the Tropical Marine Sponge Xestospongia muta with Season and Depth. *Microbial Ecology*. https://doi.org/10.1007/s00248-018-1285-y

Von Wintzingerode, F., Landt, O., Ehrlich, A., & Göbel, U. B. (2000). Peptide nucleic acid-mediated PCR clamping as a useful supplement in the determination of microbial diversity. *Applied and Environmental Microbiology*. https://doi.org/10.1128/AEM.66.2.549-557.2000

Wang, Q., Cao, R., Ning, X., You, L., Mu, C., Wang, C., Wei, L., Cong, M., Wu, H., & Zhao, J. (2016). Effects of ocean acidification on immune responses of the Pacific oyster Crassostrea gigas. *Fish and Shellfish Immunology*. https://doi.org/10.1016/j.fsi.2015.12.025

Webster, N. S., Negri, A. P., Botté, E. S., Laffy, P. W., Flores, F., Noonan, S., Schmidt, C., & Uthicke, S. (2016). Host-associated coral reef microbes respond to the cumulative pressures of ocean warming and ocean acidification. *Scientific Reports*, *6*(August 2015), 1–9. https://doi.org/10.1038/srep19324

Webster, N. S., Negri, A. P., Flores, F., Humphrey, C., Soo, R., Botté, E. S., Vogel, N., & Uthicke, S. (2013). Near-future ocean acidification causes differences in microbial associations within diverse coral reef taxa. *Environmental Microbiology Reports*, *5*(2), 243–251. https://doi.org/10.1111/1758-2229.12006

Webster, Nicole S., & Taylor, M. W. (2012). Marine sponges and their microbial symbionts: Love and other relationships. *Environmental Microbiology*, *14*(2), 335–346. https://doi.org/10.1111/j.1462-2920.2011.02460.x

Webster, Nicole S., & Thomas, T. (2016). The sponge hologenome. *MBio*. https://doi.org/10.1128/mBio.00135-16

Wickham, H. (2016). ggplot2: Elegant Graphics for Data Analysis. In *Journal of the Royal Statistical Society: Series A (Statistics in Society)*.

Wilkinson, C. R., & Vacelet, J. (1979). Transplantation of marine sponges to different conditions of light and current. *Journal of Experimental Marine Biology and Ecology*. https://doi.org/10.1016/0022-0981(79)90028-5

Williamson, P., Pörtner, H., Widdicombe, S., & Gattuso, J. (2020). *Ideas and Perspectives : When ocean acidification experiments are not the same , reproducibility is not tested*. *November*, 1–7.

Wirth, J. S., & Whitman, W. B. (2019). R uegeria . In *Bergey's Manual of Systematics of Archaea and Bacteria*. https://doi.org/10.1002/9781118960608.gbm00870.pub2

Wisshak, M., Schönberg, C. H. L., Form, A., & Freiwald, A. (2014). Sponge bioerosion accelerated by ocean acidification across species and latitudes? *Helgoland Marine Research*. https://doi.org/10.1007/s10152-014-0385-4

Yang, R. H., Su, J. H., Shang, J. J., Wu, Y. Y., Li, Y., Bao, D. P., & Yao, Y. J. (2018). Evaluation of the ribosomal DNA internal transcribed spacer (ITS), specifically ITS1 and ITS2, for the analysis of fungal diversity by deep sequencing. *PLoS ONE*. https://doi.org/10.1371/journal.pone.0206428

Yu, Z., Zhang, B., Sun, W., Zhang, F., & Li, Z. (2013). Phylogenetically diverse endozoic fungi in the South China Sea sponges and their potential in synthesizing bioactive natural products suggested by PKS gene and cytotoxic activity analysis. *Fungal Diversity*. https://doi.org/10.1007/s13225-012-0192-7

Zhang, D., Li, S., Wang, G., & Guo, D. (2011). Impacts of CO2-driven seawater acidification on survival, egg production rate and hatching success of four marine copepods. *Acta Oceanologica Sinica*. https://doi.org/10.1007/s13131-011-0165-9

Zheng, C. qun, Jeswin, J., Shen, K. li, Lablche, M., Wang, K. jian, & Liu, H. peng. (2015). Detrimental effect of CO2-driven seawater acidification on a crustacean brine shrimp, Artemia sinica. *Fish and Shellfish Immunology*. https://doi.org/10.1016/j.fsi.2014.12.027

Zheng, X., Kuo, F., Pan, K., Huang, H., & Lin, R. (2019). Different calcification responses of two hermatypic corals to CO2-driven ocean acidification. *Environmental Science and Pollution Research*. https://doi.org/10.1007/s11356-018-1376-9

Zhou, K., Zhang, X., Zhang, F., & Li, Z. (2011). Phylogenetically Diverse Cultivable Fungal Community and Polyketide Synthase (PKS), Non-ribosomal Peptide Synthase (NRPS) Genes Associated with the South China Sea Sponges. *Microbial Ecology*. https://doi.org/10.1007/s00248-011-9859-y

Zhou, Z. F., Menna, M., Cai, Y. S., & Guo, Y. W. (2015). Polyacetylenes of marine origin: Chemistry and bioactivity. In *Chemical Reviews*. https://doi.org/10.1021/cr4006507

8. SUPPLEMENTARY MATERIAL

8.1 Supplementary figures

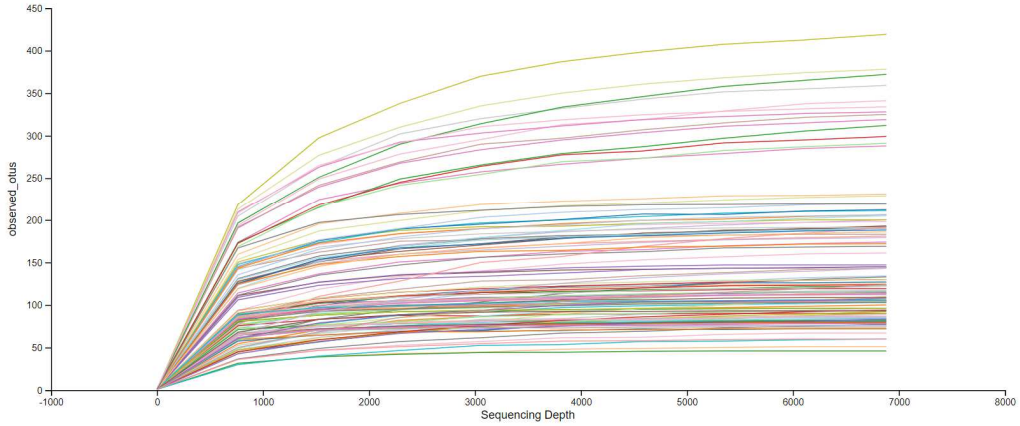

Figure S1 – Rarefaction curves of the whole dataset with threshold set up at 6881 reads per sample. No samples were lost during this process.

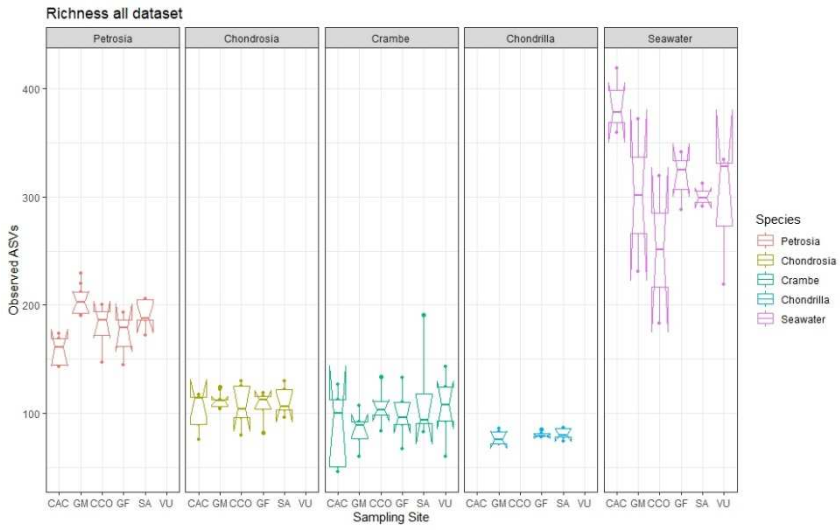

Figure S2 – Observed ASVs values plotted by sponge species and divided by sampling sites of the whole dataset.

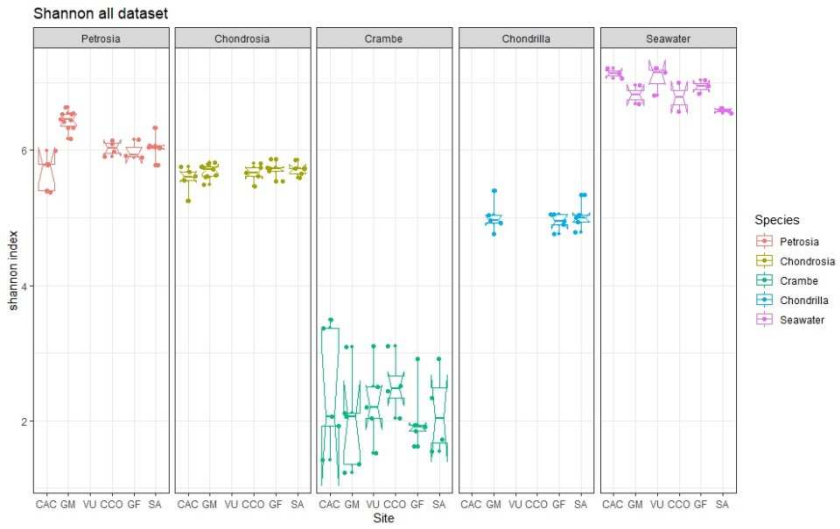

Figure S3 – Shannon values, plotted by sponge species and divided by sampling site of the whole dataset.

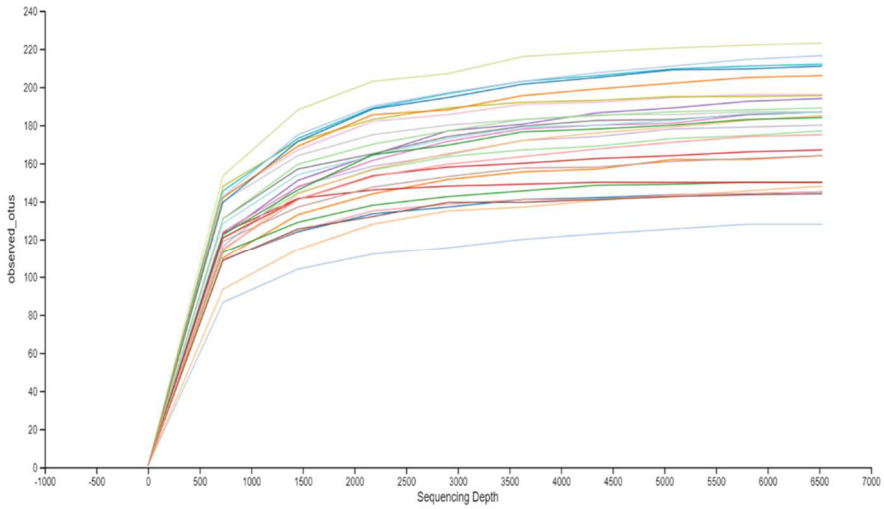

Figure S4 – Rarefaction curves of the *Petrosia ficiformis* dataset. Every sample has reached a plateau in the rarefaction and all the samples were retained in the analysis. Threshold: 6528 reads per sample.

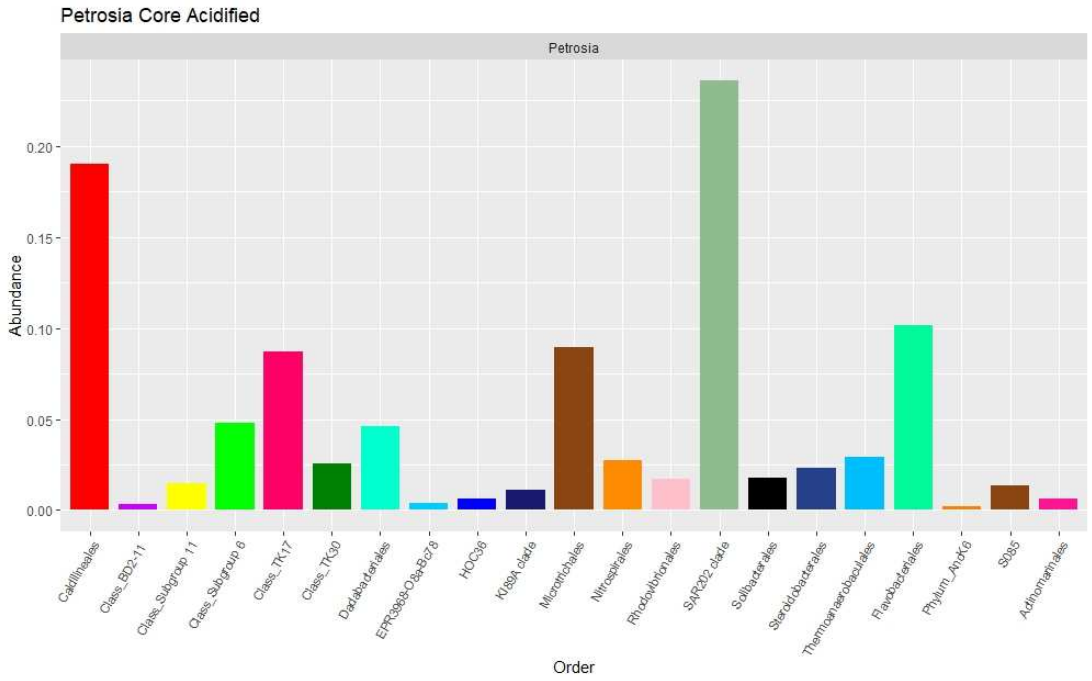

Figure S5 – Core microbial taxa associated to all the samples coming from the acidified sites for the sponge *Petrosia ficiformis*.

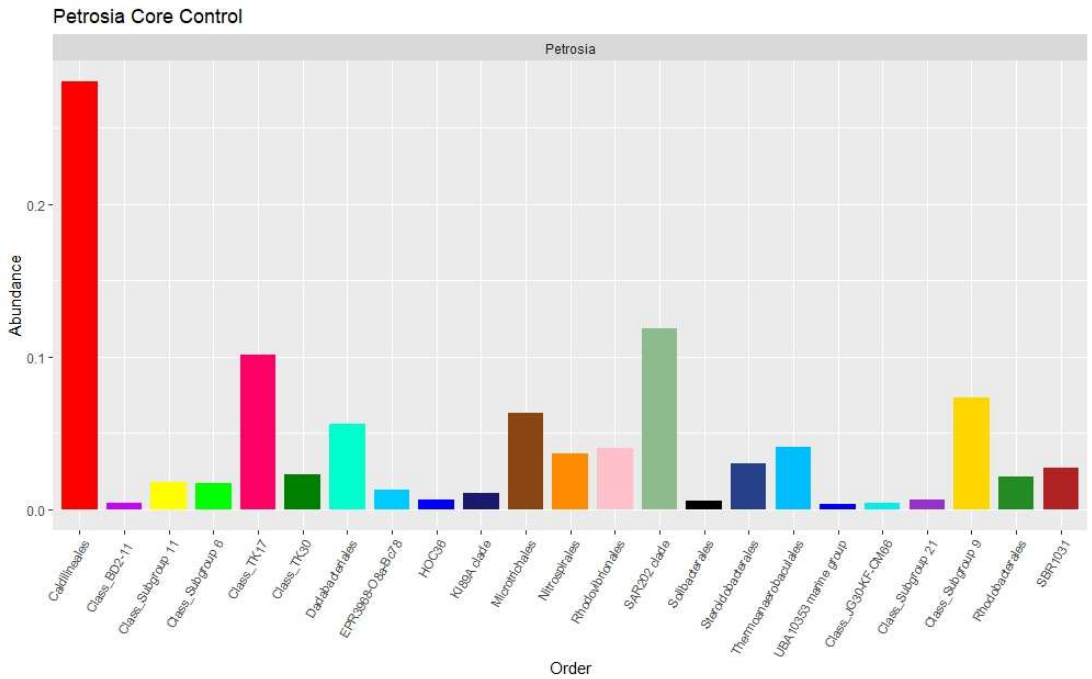

Figure S6 – Core microbial taxa associated to all the samples coming from the control's sites for the sponge *Petrosia ficiformis*.

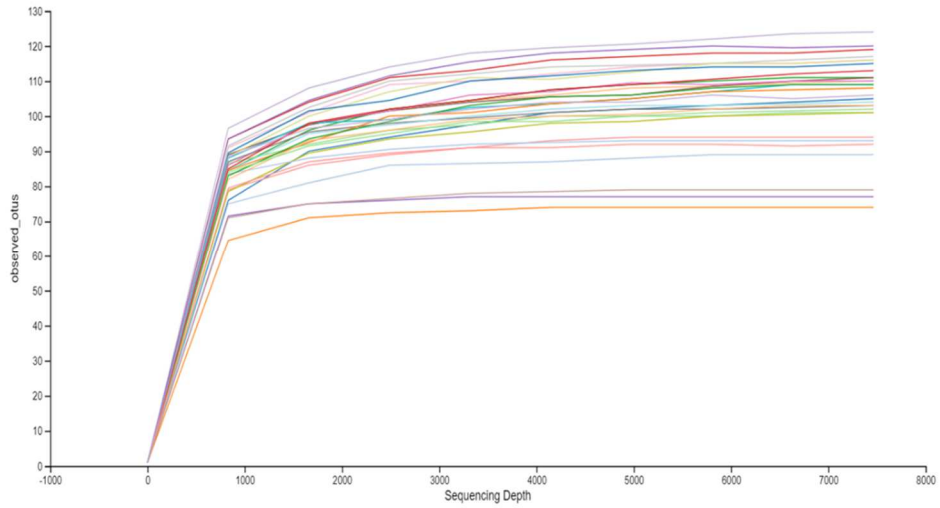

Figure S7 - Rarefaction curves of the samples belonging to the sponge species *Chondrosia reniformis*. All the samples were retained in the analysis and the curves reached a plateau. Cutoff sequences: 7.463.

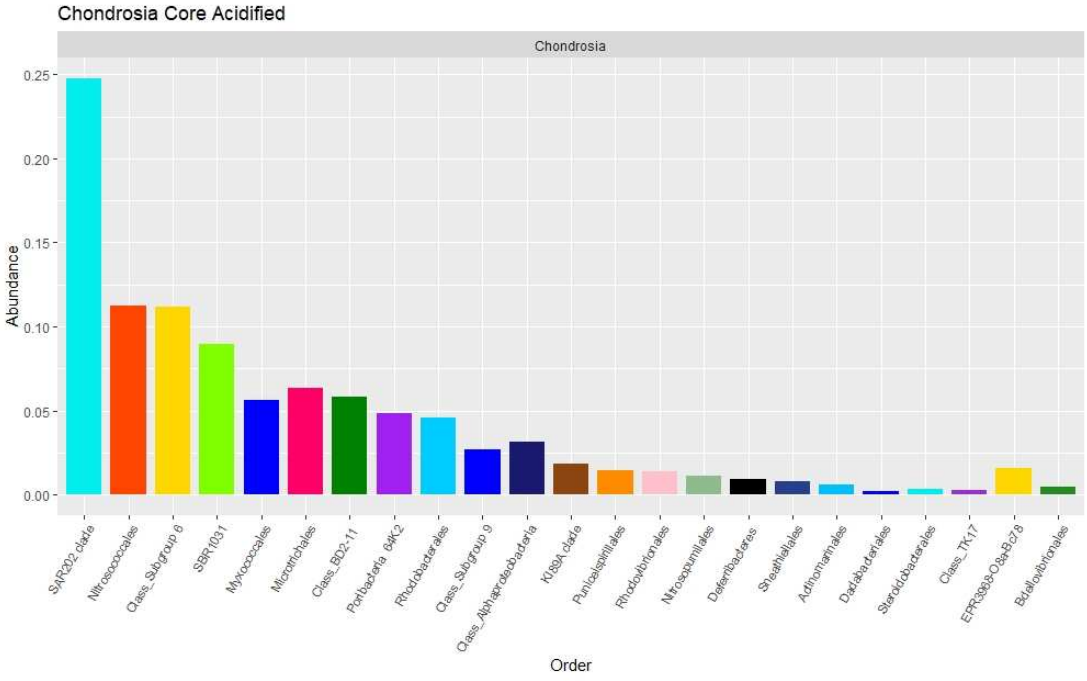

Figure S8 - Core microbial taxa associated to all the samples coming from the acidified sites for the sponge *Chondrosia reniformis*.

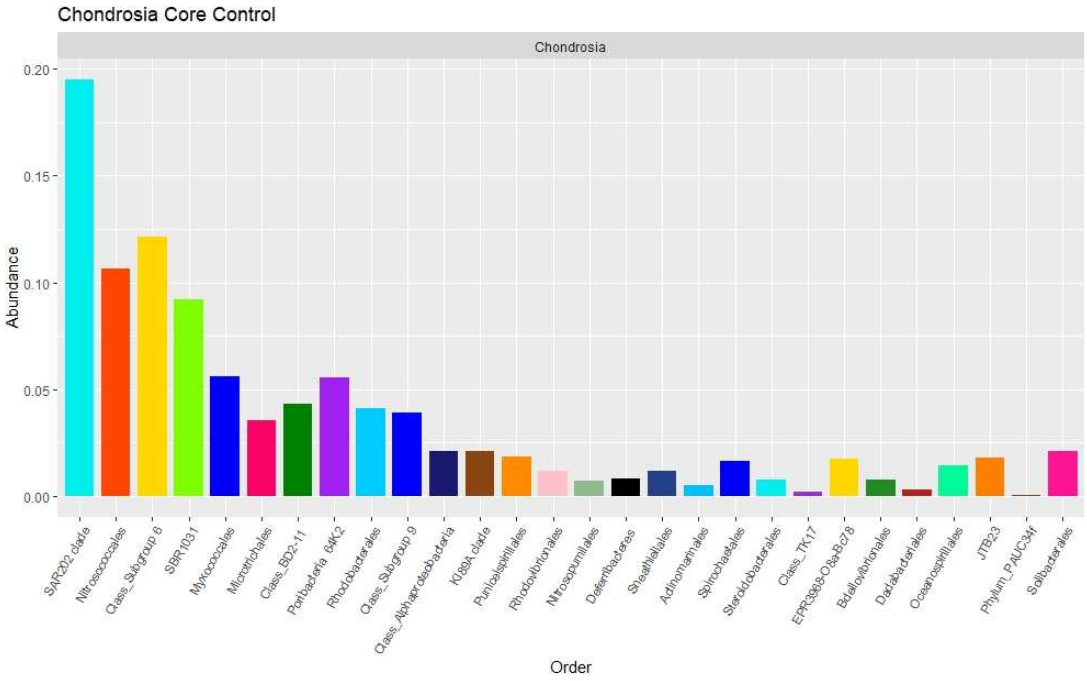

Figure S9 - Core microbial taxa associated to all the samples coming from the control sites for the sponge *Chondrosia reniformis.*

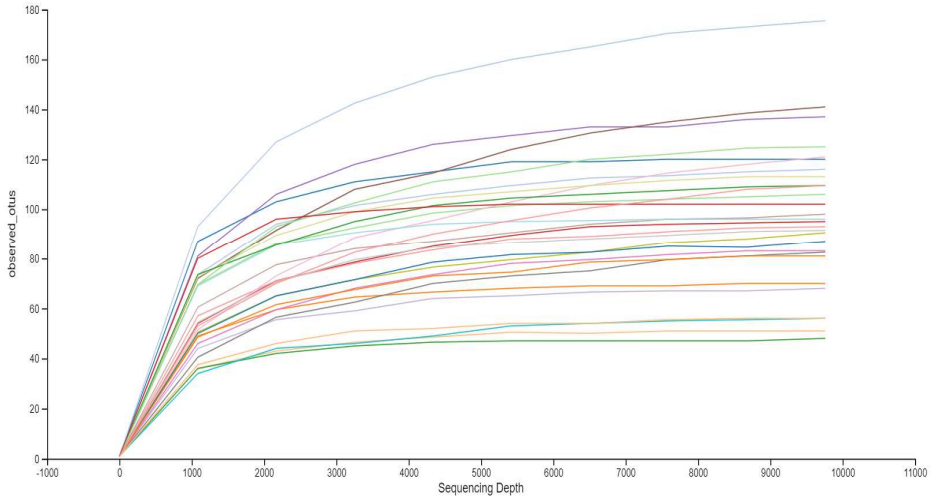

Figure S10 – Rarefaction curves for the dataset of the sponge *Crambe crambe*. Cutoff at 9.759 reads per sample.

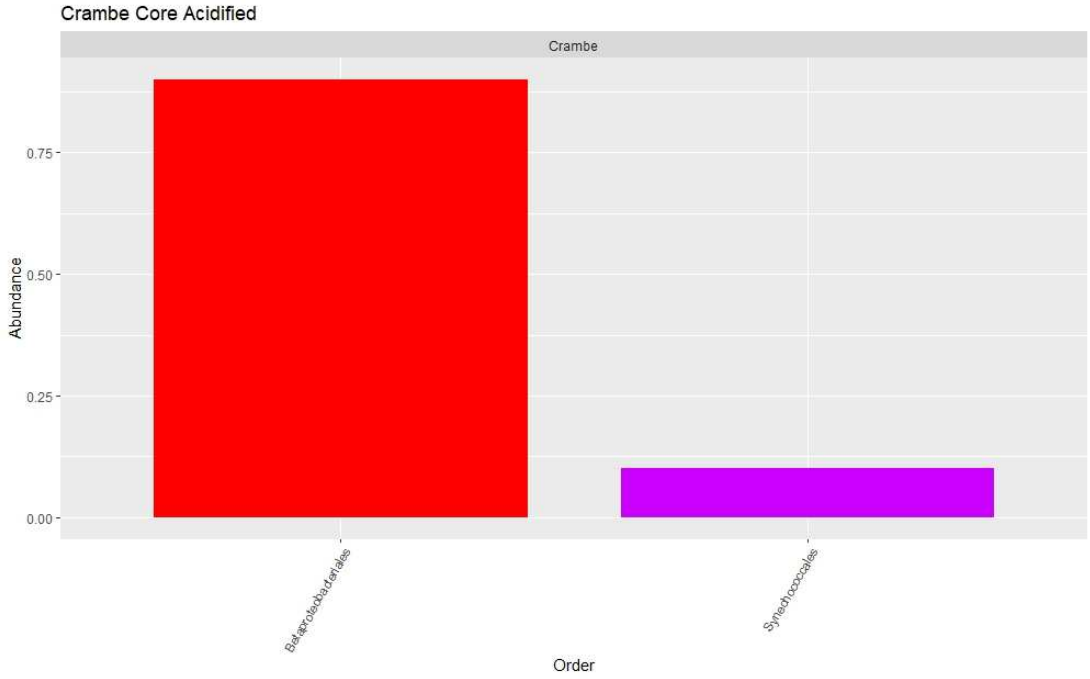

Figure S11 - Core microbial taxa associated to all the samples coming from the acidified sites for the sponge *Crambe crambe.*

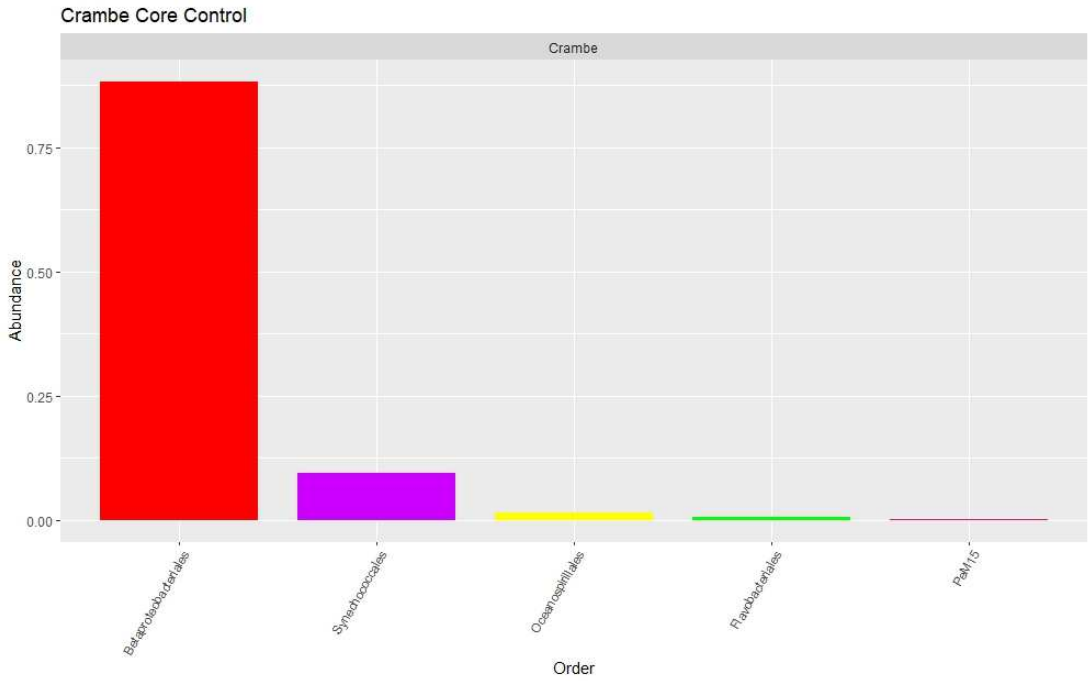

Figure S12 - Core microbial taxa associated to all the samples coming from the control sites for the sponge *Crambe crambe.*

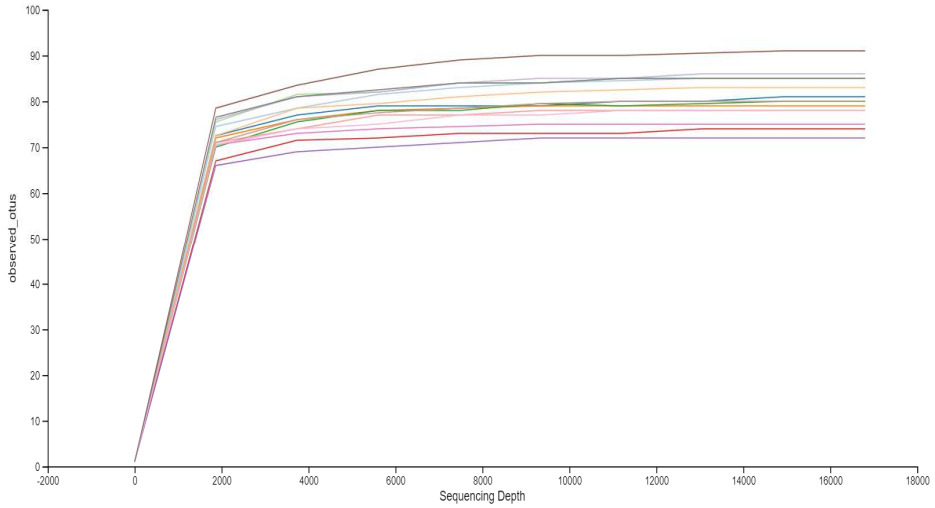

Figure S13 – Rarefaction curves for the dataset of the sponge *Chondrilla nucula.* Cutoff at 16.804 reads per sample.

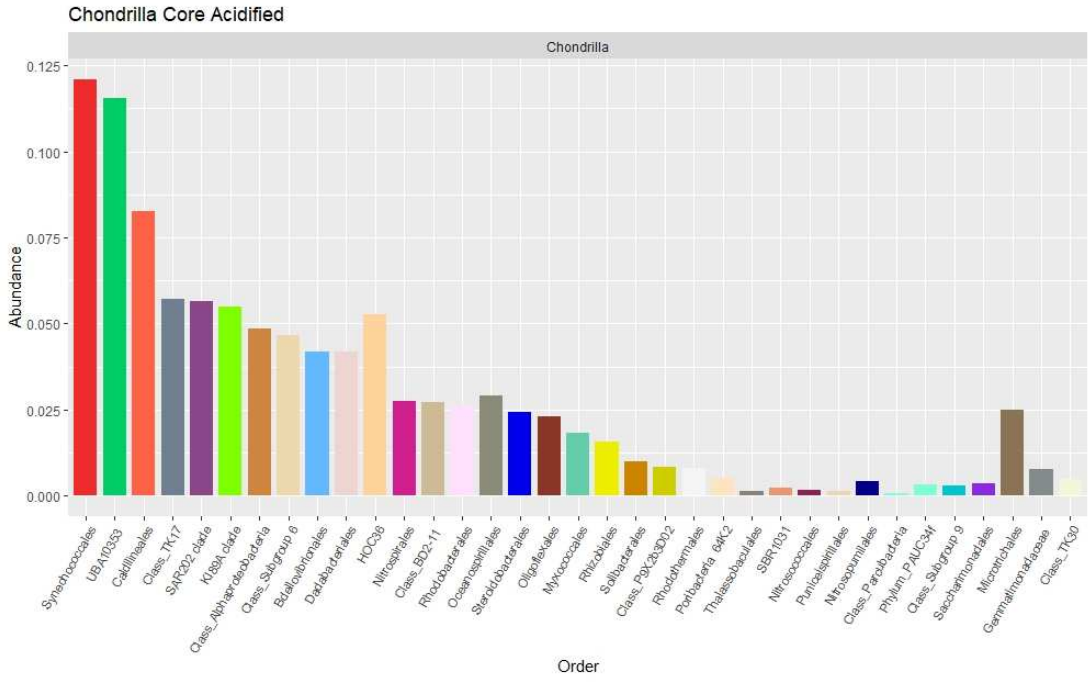

Figure S14 - Core microbial taxa associated to all the samples coming from the acidified sites for the sponge *Chondrilla nucula.*

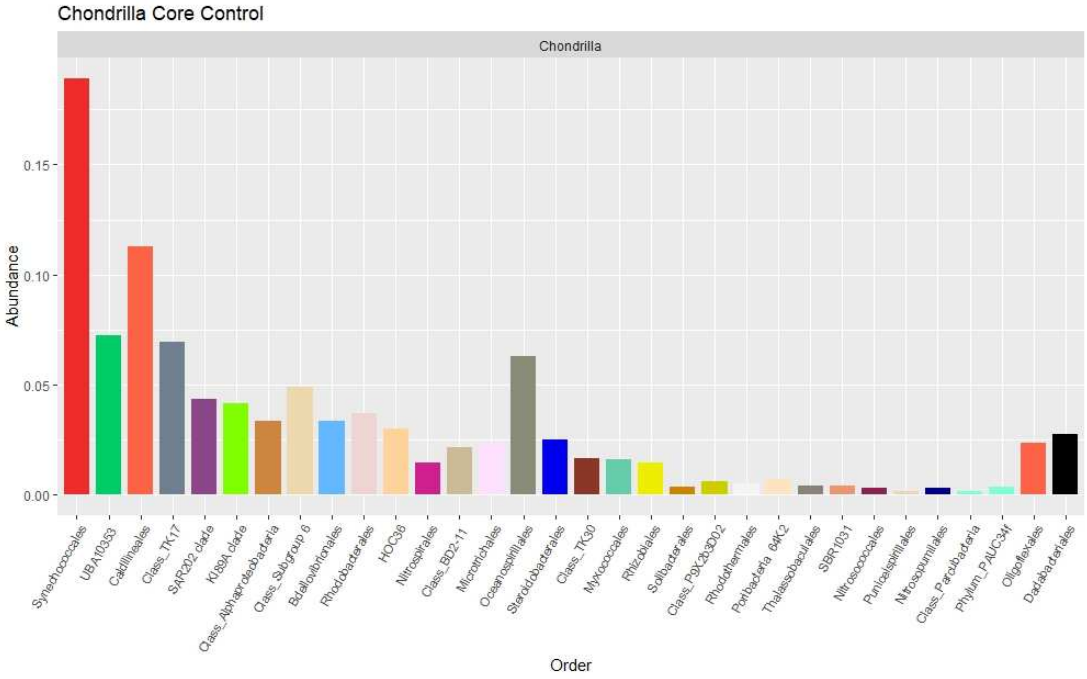

Figure S15 - Core microbial taxa associated to all the samples coming from the control sites for the sponge *Chondrilla nucula.*

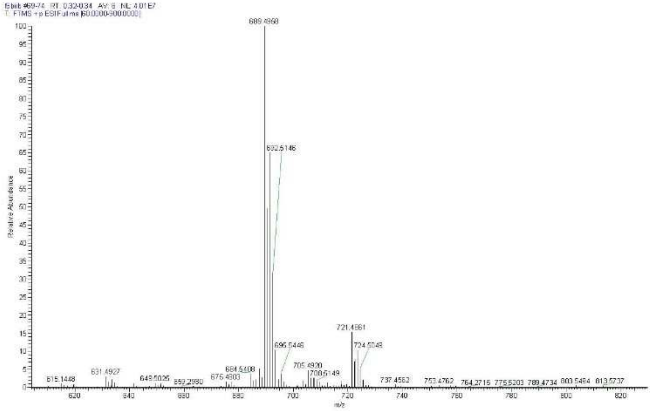

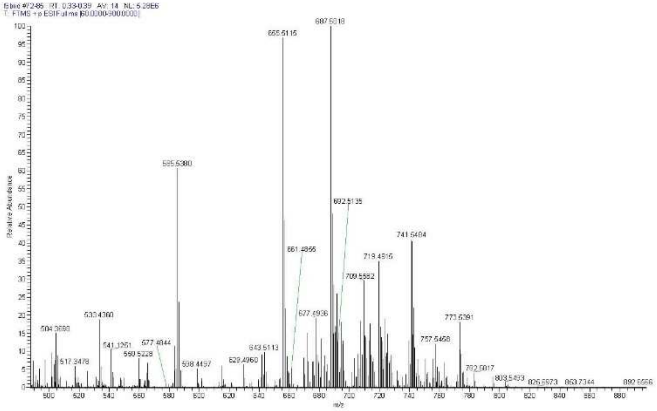

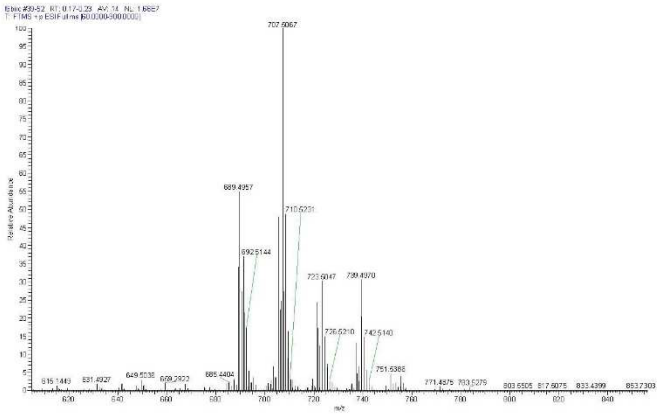

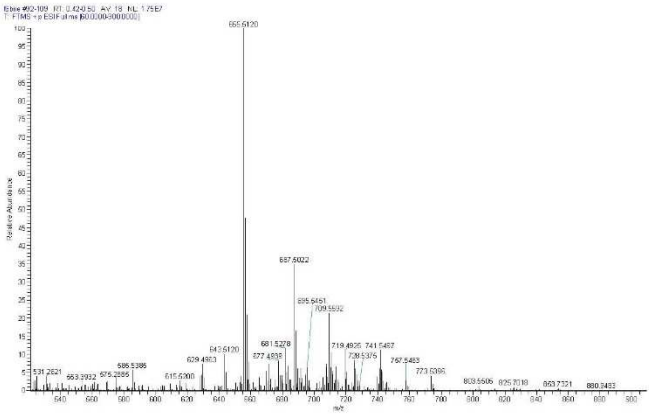

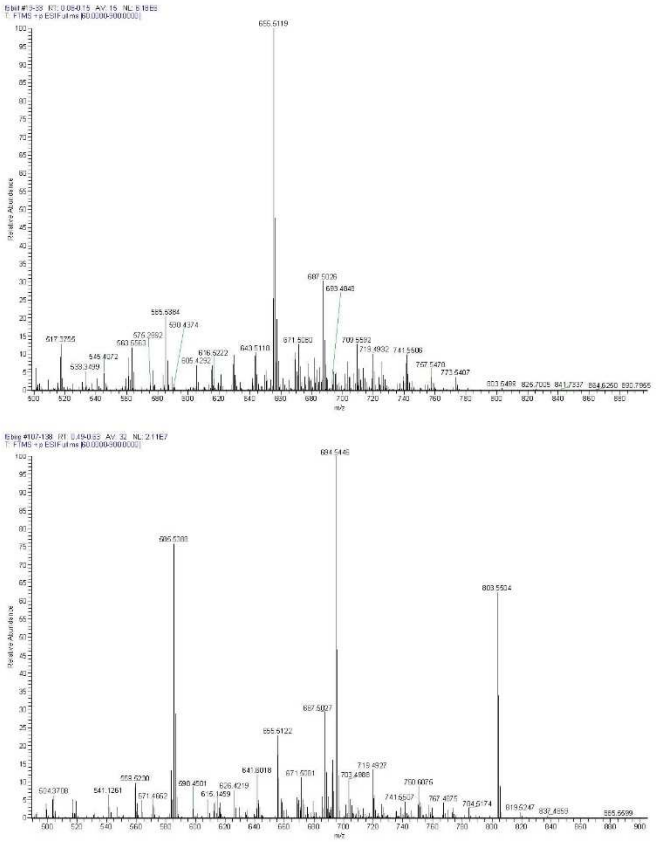

Figure S16 – Mass spectra reporting the most abundant molecular masses for each fractionating step of the sample F6BII (control).

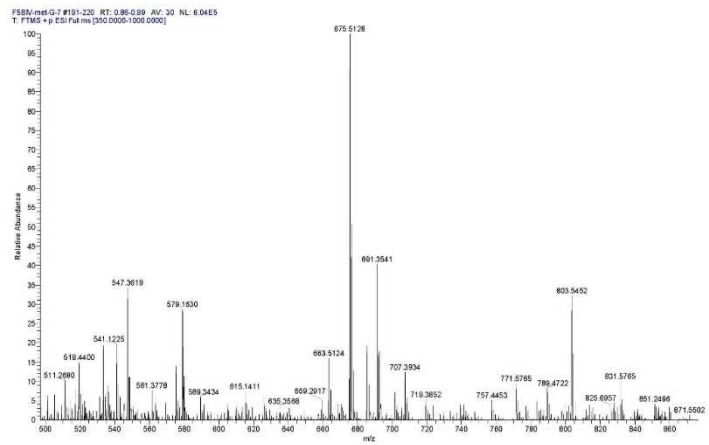

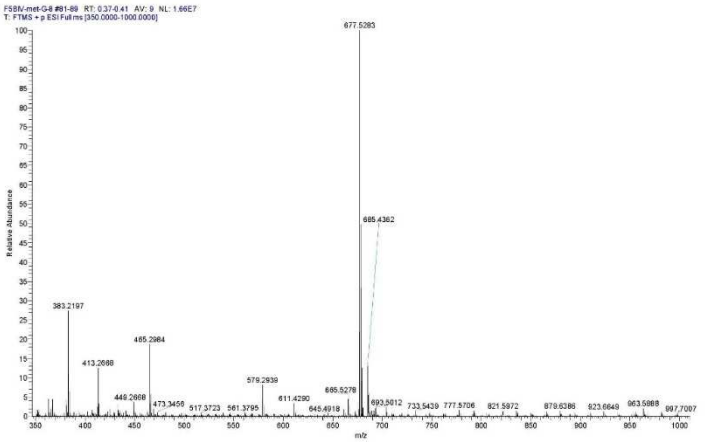

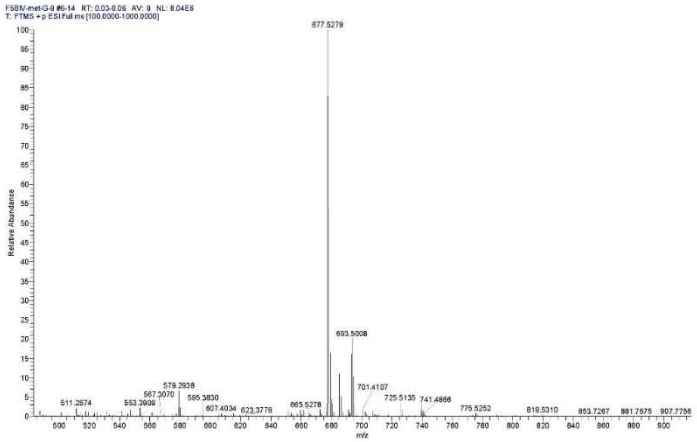

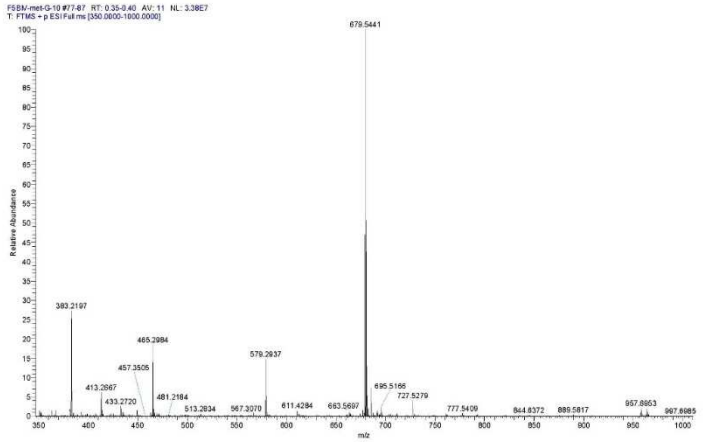

Figure S17 – Mass spectra reporting the most abundant molecular masses for each fractionating step of the sample F5BIV (acidified).

8.2 Supplementary tables

Table S1 – Supplementary information for the whole dataset.

Sponge species	*Petrosia ficiformis*	*Chondrosia reniformis*	*Crambe crambe*	*Chondrilla nucula*
Number of samples	28	30	28	15
Total reads (non-rarefied)	1.517.059	1.043.788	982.653	511.735
Total reads (rarefied)	182.784	223.890	273.252	252.060
Total ASVs (non-rarefied)	1336	630	3055	267
Total ASVs (rarefied)	511	232	523	130
Rarefaction threshold	6528	7463	9759	16804
Kingdoms	2	2	2	2
Phyla	21	17	22	13
Classes	49	29	36	26
Orders	72	47	85	40
Families	69	42	118	42
Genera	67	36	140	33

Table S2 –Statistical analyses for the whole microbiome dataset (between sponge species).

Alpha diversity microbiome

```
Kruskal-Wallis rank sum test:

Observed ASVs by sponge species
Kruskal-Wallis chi-squared = 91.066, df = 4, p-value < 2.2e-16

         Pairwise comparisons using Wilcoxon rank sum test

           Chondrilla Chondrosia Crambe  Petrosia
Chondrosia 2.2e-06    -          -       -
Crambe     0.0037     0.0425     -       -
Petrosia   2.3e-07    1.4e-09    5.2e-09 -
Seawater   2.9e-06    1.3e-07    1.4e-07 1.3e-06
```

```
Kruskal-Wallis rank sum test:

Shannon index by sponge species
Kruskal-Wallis chi-squared = 104.86, df = 4, p-value < 2.2e-16


         Pairwise comparisons using Wilcoxon rank sum test

           Chondrilla Chondrosia Crambe  Petrosia
Chondrosia 5.8e-11    -          -       -
Crambe     2.6e-11    1.3e-15    -       -
Petrosia   5.8e-11    8.4e-09    2.6e-15 -
Seawater   7.4e-09    1.0e-11    1.2e-11 1.8e-10
```

Beta diversity microbiome

PERMANOVA 9999 permutations: bray distance by sponge species

	Df	SumsOfSqs	MeanSqs	F.Model	R2	Pr(>F)	
Species	4	38.440	9.610	141.25	0.83704	9.999e-05	***
Residuals	110	7.484	0.068		0.16296		
Total	114	45.924			1.00000		

Pairwise comparisons:

	pairs	F.Model	R2	p.value	p.adjusted	sig
1	Crambe vs Chondrosia	4433.1571	0.9877455	0.001	0.001	**
2	Crambe vs Petrosia	2812.9029	0.9815067	0.001	0.001	**
3	Crambe vs Seawater	907.2116	0.9557528	0.001	0.001	**
4	Crambe vs Chondrilla	1527.5985	0.9738620	0.001	0.001	**
5	Chondrosia vs Petrosia	5287.2428	0.9898900	0.001	0.001	**
6	Chondrosia vs Seawater	2909.0654	0.9854339	0.001	0.001	**
7	Chondrosia vs Chondrilla	4005.3380	0.9896228	0.001	0.001	**
8	Petrosia vs Seawater	1535.3778	0.9739910	0.001	0.001	**
9	Petrosia vs Chondrilla	1791.5962	0.9781611	0.001	0.001	**
10	Seawater vs Chondrilla	1030.3572	0.9726249	0.001	0.001	**

PERMANOVA 9999 permutations: jaccard distance by sponge species

	Df	SumsOfSqs	MeanSqs	F.Model	R2	Pr(>F)	
Species	4	19.8344	4.9586	77.698	0.73859	9.999e-05	***
Residuals	110	7.0201	0.0638		0.26141		
Total	114	26.8545			1.00000		

Pairwise comparisons:

	pairs	F.Model	R2	p.value	p.adjusted	sig
1	Crambe vs Chondrosia	1050.47029	0.9502474	0.001	0.001	**
2	Crambe vs Petrosia	842.64715	0.9408249	0.001	0.001	**
3	Crambe vs Seawater	49.86955	0.5428300	0.001	0.001	**
4	Crambe vs Chondrilla	395.42161	0.9060541	0.001	0.001	**
5	Chondrosia vs Petrosia	786.79770	0.9357753	0.001	0.001	**
6	Chondrosia vs Seawater	1860.81150	0.9774137	0.001	0.001	**
7	Chondrosia vs Chondrilla	256.81100	0.8594429	0.001	0.001	**
8	Petrosia vs Seawater	1707.09633	0.9765459	0.001	0.001	**
9	Petrosia vs Chondrilla	327.03828	0.8910195	0.001	0.001	**
10	Seawater vs Chondrilla	805.55989	0.9652511	0.001	0.001	**

Table S3 –Statistical analyses for the whole mycobiome dataset (between sponge species).

Alpha diversity mycobiome

```
Kruskal-Wallis rank sum test:

Shannon index by Sponge_Species
Kruskal-Wallis chi-squared = 10.984, df = 4, p-value = 0.02674


Observed ASVs by sponge species
Kruskal-Wallis chi-squared = 9.7497, df = 4, p-value = 0.04486
```

Beta diversity mycobiome

```
        PERMANOVA 9999 permutations: bray distance by sponge species

                Df SumsOfSqs MeanSqs F.Model      R2 Pr(>F)
Sponge_Species   4     1.919 0.47980  1.0627 0.03787 0.2074
Residuals      108    48.761 0.45149         0.96213
Total          112    50.681                 1.00000


        PERMANOVA 9999 permutations: jaccard distance by sponge species

                Df SumsOfSqs MeanSqs F.Model      R2 Pr(>F)
Sponge_Species   4     1.999 0.49987   1.058 0.03771 0.1296
Residuals      108    51.028 0.47248         0.96229
Total          112    53.027                 1.00000
```

Table S4 – Statistical analysis for the putative functions

```
        PERMANOVA 9999 permutations: putative functions by sponge species

            Df SumsOfSqs MeanSqs  F.Model    R2    Pr(>F)
Species      3   16.4569  5.4856   142.5 0.81506 9.999e-05 ***
Residuals   97    3.7342  0.0385         0.18494
Total      100   20.1911                1.00000
---
Pairwise comparisons:

                     pairs   F.Model        R2 p.value p.adjusted sig
1   Petrosia vs Chondrosia  28.65681 0.3385057   0.001      0.001  **
2       Petrosia vs Crambe 191.14033 0.7797180   0.001      0.001  **
3   Petrosia vs Chondrilla 172.28895 0.8077725   0.001      0.001  **
4     Chondrosia vs Crambe 220.03615 0.7971280   0.001      0.001  **
5 Chondrosia vs Chondrilla 184.97368 0.8113817   0.001      0.001  **
6     Crambe vs Chondrilla  53.40415 0.5656970   0.001      0.001  **
```

Table S5 – Results of the Gneiss linear regression for the microbiome associated with the four sponge species.

No. Observations	119.0000
Model:	OLS
Rsquared:	0.7854

	mse	Rsquared	R2diff
Intercept	111.2382	0.7294	0.0560
Species[T.Chondrosia]	153.4398	0.6268	0.1587
Species[T.Crambe]	127.7264	0.6893	0.0961
Species[T.Petrosia]	157.7875	0.6162	0.1692
Species[T.Seawater]	150.6226	0.6336	0.1518
Site[T.CCO]	89.6885	0.7818	0.0036
Site[T.GF]	90.4368	0.7800	0.0054
Site[T.GM]	91.3753	0.7777	0.0077
Site[T.SA]	90.1762	0.7807	0.0048
Site[T.VU]	89.9308	0.7813	0.0042

	model_mse	Rsquared	pred_mse
fold_0	72.2941	0.7972	14.5964
fold_1	70.9822	0.7895	13.8621
fold_2	67.7666	0.8040	16.9144
fold_3	75.7496	0.7818	7.3258
fold_4	72.0477	0.7861	11.3216
fold_5	76.4482	0.7808	7.0688
fold_6	75.1960	0.7813	8.6090
fold_7	65.4088	0.7991	20.3345
fold_8	75.9851	0.7810	7.3245
fold_9	69.8418	0.7890	14.0164

Table S6 – Results of the Gneiss linear regression for the mycobiome associated with the four sponge species.

No. Observations	113.0000
Model:	OLS
Rsquared:	0.0979

	mse	Rsquared	R2diff
Intercept	23.8321	0.0658	0.0321
Sponge_Species[T.Chondrosia]	23.2994	0.0867	0.0113
Sponge_Species[T.Crambe]	23.2263	0.0895	0.0084
Sponge_Species[T.Petrosia]	23.2587	0.0882	0.0097
Sponge_Species[T.Seawater]	23.3383	0.0851	0.0128
Sampling_Site[T.CCO]	23.0120	0.0979	0.0000
Sampling_Site[T.GF]	23.0120	0.0979	0.0000
Sampling_Site[T.GM]	23.4691	0.0800	0.0179
Sampling_Site[T.SA]	23.0120	0.0979	0.0000
Sampling_Site[T.VU]	23.3767	0.0836	0.0143
Acidified[T.Control]	23.0120	0.0979	0.0000

	model_mse	Rsquared	pred_mse
fold_0	18.5719	0.1022	5.5719
fold_1	19.8364	0.1232	3.3902
fold_2	20.4482	0.1127	2.7946
fold_3	20.1549	0.1174	3.2393
fold_4	20.0208	0.1043	3.2018
fold_5	20.0948	0.1097	2.8803
fold_6	20.7805	0.1103	2.1128
fold_7	20.5301	0.1090	2.5396
fold_8	20.7573	0.1078	2.3223
fold_9	20.6595	0.1008	2.6594

Table S7 – Statistical analyses for the sponge *Petrosia ficiformis* (alpha and beta diversity).

Alpha diversity *P. ficiformis*

```
Kruskal-Wallis rank sum test: Shannon index by sampling sites

data:  shannon by Site
Kruskal-Wallis chi-squared = 19.82, df = 4, p-value = 0.000542


Pairwise comparisons using Wilcoxon rank sum test:

    CAC    CCO    GF     GM
CCO 0.0635 -      -      -
GF  0.2041 0.7143 -      -
GM  0.0067 0.0155 0.0350 -
SA  0.0926 0.7672 0.7857 0.0067

Kruskal-Wallis rank sum test: observed ASVs by sampling Sites

Kruskal-Wallis chi-squared = 18.267, df = 4, p-value = 0.001094


Pairwise comparisons using Wilcoxon rank sum test:

    CAC   CCO   GF    GM
CCO 0.289 -     -     -
GF  0.513 0.881 -     -
GM  0.026 0.028 0.103 -
SA  0.030 0.513 0.513 0.028
```

```
Kruskal-Wallis rank sum test:

Shannon index by acidification
Kruskal-Wallis chi-squared = 2.5257, df = 1, p-value = 0.112


Observed ASVs by acidification
Kruskal-Wallis chi-squared = 2.386, df = 1, p-value = 0.1224
```

Beta diversity *P. ficiformis*

```
       PERMANOVA 9999 permutations: bray distance by sampling sites

          Df SumsOfSqs  MeanSqs F.Model      R2    Pr(>F)
Site       4    1.0488 0.262195  2.9861 0.34182 9.999e-05 ***
Residuals 23    2.0195 0.087804         0.65818
Total     27    3.0683                  1.00000

Pairwise comparisons:

        pairs  F.Model        R2 p.value  p.adjusted sig
1  CAC vs CCO 3.384477 0.2972888   0.013 0.021666667   .
2   CAC vs GF 2.000898 0.2500842   0.156 0.195000000
3   CAC vs GM 9.785871 0.4294710   0.001 0.003333333   *
4   CAC vs SA 5.142568 0.3912910   0.005 0.010000000   *
5   CCO vs GF 1.191912 0.1657295   0.260 0.288888889
6   CCO vs GM 5.243935 0.2874344   0.001 0.003333333   *
7   CCO vs SA 2.517934 0.2393943   0.027 0.038571429   .
8    GF vs GM 3.705394 0.2519752   0.003 0.007500000   *
9    GF vs SA 1.219374 0.1689030   0.299 0.299000000
10   GM vs SA 8.000213 0.3809587   0.001 0.003333333   *

---
       PERMANOVA 9999 permutations: Jaccard distance by sampling sites

          Df SumsOfSqs MeanSqs F.Model      R2    Pr(>F)
Site       4    1.4037 0.35092  2.7768 0.32566 9.999e-05 ***
Residuals 23    2.9066 0.12637         0.67434
Total     27    4.3103                 1.00000

Pairwise comparisons:

        pairs   F.Model        R2 p.value p.adjusted sig
1  CAC vs CCO  3.406254 0.2986304   0.007 0.01500000   .
2   CAC vs GF  3.523082 0.3699519   0.043 0.06142857
3   CAC vs GM 15.169683 0.5385110   0.002 0.01000000   *
4   CAC vs SA  6.140786 0.4342606   0.009 0.01500000   .
5   CCO vs GF  1.918985 0.2423271   0.080 0.08888889
6   CCO vs GM  8.479668 0.3947765   0.004 0.01333333   .
7   CCO vs SA  1.199993 0.1304341   0.264 0.26400000
8    GF vs GM  8.047740 0.4225037   0.008 0.01500000   .
9    GF vs SA  2.929775 0.3280906   0.064 0.08000000
10   GM vs SA  8.349863 0.3910968   0.001 0.01000000   *
```

```
        PERMANOVA 9999 permutations: bray distance by acidification
           Df SumsOfSqs MeanSqs F.Model      R2 Pr(>F)
Acidified  1   0.30418 0.30418  2.8612 0.09914  2e-04 ***
Residuals 26   2.76409 0.10631         0.90086
Total     27   3.06826                 1.00000
---

        PERMANOVA 9999 permutations: Jaccard distance by acidification
           Df SumsOfSqs MeanSqs F.Model      R2    Pr(>F)
Acidified  1    0.4141 0.41414  2.7637 0.09608 9.999e-05 ***
Residuals 26    3.8961 0.14985         0.90392
Total     27    4.3103                 1.00000
---
```

Table S8 – Welch's test for the Songbird log-ratios in *Petrosia ficiformis* by sampling site and acidification.

```
  Welch's Heteroscedastic F Test by sampling sites
------------------------------------------------------------
  Log_Ratio and Site
  statistic  : 14.6418
  num df     : 4
  denom df   : 9.889406
  p.value    : 0.0003662443

Pairwise comparison
------------------------------------------------------------
Level (a) Level (b)      p.value   No difference
1         CAC       CCO 0.0375935508          Reject
2         CAC        GF 0.0445425128          Reject
3         CAC        GM 1.0000000000      Not reject
4         CAC        SA 0.5008924442      Not reject
5         CCO        GF 1.0000000000      Not reject
6         CCO        GM 0.0007436577          Reject
7         CCO        SA 0.7278737391      Not reject
8          GF        GM 0.0009912861          Reject
9          GF        SA 0.6787326205      Not reject
10         GM        SA 0.0468008120          Reject
------------------------------------------------------------


  Welch's Heteroscedastic F Test by acidification
------------------------------------------------------------
  Log_Ratio and Acidification
  statistic  : 37.73946
  num df     : 1
  denom df   : 24.02692
  p.value    : 2.386719e-06
```

Table S9 – Statistical analyses for the sponge *Chondrosia reniformis* (alpha and beta diversity).

Alpha diversity *C. reniformis*

```
Kruskal-Wallis rank sum test:

Shannon index by sampling sites
Kruskal-Wallis chi-squared = 2.8219, df = 4, p-value = 0.5881



Shannon index by acidification
Kruskal-Wallis chi-squared = 0.1243, df = 1, p-value = 0.7244



Oserved ASVs by sampling site
Kruskal-Wallis chi-squared = 1.0566, df = 4, p-value = 0.9011


Observed ASVs by acidification
Kruskal-Wallis chi-squared = 0.062018, df = 1, p-value = 0.8033
```

Beta diversity *C. reniformis*

```
        PERMANOVA 9999 permutations: Bray distance by sampling sites


          Df SumsOfSqs  MeanSqs F.Model     R2 Pr(>F)
Site       4   0.18519 0.046297   2.929 0.3191  2e-04 ***
Residuals 25   0.39516 0.015806         0.6809
Total     29   0.58034                  1.0000
--
Pairwise comparison:
        pairs    F.Model         R2 p.value p.adjusted sig
1  CAC vs CCO  0.4459609 0.05280167   0.713 0.71300000
2   CAC vs GF  3.1170540 0.28038489   0.065 0.10833333
3   CAC vs GM  2.0726330 0.13750969   0.112 0.14000000
4   CAC vs SA  4.6995942 0.37005861   0.020 0.04000000   .
5   CCO vs GF  2.2578510 0.22010955   0.106 0.14000000
6   CCO vs GM  1.6338307 0.11164750   0.151 0.16777778
7   CCO vs SA  3.9578660 0.33098431   0.006 0.02333333   .
8    GF vs GM  6.5669113 0.33561308   0.005 0.02333333   .
9    GF vs SA 20.0333280 0.71462539   0.015 0.03750000   .
10   GM vs SA  5.5097987 0.29766929   0.007 0.02333333   .

        PERMANOVA 9999 permutations: Jaccard distance by sampling sites
Permutation: free
Number of permutations: 10000
Terms added sequentially (first to last)
          Df SumsOfSqs  MeanSqs F.Model      R2  Pr(>F)
Site       4   0.07405 0.018512  1.5477 0.19848 0.06099
Residuals 25   0.29903 0.011961         0.80152
Total     29   0.37308                  1.00000
--
        PERMANOVA 9999 permutations: Jaccard distance by acidification


          Df SumsOfSqs  MeanSqs F.Model      R2 Pr(>F)
Acidified  1   0.04474 0.044739  2.3388 0.07709  0.018 *
Residuals 28   0.53561 0.019129         0.92291
Total     29   0.58034                  1.00000
---
        PERMANOVA 9999 permutations: Jaccard distance by acidification


          Df SumsOfSqs  MeanSqs F.Model      R2 Pr(>F)
Acidified  1   0.01937 0.019368  1.5332 0.05191  0.184
Residuals 28   0.35372 0.012633         0.94809
Total     29   0.37308                  1.00000
---
```

Table S10 – Welch's test for the Songbird log-ratios in *Chondrosia reniformis* by sampling site and acidification.

```
  Welch's Heteroscedastic F Test
------------------------------------------------------------
  Log_Ratio and Site
  statistic  : 1.495323 num df: 4 denom df: 9.747721 p.value: 0.2770643
```

```
  Welch's Heteroscedastic F Test
------------------------------------------------------------
Log_Ratio and Acidification
  statistic  : 3.228168 num df: 1 denom df: 27.69879 p.value    : 0.08329572
```

Table S11– Statistical analyses for the sponge *Crambe crambe* (alpha and beta diversity).

Alpha diversity *C. crambe*

```
Kruskal-Wallis rank sum test:

Shannon index by sampling site
Kruskal-Wallis chi-squared = 2.7251, df = 5, p-value = 0.7423


Shannon index by acidification
Kruskal-Wallis chi-squared = 0.0005305, df = 1, p-value = 0.9816


Observed ASVs by sampling site
Kruskal-Wallis chi-squared = 3.1756, df = 5, p-value = 0.6729


Observed ASVs by acidification
Kruskal-Wallis chi-squared = 1.1232, df = 1, p-value = 0.2892
```

Beta diversity *C. crambe*

```
        PERMANOVA 9999 permutations: Bray distance by sampling sites


          Df SumsOfSqs  MeanSqs F.Model     R2 Pr(>F)
Site       5   0.27755 0.055511   1.634 0.2708 0.0347 *
Residuals 22   0.74739 0.033972         0.7292
Total     27   1.02494                  1.0000
---


Pairwise comparison:

        pairs   F.Model         R2 p.value p.adjusted sig
1  CAC vs CCO 0.5440926 0.07212167   0.538      0.735
2   CAC vs GF 0.3828012 0.04566507   0.733      0.800
3   CAC vs GM 0.4953755 0.05831119   0.570      0.735
4   CAC vs SA 1.5280313 0.17917750   0.330      0.735
5   CAC vs VU 1.1610892 0.12674139   0.256      0.735
6   CCO vs GF 0.6719049 0.08757994   0.588      0.735
7   CCO vs GM 0.8272929 0.10569336   0.424      0.735
8   CCO vs SA 1.1515589 0.16102209   0.376      0.735
9   CCO vs VU 0.7460002 0.09630780   0.456      0.735
10   GF vs GM 0.1318926 0.01621918   0.800      0.800
11   GF vs SA 0.7460196 0.09631005   0.778      0.800
12   GF vs VU 0.9388604 0.10503133   0.437      0.735
13   GM vs SA 0.8900752 0.11280947   0.581      0.735
14   GM vs VU 1.2601362 0.13608182   0.355      0.735
15   SA vs VU 0.9414417 0.11854796   0.428      0.735

        PERMANOVA 9999 permutations: Jaccard distance by sampling sites

          Df SumsOfSqs MeanSqs F.Model      R2    Pr(>F)
Site       5    2.3059 0.46118  1.9535 0.30747 9.999e-05 ***
Residuals 22    5.1937 0.23608         0.69253
Total     27    7.4996                 1.00000
---


Pairwise comparison:
        pairs   F.Model        R2 p.value p.adjusted sig
1  CAC vs CCO 4.9030301 0.4119145   0.005 0.03300000   .
2   CAC vs GF 4.6484243 0.3675102   0.009 0.03300000   .
3   CAC vs GM 4.1600166 0.3421062   0.011 0.03300000   .
4   CAC vs SA 2.4033610 0.2555853   0.045 0.07050000
5   CAC vs VU 1.7412694 0.1787518   0.094 0.11750000
6   CCO vs GF 1.9087875 0.2142590   0.071 0.09681818
7   CCO vs GM 6.5752585 0.4843560   0.011 0.03300000   .
8   CCO vs SA 0.9249446 0.1335671   0.545 0.54500000
9   CCO vs VU 2.9050424 0.2932892   0.040 0.07050000
10   GF vs GM 3.3302705 0.2939268   0.047 0.07050000
11   GF vs SA 1.4607060 0.1726459   0.178 0.20538462
12   GF vs VU 2.9889294 0.2719946   0.024 0.05142857
13   GM vs SA 3.7082139 0.3462962   0.017 0.04250000   .
14   GM vs VU 4.1952351 0.3440061   0.007 0.03300000   .
15   SA vs VU 1.3488821 0.1615644   0.218 0.23357143
```

Beta diversity *C. crambe*

```
        PERMANOVA 9999 permutations: Bray distance by acidification

           Df SumsOfSqs  MeanSqs F.Model      R2 Pr(>F)
Acidified  1   0.04150 0.041500  1.0972 0.04049 0.3287
Residuals 26   0.98344 0.037825         0.95951
Total     27   1.02494                  1.00000

        PERMANOVA 9999 permutations: Jaccard distance by acidification

           Df SumsOfSqs MeanSqs F.Model      R2 Pr(>F)
Acidified  1    0.5028 0.50280  1.8684 0.06704 0.0014 **
Residuals 26    6.9968 0.26911         0.93296
Total     27    7.4996                 1.00000
```

Table S12 – Welch's test for the Songbird log-ratios in *Crambe crambe* by sampling site and acidification.

```
Welch's Heteroscedastic F Test
------------------------------------------------------------
  Log_Ratio and Site

  statistic  : 17.28303
  num df     : 5
  denom df   : 9.812469
  p.value    : 0.0001371471
------------------------------------------------------------

Pairwise comparisons

  Bonferroni Correction (alpha = 0.05)
-----------------------------------------------------
   Level (a) Level (b)     p.value   No difference
1         CAC       CCO 0.001489286          Reject
2         CAC        GF 0.027620545          Reject
3         CAC        GM 0.002388976          Reject
4         CAC        SA 0.002772186          Reject
5         CAC        VU 0.033869795          Reject
6         CCO        GF 1.000000000      Not reject
7         CCO        GM 0.565749304      Not reject
8         CCO        SA 1.000000000      Not reject
9         CCO        VU 0.097217190      Not reject
10         GF        GM 1.000000000      Not reject
11         GF        SA 1.000000000      Not reject
12         GF        VU 0.364387293      Not reject
13         GM        SA 0.356652932      Not reject
14         GM        VU 1.000000000      Not reject
15         SA        VU 0.071190656      Not reject
-----------------------------------------------------
```

```
  Welch's Heteroscedastic F Test
------------------------------------------------------------
  Log_Ratio and Acidification

  statistic  : 32.53855
  num df     : 1
  denom df   : 25.95213
  p.value    : 5.332367e-06
```

Table S13 – Statistical analyses for the sponge *Chondrilla nucula* (alpha and beta diversity).

Alpha diversity *C.nucula*

```
         Kruskal-Wallis rank sum test:

Shannon index by site
Kruskal-Wallis chi-squared = 0.14, df = 2, p-value = 0.9324

Shannon index by acidified
Kruskal-Wallis chi-squared = 0.015, df = 1, p-value = 0.9025

Observed ASVs by site
Kruskal-Wallis chi-squared = 0.6722, df = 2, p-value = 0.7146

Observed ASVs by Acidified
Kruskal-Wallis chi-squared = 0.64061, df = 1, p-value = 0.4235
```

Beta diversity *C.nucula*

```
       PERMANOVA 9999 permutations: Bray distance by site

          Df SumsOfSqs  MeanSqs F.Model      R2 Pr(>F)
Site       2   0.12063 0.060317  2.2425 0.27207 0.0123 *
Residuals 12   0.32277 0.026897         0.72793
Total     14   0.44340                  1.00000
---

Pairwise comparison:

     pairs  F.Model        R2 p.value p.adjusted sig
1 GF vs GM 3.781545 0.3209719   0.007      0.021   .
2 GF vs SA 1.576963 0.1646622   0.179      0.255
3 GM vs SA 1.499991 0.1578940   0.255      0.255
---

       PERMANOVA 9999 permutations: Bray distance by acidification


          Df SumsOfSqs  MeanSqs F.Model      R2   Pr(>F)
Acidified  1   0.08905 0.089055  3.2672 0.20084 0.009099 **
Residuals 13   0.35435 0.027257         0.79916
Total     14   0.44340                  1.00000
---

       PERMANOVA 9999 permutations: Jaccard distance by site


          Df SumsOfSqs   MeanSqs F.Model      R2 Pr(>F)
Site       2  0.026249 0.0131247  5.7398 0.48892  3e-04 ***
Residuals 12  0.027439 0.0022866         0.51108
Total     14  0.053689                  1.00000
---

Pairwise comparison:

     pairs   F.Model        R2 p.value p.adjusted sig
1 GF vs GM 10.388389 0.5649429   0.014     0.0225   .
2 GF vs SA  2.229020 0.2179114   0.168     0.1680
3 GM vs SA  5.901661 0.4245292   0.015     0.0225   .
---


       PERMANOVA 9999 permutations: Jaccard distance by acidification
          Df SumsOfSqs   MeanSqs F.Model      R2 Pr(>F)
Acidified  1  0.022432 0.0224322  9.3299 0.41782  5e-04 ***
Residuals 13  0.031256 0.0024043         0.58218
Total     14  0.053689                  1.00000
---
```

Table S14 – Welch's test for the Songbird log-ratios in *Chondrilla nucula* by sampling site and acidification.

```
Welch's Heteroscedastic F Test by sampling site
------------------------------------------------------------
  data : Log_Ratio and Site
  statistic  : 0.9945005
  num df     : 2
  denom df   : 6.953188
  p.value    : 0.4170112
------------------------------------------------------------

  Welch's Heteroscedastic F Test by acidification
------------------------------------------------------------
  data : Log_Ratio and Acidification
  statistic  : 2.016419
  num df     : 1
  denom df   : 4.971758
  p.value    : 0.215158
------------------------------------------------------------
```

Table S15 – Statistical test for the chemical analyses of *Petrosia ficiformis and Crambe crambe.*

PERMANOVA 9999 permutations: metabolomics *Petrosia ficiformis* by sampling sites

	Df	SumsOfSqs	MeanSqs	F.Model	R2	Pr(>F)	
Site	3	4.2519	1.41730	24.882	0.80571	9.999e-05	***
Residuals	18	1.0253	0.05696		0.19429		
Total	21	5.2772			1.00000		

Pairwise comparisons:

	pairs	F.Model	R2	p.value	p.adjusted	sig
1	CAC vs GM	35.268479	0.7461310	0.001	0.0030	*
2	CAC vs SA	2.599603	0.2452548	0.077	0.0770	
3	CAC vs GF	4.343547	0.4199282	0.058	0.0696	
4	GM vs SA	35.961970	0.7498018	0.001	0.0030	*
5	GM vs GF	25.507301	0.7183678	0.003	0.0060	*
6	SA vs GF	7.729059	0.5629708	0.015	0.0225	.

PERMANOVA 9999 permutations: petroformynes by sampling sites

	Df	SumsOfSqs	MeanSqs	F.Model	R2	Pr(>F)	
Site	3	2.24506	0.74835	308.66	0.98093	9.999e-05	***
Residuals	18	0.04364	0.00242		0.01907		
Total	21	2.28870			1.00000		

Pairwise comparisons:

	pairs	F.Model	R2	p.value	p.adjusted	sig
1	CAC vs SA	3.617528	0.3113853	0.059	0.0708	
2	CAC vs GM	551.209236	0.9786935	0.001	0.0060	*
3	CAC vs GF	2.897233	0.3256331	0.091	0.0910	
4	SA vs GM	589.135510	0.9800378	0.002	0.0060	*
5	SA vs GF	4.957076	0.4524086	0.054	0.0708	
6	GM vs GF	533.257015	0.9815925	0.006	0.0120	.

PERMANOVA 9999 permutations: metabolomics *Crambe crambe* by sampling sites

	Df	SumsOfSqs	MeanSqs	F.Model	R2	Pr(>F)	
Site	4	0.95022	0.237555	3.1581	0.39935	0.0017	**
Residuals	19	1.42920	0.075221		0.60065		
Total	23	2.37942			1.00000		

Pairwise comparisons:

	pairs	F.Model	R2	p.value	p.adjusted	sig
1	CAC vs VU	0.7676714	0.09882903	0.478	0.4780000	
2	CAC vs SA	1.3898074	0.16565426	0.224	0.2488889	
3	CAC vs GM	3.4278930	0.32872345	0.030	0.0875000	
4	CAC vs GF	3.3563562	0.32408659	0.059	0.1180000	
5	VU vs SA	1.7663750	0.18086291	0.136	0.2142857	
6	VU vs GM	1.8345338	0.18653999	0.150	0.2142857	
7	VU vs GF	3.1991171	0.28565797	0.035	0.0875000	
8	SA vs GM	6.2889340	0.44012618	0.009	0.0500000	.
9	SA vs GF	1.6361480	0.16979274	0.181	0.2262500	
10	GM vs GF	10.3437481	0.56388411	0.010	0.0500000	.

Table S16 – Welch's test for the Songbird log-ratios for metabolomics in *Petrosia ficiformis* and *Crambe crambe* by sampling sites.

Welch's Heteroscedastic F Test: *Petrosia ficiformis*

Log_Ratio by Site

statistic : 412.631
num df : 3
denom df : 5.901449
p.value : 3.016156e-07

Pairwise comparisons:

	Level (a)	Level (b)	p.value	No difference
1	CAC	GF	9.149833e-01	Not reject
2	CAC	GM	2.390936e-11	Reject
3	CAC	SA	4.475167e-01	Not reject
4	GF	GM	1.254616e-01	Not reject
5	GF	SA	1.000000e+00	Not reject
6	GM	SA	9.142449e-03	Reject

Welch's Heteroscedastic F Test: *Crambe crambe*

data : Log_Ratio and Site

statistic : 13.09267
num df : 4
denom df : 8.694198
p.value : 0.0009876551

Result : Difference is statistically significant.

Pairwise comparisons:

	Level (a)	Level (b)	p.value	No difference
1	CAC	GF	0.07646400	Not reject
2	CAC	GM	0.98476183	Not reject
3	CAC	SA	0.01747572	Reject
4	CAC	VU	1.00000000	Not reject
5	GF	GM	0.51699070	Not reject
6	GF	SA	1.00000000	Not reject
7	GF	VU	0.04192301	Reject
8	GM	SA	0.08923749	Not reject
9	GM	VU	0.77757934	Not reject
10	SA	VU	0.00710220	Reject

Table S17 – Statistical analyses for the molecular classes by sampling sites in *Petrosia ficiformis*.

ANOVA Triglycerides by sampling sites

```
            Df    Sum Sq   Mean Sq F value  Pr(>F)
Class        4 3.284e+15 8.210e+14   5.093 0.00635 **
Residuals   18 2.901e+15 1.612e+14
---
Pairwise comparisons:

              diff         lwr        upr     p adj
GF-CAC   28748902    713108.5 56784695.8 0.0428940
GM-CAC   14755058  -9524652.0 39034767.1 0.3838572
GMW-CAC  20929983  -3349726.8 45209692.3 0.1110116
SA-CAC   -4327537 -28607247.0 19952172.1 0.9819399
GM-GF   -13993845 -42029638.3 14041949.1 0.5698178
GMW-GF   -7818919 -35854713.1 20216874.3 0.9133826
SA-GF   -33076440 -61112233.3 -5040645.9 0.0164454
GMW-GM    6174925 -18104784.3 30454634.8 0.9362609
SA-GM   -19082595 -43362304.6  5197114.5 0.1670156
SA-GMW  -25257520 -49537229.8  -977810.7 0.0391965
```

ANOVA Monoglycerides by sampling sites

```
            Df    Sum Sq   Mean Sq F value  Pr(>F)
Class        4 4.633e+14 1.158e+14   6.354 0.00227 **
Residuals   18 3.281e+14 1.823e+13
---
Pairwise comparisons:

                diff         lwr      upr     p adj
GF-CAC     895702.86  -8532789.5 10324195 0.9983642
GM-CAC   10767433.34   2602119.5 18932747 0.0067615
GMW-CAC   7081482.59  -1083831.3 15246796 0.1078392
SA-CAC      51838.97  -8113474.9  8217153 1.0000000
GM-GF     9871730.48    443238.2 19300223 0.0376181
GMW-GF    6185779.73  -3242712.6 15614272 0.3125328
SA-GF     -843863.89 -10272356.2  8584628 0.9987045
GMW-GM   -3685950.75 -11851264.6  4479363 0.6562831
SA-GM   -10715594.37 -18880908.2 -2550281 0.0070439
SA-GMW   -7029643.62 -15194957.5  1135670 0.1117020
```

ANOVA Diglycerides by sampling sites

```
            Df    Sum Sq   Mean Sq F value   Pr(>F)
Class        4 4.415e+16 1.104e+16   9.898 0.000204 ***
Residuals   18 2.007e+16 1.115e+15
---
Pairwise comparisons:

               diff        lwr       upr     p adj
GF-CAC    3965039.9  -69779873  77709953 0.9998267
GM-CAC   88311919.0   24446951 152176887 0.0044688
GMW-CAC  89779593.1   25914625 153644561 0.0038514
SA-CAC    -539212.4  -64404180  63325755 0.9999999
GM-GF    84346879.2   10601967 158091792 0.0206430
GMW-GF   85814553.2   12069641 159559466 0.0182108
SA-GF    -4504252.3  -78249165  69240660 0.9997127
GMW-GM    1467674.0  -62397294  65332642 0.9999941
SA-GM   -88851131.5 -152716099 -24986164 0.0042313
SA-GMW  -90318805.5 -154183773 -26453838 0.0036466
```

ANOVA Phosphatidylcholines by sampling sites

```
            Df    Sum Sq  Mean Sq F value Pr(>F)
Class        4 1.308e+15 3.27e+14   1.434  0.263
Residuals   18 4.104e+15 2.28e+14
---
Pairwise comparisons:
              diff       lwr      upr     p adj
GF-CAC    15144327 -18199357 48488011 0.6512932
GM-CAC    10639844 -18236633 39516322 0.7971011
GMW-CAC    6651368 -22225110 35527846 0.9546418
SA-CAC    -6963432 -35839910 21913046 0.9468390
GM-GF     -4504483 -37848167 28839202 0.9936195
GMW-GF    -8492959 -41836643 24850725 0.9359340
SA-GF    -22107759 -55451444 11235925 0.3030205
GMW-GM    -3988476 -32864954 24888001 0.9930569
SA-GM    -17603277 -46479754 11273201 0.3809005
SA-GMW   -13614800 -42491278 15261678 0.6200122
```

ANOVA Phosphatidylethanolamines by sampling sites

```
            Df    Sum Sq   Mean Sq F value Pr(>F)
Class        4 4.754e+14 1.188e+14   1.903  0.154
Residuals   18 1.124e+15 6.247e+13
---
Pairwise comparisons:

               diff       lwr      upr     p adj
GF-CAC    8152097.5  -9300937 25605132 0.6279837
GM-CAC     765573.1 -14349198 15880344 0.9998633
GMW-CAC  -6273298.5 -21388069  8841472 0.7205078
SA-CAC   -4602315.7 -19717087 10512455 0.8851962
GM-GF    -7386524.4 -24839558 10066510 0.7063146
GMW-GF  -14425396.0 -31878430  3027638 0.1347635
SA-GF   -12754413.2 -30207447  4698621 0.2205940
GMW-GM   -7038871.5 -22153642  8075899 0.6305069
SA-GM    -5367888.8 -20482660  9746882 0.8173068
SA-GMW    1670982.8 -13443788 16785754 0.9970489
```

ANOVA Sulfatides by sampling sites

```
            Df    Sum Sq   Mean Sq F value   Pr(>F)
Class        4 2.397e+15 5.992e+14   8.142 0.000624 ***
Residuals   18 1.325e+15 7.360e+13
---

Pairwise comparisons:
              diff       lwr      upr     p adj
GF-CAC     6171632 -12773365 25116629 0.8585374
GM-CAC   -17733326 -34140174 -1326478 0.0305569
GMW-CAC  -22697151 -39103999 -6290303 0.0044514
SA-CAC   -11636043 -28042891  4770805 0.2448029
GM-GF    -23904958 -42849955 -4959961 0.0097478
GMW-GF   -28868783 -47813780 -9923786 0.0017948
SA-GF    -17807675 -36752672  1137322 0.0712920
GMW-GM    -4963825 -21370673 11443024 0.8874903
SA-GM      6097283 -10309565 22504132 0.7921668
SA-GMW    11061108  -5345740 27467956 0.2881743
```

ANOVA Wax esters by sampling sites

```
            Df    Sum Sq   Mean Sq F value   Pr(>F)
Class        4 8.688e+14 2.172e+14   9.372 0.000282 ***
Residuals   18 4.172e+14 2.318e+13
---
Pairwise comparisons:

               diff         lwr        upr     p adj
GF-CAC    -973755.1 -11604929.2  9657419.1 0.9985818
GM-CAC   14437524.1   5230657.2 23644390.9 0.0013487
GMW-CAC   8422063.2   -784803.6 17628930.1 0.0824685
SA-CAC    -172372.8  -9379239.7  9034494.0 0.9999974
GM-GF    15411279.1   4780105.0 26042453.3 0.0028997
GMW-GF    9395818.3  -1235355.8 20026992.4 0.0983201
SA-GF      801382.3  -9829791.9 11432556.4 0.9993403
GMW-GM   -6015460.8 -15222327.7  3191406.0 0.3162868
SA-GM   -14609896.9 -23816763.7 -5403030.0 0.0011956
SA-GMW   -8594436.1 -17801302.9   612430.8 0.0740290
```

ANOVA Phosphatidylinositols by sampling sites

```
            Df    Sum Sq   Mean Sq F value   Pr(>F)
Class        4 3.038e+15 7.595e+14   7.933 0.000719 ***
Residuals   18 1.723e+15 9.573e+13
---

Pairwise comparisons:

              diff       lwr         upr     p adj
GF-CAC     9034941 -12571541  30641423.0 0.7151236
GM-CAC   -17918341 -36630103    793421.2 0.0643092
GMW-CAC  -25082347 -43794109  -6370584.3 0.0058750
SA-CAC   -11379727 -30091489   7332035.4 0.3831576
GM-GF    -26953282 -48559764  -5346800.0 0.0106864
GMW-GF   -34117288 -55723770 -12510805.5 0.0012573
SA-GF    -20414668 -42021150   1191814.1 0.0692963
GMW-GM    -7164005 -25875768  11547756.9 0.7743237
SA-GM      6538614 -12173148  25250376.5 0.8256845
SA-GMW    13702620  -5009143  32414382.0 0.2189639
```

ANOVA Ceramides by sampling sites

```
            Df    Sum Sq   Mean Sq F value Pr(>F)
Class        4 1.363e+14 3.407e+13   0.584  0.678
Residuals   18 1.050e+15 5.834e+13
---

Pairwise comparisons:
               diff       lwr      upr     p adj
GF-CAC   6685081.34 -10181558 23551721 0.7522112
GM-CAC     74770.64 -14532168 14681709 1.0000000
GMW-CAC  1709432.25 -12897506 16316371 0.9963222
SA-CAC   4567547.29 -10039391 19174486 0.8752509
GM-GF   -6610310.70 -23476950 10256329 0.7595554
GMW-GF  -4975649.10 -21842289 11890990 0.8961553
SA-GF   -2117534.06 -18984174 14749105 0.9951801
GMW-GM   1634661.61 -12972277 16241600 0.9969061
SA-GM    4492776.65 -10114162 19099715 0.8815055
SA-GMW   2858115.04 -11748823 17465053 0.9746060
```

Table S18 – Statistical analyses for the molecular classes by sampling sites in *Crambe crambe*.

ANOVA Triglycerides by sampling sites

```
            Df    Sum Sq   Mean Sq F value Pr(>F)
Class        4 1.001e+15 2.501e+14    2.87 0.0498 *
Residuals   20 1.743e+15 8.715e+13
---

Pairwise comparisons:
             diff       lwr      upr     p adj
GF-CAC   9704516  -7963435 27372468 0.4885924
GM-CAC  -1754159 -19422111 15913792 0.9981514
SA-CAC  14731840  -2936111 32399792 0.1315620
VU-CAC   1420527 -16247425 19088478 0.9991915
GM-GF  -11458676 -29126627  6209276 0.3292661
SA-GF    5027324 -12640627 22695276 0.9109667
VU-GF   -8283990 -25951941  9383962 0.6328219
SA-GM   16486000  -1181952 34153951 0.0747570
VU-GM    3174686 -14493266 20842637 0.9822253
VU-SA  -13311314 -30979265  4356638 0.2008867
```

ANOVA Monoglycerides by sampling sites

```
            Df   Sum Sq   Mean Sq F value Pr(>F)
Class        4 3.79e+12 9.476e+11   1.722  0.185
Residuals   20 1.10e+13 5.502e+11
---
Pairwise comparisons:
             diff        lwr       upr     p adj
GF-CAC   92156.27 -1311692.5 1496005.0 0.9996368
GM-CAC 1061002.21  -342846.5 2464850.9 0.1985015
SA-CAC  171182.47 -1232666.3 1575031.2 0.9958968
VU-CAC  127989.26 -1275859.5 1531838.0 0.9986755
GM-GF   968845.93  -435002.8 2372694.7 0.2730374
SA-GF    79026.20 -1324822.5 1482874.9 0.9998025
VU-GF    35832.99 -1368015.7 1439681.7 0.9999915
SA-GM  -889819.74 -2293668.5  514029.0 0.3507878
VU-GM  -933012.94 -2336861.7  470835.8 0.3067392
VU-SA   -43193.21 -1447041.9 1360655.5 0.9999822
```

ANOVA Diglycerides by sampling sites

```
            Df    Sum Sq   Mean Sq F value Pr(>F)
Class        4 8.706e+13 2.176e+13   1.613   0.21
Residuals   20 2.698e+14 1.349e+13
---
Pairwise comparisons:

             diff       lwr      upr     p adj
GF-CAC  3852513.5  -3098434 10803461 0.4799435
GM-CAC   772610.7  -6178336  7723558 0.9971318
SA-CAC  4888850.7  -2062096 11839798 0.2566449
VU-CAC  1442443.8  -5508503  8393391 0.9699684
GM-GF  -3079902.8 -10030850  3871044 0.6789718
SA-GF   1036337.2  -5914610  7987284 0.9911542
VU-GF  -2410069.7  -9361017  4540877 0.8350436
SA-GM   4116240.0  -2834707 11067187 0.4159451
VU-GM    669833.1  -6281114  7620780 0.9983548
VU-SA  -3446406.9 -10397354  3504540 0.5840500
```

ANOVA Phosphatidylcholines by sampling sites

```
            Df    Sum Sq   Mean Sq F value Pr(>F)
Class        4 3.798e+15 9.496e+14   4.089  0.014 *
Residuals   20 4.645e+15 2.322e+14
---
Pairwise comparisons:
            diff         lwr      upr     p adj
GF-CAC  19883695  -8956917.3 48724308 0.2739287
GM-CAC -13203802 -42044414.1 15636811 0.6527082
SA-CAC  16447963 -12392650.0 45288575 0.4523832
VU-CAC  -2369213 -31209825.9 26471399 0.9991202
GM-GF  -33087497 -61928109.4 -4246884 0.0197292
SA-GF   -3435733 -32276345.3 25404880 0.9962496
VU-GF  -22252909 -51093521.1  6587704 0.1831256
SA-GM   29651764    811151.5 58492377 0.0420420
VU-GM   10834588 -18006024.3 39675201 0.7921059
VU-SA  -18817176 -47657788.4 10023437 0.3237050
```

ANOVA Phosphatidylethanolamines by sampling sites

```
            Df    Sum Sq  Mean Sq F value Pr(>F)
Class        4 8.520e+14 2.13e+14   3.475 0.0261 *
Residuals   20 1.226e+15 6.13e+13
---

Pairwise comparisons:
              diff         lwr      upr     p adj
GF-CAC  11301551.6  -3516378.3 26119481 0.1916552
GM-CAC  -1771257.9 -16589187.8 13046672 0.9962000
SA-CAC  12194740.7  -2623189.2 27012671 0.1395659
VU-CAC   2110824.7 -12707105.2 16928755 0.9925583
GM-GF  -13072809.5 -27890739.4  1745120 0.1003958
SA-GF     893189.2 -13924740.8 15711119 0.9997410
VU-GF   -9190726.9 -24008656.8  5627203 0.3713952
SA-GM   13965998.6   -851931.3 28783929 0.0707133
VU-GM    3882082.6 -10935847.3 18700012 0.9323096
VU-SA  -10083916.0 -24901845.9  4734014 0.2854230
```

ANOVA Cholesterol esters by sampling sites

```
            Df    Sum Sq   Mean Sq F value Pr(>F)
Class        4 7.040e+13 1.760e+13   0.526  0.718
Residuals   20 6.689e+14 3.344e+13
---

Pairwise comparisons:
               diff       lwr      upr     p adj
GF-CAC  1735383.180  -9209467 12680234 0.9888443
GM-CAC -3426463.195 -14371314  7518387 0.8791452
SA-CAC   -83429.217 -11028280 10861421 0.9999999
VU-CAC   -75843.424 -11020694 10869007 1.0000000
GM-GF  -5161846.375 -16106697  5783004 0.6278526
SA-GF  -1818812.397 -12763663  9126038 0.9867000
VU-GF  -1811226.605 -12756077  9133624 0.9869059
SA-GM   3343033.978  -7601816 14287884 0.8881679
VU-GM   3350619.770  -7594231 14295470 0.8873629
VU-SA      7585.793 -10937265 10952436 1.0000000
```

ANOVA ceramides by sampling sites

```
            Df    Sum Sq   Mean Sq F value Pr(>F)
Class        4 1.363e+14 3.407e+13   0.584  0.678
Residuals   18 1.050e+15 5.834e+13
---

Pairwise comparisons:
               diff       lwr      upr     p adj
GF-CAC   6685081.34 -10181558 23551721 0.7522112
GM-CAC     74770.64 -14532168 14681709 1.0000000
GMW-CAC  1709432.25 -12897506 16316371 0.9963222
SA-CAC   4567547.29 -10039391 19174486 0.8752509
GM-GF   -6610310.70 -23476950 10256329 0.7595554
GMW-GF  -4975649.10 -21842289 11890990 0.8961553
SA-GF   -2117534.06 -18984174 14749105 0.9951801
GMW-GM   1634661.61 -12972277 16241600 0.9969061
SA-GM    4492776.65 -10114162 19099715 0.8815055
SA-GMW   2858115.04 -11748823 17465053 0.9746060
```

9. PUBLICATIONS

International Journal of
Molecular Sciences

MDPI

Article

Molecular Network and Culture Media Variation Reveal a Complex Metabolic Profile in *Pantoea* cf. *eucrina* D2 Associated with an Acidified Marine Sponge

Giovanni Andrea Vitale [1], Martina Sciarretta [2], Chiara Cassiano [2], Carmine Buonocore [1], Carmen Festa [2], Valerio Mazzella [3], Laura Núñez Pons [3], Maria Valeria D'Auria [2,*] and Donatella de Pascale [1,4,*]

1 Institute of Biochemistry and Cell Biology, National Research Council, 80131 Naples, Italy; giovanniandrea.vitale@ibbc.cnr.it (G.A.V.); carmine.buonocore@ibbc.cnr.it (C.B.)
2 Department of Pharmacy, University of Naples "Federico II", 80131 Naples, Italy; martina.sciarretta@unina.it (M.S.); chiara.cassiano@unina.it (C.C.); carmen.festa@unina.it (C.F.)
3 Department of Integrated Marine Ecology (EMI), Stazione Zoologica Anton Dohrn, Villa Comunale, 80125 Naples, Italy; valerio.mazzella@szn.it (V.M.); laura.nunezpons@szn.it (L.N.P.)
4 Department of Marine Biotechnology, Stazione Zoologica Anton Dohrn, Villa Comunale, 80125 Naples, Italy
* Correspondence: madauria@unina.it (M.V.D.); donatella.depascale@szn.it (D.d.P.); Tel.: +39-081-5833319 (D.d.P.)

Received: 5 August 2020; Accepted: 28 August 2020; Published: 31 August 2020

Abstract: The Gram-negative *Pantoea eucrina* D2 was isolated from the marine sponge *Chondrosia reniformis*. Sponges were collected in a shallow volcanic vents system in Ischia island (South Italy), influenced by CO_2 emissions and lowered pH. The chemical diversity of the secondary metabolites produced by this strain, under different culture conditions, was explored by a combined approach including molecular networking, pure compound isolation and NMR spectroscopy. The metabolome of *Pantoea* cf. *eucrina* D2 yielded a very complex molecular network, allowing the annotation of several metabolites, among them two biosurfactant clusters: lipoamino acids and surfactins. The production of each class of metabolites was highly dependent on the culture conditions, in particular, the production of unusual surfactins derivatives was reported for the first time from this genus; interestingly the production of these metabolites only arises by utilizing inorganic nitrogen as a sole nitrogen source. Major components of the extract obtained under standard medium culture conditions were isolated and identified as N-lipoamino acids by a combination of 1D and 2D NMR spectroscopy and HRESI-MS analysis. Assessment of the antimicrobial activity of the pure compounds towards some human pathogens, indicated a moderate activity of leucine containing N-lipoamino acids towards *Staphylococcus aureus*, *Staphylococcus epidermidis* and a clinical isolate of the emerging food pathogen *Listeria monocytogenes*.

Keywords: molecular networking; hydrothermal vents; *Pantoea eucrina*; biosurfactants

1. Introduction

The Gram-negative genus *Pantoea* was only recently established as new genus within the family of Enterobacteriaceae. To date, it comprises about 20 species (https://lpsn.dsmz.de/genus/pantoea) isolated from both the host and non-host environments [1]. The high adaptability to different habitats was also accomplished by a remarkable phenotypic diversity that ranges from the pathogeny of some isolates toward plants and humans—although the actual involvement of *Pantoea* strains in the insurgence of diseases in both plants and humans is a matter of controversy—to high beneficial biotechnological and therapeutic potential.

Bioremediation of contaminated soils and water by *Pantoea* spp. was exerted through bioabsorption and metabolic transformation of heavy metal ions and/or through production of glycolipid biosurfactants, able to promote the emulsification and degradation of organic waste components and pollutants as well as of petroleum derivatives [1].

On the other hand, the mutualistic interaction with plants and insects was associated with multiple factors [2] as the metabolic cooperation, thanks to the nitrogen fixation and phosphate solubilization capabilities exhibited by some *Pantoea* species and to the production of several plant growth promoting and defense secondary metabolites [3].

Noteworthy is the production of small molecules with antimicrobial activities such pantocins, herbicolins, microcins and phenazines [1,4,5].

The study of the phenotypic features of members of this species has been so far mainly focused on the comparative genomic analysis in the search for the genetic and genomic determinants able to drive specific diversity and adaptability [6–8], whereas there are only sporadic papers dealing with the chemical profiling of members of this genus.

As part of our interest toward the biotechnological potential of bacterial strains isolated from unexplored and unique habitats, we conducted a collection of sponge samples in a volcanic vents system of Ischia island (Gulf of Naples, Italy). Here due to the effect of secondary volcanism, carbon dioxide seeps inflate CO_2 in the surrounding seawater [9], creating a unique area of naturally lowered pH. Such system represents a unique in situ laboratory for studies regarding adaptations to ocean acidification (OA) on benthic biota [10]. The volcanic CO_2 vents include areas where pH ranges from normal values (8.1–8.2) to lowered pH values (mean 7.8–7.9, minimum 7.4–7.5), mimicking the records predicted for the end of the century [11].

Marine sponges (phylum Porifera) are known to be prolific sources of bioactive metabolites, most suspected to be produced by their conspicuous microbial associates [12]. Among sponges collected in our surveys, samples from *Chondrosia reniformis* Nardo, 1847 coming from acidified zones were selected to obtain microbial isolates for downstream analyses. After culture-dependent isolations, a strain identified as *Pantoea eucrina* was selected for metabolic studies. To the best of our knowledge this is the first report of a *Pantoea* strain isolated from a marine sponge.

In this work, OSMAC (one strain many compounds) [13] and molecular networking (MN) [14] approaches were strategically combined to perform a downstream exploration of the diversity of secondary metabolites produced by *P. eucrina* D2 under different conditions. The metabolome turned out to be very complex and molecular networking analysis allowed the annotation of several metabolites that were clustered in three subgroups: lipoamino acids, diketopiperazines and surfactins.

The strain was found to be able to produce these metabolites using inorganic ammonium and nitrate salts as sole nitrogen sources. The production of specific subgroups and even of specific components within each subgroup was strongly dependent on the cultivation media, in particular the production of surfactin derivatives, here described for the first time from a *Pantoea* strain, was triggered by the use of inorganic nitrogen, while it was totally abolished under normal conditions.

The major metabolites belonging to lipoamino acids group were isolated, chemically characterized by NMR and HR-ESI-MS analysis and subjected to antimicrobial assays towards human pathogens. This hyphenate approach allowed the detection of two otherwise undetectable new surfactin derivatives, together with the isolation of several lipoamino acids derivatives, some of which never isolated before from natural sources, among them Compound **1** has never been reported even as synthetic product. Concerning the biologic activity, leucine derivatives which displayed a prominent antimicrobial activity towards Gram-positive human pathogens confirmed to be promising candidates for biotechnological applications.

2. Results and Discussion

2.1. Isolation and Identification of Bacterial Strains from the Sponge Chondrosia reniformis Living at Naturally Lowered pH Conditions

Chondrosia reniformis, a high microbial abundance (HMA) sponge [15] widespread in the Mediterranean Sea and with a rich microbiome [16], was collected in the marine area around Castello Aragonese, Ischia Island. This species is common in around the acidified area formed by local volcanic CO_2 vents [17], suggesting a long term adaptation to OA conditions. The microbiome of this sponge was hence exploited as a reservoir for the isolation and culture of bacterial strains with interesting metabolite profiles. Since the sponges were collected in an acidified environment, bacterial isolation was performed in a decreasing pH gradient. Sponge pieces were brought in a sterile manner to the lab, submersed in 0.22 µm filtered seawater and plated on MB agar plates at pH: 5, 6 and 7 for the microbial isolation. No bacteria grew at pH 5, also considering agar plates frailty at that pH, while most bacteria developed on pH 6 agar plates, resulting in nine morphologically different strains, which were all identified through the 16S rRNA sequencing (Table 1).

Table 1. Genera of the bacterial isolates at pH 6 based on their 16S sequences.

Strain	Identity
G	*Pseudoalteromonas* sp.
H	*Shewanella* sp.
S1	*Pseudomonas* sp.
U1	*Sphingobium* sp.
Z1	*Sphingobium* sp.
X1	*Stenotrophomonas* sp.
J1	*Acinetobacter* sp.
D2	*Pantoea* sp.

The isolated bacteria were identified through 16S rRNA Sanger sequencing, and sequences were submitted on BLASTn (Nucleotide Basic Local Alignment Search Tool) against GenBank database for species annotation [18]. A phylogenetic tree was built including the strain D2 along with the closest matches from GenBank using MEGA X (Figure 1). These results suggest that D2 is closely related, if not conspecific, to *Pantoea eucrina*, a poorly studied member of *Pantoea* genus. This genus was established ~30 years ago in the *Enterobacteriaceae* family. It counts only for 20 isolated species [1,19–21], and certain strains have been found to produce antimicrobial metabolites, many of which peptides [4,5,22]. In addition, a new marine strain of *Pantoea* was recently found to produce high amounts of an exopolysaccharide [23]. This is the first record of this genus associated with a sponge, in addition, its metabolome has never been deeply investigated.

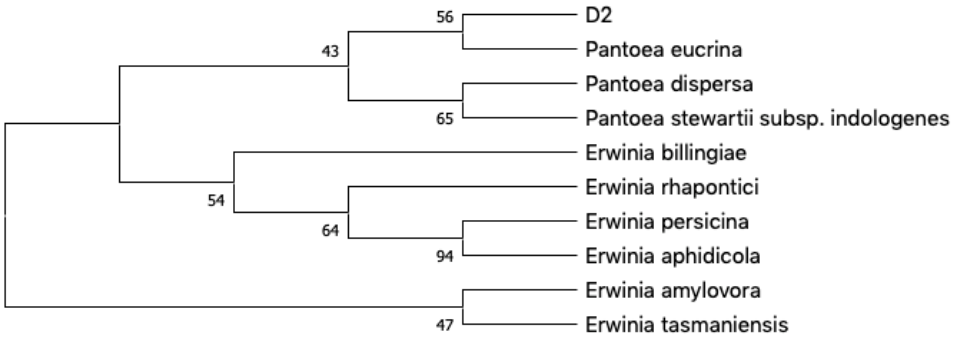

Figure 1. Phylogenetic neighbor-joining (NJ) tree generated with MEGAX based on 16S rRNA gene sequences from D2 and the most related species according to matching entries on BLAST. Next to the branches are shown the percentage of replicate trees in which the associated taxa clustered together in the bootstrap test (1000 resamples).

2.2. MS/MS-Based Molecular Networking Analysis of Pantoea eucrina D2 Metabolome Grown under Different Culture Conditions

The principle of "one strain many compounds" (OSMAC) approach is based on the principle that several microbes can potentially produce many more metabolites than they do under determined conditions. A simple and effective way to influence bacterial metabolisms is changing growth parameters such as nutrients, temperature, salinity, aeration, in this way activating or upregulating metabolic pathways which usually silenced [24]. Herein metabolites produced by the sponge-associated *P.* cf. *eucrina* D2 in different culture media were explored by modifying the sources of inorganic nitrogen and comparing them with the metabolic profile obtained in the optimal and complex TSB medium. The metabolome was investigated by analyzing the crude extracts through HPLC-MS/MS data dependent analysis. The obtained MS raw data were converted in mzXML format, processed by MZmine [25] in order to remove noise, to filter the isotopes and to align the data. Then, the output files were uploaded to Global Natural Products Social molecular networking (GNPS) [14] and used to build a feature-based molecular network [26], finally the data were exported and visualized on Cytoscape [27].

In this way, a complex web of nodes grouped in several clusters was obtained (Figure 2). Each node represents an ion found in at least one of the growth cultures, different colors are used to define their presence in different growth media, the edges size among different nodes are directly dependent on their fragmentation spectra similarity (cosine score), while the node size is directly proportional to the precursor ion intensity (sum precursor intensity). This visualization provides a scheme of the different metabolites production in the specific conditions (Figure 2).

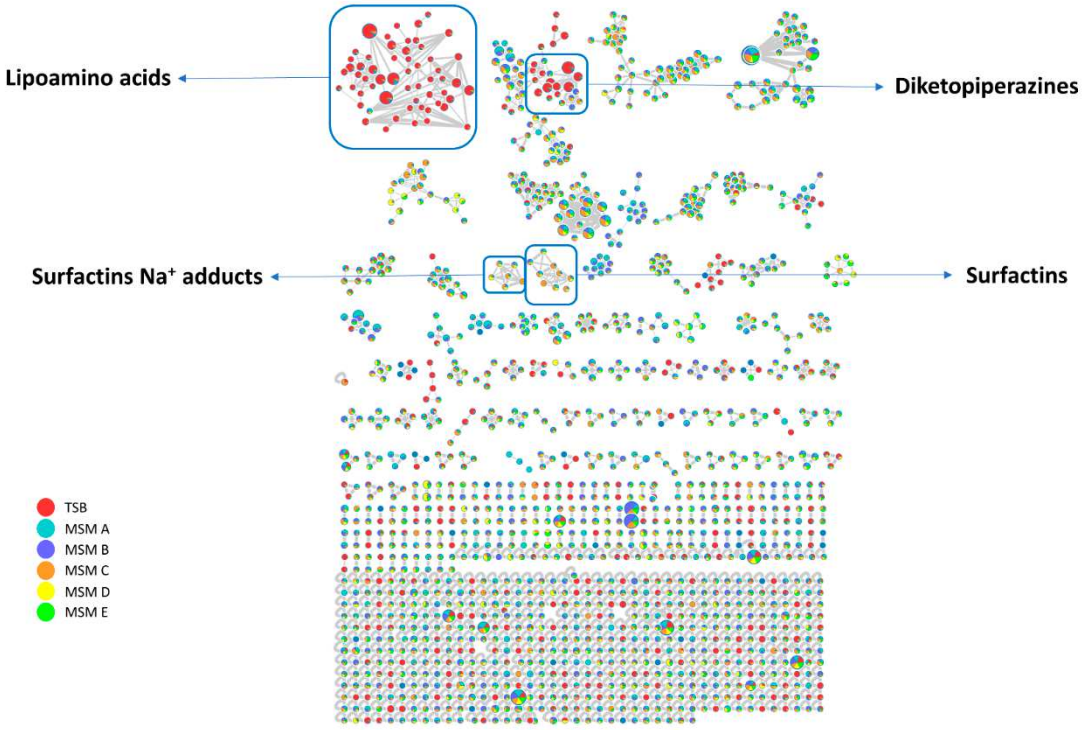

Figure 2. *Pantoea* cf. *eucrina* D2 metabolic network overview, it was obtained through global natural products social molecular networking (GNPS) and Cytoscape. The presence of lipoamino acids, diketopiperazines and surfactins clusters are displayed.

Analysis of GNPS unique library hits and analog library hits evidenced the presence of three class of metabolites: diketopiperazines, surfactins and lipoamino acids. Herein we focused our attention on two latter classes.

2.2.1. Surfactins Molecular Cluster

The analysis of the $[M + H]^+$ network in Figure 3 matched on GNPS library for surfactin C (1036 *m*/*z*) and through the clusterization suggested the occurrence of related species with *m*/*z* at 1050.7041, 1064.7197, 1078.7348, 1092.7509 in addition, another pseudomolecular ion with *m*/*z* of 1106.7681 compatible with a surfactin derivative was found in the full-MS spectrum (1000–1200 Da) (Figure S1) by manual HR data curation.

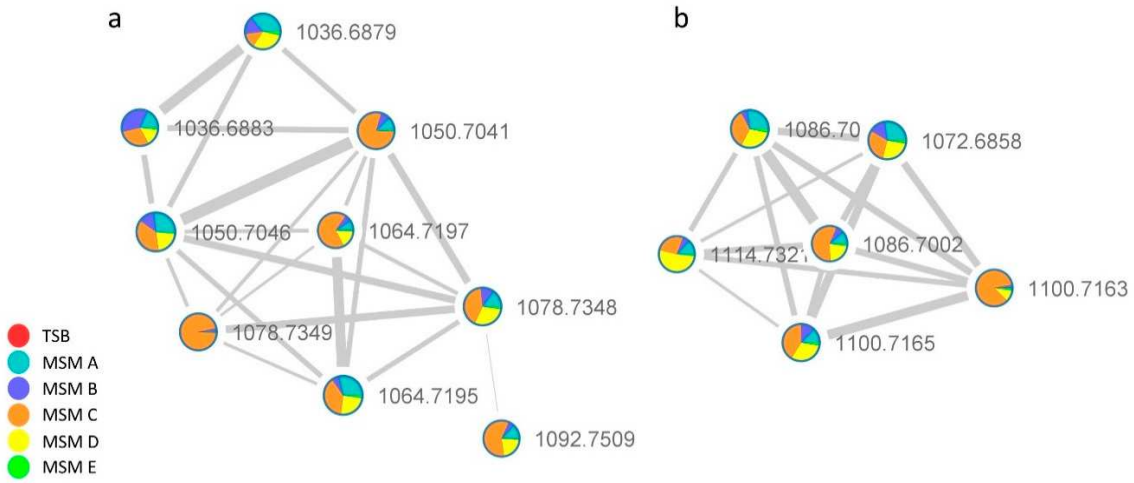

Figure 3. Surfactins (**a**) $[M + H]^+$ and (**b**) $[M + Na]^+$ adduct clusters. Color chart shows that they are only produced in the media containing inorganic nitrogen sources.

Surfactins are a family of lipopeptides produced by strains of the genus *Bacillus*. They feature a cycloheptadepsipeptide core with a terminal β-hydroxy fatty acid (β-OH FA). Culture samples of different *Bacillus* spp. were found to produce complex mixtures of surfactin congeners, which differ either in the length of the fatty acid chain or in the amino acid sequence and composition of the peptide moiety.

The extract obtained in MSM C media, which contains all the detected surfactins, was further analyzed to deepen the sequence of surfactins analogs and to reveal the potential presence of isomers.

The fragmentation pattern of surfactins has been extensively investigated. The initial cleavage of the protonated ester bond was followed by sequential loss of amino acid residues giving rise to b+ and y+ series of fragment ions useful to assign the amino acid sequence, except for the discrimination of isomeric Leu and Ile and OMet Asp and Glu.

The extracted ion chromatogram (XIC) (Figure S2) obtained for all the surfactins $[M + H]^+$ adducts displays for some of them more than one peak, which is ascribable to the presence of isomers, the XIC at 1036 *m*/*z* showed two peaks, the fragmentation spectrum of the first peak (Figure 4a) displayed the series of b+ fragment ions at *m*/*z* 1036(−H2O, 1018) → 923 → 808 → 695 → 596 → 483 → 370, compatible with the sequential loss of Leu/Ile7-Asp6-Leu/Ile5-Val4-Leu/Ile3-Leu/Ile2 from the C terminus. Moreover, the second typical set of y+ fragment ions at *m*/*z* 1036 (−H2O, 1018) → 667(+H2O, 685) → 554 → 441 is ascribable to the losses of C15 β-hydroxyl fatty acid chain-Glu1-Leu/Ile2-Ile/Leu3 from the precursor ion. Both series pointed toward a positional variant of surfactin C, recently reported by Khyati at al. [28], with a C15 β-hydroxyl fatty acid chain and the following amino acid sequence: Glu 1-Leu/Ile 2-Leu3-Val4-Leu/Ile5-Asp6-Leu/Ile7.

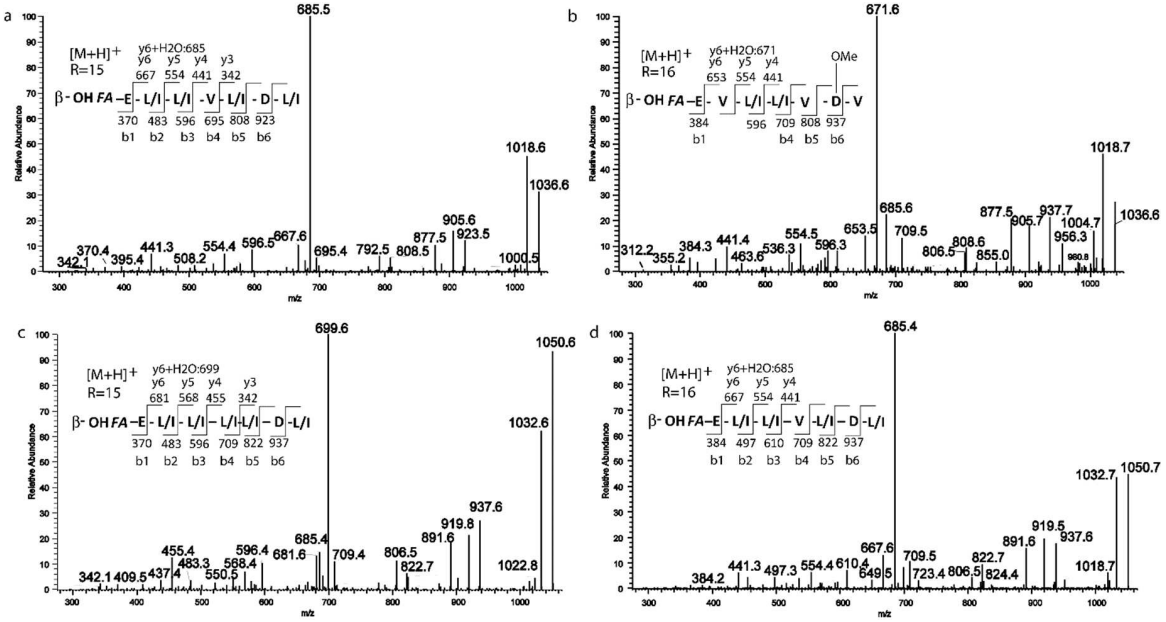

Figure 4. MS/MS spectra of the two isomers for the precursors (**a**,**b**) 1036.6 *m*/*z*; (**c**,**d**) 1050.6 *m*/*z*.

The second isoform with *m*/*z* 1036.7 (Figure 4b) gave a series of b+ ions at *m*/*z* 1036 (–H2O, 1018) → 937 → 808 → 709 → 596 → 384, compatible with the loss of Val7–OMeAsp or Glu6-Val5-Leu/Ile4-Leu/Ile3-Val2. y+ fragment ions at *m*/*z* 1036 (−H2O, 1018) → 653 (+H2O, 671) → 554 → 441 are also in line with proposed sequence and with a C16 β-hydroxyl fatty acid chain.

Although the difference of 129 between b6 and b5 ions could be ascribable both to a Glu residue or to the presence of an OMet-Asp, we proposed here the C16 β-hydroxyl fatty acid chain-Glu1-Val2-Leu/Ile3-Leu/Ile4-Val5-OMeAsp6-Val7 structure based on the observation of a ion fragment a 905, likely arising from b6 ion by MeOH loss. To the best of our knowledge, this surfactin isoform is described in this study for the first time.

Similarly, two fragmentation patterns were observed from precursor ions at 1050.7. The first one (Figure 4c) could be assigned with high confidence to C15 β-hydroxyl fatty acid chain-Glu1-Leu/Ile2-Leu/Ile3-Leu/Ile4-Leu/Ile5-Asp6-Leu/Ile7 on the basis of b+ and y+ series (b+: 937; 822; 709; 596; 483; 370—y+: 681 (+H2O, 699); 568; 455; 342) [28].

The second isomer at *m*/*z* 1050.7 (Figure 4d) showed a fragmentation pattern compatible with the substitution of Leu/Ile in position 4 with a Val and a fatty acid chain with 16 carbons (C16 β-hydroxyl fatty acid chain-Glu1-Leu/Ile2-Leu/Ile3-Val4-Leu/Ile5-Asp6-Leu/Ile7 b+: 937; 822; 709; 610; 497; 384—y+: 667 (+H2O, 685); 554; 441) [28]. Based on fragmentation profile, the three species at *m*/*z* 1064.7 1078.7, 1092.7, (Figure 5a–c) could be assigned as C16, C17 and C18 β-hydroxyl fatty acid homologs with the same peptide moiety, the C18 β-hydroxyl fatty acid isoform is here described for the first time [28].

Finally, two homologs with Glu1-Leu/Ile 2-Leu/Ile3-Leu/Ile4–OMeAsp or Glu5-Leu/Ile6-Leu/Ile7 as aminoacidic sequence and a C17 and C18 β-hydroxyl fatty acid chain were found to be ascribable to the ions with *m*/*z* at 1092.7 and 1106.7 (Figure 5d,e) [29,30].

A peculiar feature of the surfactin analogs produced by *P.* cf. *eucrina* D2 seems to be the presence of the four consecutive leucine motifs found in certain derivatives, and the reversed position of Leu5 and Asp6 compared to the canonical surfactin C (Table S1). The production of surfactins with C17/C18 β-hydroxyl fatty acid chain appear a further unusual feature, with few literature precedents [30].

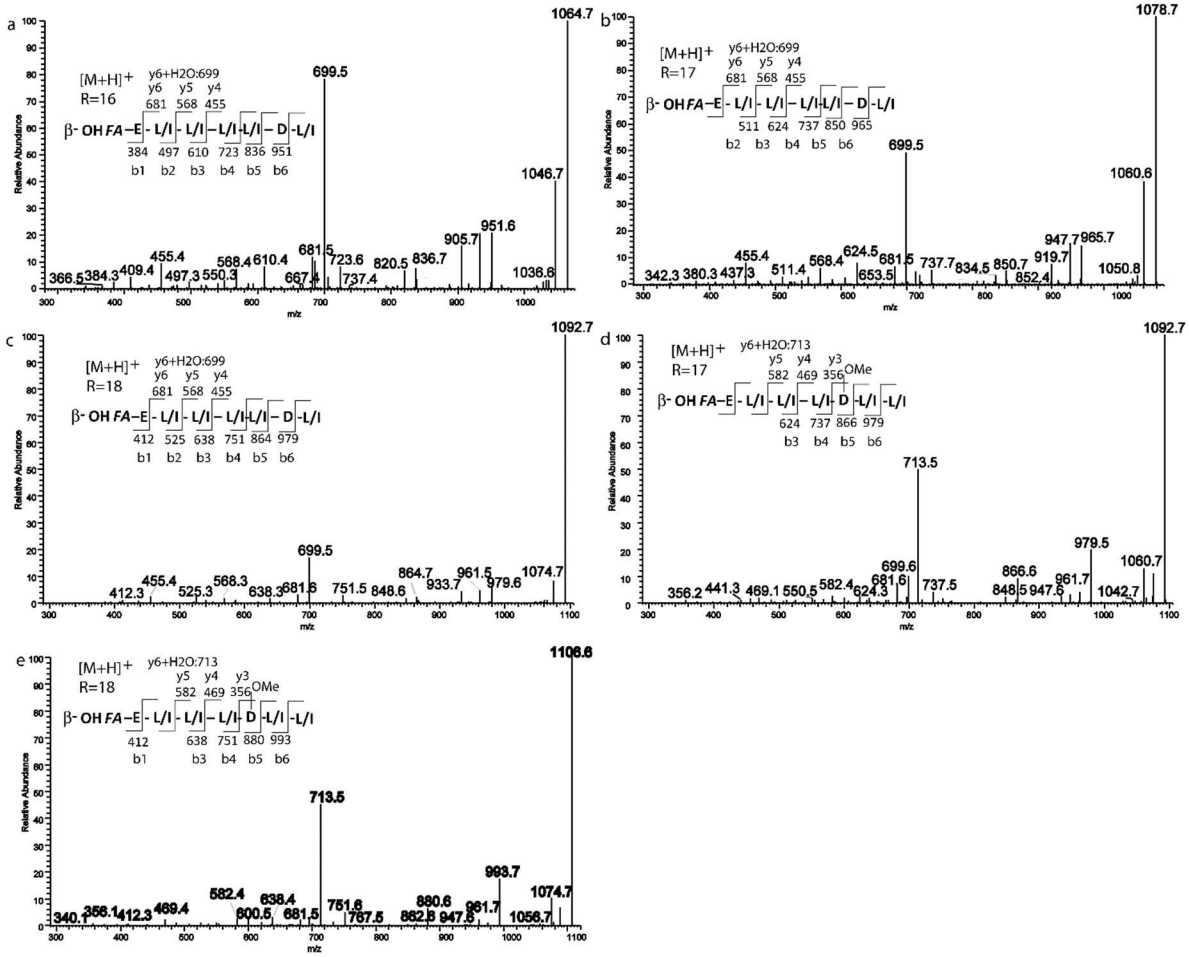

Figure 5. MS/MS spectra of precursors at (**a**) 1064.7 *m*/*z*; (**b**) 1078.7 *m*/*z*; (**c**) 1092.7 *m*/*z*; (**d**) 1092.7 *m*/*z*; (**e**) 1106.6 *m*/*z*.

To the best of our knowledge, this is the first report of the production of surfactins from a Pantoea strain. This is not surprisingly since the production of surfactins was not observed using conventional growth conditions (i.e., TBS medium) whereas it was triggered in the OSMAC media using inorganic sources of nitrogen NH_4Cl or $NaNO_3$. Similarly, the use of inorganic nitrogen sources demonstrated to be an effective tool to simulate the production of the antimicrobial peptide SBR-22 in the marine *Streptomyces psammoticus* BT-408 strain [31] and of the pigment pyocyanin in *Pseudomonas* sp. MCCB-103 [32]. As concerning the carbon sources, glycerol was found to enhance the production, when compared to glucose. The use of glycerol as cost-effective substrate for biosurfactants production by wild type and engineered strains of *Pseudomonas* has been extensively explored and rationalized [33], whereas the use of glycerol in surfactin production has been only sporadically explored [34]. Unfortunately, surfactins derivatives were detected as minor components co-eluting with major lipoamino acids, therefore we were unable to perform an isolation and chemical characterization work.

2.2.2. Lipoamino Acids Molecular Cluster

Figure 6 reports the second cluster featuring a huge number of nodes. The node at *m*/*z* 404.3149 matched the 2-(14-methylpentadecanoylamino)-3-phenylpropanoic acid, a member of lipoamino acids (also referred as N-acyl amino acids), namely conjugates of one amino acid unit linked via an amide bond to saturated or unsaturated fatty acids. In particular, this compound was recently reported as component of a complex mixture of related lipoamino acids from an entomopathogenic *Pantoea* sp.

strain isolated from an individual insect from the *Diaspididae* family [24]. This suggested that the members of this cluster could represents lipoamino acid variants differing for the amino acid and/or fatty acid moiety.

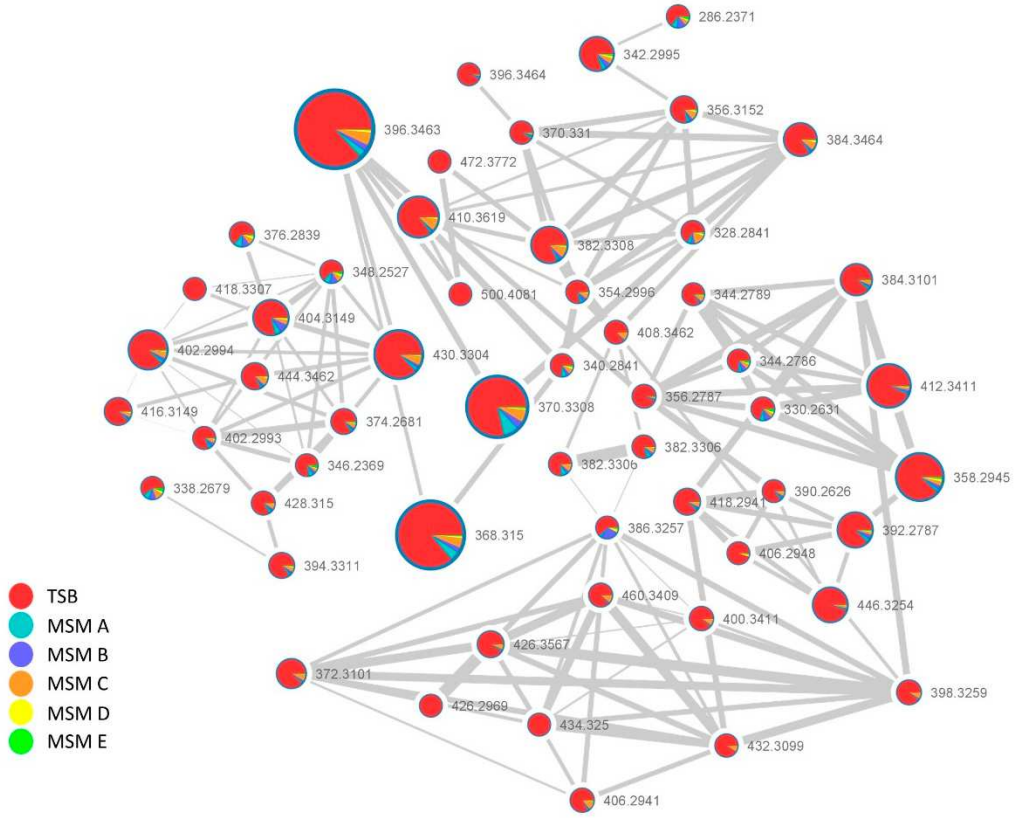

Figure 6. Lipoamino acids cluster in *P.* cf. *eucrina* D2, the size of the nodes is directly proportional to the precursor ion intensity, while the color (explained in the color chart) is dependent on the growth media in which the ion was detected.

Comprehensive manual dereplication of each node within the cluster was done by determination of the molecular formula, from the analysis of the positive pseudomolecular ion $[M + H]^+$, and from inspection of the fragmentation pattern. The key fragment arising from the cleavage of the amide bond allowed to assign the amino acid portion, and by subtraction, the length of the fatty acid subunit, whereas the presence of double bonds was inferred from the calculated round double bond equivalent (RDBE). Through the above analysis, the annotation of each node within the cluster was done and putative phenylalanine, leucine/isoleucine and valine derivatives were found with fatty acid chains ranging from C10 to C21, some of which containing one or two insaturations or an hydroxyl group, the detailed assignments are summarized in Table S2.

Our results parallel those reported by Tourè et al. [8] in what concerns the qualitative composition of the mixture except for some congeners. Although our *Pantoea* cf. *eucrina* D2 was found to produce the phenylalanine conjugates as minor components, whereas in all tested media cultivation conditions the Leu/Ile conjugates are the major components.

Interestingly, we observed that *P.* cf. *eucrina* D2 was able to produce lipoamino acids in all tested growing media containing only inorganic nitrogen sources, so showing nitrifying properties.

2.3. Isolation and Structure Elucidation of Pure Compounds

In order to solve the Leu/Ile and the configurational ambiguities left by the MS analysis and to assess the antimicrobial activity of the major pure components, a medium scale cultivation (1.8 L)

in TBS medium was performed, the crude extracellular extract (1.0 g) was fractionated by reverse Phase MPLC, and the obtained fractions were purified on UPLC equipped with a semipreparative PFP column as described in Material and methods section, affording pure Compounds **1–8** (Figure 7).

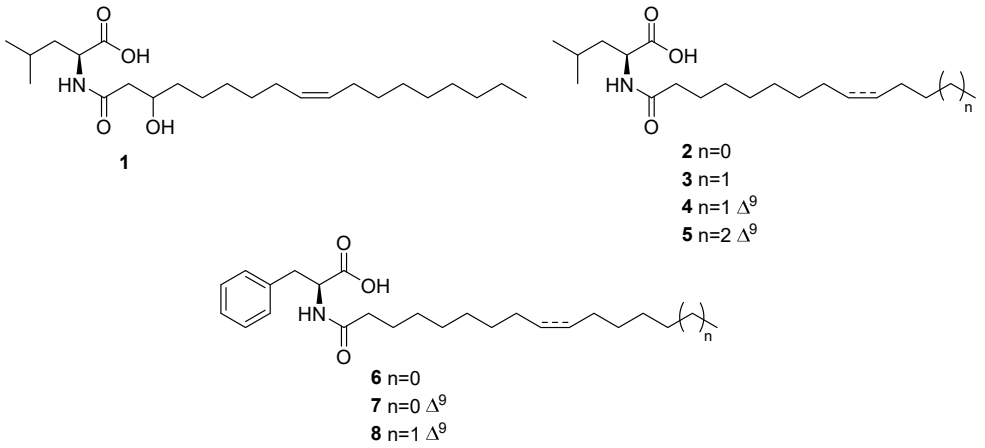

Figure 7. Structures of isolated aminolipids **1–8**.

The structures of these compounds were determined by combined MS/MS and 2D NMR analysis and by comparison with literature data.

Compound **1** gave a pseudomolecular ion $[M + H]^+$ at *m*/*z* 412.3411 $[M + H]^+$, calcd. 412.3411 $\Delta = -3.84$ ppm corresponding to the molecular formula $C_{24}H_{45}NO_4$. LC-HRMS/MS fragmentation showed a diagnostic molecular ion at *m*/*z* of 132.1017 corresponding to $C_6H_{14}O_2$ N (Ile and/or Leu).

The analysis of 2D COSY, HSQC and HMBC allowed the straightforward assignment of the leucine aminoacyl spin system (Table S5). Particularly diagnostic for the Ile/leu discrimination are the ^{1}H and ^{13}C NMR chemical shifts of two γ methyl groups (δ_H 0.96 and 0.97/δ_C 21.8 and 23.2).

Remaining NMR data were indicative of a linear acyl group (one terminal methyl δ_H 0.90, t, J = 7.0 Hz) with a double bond (δ_H 5.36, δ_C 130.1) and one hydroxy group (δ_H 4.00, δc 68.9). Key COSY and HMBC correlations were reported in Figure 8. COSY correlations between the diastereotopic methylene protons at C-2′ (δ_H 2.50 (d, J = 14.7 Hz) and 2.34 (dd; J = 14.7, 8.9 Hz) and the hydroxymethine H-3 (δ_H 4.00) and between H-3 and methylene protons H_2-4′ (δ_H 1.56 and 1.48) together the diagnostic HMBC correlations between H_2-2/C-1′, H_2-2/C-3′, H_2-2/C-4′ and H_2-4/C-3 clearly suggested the presence of 3-hydroxy unsaturated fatty acid moiety. The mass and NMR data allowed us to determine that the fatty acid moiety is 3-hydroxyoctadec-9-enoic acid.

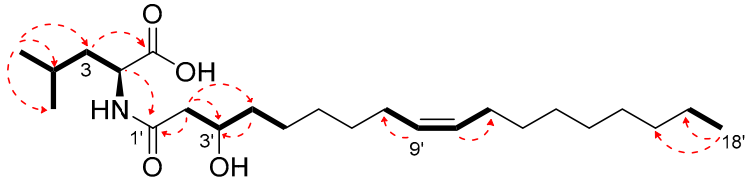

Figure 8. Key COSY (bold lines) and HMBC (red dashed arrows) correlations of Compound **1.**

The stereochemistry of the double bond was assigned as *Z*, based on the ^{13}C chemical shift of the C8-C11 allylic carbons at δ_C 27.4 ppm [35].

Marfey's analysis confirmed the identity of Leu residue and its L-configuration (Figure S18). At this stage, the stereochemistry of hydroxy-methine in position 3 remains undefined. Compound **1** was therefore identified as (Z)-*N*-(3-hydroxyoctadec-9-enoyl)-L-leucine.

Structural *N*-acylamino acid analogs **2–5** were characterized using comparative NMR, HRMS/MS and Marfey's analysis. Compounds **2–4** were already isolated as mixture of enantiomers and an

inseparable mixture together with their isoleucine congeners from *Cobetia* sp. isolated from the marine hydroid *Hydractinia echinata* [36].

N-palmitoyl-L-leucine (**4**) was already isolated by *Streptomyces* sp. and identified as a late stage inhibitor of m-RNA splicing through a high- throughput screening of 5304 pre-fractions of marine bacterial lysates [37].

Through NMR and MS analysis and by comparison with literature data [8] Compounds **6**, **7** and **8** were identified as *N*-palmitoyl-L-phenylalanine, *N*-palmitenoyl-L-phenylalanine and *N*-oleyl-L-phenylalanine, respectively. *N*-palmitenoyl-L-phenylalanine (**7**) was already isolated from *Pantoea* sp., whereas Compounds **6** and **8** were obtained in the same study by synthesis [8]. The configuration of the double bond in the acyl chain of **7** and **8** was assigned as Z on the basis of the ^{13}C NMR chemical shifts of allylic methylenes, whereas the L-configuration of the phenylalanine residue was assigned by comparison of the experimental positive optical rotation data with those reported in the literature [8].

2.4. Minimum Inhibition Concentration (MIC)

The data regarding antimicrobial activity of lipoamino acids are often dated and not widely described, in the specific case, are not reported at all for leucine N-acylamino lipids. Herein the antimicrobial potential of the pure molecules was determined by microdilution method and the MIC value was reported for each pathogen, DMSO at an initial concentration of 2% (*v*/*v*) was adopted as negative control and antibiotics at their respective breakpoint concentrations were used as positive controls. The results reported in Table 2 show that this class of molecules is ineffective against the Gram-negative strains (*Acinetobacter baumannii* 13 and *Stenotrophomonas maltophilia* ATCC 13637). In addition, the amino acid moiety seems to play an important role in the exertion of antimicrobial properties, in fact, in accordance with a recent report on phenylalanine lipoamino acids [8], Compounds **6**–**8** are totally ineffective or slightly active towards *Staphylococcus aureus* and also against *Staphylococcus epidermidis*, independently from fatty acid chain length. On the other hand, leucine- containing congeners were very active towards *Staphylococcus* spp., with the best MIC values given by Compounds **1**, **3** and **4** with 10 (µg/mL) towards *S. aureus* and by Compounds **3** and **4** with 10 (µg/mL) towards *S. epidermidis*.

Table 2. Antimicrobial activity expressed as MIC values for the pure Compounds 1–8 towards a panel of human pathogens.

	MIC (µg/mL)				
Compound	***S. aureus* 6538P**	***L. monocyogenes* MB677**	***S. epidermidis* ATCC 35984**	***A. baumannii* 13**	***S. maltophilia* ATCC 13,637**
1	10	8.0	13	–	–
2	13	8.0	13	–	–
3	10	4.0	10	–	–
4	10	6.6	10	–	–
5	128	6.6	128	–	–
6	–	4.0	–	–	–
7	64	16	128	–	–
8	–	26	–	–	–
Positive control [a]	2	1	1.7	4	3.3

Each experiment was repeated at least three times and the mean value is reported. [a] Vancomycin was used as positive control for *Staphylococcus* strains, ampicillin for *L. monocytogenes*, chloramphenicol for *S. maltophilia* and gentamicin for *A. baumannii*.

The activity of these biosurfactants towards foodborne pathogens was observed on certain shorter chain derivatives [38], where *N*-myristoyl-L-phenylalanine showed a MIC of 34 (µg/mL) towards *L. monocytogenes*, although longer chain congeners herein isolated seems to be more effective towards the clinical isolated *L. monocytogenes* strain used in this study. Additionally, it is noticeable that

phenylalanine congeners hold a comparable activity with leucine one, with the best activity value obtained for Compounds **3** and **6** (4.0 μg/mL).

3. Materials and Methods

3.1. General Experimental Procedures

1D and 2D NMR experiments were recorded on Bruker Avance NEO 400 MHz and 700 MHz spectrometers (Bruker, USA) with a RT-DR-BF/1H-5mm-OZ SmartProbe. Chemical shifts were reported in δ (ppm) and were referenced to the residual $CDCl_3$ as internal standards (δ_H = 7.26 and δ_C = 77.0 ppm) and CD_3OD as internal standards (δ_H = 3.31 e δ_C = 49.0 ppm). All of the recorded signals were in accordance with the proposed structures. Spin multiplicities are given as s (singlet), br s (broad singlet), d (doublet), t (triplet) or m (multiplet).

The LC-HRMS and MS/MS analysis were carried out on an LTQ XL-Orbitrap high-resolution mass spectrometry system (Thermo Scientific) equipped with an Accelera 600 pump HPLC (LCHRMS).

Further fragmentation analysis was carried out on an LTQ XL mass spectrometry system (Thermo Scientific) equipped with a HESI source and connected to an Ultimate 3000 HPLC pump.

The first purification step was run on a User Manual PuriFlash XS 520 Plus equipped with UV detector. Purification of single molecules was performed on an Acquity UPLC H-CLASS connected to a PDA detector (Waters).

The 96-well plates were read on a Biotek ELX800, monitoring the absorbance at 600 nm at room temperature.

3.2. Media and Buffers

Tryptic soy broth (TSB): 3.0-g/L papaic digest of soya, 2.5-g/L D (+)-glucose, 17-g/L pancreatic digest of casein, 2.5-g/L di-potassium hydrogen phosphate, 5-g/L sodium chloride.

Modified mineral salt medium (MSM mod): 0.7-g/L KH_2PO_4, 0.9-g/L Na_2HPO_4, 0.4-g/L $MgSO_4$, 0.1-g/L $CaCl_2$.

MSM A: MSM mod + glucose 1% *v*/*v* + 1-g/L NH_4Cl

MSM B: MSM mod + glucose 1% *v*/*v* + 2-g/L NH_4Cl

MSM C: MSM mod + glycerol 1% *v*/*v* + 1-g/L NH_4Cl

MSM D: MSM mod + glucose 1% *v*/*v* + 2-g/L $NaNO_3$

MSM E: MSM mod + glucose 1% *v*/*v* + 4-g/L $NaNO_3$

Cation-adjusted Mueller–Hinton broth (CAMHB) [39]

Marine broth (MB): 19.4-g/L NaCl, 8.8-g/L $MgCl_2$, 5-g/L peptone, 3.24-g/L Na_2SO_4, 1.8-g/L $CaCl_2$, 1-g/L yeast extract, 0.55-g/L KCl, 0.16-g/L $NaHCO_3$, 0.10-g/L Fe(III) citrate, 0.08-g/L KBr, 0.034-g/L $SrCl_2$, 0.022-g/L H_3BO_3, 0.008-g/L Na_2HPO_4, 0.004-g/L sodium silicate, 0.0024-g/L NaF, 0.0016-g/L NH_4NO_3

3.3. Sponge Collection and Bacterial Isolation at Different pH

Specimens of the sponge *Chondrosia reniformis* were collected by scuba diving at 2-m depth in several spots influenced by CO_2 emissions and low pH close to Castello Aragonese, Ischia, Italy (40°43.84′ N 13°57.08′ E). Immediately after the collection some sponge pieces were stored at 15 °C submersed in 0.22 μm filtered seawater and taken to the laboratory for the microbial isolation. Bacterial isolation was performed at different pH values. Sponge pieces were shredded and mixed with 20 mL sterile seawater, then the solution was shaken for 30 min, and finally the bacterial suspension was serially diluted (10^{-1}, 10^{-2} and 10^{-3} in 10 mL) and 100 μL of each dilution was plated on different MB agar plates, previously adjusted with HCL 1 M to the three chosen pH values: 5, 6 and 7.

The petri dishes were incubated at 15 °C for 15 days, which is the same temperature of the seawater registered during the sampling session. After the incubation period, morphologically different colonies were picked by a sterile loop, grown in liquid MB broth and finally pure bacteria cultures were stored at -80 °C in sterile cryovials with glycerol 20% *w*/*w*.

3.4. 16S Sequencing

PCR was carried out in a total volume of 50 µL containing 25 µL of PCR Master Mix 2× (a ready-to-use solution containing TaqPol, buffer, MgCl2 and dNTPs), 0.2 µM of both primers 27F (5'-AGAGTTTGATCCTGGCTCAG-3') and 1492R (5'-GGTTACCTTGTTACGACTT-3'), and 100 ng of DNA. PCR protocol is reported in Table S3. Five microliters of each PCR product were run on 1% agarose gel at 110 V for 45 min to check the quality of DNA and observed under UV light. Then PCR products were purified with the GeneAll kit according to manufacturer's instructions and the obtained amplicons were send to Eurofins Genomics for the sequencing. Finally, the sequences were used as template for a taxonomic annotation via BLASTn tool against GenBank database, using the 16S RNA sequences collection. The contig obtained submitting the forward and the reverse sequences to Prabi CAP3 (http://doua.prabi.fr/software/cap3) was submitted to BLASTn for the affiliation analysis. Evolutionary analyses involved ten nucleotide sequences, our D2 strain along with nine close matching entries according to BLASTn, and were conducted in MEGA X [40]. A phylogenetic tree was inferred using the neighbor-joining method [41]. The evolutionary distances were computed using the Kimura 2-parameter method [42] and are in the units of the number of base substitutions per site. All ambiguous positions were removed for each sequence pair (pairwise deletion option). Bootstrap values were calculated with 1000 resamples.

3.5. Bacterial Cultivation, OSMAC Cultures and Extraction Methodologies

To produce the extracts in the complex media TSB, a single CFU of D2 was used to inoculate 3 mL of TSB, in sterile bacteriological tubes. After 24 h of incubation at 20 °C and 210 rpm, the inoculum was employed to inoculate 125 mL of the respective media in a 500-mL flask, at the initial cell concentration of 0.01 OD_{600}/mL. The flask was incubated for 5 days at the same conditions.

The OSMAC (one strain many compounds) approach was used to trigger the production of metabolites unexpressed or underexpressed under normal conditions. Different D2 cultures have been set utilizing MSM mod liquid media as base, glucose or glycerol as carbon source, while the inorganic nitrogen salts NH_4Cl or $NaNO_3$ were used as sole nitrogen sources at different concentrations. In this case, a different protocol was used to inoculate the strain: a D2 single colony was picked from a pure plate and inoculated in 3 mL of TSB. After 2 days of incubation at 20 °C and 210 rpm, the culture was centrifuged, the medium was discarded, and the cells were resuspended in 1 mL of MSM mod. The absorbance was measured at the spectrophotometer and was inoculated in 125 mL of each different medium in a 500-mL flask at the same conditions previously described.

The medium-scale fermentation was set by inoculating 1.8 L of TSB with the same procedure described above at 20 °C for 5 days to afford 1 g of crude extract.

After the incubation time, all the cultures were centrifuged at 6800× *g* at 4 °C for 45 min, and the supernatant was extracted with 2 volumes of ethyl acetate, then the organic phase was dried under vacuum at the rotary evaporator to afford the crude extract.

3.6. Mass Spectrometry Analysis

The TSB and OSMAC extracts were first subjected to a desalination step by using the Sep-Pak tC18 Plus Short Cartridge 400 mg. Each extract was dissolved in the minimum amount of MeOH and upload on a cartridge, then 3 beds of MQ H_2O were used to wash the extract and 3 beds of MeOH and MeOH + TFA 0.01% to eluate the metabolites. Then the methanolic extracts were dried under nitrogen flux and subjected to mass spectrometric analysis.

Both low resolution and high resolution data dependent analysis were carried out performing chromatographic separation of samples on a Synergi 2.5 mm Fusion_RP 100 × 2 by means of a linear gradient of B in 27 min (Buffer A: H_2O + 0.1% Formic acid (FA), Buffer B: ACN 0.1% + FA). Full MS spectra were acquired in the mass range 150–1500 with 10 data-dependent MS/MS events of the 10 most intense ions.

3.7. Molecular Networking Building

The MS data were treated with MZmine [25] upon being converted from *.raw extension to *.mzXML extension using the tool MSConvert by ProteoWizard.

Version 2.53 of MZmine was used to process the data and the parameters used in each step are listed in the Table S4, the job was exported as two output data, one quantification table (.csv) and one file containing the MS and MS/MS features (.mgf).

These data were submitted to GNPS website (https://gnps.ucsd.edu) [14] and the network was created with the feature-based molecular networking (FBMN) workflow [26]. The parameters were changed in accordance with the data and the used mass spectrometer, the precursor ion mass tolerance was set to 0.05 Da, the fragment Ion mass tolerance was set to 0.05 Da. The molecular network was created with a maximum of 100 nodes for each cluster, edges were filtered to have cosine score above 0.7 and at least 3 matching peaks, more edges among two nodes were kept only if each of the nodes is, respectively in each other list of the 10 more similar nodes. Analogs for each node were also searched, with a maximum mass difference of 300 Da, here at the same way all the analogs hits had to show a cosine score above 0.7 and at least 3 matching peaks. Finally the network was visualized by Cytoscape [27].

The MN job can be publicly accessed through this link https://gnps.ucsd.edu/ProteoSAFe/status.jsp?task=26db58f686234915b9e8884718f25085.

3.8. Medium-Scale Cultivation and Isolation of Pure Lipoamino Acids

The medium-scale fermentation was set by inoculating 1.8 L of TSB with the same procedure previously described for the small cultures, at 20 °C for 5 days.

The culture was centrifuged at 6800× *g* at 4 °C for 45 min, and the supernatant was extracted with 2 volumes of ethyl acetate, then the organic phase was dried under vacuum at the rotary evaporator to afford about 1 g of crude extract. The extracellular extract was fractionated in two runs by MPLC on RP-column (C18 spherical 20–35-µM 100A, 12 g) using a linear gradient of H_2O/MeOH (*v*/*v*, from 90:10 to 0:100 over 1 h) to give six main fractions, labeled A to G. Fraction F (110 mg), eluted with MeOH:H_2O 90:10, was purified by UPLC using a Luna® PFP(2) column (5 µM, 250 mm × 10 mm i.d.) with ACN/H_2O 62% with 0.1% TFA as mobile phase (flow rate 2.00 mL/min) giving Compounds **1** (1.6 mg, t_R 32 min); **2** (5 mg, t_R 34 min), **4** (11 mg, t_R 39 min) and **7** (0.6, t_R 41 min). Fraction G (160 mg), eluted with MeOH:H_2O 90:10, was subjected to UPLC using a Luna® PFP(2) column (5 µM, 250 mm × 10 mm i.d.) and ACN/H_2O 62% with 0.1% TFA as mobile phase (flow rate 2.00 mL/min) to yield Compounds **3** (9.9 mg, t_R 42 min), **6** (3.3 mg, t_R 44 min), **5** (8 mg, t_R 47 min) and **8** (7 mg, t_R 49 min).

Compound **1**: white powder; $[\alpha]_D^{25}$ -7 (c 0.16, MeOH); ^{1}H and ^{13}C NMR (700 and 175 MHz, $CDCl_3$) spectroscopic data, see Table S5 and Figures S3–S6; HR-ESIMS *m*/*z* 412.3411 $[M + H]^+$ (calculated for $C_{24}H_{45}O_4\ N^+$, 412.3421).

N-myristoyl-L-leucine (**2**): white powder; $[\alpha]_D^{25}$ − 9 (c 0.5, MeOH); ^{1}H NMR (400 MHz, $CDCl_3$) spectroscopic data, see Figure S7, δ_H 6.06 (NH, d, *J* = 6.9 Hz), 4.58 (1H, m), 2.26 (2H, t, *J* = 7.4 Hz), 1.72 (2H, m), 1.65 (3H, m), 1.29 (20H, m), 0.98 (3H, d, *J* = 6.2 Hz), 0.96 (3H, d, *J* = 6.2 Hz), 0.90 (3H, t, *J* = 6.8 Hz); HR-ESIMS *m*/*z* 342.2995 $[M + H]^+$ (calculated for $C_{20}H_{40}O_3N^+$, 342.3003).

N-palmitoyl-L-leucine (**3**): white powder; $[\alpha]_D^{25}$ − 14 (c 0.34, MeOH); ^{1}H and ^{13}C NMR (700 and 175 MHz, $CDCl_3$) spectroscopic data, see Table S6, Figure S8 and S9; HR-ESIMS *m*/*z* 370.3308 $[M + H]^+$ (calculated for $C_{22}H_{44}O_3N^+$, 370.3316).

N-palmitoleoyl-L-leucine (**4**): white powder; $[\alpha]_D^{25}$ − 7 (c 1.0, MeOH); ^{1}H and ^{13}C NMR (400 and 100 MHz, $CDCl_3$) spectroscopic data, see Table S6, Figures S10 and S11; HR-ESIMS *m*/*z* 368.3150 $[M + H]^+$ (calculated for $C_{22}H_{42}O_3N^+$, 368.3159).

N-oleoyl-L-leucine (**5**): white powder; $[\alpha]_D^{25}$ − 8 (c 0.41, MeOH); ^{1}H and ^{13}C NMR (400 and 100 MHz, $CDCl_3$) spectroscopic data, see Table S6, Figures S12 and S13; HR-ESIMS *m/z* 396.3463 $[M + H]^+$ (calculated for $C_{24}H_{46}O_3N^+$, 396.3472)

N-palmitoyl-L-phenylalanine (**6**): white powder; $[\alpha]_D^{25}$ + 41 (c 0.04, MeOH); selected ^{1}H NMR (400 MHz, CD_3OD) spectroscopic data, see Figure S14; δ_H 7.25 (5H, m), 4.68 (1H, dd, *J* = 9.5 and 4.5 Hz), 3.22 (1H, dd, *J* = 14.0 and 4.5 Hz), 2.94 (1H, dd, *J* = 14.0 and 9.5 Hz), 2.16 (2H, t, *J* = 7.4 Hz), 1.49 (2H, m), 1.29 (24H, m), 0.90 (3H, t, *J* = 6.8 Hz); HR-ESIMS *m/z* 404.3149 $[M + H]^+$ (calculated for $C_{25}H_{42}O_3N^+$, 404.3159).

N-palmitoleoyl-L-phenylalanine (**7**): white powder; $[\alpha]_D^{25}$ + 20 (c 0.06, MeOH); (400 MHz, CD_3OD) spectroscopic data, see Figure S15; δ_H 7.25 (5H, m), 5.35 (2H, m), 4.64 (1H, dd, *J* = 9.6 and 4.8 Hz), 3.24 (1H, dd, *J* = 13.9 and 4.7 Hz), 2.93 (1H, dd, *J* = 13.9 and 9.3 Hz), 2.14 (2H, t, *J* = 7.4 Hz), 2.04 (2H, m), 1.49 (2H, m), 1.31 (16H, m), 0.89 (3H, t, *J* = 7.0 Hz); HR-ESIMS *m/z* 402.2993 $[M + H]^+$ (calculated for $C_{25}H_{40}O_3N^+$, 402.3003).

N-oleoyl-L-phenylalanine (**8**): white powder; $[\alpha]_D^{25}$ + 44 (c 0.06, MeOH); ^{1}H NMR (400 MHz, CD_3OD) see Figure S16; δ_H 7.24 (5H, m), 5.36 (2H, m), 4.68 (1H, dd, *J* = 9.6 and 4.8 Hz), 3.21 (1H, dd, *J* = 13.9 and 4.8 Hz), 2.94 (1H, dd, *J* = 13.9 and 9.6 Hz), 2.13 (2H, t, *J* = 7.5 Hz), 2.04 (2H, m), 1.48 (2H, m), 1.30 (20H, m), 0.90 (3H, t, *J* = 7.0 Hz); ^{13}C NMR (100 MHz, CD_3OD) see Figure S17, δ_C 176.2, 175.7, 138.9, 131.0, 130.6 (2C), 129.5, 127.7, 55.5, 38.6, 37.3, 33.2, 31.1 (2C), 30.9 (2C), 30.8 (2C), 30.7 (2C), 30.5, 30.4, 28.5 (2C), 27.3, 23.9, 14.6; HR-ESIMS *m/z* 430.3304 $[M + H]^+$ (calculated for $C_{27}H_{44}O_4N^+$, 430.3316).

3.9. Hydrolysis and Advanced Marfey's Analysis.

Compound **3** (0.8 mg) was hydrolyzed with 6-N HCl 120 °C for 12 h. The residual HCl fumes were removed under vacuum. The hydrolysate of **3** was split and dissolved in TEA/acetone (2:3, 100 µL), and the solution was treated with 100 µL of 1% 1-fluoro-2,4-dinitrophenyl-5-D-alaninamide (D-FDAA) and 1-fluoro-2,4-dinitrophenyl-5-L-alaninamide (L-FDAA) in CH_3CN/acetone (1:2).

The vial was heated at 50 °C for 1.5 h. The mixture was dried, and the resulting D-FDAA and L-FDAA derivatives were dissolved in MeOH (200 µL) for subsequent analysis. Authentic standards of L-Leu, L-Ile and D-Allo-Ile were treated with L-FDAA and D-FDAA as described above and yielded the L-FDAA and D-FDAA standards. Marfey's derivatives of **3** were analyzed by LC–ESI–MS, and their retention times were compared with those from the authentic standard derivatives. A Luna Omega 3 µm Polar C18 column (100 × 2.1 mm) maintained at 25 °C was eluted at 300 µL/min with 0.1% HCOOH in H_2O and ACN. The gradient program was as follows: 10% ACN 2 min, 10% → 95% ACN over 10 min, 100% ACN 3 min. Mass spectra were acquired in positive ion detection mode, and the data were analyzed using the Xcalibur suite of programs.

3.10. Minimum Inhibition Concentration (MIC) Assessment

The antimicrobial activity of the pure lipoamino acids was determined by microdilution method and MIC values were determined comparing them with appropriate antibiotics, how described by the Clinical and Laboratory Standard Institute (CLSI) [39]. The antimicrobial assay was performed in CAMHB as medium, pure compounds were dissolved in DMSO and were 2-fold serially diluted from in a final volume of 100 µL of CAMHB medium in a 96-well microtiter plate (Sarstedt), obtaining concentration in the range 128–1 µg/mL. DMSO at an initial concentration of 2% (*v*/*v*) was adopted as negative control. Each well contained 50 µL of a pure molecule solution at twice the desired final concentration, therefore it was inoculated with 50 µL of bacterial culture grown overnight at 37 °C, resulting in a final inoculum of 4 × 105 CFU/mL in a 100 µL final volume of each well. Then, each plate was incubated for 20 h at 37 °C to allow optimal bacterial growth. The pathogenic strains used in the liquid inhibition assay are: *S. aureus* 6538P [43], *L. monocyogenes* MB677 [44], *S. epidermidis* ATCC 35,984 [45], *A. baumannii* 13 [46] and, *S. maltophilia* [47].

4. Conclusions

In this study, MN and OSMAC integrated strategies were used to study the secondary metabolism of the endophytic strain *Pantoea* cf. *eucrina* D2 isolated from the sponge *Chondrosia reniformis* adapted to OA conditions. The study evidenced the production of otherwise silent surfactin biosurfactants induced by using inorganic nitrogen as sole nitrogen source.

The molecular networking-based approach confirmed the production of lipoamino acids as chemotaxonomic markers of members of *Pantoea* genus [8] and guided towards the isolation of six new structural variants of this growing family of bacterial secondary metabolites, together with two known derivatives.

All isolated compounds exhibited antimicrobial activity. It is currently suggested that lipoamino acids exert a protective role in the endosymbiotic interaction with the host [8] and that the observed species-specific tight regulation of the composition of lipoamino acid mixtures [48,49] may be the result of the epigenetic regulation of their biosynthesis in response to specific environmental pressures. The leucine-based N-acylamino acids were found to possess a good antimicrobial potential towards Gram-positive strains, in particular towards a clinical isolate of the foodborne pathogen *L. monocytogenes*. The natural presence of *Pantoea* cf. *eucrina* D2 in *Chondrosia reniformis* may likely afford the sponge with advantages, in what regards defense from other undesirable invasive microbes by out-competition and antimicrobial properties. However, also, the production of exopolysaccharides and surfactant-type chemicals, may create protective envelopes for beneficial endosymbiotic microorganisms (e.g., N-fixing microbes) sensitive to low pH scenarios [1,23].

Further studies will be devoted to the optimization of the production of both biosurfactant families and to the exploration of the biotechnological potential of *Pantoea eucrina* D2 in bioremediation, biocontrol and food preservation fields.

Supplementary Materials: Supplementary Materials can be found at http://www.mdpi.com/1422-0067/21/17/6307/s1.

Author Contributions: Conceptualization, M.V.D. and D.d.P.; organismal sampling, L.N.P. and V.M.; formal analysis and investigation, G.A.V., C.C., M.S., C.B. and V.M.; data curation, G.A.V., C.C. and M.S., C.F.; writing—original draft preparation, M.V.D. and G.A.V.; supervision, M.V.D.; project administration, D.d.P. and L.N.P.; funding acquisition, D.d.P., L.N.P. and M.V.D. All authors have read and agreed to the published version of the manuscript.

Funding: This work was supported by MIUR (PRIN 2017; 2017A95NCJ/2017A95NCJ_002, "Stolen molecules—Stealing natural products from the depot and reselling them as new drug candidates"); H2020-MSCA-ITN-ETN MarPipe, Grant Number 721421 and by H2020-MSCA-RISE: Ocean Medicines Grant Number 690944

Acknowledgments: Special thanks are due to B. Iacono for scuba diving assistance. The authors thank the H2020-MSCA-RISE Ocean Medicines, GA 690944, the H2020-MSCA-ITN-ETN MarPipe, GA 721421, and the University of Campania Luigi Vanvitelli for partial support.

Conflicts of Interest: The authors declare no conflict of interest.

References

1. Walterson, A.M.; Stavrinides, J. Pantoea:insights into a highly versatile and diverse genus within the Enterobacteriaceae. *FEMS Microbiol. Rev.* **2015**, *39*, 968–984. [CrossRef] [PubMed]
2. Dutkiewicz, J.; Mackiewicz, B.; Lemieszek, M.; Golec, M.; Milanowski, J. Pantoea agglomerans: A mysterious bacterium of evil and good. Part IV. Beneficial effects. *Ann. Agric. Environ. Med.* **2016**, *23*, 206–222. [CrossRef] [PubMed]
3. Ferreira, C.M.H.; Soares, H.M.; Soares, H.M. Promising bacterial genera for agricultural practices: An insight on plant growth-promoting properties and microbial safety aspects. *Sci. Total Environ.* **2019**, *682*, 779–799. [CrossRef] [PubMed]
4. Smits, T.; Duffy, B.; Blom, J.; Ishimaru, C.A.; Stockwell, V.O. Pantocin A, a peptide-derived antibiotic involved in biological control by plant-associated Pantoea species. *Arch. Microbiol.* **2019**, *201*, 713–722. [CrossRef]
5. Teng, T.; Li, X.; Zhang, L.; Li, Y. Identification and Characterization of pantocin wh-1, a Novel Cyclic Polypeptide Produced by Pantoea dispersa W18. *Molecules* **2020**, *25*, 485. [CrossRef]

6. De Maayer, P.; Chan, W.Y.; Blom, J.; Venter, S.; Duffy, B.; Smits, T.H.; Coutinho, T.A. The large universal Pantoea plasmid LPP-1 plays a major role in biological and ecological diversification. *BMC Genom.* **2012**, *13*, 625. [CrossRef]
7. Rezzonico, F.; Smits, T.; Duffy, B. Misidentification slanders Pantoea agglomerans as a serial killer. *J. Hosp. Infect.* **2012**, *81*, 137–139. [CrossRef]
8. Touré, S.; Desrat, S.; Péllissier, L.; Allard, P.-M.; Wolfender, J.-L.; Dusfour, I.; Stien, D.; Eparvier, V. Characterization, Diversity, and Structure-Activity Relationship Study of Lipoamino Acids from Pantoea sp. and Synthetic Analogues. *Int. J. Mol. Sci.* **2019**, *20*, 1083. [CrossRef]
9. Gambi, M.; Gaglioti, M.; Teixido, N. I sistemi di emissione di CO2 dell'isola d'Ischia. *Mem. Della Carta Geol. D'italia* **2019**, *105*, 55–64.
10. Foo, S.A.; Byrne, M.; Ricevuto, E.; Gambi, M.C. The Carbon Dioxide Vents of Ischia, Italy, A Natural System to Assess Impacts of Ocean Acidification on Marine Ecosystems: An Overview of Research and Comparisons with Other Vent Systems. *Oceanogr. Mar. Biol.* **2018**, 237–310. [CrossRef]
11. Hall-Spencer, J.M.; Rodolfo-Metalpa, R.; Martin, S.; Ransome, E.; Fine, M.; Turner, S.M.; Rowley, S.J.; Tedesco, D.; Buia, M.C. Volcanic carbon dioxide vents show ecosystem effects of ocean acidification. *Nature* **2008**, *454*, 96–99. [CrossRef] [PubMed]
12. Taylor, M.W.; Radax, R.; Steger, D.; Wagner, M. Sponge-Associated Microorganisms: Evolution, Ecology, and Biotechnological Potential. *Microbiol. Mol. Biol. Rev.* **2007**, *71*, 295–347. [CrossRef] [PubMed]
13. Pan, R.; Bai, X.; Chen, J.; Zhang, H.; Wang, H. Exploring Structural Diversity of Microbe Secondary Metabolites Using OSMAC Strategy: A Literature Review. *Front. Microbiol.* **2019**, *10*, 294. [CrossRef]
14. Wang, M.; Carver, J.J.; Phelan, V.V.; Sanchez, L.M.; Garg, N.; Peng, Y.; Nguyen, D.D.; Watrous, J.; Kapono, C.A.; Luzzatto-Knaan, T.; et al. Sharing and community curation of mass spectrometry data with Global Natural Products Social Molecular Networking. *Nat. Biotechnol.* **2016**, *34*, 828–837. [CrossRef] [PubMed]
15. Erwin, P.M.; Coma, R.; López-Sendino, P.; Serrano, E.; Ribes, M. Stable symbionts across the HMA-LMA dichotomy: Low seasonal and interannual variation in sponge-associated bacteria from taxonomically diverse hosts. *FEMS Microbiol. Ecol.* **2015**, *91*, 91. [CrossRef] [PubMed]
16. Björk, J.R.; O'Hara, R.B.; Ribes, M.; Coma, R.; Montoya, J.M. The dynamic core microbiome: Structure, stability and resistance. *bioRxiv* **2017**, 137885. [CrossRef]
17. Goodwin, C.E.; Rodolfo-Metalpa, R.; Picton, B.; Hall-Spencer, J.M. Effects of ocean acidification on sponge communities. *Mar. Ecol.* **2013**, *35*, 41–49. [CrossRef]
18. Altschul, S.F.; Gish, W.; Miller, W.; Myers, E.W.; Lipman, D.J. Basic local alignment search tool. *J. Mol. Biol.* **1990**, *215*, 403–410. [CrossRef]
19. Brady, C.L.; Cleenwerck, I.; Venter, S.; Vancanneyt, M.; Swings, J.; Coutinho, T.A. Phylogeny and identification of Pantoea species associated with plants, humans and the natural environment based on multilocus sequence analysis (MLSA). *Syst. Appl. Microbiol.* **2008**, *31*, 447–460. [CrossRef] [PubMed]
20. Brady, C.L.; Cleenwerck, I.; Venter, S.N.; Engelbeen, K.; De Vos, P.; Coutinho, T.A. Emended description of the genus Pantoea, description of four species from human clinical samples, *Pantoea septica* sp. nov., *Pantoea eucrina* sp. nov., *Pantoea brenneri* sp. nov. and *Pantoea conspicua* sp. nov., and transfer of *Pectobacterium cypripedii* (Hori 1911) Brenner et al. 1973 emend. Hauben et al. 1998 to the genus as *Pantoea cypripedii* comb. nov. *Int. J. Syst. Evol. Microbiol.* **2010**, *60*, 2430–2440. [CrossRef]
21. Tindall, B.J. The combination *Enterobacter agglomerans* is to be cited as *Enterobacter agglomerans* (Beijerinck 1888) Ewing and Fife 1972 and the combination *Pantoea agglomerans* is to be cited as *Pantoea agglomerans* (Beijerinck 1888) Gavini et al. 1989. Opinion 90. Judicial Commission of the International Committee on Systematics of Prokaryotes. *Int. J. Syst. Evol. Microbiol.* **2014**, *64*, 3582–3583. [CrossRef]
22. Brady, S.F.; Wright, S.A.; Lee, J.C.; Sutton, A.E.; Zumoff, C.H.; Wodzinski, R.S.; Beer, S.V.; Clardy, J. Pantocin B, an antibiotic from Erwinia herbicola discovered by heterologous expression of cloned genes. *J. Am. Chem. Soc.* **1999**, *121*, 11912–11913. [CrossRef]
23. Silvi, S.; Barghini, P.; Aquilanti, A.; Juárez-Jiménez, B.; Fenice, M. Physiologic and metabolic characterization of a new marine isolate (BM39) of *Pantoea* sp. producing high levels of exopolysaccharide. *Microb. Cell Factories* **2013**, *12*, 10. [CrossRef] [PubMed]
24. Romano, S.; Jackson, S.A.; Patry, S.; Dobson, A.D. Extending the "One Strain Many Compounds" (OSMAC) Principle to Marine Microorganisms. *Mar. Drugs* **2018**, *16*, 244. [CrossRef] [PubMed]

25. Pluskal, T.; Castillo, S.; Villar-Briones, A.; Orešič, M. MZmine 2: Modular framework for processing, visualizing, and analyzing mass spectrometry-based molecular profile data. *BMC Bioinform.* **2010**, *11*, 395. [CrossRef] [PubMed]
26. Nothias, L.-F.; Petras, D.; Schmid, R.; Dührkop, K.; Rainer, J.; Sarvepalli, A.; Protsyuk, I.; Ernst, M.; Tsugawa, H.; Fleischauer, M.; et al. Feature-based molecular networking in the GNPS analysis environment. *Nat. Methods* **2020**, 1–4. [CrossRef]
27. Shannon, P.; Markiel, A.; Ozier, O.; Baliga, N.S.; Wang, J.T.; Ramage, D.; Amin, N.; Schwikowski, B.; Ideker, T. Cytoscape: A Software Environment for Integrated Models of Biomolecular Interaction Networks. *Genome Res.* **2003**, *13*, 2498–2504. [CrossRef]
28. Pathak, K.V.; Bose, A.; Keharia, H. Characterization of Novel Lipopeptides Produced by Bacillus tequilensis P15 Using Liquid Chromatography Coupled Electron Spray Ionization Tandem Mass Spectrometry (LC–ESI–MS/MS). *Int. J. Pept. Res. Ther.* **2013**, *20*, 133–143. [CrossRef]
29. Bartal, A.; Vigneshwari, A.; Bóka, B.; Vörös, M.; Takacs, I.; Kredics, L.; Manczinger, L.; Varga, M.; Vágvölgyi, C.; Szekeres, A. Effects of Different Cultivation Parameters on the Production of Surfactin Variants by a Bacillus subtilis Strain. *Molecules* **2018**, *23*, 2675. [CrossRef]
30. Kecskeméti, A.; Bartal, A.; Bóka, B.; Kredics, L.; Manczinger, L.; Kadaikunnan, S.; Alharby, N.S.; Khaled, J.M.; Varga, M.; Vágvölgyi, C.; et al. High-Frequency Occurrence of Surfactin Monomethyl Isoforms in the Ferment Broth of a Bacillus subtilis Strain Revealed by Ion Trap Mass Spectrometry. *Molecules* **2018**, *23*, 2224. [CrossRef]
31. Peela, S.; Raju, K.B.; Ramana, T. Studies on a new marine streptomycete BT-408 producing polyketide antibiotic SBR-22 effective against methicillin resistant Staphylococcus aureus. *Microbiol. Res.* **2005**, *160*, 119–126. [CrossRef]
32. Preetha, R.; Jayaprakash, N.; Philip, R.; Singh, I.S.B. Optimization of carbon and nitrogen sources and growth factors for the production of an aquaculture probiotic (Pseudomonas MCCB 103) using response surface methodology. *J. Appl. Microbiol.* **2006**, *102*, 1043–1051. [CrossRef] [PubMed]
33. Poblete-Castro, I.; Wittmann, C.; Nikel, P.I. Biochemistry, genetics and biotechnology of glycerol utilization in Pseudomonas species. *Microb. Biotechnol.* **2020**, *13*, 32–53. [CrossRef]
34. Zhou, D.; Hu, F.; Lin, J.; Wang, W.; Li, S. Genome and transcriptome analysis of Bacillus velezensis BS-37, an efficient surfactin producer from glycerol, in response to D-/L-leucine. *MicrobiologyOpen* **2019**, *8*, e00794. [CrossRef]
35. Bus, J.; Sies, I.; Jie, M.S.L.K. 13C-NMR of methyl, methylene and carbonyl carbon atoms of methyl alkenoates and alkynoates. *Chem. Phys. Lipids* **1976**, *17*, 501–518. [CrossRef]
36. Guo, H.; Rischer, M.; Sperfeld, M.; Weigel, C.; Menzel, K.D.; Clardy, J.; Beemelmanns, C. Natural products and morphogenic activity of γ-Proteobacteria associated with the marine hydroid polyp Hydractinia echinata. *Bioorganic Med. Chem.* **2017**, *25*, 6088–6097. [CrossRef] [PubMed]
37. Effenberger, K.A.; James, R.C.; Urabe, V.K.; Dickey, B.J.; Linington, R.G.; Jurica, M. The Natural Product N-Palmitoyl-l-leucine Selectively Inhibits Late Assembly of Human Spliceosomes. *J. Biol. Chem.* **2015**, *290*, 27524–27531. [CrossRef]
38. McKellar, R.; Paquet, A.; Ma, C.-Y. Antimicrobial activity of fatty N-acylamino acids against Gram-positive foodborne pathogens. *Food Microbiol.* **1992**, *9*, 67–76. [CrossRef]
39. CLSI. *Methods for Dilution Antimicrobial Susceptibility Tests for Bacteria That Grow Aerobically: Approved Standard*, 10th ed.; Clinical and Laboratory Standards Institute: Wayne, PA, USA, 2015; Volume 35.
40. Kumar, S.; Stecher, G.; Li, M.; Knyaz, C.; Tamura, K. MEGA X: Molecular Evolutionary Genetics Analysis across Computing Platforms. *Mol. Biol. Evol.* **2018**, *35*, 1547–1549. [CrossRef]
41. Saitou, N.; Nei, M. The neighbor-joining method: A new method for reconstructing phylogenetic trees. *Mol. Biol. Evol.* **1987**, *4*, 406–425. [CrossRef]
42. Kimura, M. A simple method for estimating evolutionary rates of base substitutions through comparative studies of nucleotide sequences. *J. Mol. Evol.* **1980**, *16*, 111–120. [CrossRef] [PubMed]
43. Connolly, P.; Bloomfield, S.F.; Denyer, S. The use of impedance for preservative efficacy testing of pharmaceuticals and cosmetic products. *J. Appl. Bacteriol.* **1994**, *76*, 68–74. [CrossRef] [PubMed]

44. Werbrouck, H.; Vermeulen, A.; Van Coillie, E.; Messens, W.; Herman, L.; Devlieghere, F.; Uyttendaele, M. Influence of acid stress on survival, expression of virulence genes and invasion capacity into Caco-2 cells of Listeria monocytogenes strains of different origins. *Int. J. Food Microbiol.* **2009**, *134*, 140–146. [CrossRef] [PubMed]
45. Christensen, G.D.; Bisno, A.L.; Parisi, J.T.; McLaughlin, B.; Hester, M.G.; Luther, R.W. Nosocomial Septicemia Due to Multiply Antibiotic-Resistant Staphylococcus epidermidis. *Ann. Intern. Med.* **1982**, *96*, 1. [CrossRef]
46. Corvec, S.; Poirel, L.; Naas, T.; Drugeon, H.; Nordmann, P. Genetics and Expression of the Carbapenem-Hydrolyzing Oxacillinase Gene blaOXA-23 in *Acinetobacter baumannii*. *Antimicrob. Agents Chemother.* **2007**, *51*, 1530–1533. [CrossRef]
47. Zhang, L.; Li, X.-Z.; Poole, K. Fluoroquinolone susceptibilities of efflux-mediated multidrug-resistant *Pseudomonas aeruginosa*, *Stenotrophomonas maltophilia* and *Burkholderia cepacia*. *J. Antimicrob. Chemother.* **2001**, *48*, 549–552. [CrossRef]
48. Brady, S.F.; Clardy, J. Long-ChainN-Acyl Amino Acid Antibiotics Isolated from Heterologously Expressed Environmental DNA. *J. Am. Chem. Soc.* **2000**, *122*, 12903–12904. [CrossRef]
49. Pohnert, G.; Jung, V.; Haukioja, E.; Lempa, K.; Boland, W. New fatty acid amides from regurgitant of Lepidopteran (Noctuidae, Geometridae) caterpillars. *Tetrahedron* **1999**, *55*, 11275–11280. [CrossRef]

PLOS ONE

RESEARCH ARTICLE

Ocean acidification influences plant-animal interactions: The effect of *Cocconeis scutellum parva* on the sex reversal of *Hippolyte inermis*

Mirko Mutalipassi*, Valerio Mazzella, Valerio Zupo

Integrated Ecology Department, Benthic Ecology Centre, Stazione Zoologica Anton Dohrn, Ischia, Italy

* Mirko.mutalipassi@gmail.com

Citation: Mutalipassi M, Mazzella V, Zupo V (2019) Ocean acidification influences plant-animal interactions: The effect of *Cocconeis scutellum parva* on the sex reversal of *Hippolyte inermis*. PLoS ONE 14(6): e0218238. https://doi.org/10.1371/journal.pone.0218238

Editor: Gustavo M. Martins, Universidade dos Acores, PORTUGAL

Received: July 4, 2018

Accepted: May 30, 2019

Published: June 26, 2019

Data Availability Statement: All relevant data are within the paper and its Supporting Information files.

Funding: M. Mutalipassi conducted these researches within the project EXCITE funded by the Italian Ministry of Foreign Affairs within Italy-Israel cooperation activities. The funder had no role in study design, data collection and analysis, decision to publish, or preparation of the manuscript.

Competing interests: The authors have declared that no competing interests exist.

Abstract

Ocean acidification (O.A.) influences the ecology of oceans and it may impact plant-animal interactions at various levels. Seagrass meadows located at acidified vents in the Bay of Naples (Italy) are considered an open window to forecast the effects of global-changes on aquatic communities. Epiphytic diatoms of the genus *Cocconeis* are abundant in seagrass meadows, including acidified environments, where they play key ecological roles. A still-unknown apoptogenic compound produced by *Cocconeis* triggers the suicide of the androgenic gland of *Hippolyte inermis* Leach 1816, a protandric hermaphroditic shrimp distributed in *P. oceanica* meadows located both at normal pH and in acidified vents. Feeding on *Cocconeis sp*. was proven important for the stability of the shrimp's natural populations. Since O.A. affects the physiology of diatoms, we investigated if, in future scenarios of O.A., *Cocconeis scutellum parva* will still produce an effect on shrimp's physiology. Cell densities of *Cocconeis scutellum parva* cultivated in custom-designed photobioreactors at two pH conditions (pH 7.7 and 8.2) were compared. In addition, we determined the effects of the ingestion of diatoms on the process of sex reversal of *H. inermis* and we calculated the % female on the total of mature individuals^{-1} (F/mat). We observed significant differences in cell densities of *C. scutellum parva* at the two pH conditions. In fact, the highest cell densities (148,808 ±13,935 cells. mm^{-2}) was obtained at day 13 (pH 7.7) and it is higher than the highest cell densities (38,066 (±4,166) cells. mm^{-2}, day 13) produced at pH 8.2. Diatoms cultured at acidified conditions changed their metabolism. In fact, diatoms grown in acidified conditions produced in *H. inermis* a proportion of females (F/mat 36.3 ±5.9%) significantly lower than diatoms produced at normal pH (68.5 ±2.8), and it was not significantly different from that elicited by negative controls (31.7 ±5.6%).

Introduction

Hippolyte inermis Leach is a shrimp mainly inhabiting meadows of *Posidonia oceanica* [1] and in other seagrasses [2]. *Hippolyte inermis* is a key component of their food webs, as a link between primary producers, fishes and other carnivores [3]. The shrimp naturally undergoes a process of protandric sex reversal [4,5].

However, it was demonstrated the presence of two distinct reproductive periods, in spring and in fall. The offspring born during the fall period are characterised by males that undergo sex reversal after the next spring recruitment period, producing "alpha" females [6]. On the

contrary, the spring period is characterised by offspring consisting of directly developing males and females. The presence of spring early-developed females ("beta" females) contributes to the fall reproductive burst and these "beta" females exhibits the maximum abundance in association with blooms of epiphytic diatoms [7]. The early-developed females demonstrated a peculiar dietetic pattern: in spring, gut contents of "beta" females are dominated by benthic diatoms, among which *Cocconeis* spp. are particularly abundant. In contrast, males and "alpha" females are generalist grazers feeding on common epiphytes of *P. oceanica* leaves such as micro and macroalgae, bryozoans and foraminiferids [3]. It has been demonstrated that a) the ingestion of *Cocconeis* diatoms influences in a narrow time window the physiology of *H. inermis* [8]; b) the production of "beta females" is triggered by a still unknown lipophilic compound produced by diatoms after wounding and c) the compound has a highly selective apoptogenic power targeted on the shrimp's androgenic glands (A.G.) [9]. The destruction of the A.G. in males of *H. inermis* by apoptosis represents a stabilizing factor for natural populations [7] by triggering an increase of ovigerous females during the fall reproductive season.

Various diatoms dramatically change their productivity and growth dynamics, as well as the composition and concentration of secondary metabolites, in different culture conditions, influenced by light irradiance [10,11], presence of pollutants [12], nutrient limitations [13] and light spectrum [14,15].

Ocean acidification affects the ecology of oceans and the physiology of marine organisms and various direct and indirect effects on the marine biota are forecasted. Concentration of CO_2 in oceans increased in the last decades due to anthropogenic emissions [16] and a decrease in 0.43 pH units is forecasted to occur over the next century [17]. Thus, the chemistry of oceans and consequently various biological processes will be deeply affected by increasing concentrations of atmospheric carbon dioxide. O.A. combined with such factors as eutrophication and temperature rising, may cause a significant decrease in the abundance and diversity of calcareous algae [18]. Indeed, O.A. may have a deep effects on plant-animal interactions, algal growth, calcification rates of various algae [19,20] as well as other physiological processes such as nutrient uptake [18], and metabolisms [21–24]. In addition, algae living in acidified environments may modify their patterns of production of secondary metabolites which, in turn, may impact marine food webs. In the "Castello" vents off the island of Ischia (Bay of Naples, Italy), considered as a natural laboratory to simulate future O.A. scenarios, previous researchers identified more than 22 diatom genera in the epiphytic community on *P. oceanica* leaves among which *Cocconeis* spp. were numerically the dominant ones [25].

Aims

This study aimed at investigating how O.A. can affect the cell density of *Cocconeis scutellum parva* benthic diatoms simulating the present status (pH 8.2) and a hypothetical future condition (pH 7.7). Since the shrimp *H. inermis* is the only known "biological sensor" that is able to track the presence of the active apoptogenic compound produced by the diatom, the effects of *Cocconeis* spp. cultivated at the two pH scenarios on shrimps' post-larvae diet was examined to test its potential effect on plant-animal interactions. To compare the effects of *C. scutellum parva*, *C. scutellum posidoniae*, a strictly related variety that has been proved to be able to produce apoptogenic metabolite [26], was also tested as positive control.

Materials and methods

Stock cultures and inoculation process

Two *Cocconeis spp*. were taken into consideration, *i.e*., *C. scutellum parva and C. scutellum posidoniae*. All the diatoms used in this investigation belong to our stock culture that were

collected in 2014 in Lacco Ameno, Ischia, Italy. Each species was cultured in continuous axenic conditions in 6 mL multi-wells containing 4 mL of Guillard's *f*/2 medium with silica (Sigma-Aldrich, Milan, Italy). Cultures were kept under controlled conditions in a thermostatic chamber at 18˚C with 12:12 light:dark photoperiod. Light was provided by Sylvania GroLux (Osram Sylvania Inc., USA) at an irradiance of 140 μE. m^{-2}. s^{-1}.

At the 16th day of grow-out, the surface of the multi-wells was almost completely covered by diatoms and cells were scraped and collected by a Pasteur pipette, then pooled in a sterilized beaker; the suspension was divided and transferred into 10 Petri dishes (diameter 7 cm) filled with 50 mL of *f*/2 medium. At the end of the next grow-out phase (16 days), diatoms were collected by gently scraping off (with the aid of a Pasteur pipette) the bottom of the culture vessels. Diatoms were pooled again in a sterilized beaker and the suspension was partitioned into three photobioreactors filled with 2 litres of *f*/2 medium each. Given the adhesive properties of *Cocconeis* spp., only part of diatoms inoculated in each photobioreactor survived each grow-out phase; for this reason, the diatom concentration in the suspension was not determined at the moment of the inoculation [15].

Seawater carbonate chemistry

Samples of culture medium (50 mL of volume) were collected from each replicate each 3 days to perform analysis of the seawater carbonate chemistry. Salinity was measured with a HI-96822 refractometer for seawater (Hanna Instruments, Woonsocket, Rhode Island, United States). Total alkalinity (TA) and pH (NBS scale; pH_{NBS}) was determined using the total Alkalinity mini titrator for water analysis HI-84531-02. Three points electrode calibration (pH 4.01, 7.01 and 8.30 at 25˚C) and pump calibration (using a HI 84531–55 calibration standard) were performed before each set of titrations to assure high accuracy. Working temperature (18˚C) was automatically adjusted by the instrument using the automatic temperature compensation feature. Samples were analysed immediately after obtained from replicate photobioreactors carefully avoiding the formation of any air bubble in the instrument that could alter the measurement.

Seawater partial pressure of CO_2 analyses were performed using the CO_2Sys EXCEL Macro [27–29] from pH_{NBS}, TA, temperature, and salinity data. Carbonic acid dissociation constants (i.e., pK_1 and pK_2, [30]), ion HSO_4 constant [31] and borate dissociation constant [32] were used for the computation.

Photobioreactors

Special photobioreactors adapted for benthic diatoms were *ad-hoc* designed to perform at normal and acidified conditions. Each photobioreactor was assembled using a Pyrex dish with a total volume of 2.4 L (300 mm x 200 mm x 40 mm; Fig 1).

The vessel was covered with a heat resistant glass plate, provided with a narrow opening at its centre, where a pH probe was housed (InLab Micro pH, Mettler Toledo). A secondary opening was placed sideways, where a plastic stripette was fixed. The InLab Micro probe is designed to work even in a reduced volume of water and up to a thickness of 3 mm. A pH controller (pH 201, Aqualight) was connected to the Inlab Micro Probe (via a BNC cable) by an electronic valve which was connected to a CO_2 regulator (CO_2 Energy, Ferplast). To avoid water stratification and the formation of any pH gradient along the photobioreactor, a centrifuge pump (Askoll Pure pump 300) was added. The centrifuge pump was temporized by a micro-controller (EnerGenie EG-PMS2-LAN) that cyclically activated the pump each 30 minutes (1 minute on, 29 minutes off). The pH, in both treatments (pH 8.2 and pH 7.7) was regulated by a pH controller that opened and closed the electronic valve, when necessary,

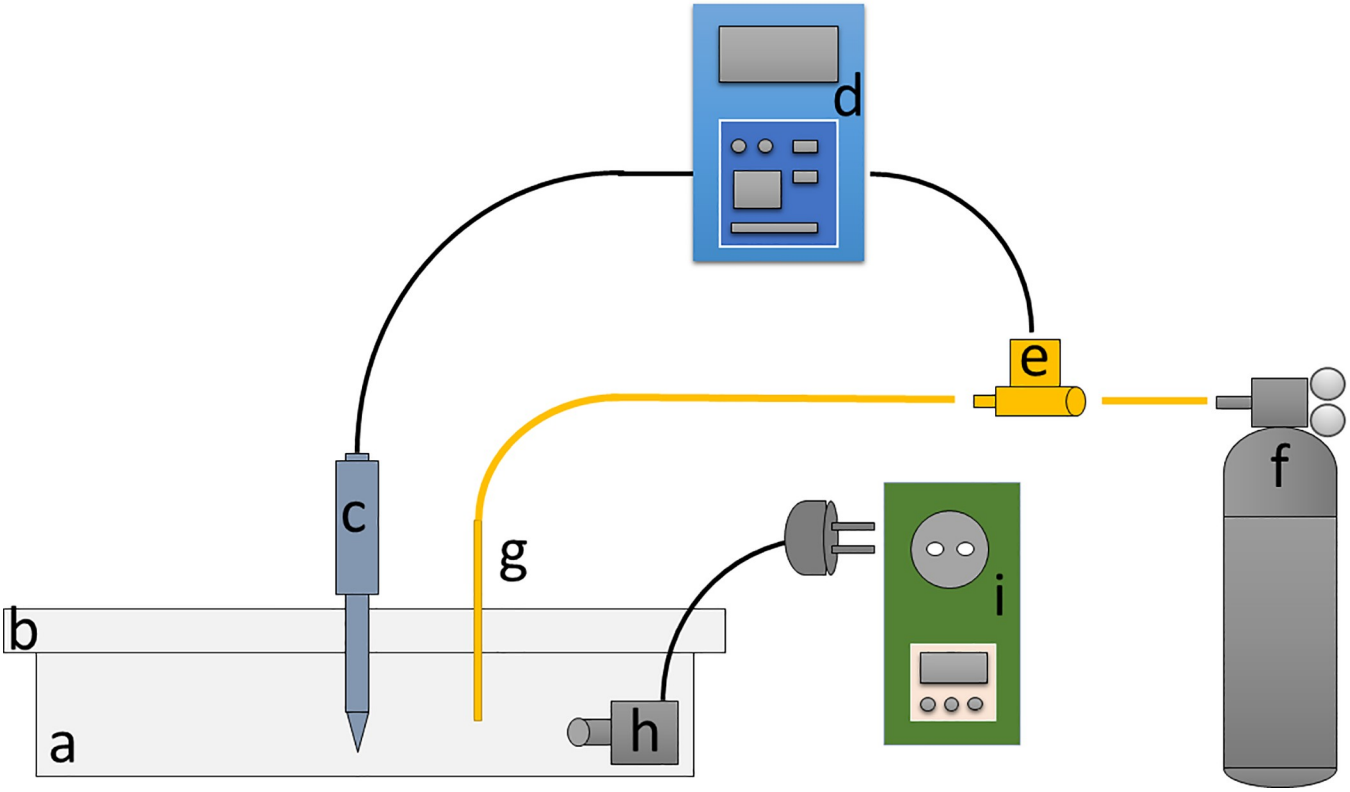

Fig 1. Photobioreactors devised to culture benthic algae at normal and acidified pH. Each reactor was constructed using a Pyrex dish (a) covered with a heat resistant glass plate (b). In the opening at the center of the cover was housed a pH probe (InLab Micro pH, Mettler Toledo; c). The pH probe was connected to a pH controller (pH 201, Aqualight; d) that controls an electronic valve (e). The electronic valve is connected, on one side, to the CO_2 regulator (CO_2 Energy, Ferplast; f), and on the other side to a plastic stripette (g), fixed in a secondary opening in the glass cover. A centrifuge pump (Askoll Pure pump 300; h) was placed on one side of the photobioreactor to avoid water stratification and was temporized by a microcontroller (EnerGenie EG-PMS2-LAN; i).

https://doi.org/10.1371/journal.pone.0218238.g001

dispensing the CO_2 through a plastic stripette into the photobioreactors. The pH of the medium was checked five times a day to guarantee that pH oscillations were lower than 0.05.

Photobioreactors were used to culture *C. scutellum parva* at pH 7.7 and 8.2. In addition, *C. scutellum posidoniae* was cultivated at normal pH (8.2). Three replicates were produced for each diatom and condition. The growth of diatoms into photobioreactors continued for 16 days. To estimate the number of cells. mm^{-2} into photobioreactors, 24 microscopy cover-slides (1 cm^2), glued to a nylon wire in order to facilitate the picking operations, were placed into each photobioreactor. In each cover-slide, 24 areas of 0.04 mm^2 were randomly selected and examined under the inverted microscope to record the number of cells grown. Every 3 days, 4 cover-slides per replica were collected and examined, and the average number of cells present per surface area was computed. Examined cover slides were trashed to avoid contamination in the culture photobioreactors. Average number of cells for each species of diatoms and standard deviations among replicates were also computed. Diatom transfers and collections were performed under a laminar flow hood and all dishes and culture instruments were previously sterilized at 120˚C. All the intact cells of benthic diatoms strongly adhere to the bottom of glass cups 24 hours after the inoculation.

After 16 days the medium in each photobioreactor was removed and the vessels were quickly rinsed with distilled water to remove residual salts. Emptied vessels containing a diatom film on their bottom were immediately frozen at -20˚C, then freeze-dried. Dry diatoms

were scraped off using an iron blade, then weighed and kept in dry vessels at −20˚C up to their use for bioassays on shrimps.

Bioassays on *Hippolyte inermis*

We followed the techniques described by Zupo and Messina [33] to tests the effects of diatoms on the target shrimp *Hippolyte inermis*. Ovigerous females of *H. inermis* were collected in a *Posidonia oceanica* meadow off Castello Aragonese (Island of Ischia, bay of Naples, Italy), sorted on boat and kept in plastic bags to be transferred to the laboratory. Ovigerous females were then transferred into 2 L conical flasks (2 ind. in each flask), containing 1.8 L of filtered seawater and small portions of *P. oceanica* leaves which were added to provide a shelter for shrimps. They were kept at 18˚C in a thermostatic chamber at a mean irradiance of 250 μmol m^{-2} s^{-1} with a photoperiod of 10:14 h light: dark. Once a sufficient number of larvae has been released by females and collected, the breeders have been returned to the sea.

Larvae produced were collected daily and transferred to 10 conical flasks containing 800 mL (total volume 1 litre) of filtered seawater (pH 8.2) in pools of 80 individuals. Larvae were fed with *Artemia salina* nauplii and *Brachionus plicatilis* (4 individuals per mL) for 7 days. *Artemia salina* nauplii were enriched daily with Algamac Biomarine (Hawthorne, CA, USA). Survival rates were recorded daily, by collecting larvae using a Pasteur pipette and transferring them into a fresh culture medium (filtered sea-water). Larvae already metamorphosed into post-larvae (in about 26 days) were randomly pooled and further divided in groups of 5 replicates of 25 post-larvae for each treatment. Post-larval culture vessels consisted of 14 cm diameters crystallizing dishes containing 400 mL of filtered seawater. Negative controls were fed with a base food composed of equal proportions of SHG "Artemia Enriched", SHG "Microperle" and SHG "Pure Spirulina" (produced by Super High Group, Ovada, Italy). Treatments were fed with dried cells of *C. scutellum parva* cultured at pH 7.7 or 8.2 added to the basic food in a ratio of 2:1 (w/w), according to treatments. Positive control replicates were fed with dried cells of *C. scutellum posidoniae* in addition of the base food with the same proportions used for the bioassays. Dry feeds were prepared and stored at -20˚C. Each post-larval replicate received daily a 5 mg ration of feed. Post-larvae medium (filtered sea-water) was daily replaced, the crystallizing dishes were washed and shrimps transferred. Post-larvae aged 40 days were sacrificed and fixed in 70% ethanol. Their total body length was measured using millimetric paper under a dissecting macroscope (Leica Z16 APO) and pleopods II were cut, mounted on a slide and observed under an optical microscopy (Leica DMLB) to determine their sex based on the presence/absence of a masculine appendix [34].

Statistical analyses

Average survival rates in larval cultures were evaluated and plotted by Prism 7 (Graph-Pad Software, La Jolla, USA). Diatom growth curves were computed according to the following equation:

$$Y = (Y_0 - a).e^{(-b.X)} + a$$

where:

"a" is the Y value at infinite times;

"Y_0" is Y value when X is zero;

"b" is the rate constant, expressed in reciprocal of the X axis time units;

Cell densities obtained for *C. scutellum parva* at the two pH conditions were compared by a paired t-test. Cell densities and pCO_2, at each replicate and time interval, were statistically compared in the two pH conditions. The time evolution of cell densities according to the

pCO_2 concentration was evaluated according to the equation:

$$Normalized\ cell\ densities = (Number\ of\ cells.mm^{-2}).pCO_2^{-1}$$

in order to relate the actual densities of diatoms to the abundance of carbon. The differences in the time evolution of cell densities in various pH conditions were analysed by a Spearman correlation analysis (Prism 7, Graph-Pad Software, La Jolla, USA).

The percentage of females normalized to the total number of mature individuals (% Female. mature individuals^{-1}) was computed. The % female. mature individuals^{-1} (F/mat) index permits to determine the effects of diatom on mature *H. inermis*, avoiding the bias due to immature individuals or shrimp with corroded pleopods due to bacterial infections.

The significance of differences among treatments and controls was tested by one-way analysis of variance (ANOVA), adopting the Tukey's multiple comparisons post-hoc test (Prism software) to the observed F/mat scores.

Results

Photobioreactors and diatom cultures

The photobioreactors here developed permitted to keep the pH of the medium constant during the whole experimental period, by adjusting the pCO_2 with small additions of gas immediately dissolved by the movements of the applied pumps (Table 1).

The maximum deviation of the pH from the values set on the control instrument was 0.05. At the end of the culture periods, we observed an average pH of 7.695 (±0.033), 8.19 (± 0.046) and 8.2 (±0.030) in *C. scutellum parva* cultures at pH 7.7, at pH 8.2 and in *C. scutellum posidoniae* cultures, respectively. The cell density at the beginning of the experiment (24 hours after inoculation) in replicates at pH 7.7 and 8.2 was 14,183 (±3,975) and 3,546 (±994) cells. mm^{-2}, respectively (Fig 2).

However, steady state was consistently reached within 10 days of incubation at both tested conditions. *Cocconeis scutellum parva*, cultured at two pH conditions (pH 7.7 and 8.2) produced significant differences in the cell density (t test; $P \leq 0.01$). The highest cell densities were recorded at pH 7.7, with 144,283 (±15,048) and 148,808 (±13,935) cells. mm^{-2} reached at

Table 1. Seawater carbonate chemistry variables (mean values ± standard deviation) in photobioreactors at the two pH conditions (pH 7.7 and 8.2).

Conditions	Day	pH_{NBS}		TA		pCO_2	
		Mean	SD	Mean	SD	Mean	SD
pH 8.2	1	7.702	±0.025	3,030.3	±5.5	1,812.2	±76.4
	4	7.701	±0.026	3,025.3	±6.4	1,814.4	±111.4
	7	7.691	±0.044	3,023.7	±12.1	1,837.8	±136.3
	10	7.683	±0.042	3,031.3	±4.6	1,862.1	±168.9
	13	7.703	±0.042	3,023.7	±6.7	1,815.2	±147.5
	16	7.691	±0.046	3,031.3	±6.4	1,843.7	±147.9
pH 7.7	1	8.175	±0.054	3,025.7	±8.1	530.2	±65.7
	4	8.209	±0.055	3,032.3	±7.2	491.1	±65.1
	7	8.208	±0.049	3,032.3	±3.8	488.3	±57.4
	10	8.196	±0.045	3,028.7	±5.0	501.6	±63.8
	13	8.175	±0.050	3,026.3	±7.5	520.9	±68.6
	16	8.177	±0.056	3,026.7	±9.6	524	±62.8

pH_{NBS} = measured pH (NBS scale); TA = total alkalinity; pCO_2 = CO_2 partial pressure.

https://doi.org/10.1371/journal.pone.0218238.t001

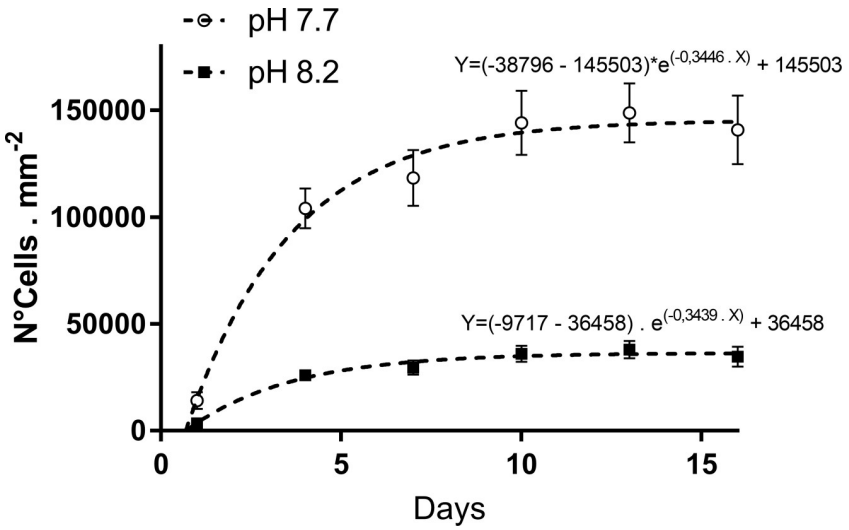

Fig 2. Growth curve of *Cocconeis scutellum parva* at pH 7.7 (white dots) and at pH 8.2 (black square) obtained over 16 days of culture. Error bars indicate the standard deviation among cell counts obtained in the same day in all replicates.

https://doi.org/10.1371/journal.pone.0218238.g002

the days 10 and 13, respectively. *Cocconeis scutellum parva* cultured at pH 8.2 produced, over the same period of time, cell densities of 36,070 (±3,762) and 38,066 (±4,166) cells. mm^{-2}, respectively. The pCO_2 significantly influenced the cell densities reached in each plate (Spearman test, $P \leq 0.1$, rs = 0.9429).

Bioassay

On average 81.8 (±19.3) larvae were produced by each of ten ovigerous females. During 24.5 (±1.08) days of larval growth, survival rate was 78.26% (±3.6; Fig 3).

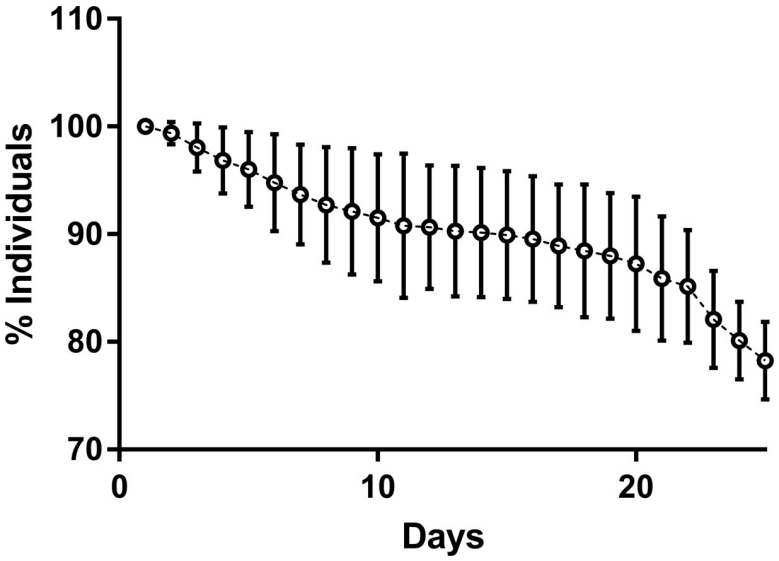

Fig 3. Percent survival rates of *Hippolyte inermis* cultured 26 days in conical flask (10 replicates). Dots indicate the average values and vertical bars their standard deviations.

https://doi.org/10.1371/journal.pone.0218238.g003

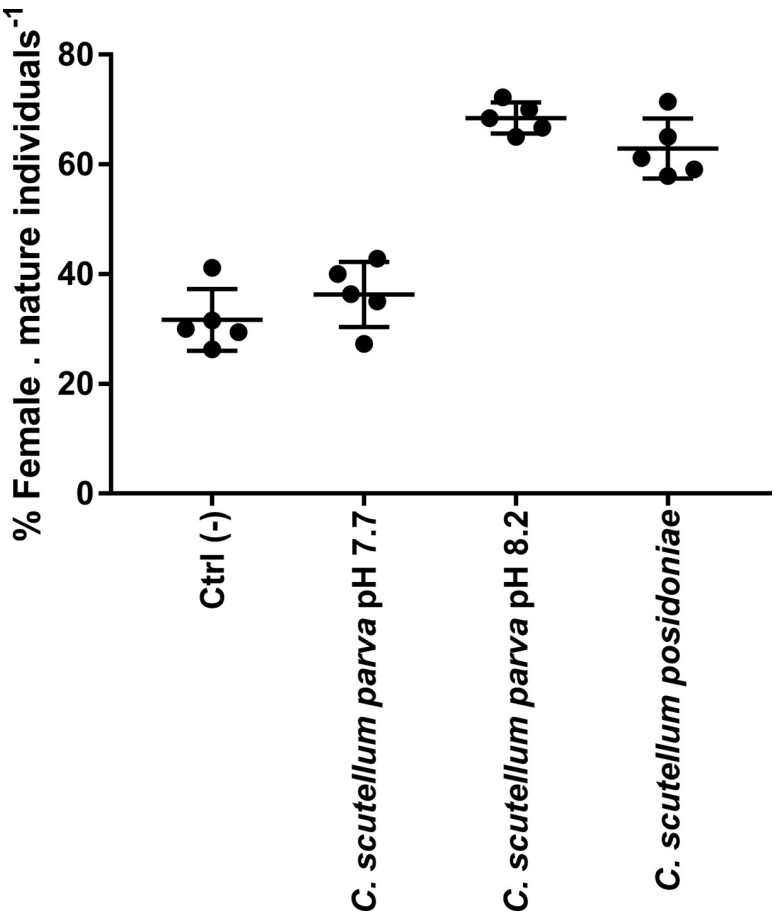

Fig 4. Female/Mature ratio obtained for each diet. Average values, standard deviations and the value of each replicate are reported.

https://doi.org/10.1371/journal.pone.0218238.g004

After 25 days of larval culture all the individuals settled and metamorphosed into post-larvae.

A survival rate of 80 (±4.9) %, a percentage of 6.4 (±4.6) % immature individuals and an average size of 7.63 (±0.65) mm were recorded in fixed shrimps, at the end of post-larval culture. Treatments fed on *C. scutellum parva* cultured in acidified conditions (pH 7.7) produced a survival rate of 87.2 (±7.7) %, a percentage of immatures of 7.2 (±5.9) % and an average size of 7.52 (±0.63) mm. In treatments fed on *C. scutellum parva* cultured at normal conditions (pH 8.2) a survival rate of 82.4 (±2.2) %, 4.0 (±4.0) % of immatures and an average size of 7.80 (±0.60) mm were recorded.

Treatments fed on *Cocconeis scutellum posidoniae* produced a survival rate of 86.4 (±5.4) %, a percentage of immature of 4.8 (±1.8) % and an average size of 7.75 (±0.63) mm. During the post-larvae phase, all individuals experiences the same culture conditions and they were cultured contemporaneously in the same thermostatic chamber.

The highest activity (highest ratio of sex reversed individuals, evaluated according to the presence/absence of *masculinae* appendices on shrimp's pleopods) was measured in replicates fed on *C. scutellum parva* cultured at normal conditions (pH 8.2), where a percentage of 68.5 (±2.8) % female. mature individuals^{-1} was recorded (Fig 4). Positive controls produced a high number of females with 63.4 F/mat ±2.8% in replicates fed on *C. scutellum posidoniae*. Replicates fed on *C. scutellum parva* cultured in acidified conditions (pH 7.7) as well as negative

controls, produced a low number of females (36.3 F/mat ±5.9% and 31.7 F/mat ±5.6% respectively) and significant differences among treatments were indicated by ANOVA ($P \leq 0.0001$; S1A Table). Notably, no differences in the percentage of F/mat were observed between negative controls and *C. scutellum parva* cultured at acidified conditions (Tukey's, $P \geq 0.05$; S1B Table) as well as between *C. scutellum parva* cultured at normal conditions and *C. scutellum posidoniae* (Tukey's, $P \geq 0.05$; S1B Table). In contrast, significant differences were found between *C. scutellum parva* cultured both at normal and acidified conditions and negative controls (Tukey's, $P \leq 0.0001$; S1B Table).

Discussion

Our results demonstrated that *Cocconeis scutellum parva* cultured at acidified conditions (pH 7.7) produced four times more cells than the same diatoms cultured at normal conditions (pH 8.2). The pCO_2 recorded at pH 7.7 is quite higher (about 4 times) then the one recorded at pH 8.2 and, similarly, the cell densities recorded at pH 7.7 are significantly higher (about 4 times) than the ones recorded at pH 8.2. In fact, the time trends of cell densities are significantly correlated to the pCO_2. Our results on the growth of *C. scutellum parva* in photobioreactors are in accordance with studies performed at Castello Aragonese meadows, where species populating the vent include a suite of organisms resilient to naturally high concentrations of pCO_2 and the massive presence of *Cocconeis sp*. may indicate that these species may have a competitive advantage under low pH conditions, in the field. The effect of CO_2 on the growth of diatoms is quite complex and, probably, depends on the particular physiology of each species. It has been shown that species can use different carbon sources, with some utilizing CO_2 as main carbon source, whereas others mostly drawing carbon from HCO_3^- [35]. Elevated CO_2 concentration did not cause significant differences in growth in diatoms such as *Asterionella glacialis*, *Thalassiosira punctigera*, *Coscinodiscus wailesii*, *Phaeodactylum tricornutum* [36–38]. In the case of *Chaetoceros gracilis*, the maximum number of cells was obtained at a carbon dioxide concentration of 385 μatm and a lower cell number was obtained at lower (control and 280 μatm) and higher levels of carbon dioxide (1,050 μatm) [35]. In other species, such as *Thalassiosira weissflogii*, algal density decreased with the decreasing pH [39] probably because, when the acidity is lower than a certain concentration, it will impair algal physiological functioning [40]. In contrast, previous studies [41] demonstrated an advantage of larger planktonic diatom species, more than 40 μm in diameter, over smaller-sized ones with an enhanced growth rate under elevated pCO_2 due to a combination of increased diffusion rates, a lowering of metabolic costs and a lower susceptibility to photo-inactivation of PSII.

Cocconeis spp., particularly abundant in the field at both normal and acidified areas of Castello Aragonese (Ischia, Naples, Italy), are a food source of *H. inermis* as demonstrated by the abundance of their thecae in its gut contents [42], especially in spring. Diatoms have been demonstrated to influence the ecology and the life cycle of other crustaceans [43–45] but in this species, according to co-evolutionary processes (triggering, in the shrimp, the development of beta females due to apoptotic disruption of the male gonadic buds;[42]), the toxic effect of diatoms are translated into their role as spring signals to set the reproductive cycle. Although it is known that acidification produces a change in the set of secondary metabolites produced by diatoms [22], here we demonstrated that the plant-animal relationship between *C. scutellum parva* and *H. inermis* is deeply affected by O.A. Although *H. inermis* is a polytrophic species [42], it strongly depends on *Cocconeis sp*. to keep the size of natural stocks constant. The development of beta females has been demonstrated to be a crucial factor in maintaining a constant sex ratio in this species, allowing for a fall large reproductive burst [6].

To obtain correct bioassays responses, the quality of shrimp larvae is of primary importance. For this reason, it is important to follow survival and growth, in larval and post-larval cultures of *H. inermis*, to evaluate their specific stress levels [46,47]. The reduction of stress factors, in studies on physiology of model organisms, should be taken into account to avoid bias in the reaching of actual sex ratios. Indeed, it was demonstrated that stress may influence sex ratios in protandric decapods [33,48,49]. Number of larvae produced by each female (81.8 ±19.3), low larval mortality and the duration of the larval period were in agreement to the health status of cultures in previous studies on *H. inermis* [7,8,50–52] and they may indicate absence of stress in cultured shrimps. A further demonstration of the low level of stress reached in larval and post-larval cultures was given by the low mortality, the size reached by most shrimps at the end of the feeding experiments and the low female/mature ratio observed in negative controls, as compared to previous studies [7,8,33].

Our bioassays confirmed the activity of *C. scutellum parva* compounds targeted the androgenic gland of *H. inermis* post-larvae [6–8,33,42]. It is worth observing that *Cocconeis scutellum parva* cultured in normal conditions (pH 8.2) was the most effective diatom with a 68.5 (±2.8) % females. mature individuals^{-1}. On the contrary, *Cocconeis scutellum parva* cultured in acidified conditions produced the lowest female/matures ratio, with no significant differences in comparison to negative controls.

In order to culture highly adhesive benthic diatoms, the use of photobioreactors is convenient due to low operational time and perfect repeatability of procedures and it permits an optimization of space in thermostatic chambers [15] avoiding time consuming procedures of cultures in Petri dishes [53]. Various custom-made photobioreactors were designed to mass culture planktonic [54–56] and low adhesive benthic microalgae [57–59] but a few of them are specific for high adhesive benthic diatoms and, at the same time, are capable of manipulating pH [60]. The photobioreactor here described was proven to be effective in manipulating the pH in microalgal cultures and, in addition, they demonstrated to be capable of culture slow-growing, highly adhesive, benthic diatoms in axenic conditions.

It has been demonstrated that *Posidonia oceanica* meadows growing in acidified conditions show altered epiphyte and vagile fauna communities [61], with a strong reduction in organisms bearing aragonite skeletons. The seasonal correlation of the life cycle of *H. inermis* with the patterns of abundance of epiphytic *Cocconeis sp*. in *Posidonia oceanica* meadows [6] will be modified by climate change. In the future, *H. inermis* is forecasted to still be able to find *Cocconeis* spp. in the field, as the dominant epiphyte in acidified meadows [62] but the plant-animal co-evolutionary relationship will be probably lost, due to changes in the secondary metabolites produced by the microalga. For this reason, *Hippolyte inermis* could miss, in future, the possibility to obtain crucial infochemicals (e.g., the still unidentified apoptogenic compound) fundamental to triggering the apoptosis of cells in the androgenic gland of these shrimps facilitating its sex reversal. In an acidified environment, the abundance of *Cocconeis* spp. increase but this correspond to a lack of some key metabolites which impacts *H. inermis* life cycle, modifying its peculiar sex ratio.

The present study demonstrates that, besides basic processes directly influencing the life and the production of marine organisms, more complex mechanisms will determine the future of marine associations in acidified oceans.

Supporting information

S1 Table. Statistical analyses on the bioassay on *H. inermis*. A) ONE-way ANOVA compared the percentage of female/mature individuals among treatments. B) Tukey's multiple

comparisons test among treatments.
(XLSX)

S2 Table. Minimal data sets.
(XLSX)

Acknowledgments

We thank Cpt. Rando for the collection of shrimps on board of the SV Phoenicia, of Stazione Zoologica. We thank Dr. Lucia Porzio for the taxonomical confirmation of the diatoms herein described and M. Lorenti of the Unit EMI for the analyses of pH in the cultures of diatom at normal and acidified conditions. M. Mutalipassi conducted these researches within the project EXCITE funded by the Italian Ministry of Foreign Affairs within Italy-Israel cooperation activities.

The authors would like to thank the referees for their valuable comments which helped to improve the manuscript.

All animal experiments were carried in accordance with the EU Directive 2010/63/EU and The Code of Ethics of the World Medical Association (Declaration of Helsinki) for animal experiments.

Author Contributions

Conceptualization: Mirko Mutalipassi, Valerio Zupo.

Formal analysis: Mirko Mutalipassi.

Investigation: Mirko Mutalipassi, Valerio Mazzella.

Methodology: Mirko Mutalipassi.

Supervision: Valerio Zupo.

Writing – original draft: Mirko Mutalipassi.

Writing – review & editing: Mirko Mutalipassi.

References

1. Gambi MC, Lorenti M, Russo GF, Scipione MB, Zupo V. Depth and seasonal distribution of some groups of the vagile fauna of the *Posidonia oceanica* leaf stratum: structural and trophic analyses. Mar Ecol. Wiley Online Library; 1992; 13: 17–39. https://doi.org/10.1111/j.1439-0485.1992.tb00337.x
2. Perez-Barros P, Tapella F, Romero MC, Calcagno JA, Lovrich GA. Benthic decapod crustaceans associated with captures of *Munida* spp. (Decapoda: Anomura) in the Beagle Channel, Argentina. Sci Mar. 2004; 68: 237–246. https://doi.org/10.3989/scimar.2004.68n2237
3. Zupo V, Fresi E. A study on the food web of the *Posidonia oceanica* (L.) Delile ecosystem: analysis of the gut contents of decapod crustaceans. Rapp Comm int Mer Médit. 1985; 29: 189–192.
4. Yaldwyn JC. Protandrous hermaphroditism in decapod prawns of the families Hippolytidae and Campylonotidae. Nature. 1966; 209: 1366. https://doi.org/10.1038/2091366a0
5. Veillet A, Dax J, Vouax A. Inversion sexuelle et parasitisme par *Bophyrina virbii* (Walz) chez la crevette *Hippolyte inermis* (Leach). C R Acad Sci Paris. 1963; 256: 790–791.
6. Zupo V. Strategies of sexual inversion in *Hippolyte inermis* Leach (Crustacea, Decapoda) from a Mediterranean seagrass meadow. J Exp Mar Bio Ecol. Elsevier; 1994; 178: 131–145. https://doi.org/10.1016/0022-0981(94)90229-1
7. Zupo V. Effect of microalgal food on the sex reversal of *Hippolyte inermis* (Crustacea: Decapoda). Mar Ecol Prog Ser. Inter-Research; 2000; 201: 251–259. https://doi.org/10.3354/meps201251

8. Zupo V, Messina P, Carcaterra A, Aflalo E d., Sagi A. Experimental evidence of a sex reversal process in the shrimp *Hippolyte inermis*. Invertebr Reprod Dev. Taylor & Francis; 2008; 52: 93–100. https://doi.org/10.1080/07924259.2008.9652276
9. Maibam C, Fink P, Romano G, Buia MC, Gambi MC, Scipione MB, et al. Relevance of wound-activated compounds produced by diatoms as toxins and infochemicals for benthic invertebrates. Mar Biol. Springer; 2014; 161: 1639–1652. https://doi.org/10.1007/s00227-014-2448-0
10. Affan A, Karawita R, Jeon Y-J, Lee J-B. Growth characteristics and antioxydant properties of the benthic diatom *Navicula incerta* (Bacillariophyceae) from Jeju island, Korea. J Phycol. Wiley Online Library; 2007; 43: 823–832. https://doi.org/10.1111/j.1529-8817.2007.00367.x
11. Chundi L, Aimin L, Wen Y, Fujun M, Shaoyong C. Marine diatom *Thalassirosira weissflogii* nutrient drawdown and its physiological status variation challenged to zinc and cadmium exposure. Acta Oceanol Sin. 2007; 26: 51–61.
12. Eker-Develi E, Kideys AE, Tugrul S. Effect of nutrients on culture dynamics of marine phytoplankton. Aquat Sci. Springer; 2006; 68: 28–39. https://doi.org/10.1007/s00027-005-0810-5
13. Göksan T, Durmaz Y, Gökpinar Ş. Effects of light path lengths and initial culture density on the cultivation of *Chaetoceros muelleri* (Lemmermann, 1898). Aquaculture. Elsevier; 2003; 217: 431–436. https://doi.org/10.1016/S0044-8486(01)00854-7
14. Mouget JL, Rosa P, Vachoux C, Tremblin G. Enhancement of marennine production by blue light in the diatom *Haslea ostrearia*. J Appl Phycol. Springer; 2005; 17: 437–445. https://doi.org/10.1007/s10811-005-0561-7
15. Raniello R, Iannicelli MM, Nappo M, Avila C, Zupo V. Production of *Cocconeis neothumensis* (Bacillariophyceae) biomass in batch cultures and bioreactors for biotechnological applications: light and nutrient requirements. J Appl Phycol. Springer; 2007; 19: 383–391. https://doi.org/10.1007/s10811-006-9145-4
16. Diaz-Pulido G, Cornwall C, Gartrell P, Hurd C, Tran D V. Strategies of dissolved inorganic carbon use in macroalgae across a gradient of terrestrial influence: implications for the Great Barrier Reef in the context of ocean acidification. Coral Reefs. Springer; 2016; 35: 1327–1341. https://doi.org/10.1007/s00338-016-1481-5
17. Pachauri RK, Allen MR, Barros VR, Broome J, Cramer W, Christ R, et al. Climate change 2014: synthesis report. Contribution of Working Groups I, II and III to the fifth assessment report of the Intergovernmental Panel on Climate Change. IPCC; 2014. https://doi.org/10.1046/j.1365-2559.2002.1340a.x
18. Koch M, Bowes G, Ross C, Zhang XH. Climate change and ocean acidification effects on seagrasses and marine macroalgae. Glob Chang Biol. 2013; 19: 103–132. https://doi.org/10.1111/j.1365-2486.2012.02791.x PMID: 23504724
19. Bradassi F, Cumani F, Bressan G, Dupont S. Early reproductive stages in the crustose coralline alga *Phymatolithon lenormandii* are strongly affected by mild ocean acidification. Mar Biol. 2013; 160: 2261–2269. https://doi.org/10.1007/s00227-013-2260-2
20. Gao K, Zheng Y. Combined effects of ocean acidification and solar UV radiation on photosynthesis, growth, pigmentation and calcification of the coralline alga *Corallina sessilis* (Rhodophyta). Glob Chang Biol. Wiley Online Library; 2010; 16: 2388–2398. https://doi.org/10.1007/s10811-016-0840-5
21. Hurd CL, Hepburn CD, Currie KI, Raven JA, Hunter KA. Testing the effects of ocean acidification on algal metabolism: Considerations for experimental designs. J Phycol. 2009; 45: 1236–1251. https://doi.org/10.1111/j.1529-8817.2009.00768.x PMID: 27032579
22. Poore AGBB, Graba-Landry A, Favret M, Sheppard Brennand H, Byrne M, Dworjanyn SA, et al. Direct and indirect effects of ocean acidification and warming on a marine plant—herbivore interaction. Oecologia. Springer; 2013; 173: 1113–1124. https://doi.org/10.1007/s00442-013-2683-y PMID: 23673470
23. Porzio L, Garrard SL, Buia MC. The effect of ocean acidification on early algal colonization stages at natural CO_2 vents. Mar Biol. 2013; 160: 2247–2259. https://doi.org/10.1007/s00227-013-2251-3
24. Porzio L, Buia MC, Hall-Spencer JM. Effects of ocean acidification on macroalgal communities. J Exp Mar Bio Ecol. 2011; 400: 278–287. https://doi.org/10.1016/j.jembe.2011.02.011
25. Porzio L, Buia MC, de Stefano M. Epiphytic diatom community response to ocean acidification. XXII International Diatom Symposium. 2012. p. 205.
26. Maibam C. Wound-activated algal compounds: toxic, apoptogenic and behavioural effects on marine invertebrates. Thesis (PhD)—Open University.; 2012;
27. Pierrot D, Lewis E, Wallace DWR. MS Excel program developed for CO_2 system calculations. ORNL/CDIAC-105a. Carbon Dioxide Information Analysis Center, Oak Ridge National Laboratory, US Department of Energy, Oak Ridge, Tennessee. 2006.
28. Riebesell U, Fabry VJ, Hansson L, Gattuso J-P. Guide to best practices for ocean acidification research and data reporting. Office for Official Publications of the European Communities; 2011.

29. Gattuso JP, Lee K, Rost B, Schulz K. Approaches and tools to manipulate the carbonate chemistry. Publications Office of the European Union; 2010.

30. Millero FJ. Carbonate constants for estuarine waters. Mar Freshw Res. CSIRO; 2010; 61: 139–142.

31. Dickson AG. Standard potential of the reaction: AgCl (s)+ $12H_2$ (g) = Ag (s)+ HCl (aq), and and the standard acidity constant of the ion HSO4-. J Chem Thermodyn. Elsevier; 1990; 22: 113–127.

32. Lee K, Kim T-W, Byrne RH, Millero FJ, Feely RA, Liu Y-M. The universal ratio of boron to chlorinity for the North Pacific and North Atlantic oceans. Geochim Cosmochim Acta. Elsevier; 2010; 74: 1801–1811.

33. Zupo V, Messina P. How do dietary diatoms cause the sex reversal of the shrimp *Hippolyte inermis* Leach (Crustacea, Decapoda). Mar Biol. 2007; 151: 907–917. https://doi.org/10.1007/s00227-006-0524-9

34. Mutalipassi M, Maibam C, Zupo V. The sex change of the caridean shrimp *Hippolyte inermis* Leach: temporal development of the gonopore morphology. Zoomorphology. Springer Berlin Heidelberg; 2018; 137: 377–388. https://doi.org/10.1007/s00435-018-0405-z PMID: 30174371

35. Khairy HM, Shaltout NA, El-Naggar MF, El-Naggar NA. Impact of elevated CO_2 concentrations on the growth and ultrastructure of non-calcifying marine diatom (*Chaetoceros gracilis* F.Schütt). Egypt J Aquat Res. National Institute of Oceanography and Fisheries; 2014; 40: 243–250. https://doi.org/10.1016/j.ejar.2014.08.002

36. Burkhardt S, Riebesell U, Zondervan I. Effects of growth rate, CO_2 concentration, and cell size on the stable carbon isotope fractionation in marine phytoplankton. Geochim Cosmochim Acta. 1999; 63: 3729–3741. https://doi.org/10.1016/S0016-7037(99)00217-3

37. Li W, Gao K, Beardall J. Interactive effects of Ocean Acidification and nitrogen-limitation on the diatom *Phaeodactylum tricornutum*. PLoS One. 2012; 7: 1–8. https://doi.org/10.1371/journal.pone.0051590 PMID: 23236517

38. James RK, Hepburn CD, Cornwall CE, McGraw CM, Hurd CL. Growth response of an early successional assemblage of coralline algae and benthic diatoms to ocean acidification. Mar Biol. 2014; 161: 1687–1696. https://doi.org/10.1007/s00227-014-2453-3

39. Liu FJ, Li SX, Huang BQ, Zheng FY, Huang XG. Effect of excessive CO_2 on physiological functions in coastal diatom. Sci Rep. Nature Publishing Group; 2016; 6: 1–9. https://doi.org/10.1038/s41598-016-0001-8

40. Shi D, Xu Y, Morel FMM. Effects of the pH/pCO_2 control method on medium chemistry and phytoplankton growth. Biogeosciences. Copernicus GmbH; 2009; 6: 1199–1207.

41. Wu Y, Campbell DA, Irwin AJ, Suggett DJ, Finkel Z V. Ocean acidification enhances the growth rate of larger diatoms. Limnol Oceanogr. 2014; 59: 1027–1034. https://doi.org/10.4319/lo.2014.59.3.1027

42. Zupo V. Influence of diet on sex differentiation of *Hippolyte inermis* Leach (Decapoda: Natantia) in the field. Hydrobiologia. Springer; 2001; 449: 131–140. https://doi.org/10.1023/A:1017553422113

43. Buttino I, Miralto A, Ianora A, Romano G, Poulet SA. Water-soluble extracts of the diatom *Thalassiosira rotula* induce aberrations in embryonic tubulin organisation of the sea urchin *Paracentrotus lividus*. Mar Biol. 1999; 134: 147–154. https://doi.org/10.1007/s002270050533

44. Barreiro A, Carotenuto Y, Lamari N, Esposito F, D'Ippolito G, Fontana A, et al. Diatom induction of reproductive failure in copepods: the effect of PUAs versus non volatile oxylipins. J Exp Mar Bio Ecol. Elsevier B.V.; 2011; 401: 13–19. https://doi.org/10.1016/j.jembe.2011.03.007

45. Miralto A, Guglielmo L, Zagami G, Buttino I, Granata A, Ianora A. Inhibition of population growth in the copepods *Acartia clausi* and *Calanus helgolandicus* during diatom blooms. Mar Ecol Prog Ser. Inter-Research; 2003; 254: 253–268. https://doi.org/10.3354/meps254253

46. Calado R, Vitorino A, Reis A, Lopes Da Silva T, Dinis MT. Effect of different diets on larval production, quality and fatty acid profile of the marine ornamental shrimp *Lysmata amboinensis* (de Man, 1888), using wild larvae as a standard. Aquac Nutr. 2009; 15: 484–491. https://doi.org/10.1111/j.1365-2095.2008.00614.x

47. Racotta IS, Palacios E, Ibarra AM. Shrimp larval quality in relation to broodstock condition. Aquaculture. Elsevier; 2003; 227: 107–130.

48. Bauer BT. Simultaneous hermaphoditism in caridean shrimps: a unique and puzzling sexual system in the decapoda. J Crustac Biol. JSTOR; 2000; 2: 116–128.

49. Calado R, Figueiredo J, Rosa R, Nunes ML, Narciso L. Effects of temperature, density, and diet on development, survival, settlement synchronism, and fatty acid profile of the ornamental shrimp *Lysmata seticaudata*. Aquaculture. Elsevier; 2005; 245: 221–237. https://doi.org/10.1016/j.aquaculture.2004.11.034

50. Zupo V, Buttino I. Larval development of decapod crustaceans investigated by confocal microscopy: an application to *Hippolyte inermis* (Natantia). Mar Biol. Springer; 2001; 138: 965–973. https://doi.org/10.1007/s002270000523

51. Michèl R. Survey of the nutrition in *Hippolyte inermis* LEACH (Decapoda, Natantia) during its larval development in the laboratory. Int Rev der gesamten Hydrobiol und Hydrogr. Wiley-Blackwell; 2007; 54: 749–764. https://doi.org/10.1002/iroh.19690540506

52. Mutalipassi M, Di Natale M, Mazzella V, Zupo V. Automated culture of aquatic model organisms: Shrimp larvae husbandry for the needs of research and aquaculture. Animal. 2018; 12: 155–163. https://doi.org/10.1017/S1751731117000908 PMID: 28462769

53. Zupo V, Jüttner F, Maibam C, Butera E, Blom JF, Juttner F, et al. Apoptogenic metabolites in fractions of the benthic diatom *Cocconeis scutellum parva*. Mar Drugs. 2014; 12: 547–567. https://doi.org/10.3390/md12010547 PMID: 24451194

54. Ozkan A, Rorrer GL. Effects of CO_2 delivery on fatty acid and chitin nanofiber production during photobioreactor cultivation of the marine diatom *Cyclotella* sp. Algal Res. Elsevier; 2017; 26: 422–430. https://doi.org/10.1016/j.algal.2017.07.003

55. Beuzenberg V, Goodwin EO, Puddick J, Romanazzi D, Adams SL, Packer MA. Optimising conditions for growth and xanthophyll production in continuous culture of *Tisochrysis lutea* using photobioreactor arrays and central composite design experiments. New Zeal J Bot. Taylor & Francis; 2017; 55: 64–78. https://doi.org/10.1080/0028825X.2016.1238398

56. Yen H-W, Hu IC, Chen C-Y, Chang J-S. Design of photobioreactors for algal cultivation. Biofuels from Algae. 2014; 23–45. http://dx.doi.org/10.1016/B978-0-444-59558-4.00002-4

57. Lebeau T, Gaudin P, Moan R, Robert JM. A new photobioreactor for continuous marennin production with a marine diatom: Influence of the light intensity and the immobilised-cell matrix (alginate beads or agar layer). Appl Microbiol Biotechnol. 2002; 59: 153–159. https://doi.org/10.1007/s00253-002-0993-9 PMID: 12111140

58. Silva-Aciares FR, Riquelme CE. Comparisons of the growth of six diatom species between two configurations of photobioreactors. Aquac Eng. 2008; 38: 26–35. https://doi.org/10.1016/j.aquaeng.2007.10.005

59. Avendaño-Herrera RE, Riquelme CE. Production of a diatom-bacteria biofilm in a photobioreactor for aquaculture applications. Aquac Eng. 2007; 36: 97–104. https://doi.org/10.1016/j.aquaeng.2006.08.001

60. Granum E. A photobioreactor with pH control: demonstration by growth of the marine diatom *Skeletonema costatum*. J Plankton Res. 2002; 24: 557–563. https://doi.org/10.1093/plankt/24.6.557

61. Hall-Spencer JM, Rodolfo-Metalpa R, Martin S, Ransome E, Fine M, Turner SM, et al. Volcanic carbon dioxide vents show ecosystem effects of ocean acidification. Nature. Nature Publishing Group; 2008; 454: 96–99. https://doi.org/10.1038/nature07051 PMID: 18536730

62. Garrard SL, Gambi MC, Scipione MB, Patti FP, Lorenti M, Zupo V, et al. Indirect effects may buffer negative responses of seagrass invertebrate communities to ocean acidification. J Exp Mar Bio Ecol. Elsevier; 2014; 461: 31–38. https://doi.org/10.1016/j.jembe.2014.07.011

© 2019. Published by The Company of Biologists Ltd | Biology Open (2019) 8, bio043604. doi:10.1242/bio.043604

RESEARCH ARTICLE

Growth and toxicity of *Halomicronema metazoicum* (Cyanoprokaryota, Cyanophyta) at different conditions of light, salinity and temperature

Mirko Mutalipassi[1], Valerio Mazzella[2], Giovanna Romano[1], Nadia Ruocco[1], Maria Costantini[1], Francesca Glaviano[1] and Valerio Zupo[1,*]

ABSTRACT

Cyanobacteria may live in the water column and in the benthos of aquatic environments, or be symbionts of other organisms, as in the case of *Phormidium*-like cyanobacteria, known to influence the ecology of freshwater and marine ecosystems. A strain of *Phormidium*-like cyanobacteria has been recently isolated as a free-living epiphyte of leaves of *Posidonia oceanica* (L.) Delile in the Mediterranean sea and its biology and ecology are herein investigated. It was identified as *Halomicronema metazoicum*, previously known uniquely as a symbiont of marine sponges. We cultivated it in a range of light irradiances, temperatures and salinities, to establish the most suitable conditions for the production of allelopathic and toxic compounds. The bioactivity of its spent culture medium was measured by means of standard toxicity tests performed on two model organisms. Our results indicate that at least two bioactive compounds are produced, at low and high irradiance levels and at two temperatures. The main compounds influencing the survival of model organisms are produced at the highest temperature and high or intermediate irradiance levels. The present research contributes to the understanding of critical toxigenic relationships among cyanobacteria and invertebrates, possibly influencing the ecology of such a complex environment as *P. oceanica*. Future isolation, identification and production of bioactive compounds will permit their exploitation for biotechnologies in the field of ecological conservation and medical applications.

KEY WORDS: Cyanobacterium, Toxins, Environment, Sea urchin, Rotifers

INTRODUCTION

Photosynthetic cyanobacteria, also known as 'blue-green algae', are distributed worldwide in any photic and moist environment (Gaylarde et al., 2004), including marine waters, freshwaters, natural grounds and extreme environments (Dahms et al., 2006). These prokaryotes, living either as unicellular or colonial forms, exhibit a remarkable taxonomic diversity (Whitton, 1992; Usher et al., 2004) and an even more notable functional diversity (Barberousse et al., 2006). As a matter of fact, physiologic differences among strains may largely encompass the dissimilarities among species and genera (Pfeiffer and Palińska, 2002), and their noteworthy diversity also explains the importance as potential producers of novel bioactive substances with economic potential (Shimizu, 2003; Blunt et al., 2006). A long tradition of screening and separation of active biomolecules took advantage of the secondary metabolites produced by cyanobacteria to develop antifouling agents (Abarzua et al., 1999), antibiotics (Bloor and England, 1989), sunscreens (Böhm et al., 1995), antimycotics (Bonjouklian et al., 1991) and a plethora of useful applications (Burja et al., 2001). Such an abundance of uses is due to the variety of secondary metabolites synthesized, ranging from carotenoids and phycobiliprotein pigments – having commercial value as feed additives and colour enhancers for foods (Shimizu, 2003) – to toxic polysaccharides used as pesticides or in clinical applications (Kulik, 1995). Various cyanobacteria also produce vitamins of the B and E complexes (Plavšić et al., 2004) and they are exploited for large-scale productions in special photobioreactors.

Cyanobacteria also play key ecological roles (Pietsch et al., 2001) and exhibit a wide diffusion thanks to their aptitude to colonize any habitat, and produce active biomolecules reaching the environment by simple leaching from their mattes (Jüttner et al., 2001). Other secondary metabolites are wound-activated by grazers (Manivasagan et al., 2017). They were demonstrated to control the presence of other organisms in benthic environments (Borges et al., 2015), as well as in planktonic environments (Dias et al., 2017) and influence the quality of waters destined for human consumption (Jüttner et al., 2001), when diffused in freshwater basins.

However, cyanobacteria may be also symbiotically associated with animals and algae. For example, their association with demospongiae is quite frequent in the marine environment (Caroppo et al., 2012), as well as with corals and other invertebrates (Taylor et al., 2007). Recent findings indicate that a species of cyanobacteria, *Halomicronema metazoicum*, may be both a symbiont of marine sponge and a free-living organism associated to leaves of the seagrass *Posidonia oceanica* (Ruocco et al., 2019). The host sponge *Petrosia ficiformis* exhibited haemolytic activity and influenced brine shrimp vitality and sea urchin development (Pagliara and Caroppo, 2010, 2011) and these activities were supposed to be mediated by symbiotic cyanobacteria strains (Caroppo et al., 2012). These cyanobacteria were previously assigned to the genus *Phormidium* (Geitler 1932) according to the botanical code, and to the *Lyngbya/ Plectonema/ Phormidium*-group B (Rippka et al., 1979) according to the bacteriological system.

Cyanobacteria with *Phormidium*-like morphologies do not form a monophyletic group (Giovannoni et al., 1988), but their collective

[1]Marine Biotechnology Department, Stazione Zoologica Anton Dohrn, Villa Comunale, 80121, Napoli, Italy. [2]Integrative Marine Ecology Department, Benthic Ecology Centre, Stazione Zoologica Anton Dohrn, Punta San Pietro, 80077 Ischia, Italy.

*Author for correspondence (vzupo@szn.it)

V.Z., 0000-0001-9766-8784

Received 3 April 2019; Accepted 7 October 2019

Biology Open (2019) 8, bio043604. doi:10.1242/bio.043604

ability to produce toxic exudates is well known (Dias et al., 2017; Wood et al., 2017). The new species *H. metazoicum* was established to classify non-heterocystous, thin filamentous symbiotic cyanobacteria (Caroppo et al., 2012) and further studies (Ruocco et al., 2019) indicated that this species may also live as an epiphyte of *P. oceanica* leaves. Given the known complexity of interactions among plant and animal communities associated to seagrass leaves (Mazzella et al., 1991), and the ability of cyanobacteria to produce allopathic compounds (Dias et al., 2017; Devlin et al., 1977), their presence may likely influence life and evolution of various organisms.

Proliferations of benthic mat-forming *Phormidium* have been reported in various sites and they commonly produce a range of neurotoxins, collectively known as anatoxins, prompting risks to human and animal health (Dias et al., 2017). In addition, *Phormidium*-like cyanobacteria are known to produce a range of natural toxins including anatoxin-a, homoanatoxin-a, microcystins, portoamides and saxitoxins (Borges et al., 2015; Gugger et al., 2005; Teneva et al., 2005; Kouzminov et al., 2007). Since their presence may produce acute toxicity for animals and humans (Wood et al., 2017) and their natural blooms correspond to deadly conditions for various organisms in the same communities (Shurin and Dodson, 1997), there is rising awareness of the risks driven by *Phormidium* proliferations (Catherine et al., 2013; Echenique-Subiabre et al., 2016).

The production of toxic compounds is often modulated by salinity, light irradiance and temperature (Caroppo et al., 2012) and the aim of this study was to characterize the environmental conditions maximizing the production of allochemicals and toxins produced by *Phormidium*-like cyanobacteria (Dias et al., 2017). We also aim at defining sensible experimental tools to detect and measure their toxicity, to identify possible influences on organisms in the leaf stratum of Mediterranean seagrasses. Since previous tests revealed toxic compounds naturally released in the water by similar cyanobacteria (Dias et al., 2017), and preliminary research confirmed the toxicity of *H. metazoicum* on *Artemia salina* nauplii (Zupo et al., 2019), we investigated the toxicity of natural exudates in a range of environmental conditions. A strain of *H. metazoicum* isolated from *P. oceanica* leaves (Ruocco et al., 2019) has been cultivated in the laboratory in three conditions of light irradiance, temperature and salinity, and its natural harmfulness has been assayed on model organisms using standard toxicity tests (Dahms et al., 2011). Since the relevance of culturing cyanobacteria also derives from their ability to produce compounds for biotechnological applications (Moore et al., 1988; Gerçe et al., 2009), this investigation will improve our ability to maximise the production of bioactive metabolites (Sivonen and Börner, 2008; Raniello et al., 2007).

RESULTS

The strains of *H. metazoicum* isolated and cultured for the purposes of this study appeared clean of contaminants and shaped as dense mattes of non-heterocystous, thin filaments (Fig. 1), containing small aggregates of mucous exudates. The spent culture medium, after 40 d of growth, appeared brownish but transparent. Various culture conditions produced complex patterns of responses in *Brachionus plicatilis*, according to the time of exposure, temperature, irradiance and salinity. Negative controls (containing fresh *f/2* medium at the corresponding concentrations, as above specified) exhibited an almost constant number of individuals during the experiment and, after 24 h, the survivorships were still 94% (±7.21), while the survival rates accounted for 100% both 5 and 60 min after the start of the experiment. Overall, the time of exposure did not produce an evident effect among treatments (ANOVA, $P>0.05$). Only, in a few conditions (e.g. at salinity 40, irradiance 80 µE and temperature 22°C) there was a significant difference between the records obtained at 24 h and those obtained at 5 and 60 min ($P<0.01$). In addition, the records obtained at 5 and 60 min exhibited no significant differences between them, when analysed by Wilcoxon test and in most cases there was no effect on the survival rates compared with those of negative controls (survival close to 100%). For this reason it is useful to analyse the results obtained at 24 h, exhibiting the largest differences (Fig. 2). Survival rates at the highest irradiances decreased in most treatments in a dose-dependent manner, with higher slopes between the concentrations 1:100–1:10 and the highest mortalities recorded between 1:10−1:5 (Fig. 2D,G,H). The factors mainly influencing the differences in mortality rates were temperature and irradiance. Salinity produced significant differences (ANOVA, $P<0.01$) at 18°C and 22°C, especially at the lowest (Fig. 2F,I) and the highest (Fig. 2D,G) irradiance levels. The highest temperatures (Fig. 2G–I), salinities and irradiances (Fig. 2D,G) represent the conditions maximizing the production of toxic compounds. Low temperatures (Fig. 2A–C) and low irradiances (Fig. 2C,F,I) produced media having scarce or null toxigenic effects on *B. plicatilis*.

Fig. 1. Scanning Electron Microphoto of a sample of cyanobacteria showing a dense matte of non-heterocystous thin filaments. Some small vesicles of amorphous exudates are present on their surface.

In the case of sea urchin embryos, various development phases offered different results. Negative controls produced 99.0% (±0.4) of divided embryos, recorded 1 h after the *in vitro* fertilization of eggs. In contrast, in all treatments, regardless of salinity, temperature and irradiance (ANOVA, $P>0.05$) the concentration 1:1000 blocked the development at the first division (Fig. 3), while the effect of lower concentration was low or null.

The development of sea urchin embryos to gastrulae, passing through the stage of blastulae, offered a complex array of results (Fig. 4). Also in this case, a threshold was represented by the concentration 1:1000, blocking or retarding the development, while the concentrations 1:10,000 and 1:100,000 produced results not significantly different from those exhibited by negative controls. The effect of salinity on gastrulation was generally not significant, with a few differences in various treatments (e.g. Fig. 4E,H,I). As well, the patterns of development to normal plutei were complex, but confirmed the efficacy of the highest concentration (Fig. 5). In

Biology Open (2019) 8, bio043604. doi:10.1242/bio.043604

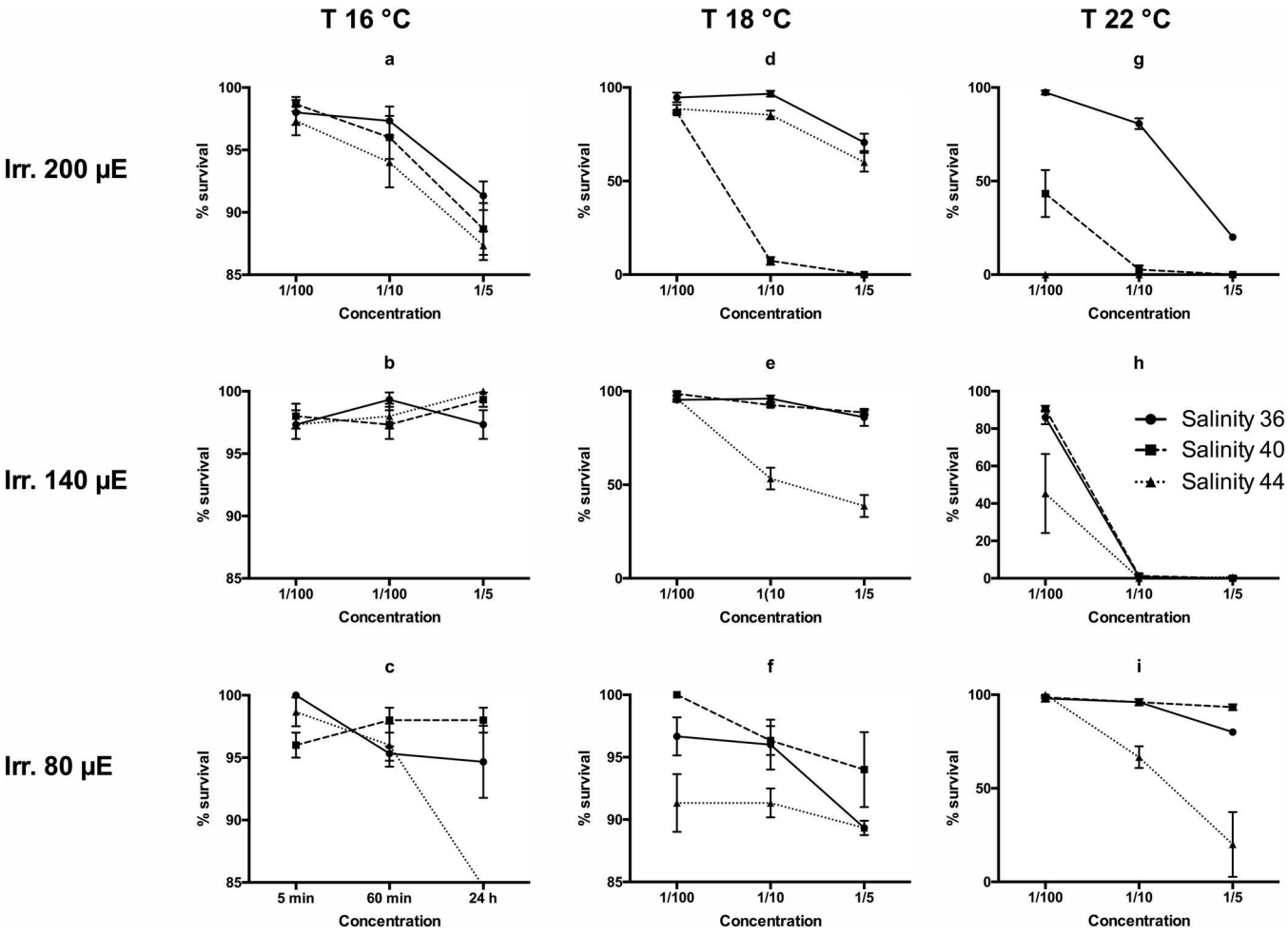

Fig. 2. Survival rates of *B. plicatilis* recorded after 24 h of exposure to three concentrations of the spent culture medium of *H. metazoicum*, cultivated at three temperatures, three irradiance levels and three salinities.

this case, the maximum efficacy was recorded at the lowest temperature (16°C) and the lowest irradiance, generating the lowest percentages of normal plutei (Fig. 5A–C,F). Salinity showed contrasting results at the highest temperature. The effective dose was consistently between 1:10,000 and 1:1000.

DISCUSSION

The grow-out of cyanobacteria was continuous in our experimental conditions (Ruocco et al., 2019) and the cultures were free of contaminants. The absence of other organisms was likely due to toxic compounds naturally produced by cyanobacteria (Dias et al., 2017), having an allopathic effect on bacteria, protozoans and algae (Snell and Carmona, 1995; Hughes et al., 1958). The same compounds were active on the rotifer (Preston and Snell, 2001) at a concentration comprised between 1:10 and 1:5. The effects were slightly increasing upon time but in most treatments they were evident after 24 h, indicating an acute toxicity clearly affecting the vitality and the survival of tested organisms. Trends of toxicity were consistent among treatments at various times and we chose to take into account the final readings at 24 h, to simplify the evaluation of the median lethal concentration (Dahms and Hellio, 2009).

The results of toxicology tests performed on rotifers were quite reproducible and the differences among replicates were generally low (Suga et al., 2007). However, the patterns of responses according to salinity were puzzling, if various irradiances and temperatures were compared. In general, the maximum efficacy was reached at intermediate irradiance (140 µE) and higher temperatures (18–22°C) and salinities (40–44). However, the highest salinity was consistently effective at lower (80 µE) irradiance while intermediate salinity (40) was effective mainly at the highest irradiance (200 µE). The production of toxic exudates was maximum at 22°C, 140–200 µE and salinity 44, producing total mortality at a concentration of 1:10. The temperature is a critical factor because the toxicity was lowest in cultures cultivated at 16°C. Interestingly, at the salinity characterizing most oceans (36 psu) the highest irradiance (200 µE) induced a decrease in the toxicity of cyanobacteria. However, the result of these acute toxicology tests measure the effects of given compounds in specific experimental conditions (Preston et al., 1999) and we cannot exclude that various families of bioactive compounds (Raniello et al., 2007), having different effects over longer times of exposure, are produced by the same strain.

For this reason it is useful to compare the results with those obtained in standard toxicology tests performed on sea urchin embryos (Romano et al., 2003). In this case, toxic compounds appear to affect selected phases of embryo development. The first division is strongly affected by the presence of cyanobacteria toxins at a concentration comprised between 1:100,000 and 1:10,000 with no reference to salinity, irradiance or temperature. In fact, all

Biology Open (2019) 8, bio043604. doi:10.1242/bio.043604

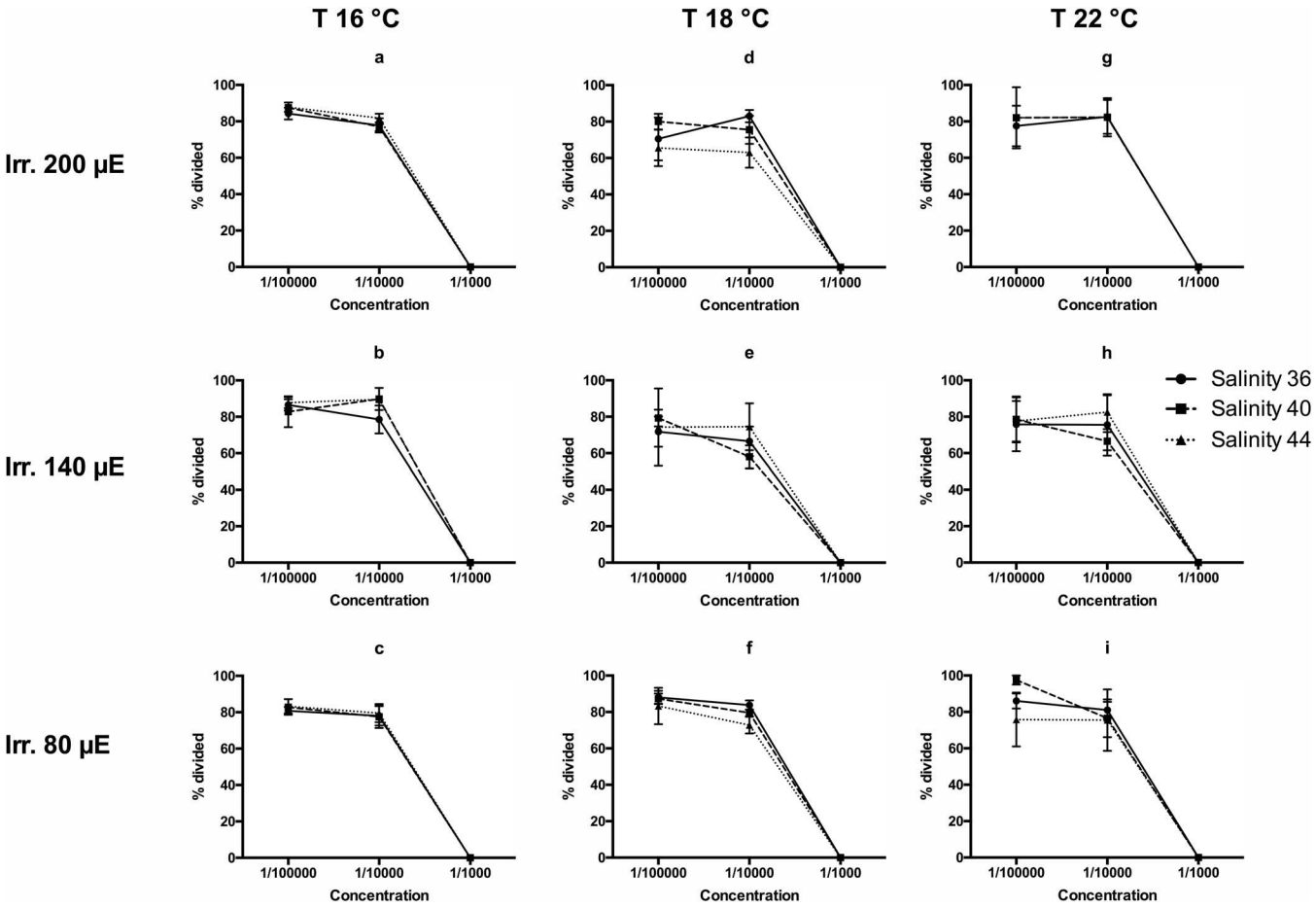

Fig. 3. Rates of first divisions of embryos of *P. lividus* recorded after 1 h of exposure to three concentrations of the spent culture medium of *H. metazoicum*, cultivated at three temperatures, three irradiance levels and three salinities.

experimental conditions produced high percentages of divided embryos at 1:100,000 and total block of embryo development at 1:10,000. A slight increase of toxicity was observed at the highest temperature (22°C) and the highest salinity (44), coherently to what observed in *B. plicatilis* tests, but the differences in this case are scarcely significant. Similar trends were observed in the influences on the gastrulation process, since the strongest effects were triggered by the media obtained at the highest temperature (22°C), especially when coupled with intermediate and highest salinities (40–44) and low or medium irradiances (80–140 µE). Thus, a different class of compounds could be responsible for this activity, or the changed metabolism of embryos in this phase could be influenced by different compounds, in the range of metabolites produced by cyanobacteria. The patterns were totally inverted when the development of plutei was considered. In this case, in fact, the lowest percentages of normal plutei were triggered by spent medium collected at the lowest temperature (16°C) regardless of irradiance and salinity. In contrast, the highest temperature (22°C) triggered similar effects only at the highest (44) or intermediate (40) salinity, in accordance with *B. plicatilis* bioassays. We conclude that the compounds influencing the development of larvae, mainly produced at lower temperatures, are different from those influencing the mortality of *B. plicatilis* and the development of the sea urchin until the gastrula stage, mainly produced at the highest temperatures and intermediate or low irradiances. In contrast, the first division of sea urchin embryos appears to be a delicate process, blocked at the same rate by compounds produced in any condition of light, temperature and salinity.

Interestingly, the median lethal concentration (Boudou and Ribeyre, 1989) of allopathic compounds produced at higher temperature (22°C), medium irradiance (140 µE) and medium-high salinities, was different in *B. plicatilis* and sea urchin embryos. The latter reacted at concentrations of the spent medium at least 2 orders of magnitude lower than those active on rotifers. A second class of compounds could be produced at low temperature (16°C) without distinction of irradiance and salinity, and it influenced the process of development of sea urchin plutei at very low concentrations, comprised between 1:100,000 and 1:10,000. These compounds produced at low-temperature influenced *B. plicatilis* at concentrations as high as 1:5, but we still ignore both their concentration in the spent medium and their chemical nature.

We must consider, however, that proteins and polypeptides (Zhang et al., 2011) are among the most important toxic compounds produced by cyanobacteria and it is known that changes in environmental conditions (e.g. salinity, pH and temperature), modify their structure and may cause the formation of cytotoxic protein aggregates, with the synthesis of 'stress' proteins (Gross, 2004). Portoamides, for example, are cyclic peptides having a clear allopathic activity and an antiproliferative effect on human lung-carcinoma cells (Ribeiro et al., 2017). They are among the most interesting compounds produced and released by *Phormidium*-like cyanobacteria. The

Biology Open (2019) 8, bio043604. doi:10.1242/bio.043604

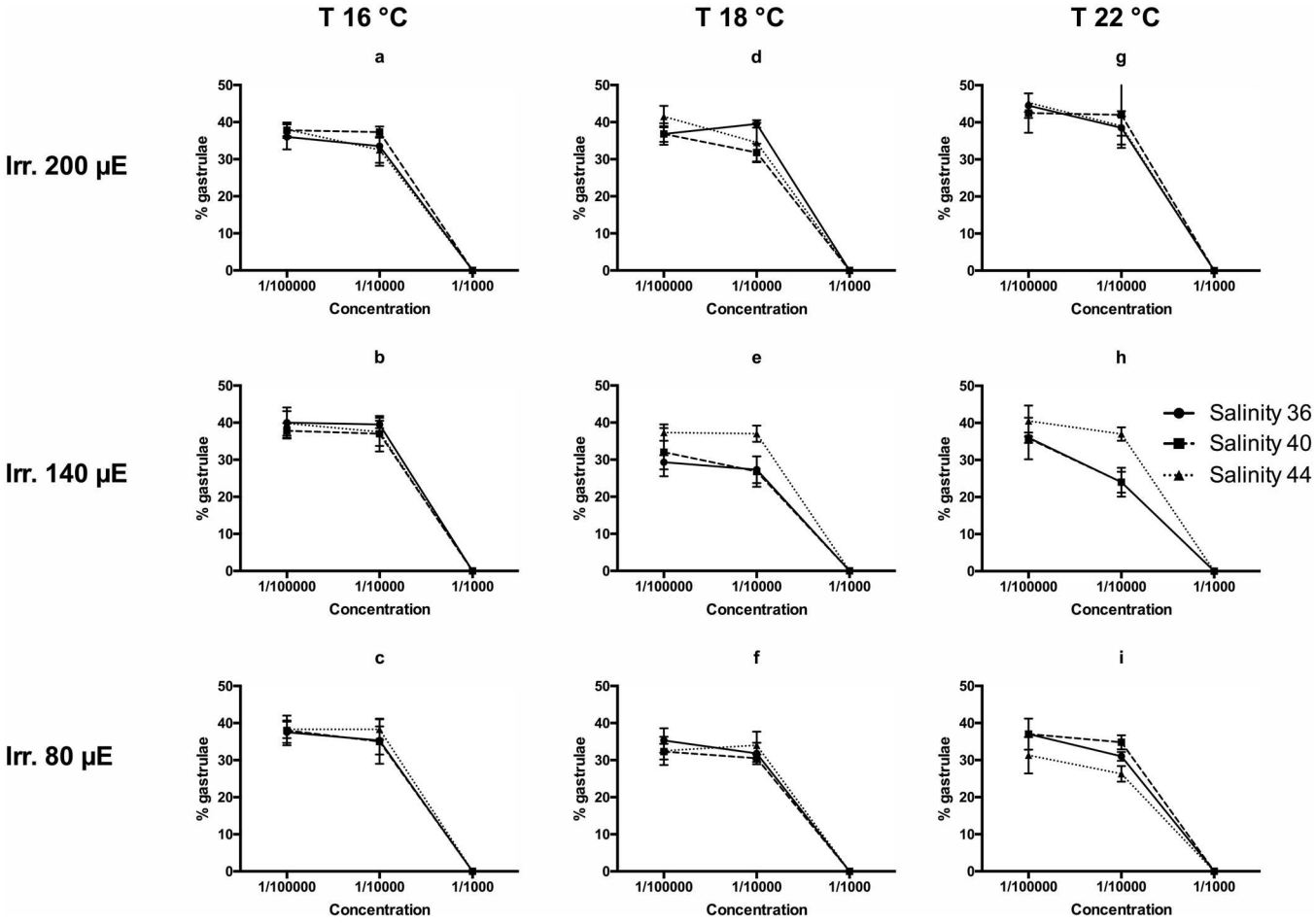

Fig. 4. Rates of gastrulation of embryos of *P. lividus* recorded after 8 h of exposure to three concentrations of the spent culture medium of *H. metazoicum*, cultivated at three temperatures, three irradiance levels and three salinities.

differences in toxicity detected at different salinities and temperatures are in line with previous findings (Chorus et al., 2000) and indicate that cyclic polypeptides (e.g. microcystins and portoamides), typically produced by these organisms, could be the main products influencing the survival of different model organisms, at corresponding median lethal concentrations.

In addition, some families of microcystins are known to induce apoptosis in various organisms and these compounds, produced at low temperatures, could be responsible for the irregular development of plutei. Microcystins can also trigger cytoskeleton disruption in human hepatocytes (Falconer and Yeung, 1992), after disorganization of cytoplasmic microtubules, cytokeratin intermediate filaments and actin microfilaments (Ding et al., 2000). They were demonstrated to produce oxidative stress, exposing cells to the activity of reactive oxygen species (ROS). For example, the exposure to microcystins causes oxidative stress in Sertoli cells of rats, through decreased antioxidative enzyme activity and increased ROS activity (Yi et al., 2011). Oxidative stress and apoptosis are related processes and the production of ROS has been suggested to be involved in programmed cell death under various conditions, including chemical injury (Buttke and Sandstrom, 1994; Tan et al., 1998; Kannan and Jain, 2000). Thus these compounds, produced at higher temperatures and irradiances, could be responsible for the block of cell divisions in sea urchin embryos.

These compounds might reveal interesting biotechnological applications even in the field of human medicine (Thompson, 1995) since they might have antitumor activity against some cell lines. Indeed, sea urchin embryos have been successfully used to test the antimitotic activity of candidate compounds for chemotherapy, in oncological research (Leite et al., 2012), and the induction of blockage at the first mitotic division might suggest a similar antimitotic effect on fast dividing tumour cells (Gutierrez, 2016). Different tissues demonstrated variable responses to microcystins (Yi et al., 2011) and a recent study (Zhang et al., 2011) demonstrated that the expression level of p53 increased when human Sertoli cells were exposed to microcystins, suggesting that they induce apoptosis by modulating the expression of p53, as well as modulating the expression of Bcl-2 proteins. Hence, some of the putative compounds responsible for the observed toxic effects play key roles in various mechanisms involved in the apoptotic pathways. In particular, p53, bcl-2, bax and caspase-3 are probably involved in cyanobacteria-induced cell damage and toxicity (Dias et al., 2017), and further investigations on the toxicological role of cyanobacterial products in apoptosis-related signalling pathways (Ribeiro et al., 2017) will clarify the nature, the specificity and the mechanism of action of the compounds produced at low and high temperatures by *H. metazoicum*.

MATERIAL AND METHODS

Collection of cyanobacteria samples

Cyanobacteria mattes were collected in spring from leaves of *P. oceanica*, in a meadow off Lacco Ameno d'Ischia (Bay of Naples, Italy, 40°44′56″ N,

Biology Open (2019) 8, bio043604. doi:10.1242/bio.043604

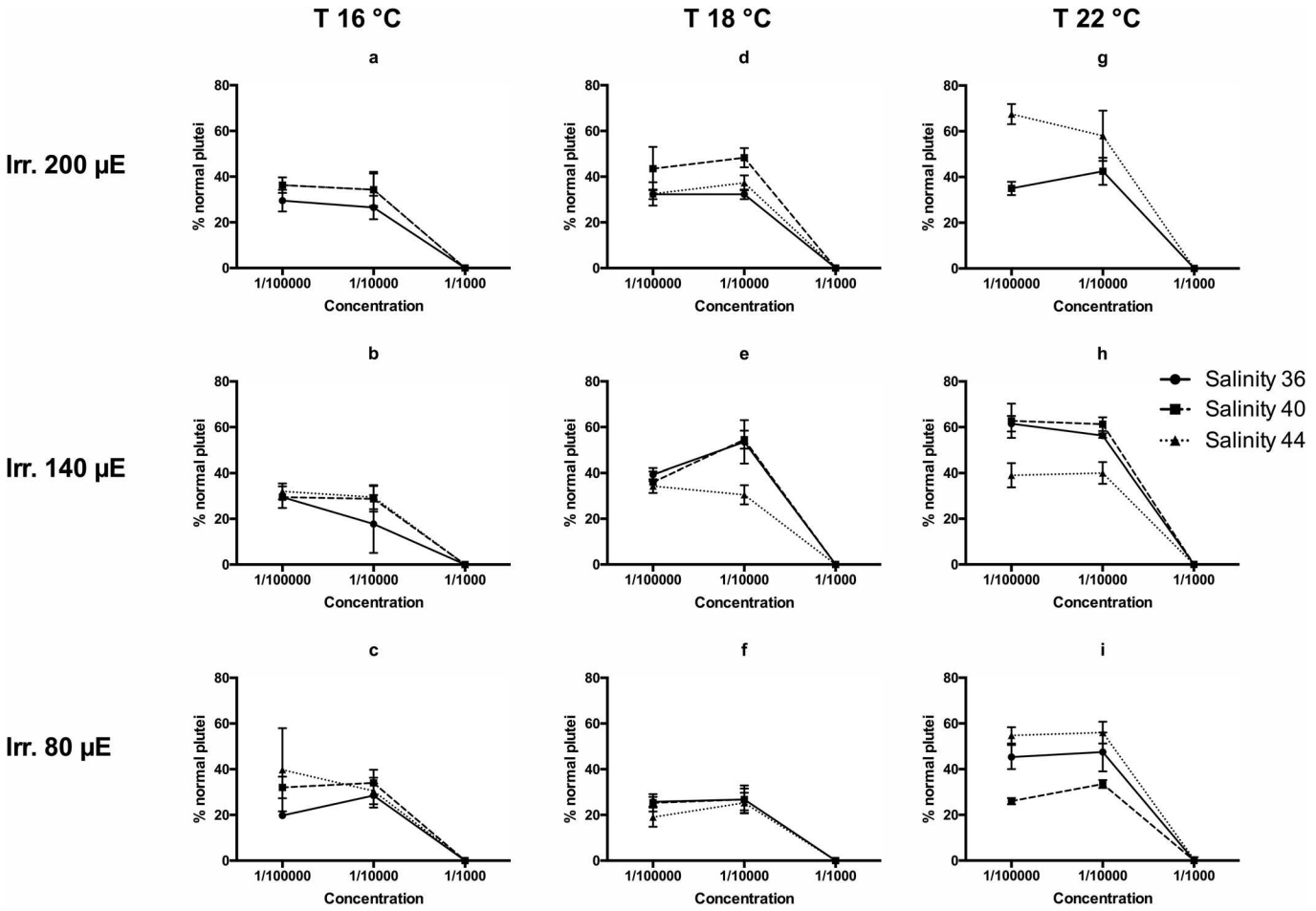

Fig. 5. Rates of production of normal plutei of *P. lividus* recorded after 48 h of exposure to three concentrations of the spent culture medium of *H. metazoicum*, cultivated at three temperatures, three irradiance levels and three salinities.

13°53′13″ E), using sterilized forceps. They were transferred to multi-well dishes filled with 4 ml of *f/2* medium. Cultures were renovated various times up to a complete purification. Morphological analyses and molecular tools (Ruocco et al., 2019) were applied and a free-living strain of *H. metazoicum* was identified. No contamination was detectable under both light microscopy and SEM in exponentially growing cultures of this uni-cyanobacterial culture, even under high magnification, probably due to the antibiotic properties attributed to their exudates (Dias et al., 2017). Pure strains were cultured in *f/2* medium in 400 ml glass dishes kept in a thermostatic chamber at a temperature of 18°C, with light irradiance of about 200 µE and 12/12 h dark/light photoperiod. The medium was renovated every 15 days to avoid changes of culture conditions due to evaporation.

Production of spent medium

Small portions of cyanobacteria mattes were collected from mother cultures, cut in pieces of about 5 g (fresh weight) and individually cultured in 2 l Erlenmeyer flasks containing 1.5 l of *f/2* medium. Two replicate flasks were cultivated under each condition of light, temperature and salinity, according to a factorial experimental plane (Table 1) containing 27 combinations. In particular, we tested conditions of salinity, temperature and irradiance that could be found in various habitats of the Mediterranean sea and combined them to test the production of bioactive compounds. Cyanobacteria were cultivated 40 days in these conditions, to facilitate an accumulation of secondary metabolites in the medium. Spent culture media were collected at the end of the production period, filtered over a 0.22 µm Millipore filter, stored in glass vessels and kept at −20°C up to the start of bioassays.

Preparation of toxicity tests

Toxicity tests were performed on two model organisms, to compare the results on taxa exhibiting a different resistance to toxic pollutants and, in particular, on adults of the rotifer *B. plicatilis* (Snell and Carmona, 1995) and embryos of the sea urchin *Paracentrotus lividus* (Romano et al., 2003). The contents of the above described two replicate flasks produced for each culture condition, were pooled prior to the tests. The spent medium was sampled and diluted at various concentrations in filtered seawater, according to the sensitivity of target models. Basically, we took into account the following six dilutions of the culture medium in filtered seawater: 1:5, 1:10, 1:100, 1:1000, 1:10,000, 1:100,000 in volume. However, in the case of *P. lividus*, the highest concentrations (1:5, 1:10, 1:100) were not considered in further analyses, because they produced immediate mortality of sensitive embryos (Romano et al., 2003). In the case of *B. plicatilis* the lowest concentrations (1:1000, 1:10,000, 1:100,000) were not considered in further analyses, because they did not produce any effect on this stronger organism, able to partially detoxify poisons (Dahms et al., 2011).

Toxicity tests on *B. plicatilis*

A single clone of *B. plicatilis*, maintained in continuous culture at the Stazione Zoologica Anton Dohrn, has been used to perform tests on rotifers. This clone continuously produces offspring when cultivated at 20°C and it is fed on cultures of *Dunaliella* sp. replaced every 5 days. As referred to above, three concentrations of spent medium were employed for bioassays on *B. plicatilis*, i.e. 1:5, 1:10 and 1:100 in volume, after preliminary tests indicating concentrations lower than 1:100 did not produce any effect in respect to controls (Dahms et al., 2011). Fifty adult individuals of

Biology Open (2019) 8, bio043604. doi:10.1242/bio.043604

Table 1. Experimental conditions imposed to the culture of cyanobacteria to obtain three combinations of salinity (36, 40, 44), irradiance (80, 140, 200 µE) and temperature (16, 18, 22°C) for the toxicity test treatments

Treatment Condition	Salinity %°	Irradiance µE	Temperature °C
1	36	80	16
2	40	80	16
3	44	80	16
4	36	140	16
5	40	140	16
6	44	140	16
7	36	200	16
8	40	200	16
9	44	200	16
10	36	80	18
11	40	80	18
12	44	80	18
13	36	140	18
14	40	140	18
15	44	140	18
16	36	200	18
17	40	200	18
18	44	200	18
19	36	80	22
20	40	80	22
21	44	80	22
22	36	140	22
23	40	140	22
24	44	140	22
25	36	200	22
26	40	200	22
27	44	200	22

B. plicatilis were transferred into three replicates of 5 ml multi-well plates filled with 4 ml of solution (spent medium diluted in seawater) for each of the above-mentioned concentrations, and their motility and survival rates were checked at 5 min, 60 min and 24 h, for each of the experimental conditions.

Toxicity tests on *P. lividus* embryos

Three dilutions of spent medium were assayed on *P. lividus* embryos, 1:1000, 1:10,000 and 1:100,000, in volume. Higher concentrations (1:5, 1:10, 1:100) produced immediate block of embryo development at the first division and they were not considered in further analyses. The test was prepared starting from two mature females and one male of *P. lividus* collected in the Bay of Naples (Italy). Sea urchins were injected with 1 ml of 0.5 M KCl into the coelom through the soft derma around the mouthparts, to stimulate the contraction of gonads. They were vigorously shaken and females were placed with mouths up, over a 50 ml beaker, until the gametes were released into filtered (0.22 µm, Millipore) seawater, to facilitate the collection of eggs. Eggs were further rinsed three times with clean seawater to remove possible organic residuals (Chapman, 1995). Sperm were collected 'dry', using a Pasteur pipette and sucking over the surface of male gonopores, to avoid premature activation. The gametes obtained from each individual were conserved in plastic vessels until fertilization, when sub-samples of eggs were collected and added with a drop of sperm suspension. Egg activation was revealed by the elevation of the fertilization membrane within 40–80 s, appearing as a clear circle. Pools of embryos exhibiting percentages of fertilization lower than 95% were discarded. Pools exhibiting viable embryos were used for bioassays. To this end, groups of 500 embryos obtained from each replicate female were collected in duplicate and transferred into 5 ml multi-well dishes filled with appropriate dilutions of the cyanobacteria spent media, as specified above.

Four replicate tests were run at each concentration of the spent culture medium, plus four negative controls prepared using only seawater added with corresponding proportions of fresh *f/2* medium. The results were recorded at various time intervals and according to each concentration. In particular, multi-wells were inspected after 1 h under the inverted microscope to record the percentage of individuals showing normal cell division and, eventually, the presence of apoptosis hallmarks, such as blebbings. After 6 h and 24 h, 1 ml of egg suspension was fixed with the addition of a drop of 40% buffered formalin and replicates examined to record the percentage of individuals at the blastula, gastrula and prism stages, respectively. The percentage of individuals that were still at the first stages of divisions and those blocked or apoptotic was recorded as well. The remaining content of wells was fixed after 48 h and examined to record the percentage of normal plutei.

Statistical analyses

Means and standard deviations of the readings obtained from various replicates, for each set of measurements, were organized in matrices. Raw data were analysed using factorial ANOVA that builds a linear model to include main-effects and interactions for categorical predictors. Multivariate (multiple continuous dependent variables) designs were analysed using Statistica version 10 (StatSoft Inc., Tulsa, OK, USA). The variance/covariance matrix of dependent variables was tested for normality and homogeneity of variances by the Kolmogorov–Smirnov and Levene's tests, respectively. Wilcoxon test was used to check the significance of differences between individual treatments. Other graphs and statistical analyses were computed using GraphPad Prism version 6.00 for Macintosh (GraphPad Software, La Jolla, CA, USA, www.graphpad.com).

Ethical approval and consent to participate

All animal experiments were carried in accordance with the EU Directive 2010/63/EU and The Code of Ethics of the World Medical Association (Declaration of Helsinki) for animal experiments.

Acknowledgements

Samples for electron microscopy were prepared and SEM images were produced by F. Iamunno, R. Graziano and G. Lanzotti of the AMOBIO Unit of Stazione Zoologica Anton Dohrn (SZN). We thank the unit MEDA for the collection of sea urchins and Mr A. Macina and D. Caramiello of the unit MaRe for the preparation of sea urchin gametes. Cpt. Rando, on board the SZN vessel Phoenicia, collected the seagrass leaves used for isolation of Cyanobacteria. Results in this paper are reproduced from the PhD thesis of Mirko Mutalipassi (UK Open University, 2018). English text was kindly revised by R. Messina.

Competing interests

The authors declare no competing or financial interests.

Author contributions

Conceptualization: M.C., V.Z.; Methodology: M.C., V.Z.; Formal analysis: M.M., V.Z.; Investigation: M.M., V.M., G.R., N.R., F.G., V.Z.; Resources: V.Z.; Writing - original draft: V.Z.; Writing - review & editing: V.Z.; Supervision: M.C., V.Z.; Project administration: V.Z.; Funding acquisition: V.Z.

Funding

M.M. and N.R. performed these investigations while funded by a Stazione Zoologica Anton Dohrn-Open University and a Stazione Zoologica Anton Dohrn-Università degli Studi di Napoli Federico II PhD project, respectively. F.G. was funded by the Flagship project ModRes under the supervision of V.Z. This research did not receive other specific grants from funding agencies in the public, commercial, or not-for-profit sectors.

Data availability

The datasets analysed during the current study are available from the corresponding author on request.

References

Abarzua, S., Jakubowski, S., Eckert, S. and Fuchs, P. (1999). Biotechnological investigation for the prevention of marine biofouling ii. blue-green algae as potential producers of biogenic agents for the growth inhibition of microfouling organisms. *Bot. Mar.* **42**, 459-465. doi:10.1515/BOT.1999.053

Barberousse, H., Lombardo, R. J., Tell, G. and Coute, A. (2006). Factors involved in the colonisation of building facades by algae and cyanobacteria in France. *Biofouling* **22**, 69-77. doi:10.1080/08927010600564712

Bloor, S. and England, R. R. (1989). Antibiotic production by the cyanobacterium *Nostoc muscorum*. *J. Appl. Phycol.* **1**, 367-372. doi:10.1007/BF00003474
Blunt, J. W., Copp, B. R., Munro, M. H. G., Northcote, P. T., Prinsep, M. R. (2006). Marine natural products.
Böhm, G. A., Pfleiderer, W., Böger, P. and Scherer, S. (1995). Structure of a novel oligosaccharide-mycosporine-amino acid ultraviolet A/B sunscreen pigment from the terrestrial cyanobacterium *Nostoc commune*. *J. Biol. Chem.* **270**, 8536-8539. doi:10.1074/jbc.270.15.8536
Bonjouklian, R., Smitka, T. A., Doolin, L. E., Molloy, R. M., Debono, M., Shaffer, S. A., Moore, R. E., Stewart, J. B. and Patterson, G. M. L. (1991). Tjipanazoles, new antifungal agents from the blue-green alga *Tolypothrix tjipanasensis*. *Tetrahedron* **47**, 7739-7750. doi:10.1016/S0040-4020(01)81932-3
Borges, H. L. F., Branco, L. H. Z., Martins, M. D., Lima, C. S., Barbosa, P. T., Lira, G. A. S. T., Bittencourt-Oliveira, M. C. and Molica, R. J. R. (2015). Cyanotoxin production and phylogeny of benthic cyanobacterial strains isolated from the northeast of Brazil. *Harmful Algae* **43**, 46-57. doi:10.1016/j.hal.2015.01.003
Boudou, A. and Ribeyre, F. (1989). *Aquatic Ecotoxicology: Fundamental Concepts and Methodologies*. Boca Raton, Fla: CRC Press.
Burja, A. M., Banaigs, B., Abou-Mansour, E., Grant, J. and Wright, P. C. (2001). Marine cyanobacteria — A prolific source of natural products. *Tetrahedron* **57**, 9347-9377. doi:10.1016/S0040-4020(01)00931-0
Buttke, T. M. and Sandstrom, P. A. (1994). Oxidative stress as a mediator of apoptosis. *Immunol. Today* **15**, 7-10. doi:10.1016/0167-5699(94)90018-3
Caroppo, C., Albertano, P., Bruno, L., Montinari, M., Rizzi, M., Vigliotta, G. and Pagliara, P. (2012). Identification and characterization of a new *Halomicronema* species (Cyanobacteria) isolated from the Mediterranean marine sponge *Petrosia ficiformis* (Porifera). *Fottea* **12**, 315-326. doi:10.5507/fot.2012.022
Catherine, Q., Susanna, W., Isidora, E.-S., Mark, H., Aurélie, V. and Jean-François, H. (2013). A review of current knowledge on toxic benthic freshwater cyanobacteria–ecology, toxin production and risk management. *Water Res.* **47**, 5464-5479. doi:10.1016/j.watres.2013.06.042
Chapman, G. A. (1995). *Sea Urchin Sperm Cell Test. Fundam. Aquat. Toxicol. Eff. Environ. Fate Risk Assessment*, 2nd edn, pp. 189-205. Philadelphia: Taylor Fr.
Chorus, I., Falconer, I. R., Salas, H. J. and Bartram, J. (2000). Health risks caused by freshwater cyanobacteria in recreational waters. *J. Toxicol. Environ. Heal. Part B Crit. Rev.* **3**, 323-347. doi:10.1080/109374000436364
Dahms, H. U. and Hellio, C. (2009). Laboratory bioassays for screening marine antifouling compounds. In *Advances in Marine Antifouling Coatings and Technologies* (eds C. Hellio and D. Yebra), pp. 275-307. Cambridge: Woodhead Publishing.
Dahms, H. U., Ying, X. and Pfeiffer, C. (2006). Antifouling potential of cyanobacteria: A mini-review. *Biofouling* **22**, 317-327. doi:10.1080/08927010600967261
Dahms, H. U., Hagiwara, A. and Lee, J.-S. (2011). Ecotoxicology, ecophysiology, and mechanistic studies with rotifers. *Aquat. Toxicol.* **101**, 1-12. doi:10.1016/j.aquatox.2010.09.006
Devlin, J. P., Edwards, O. E., Gorham, P. R., Hunter, N. R., Pike, R. K. and Stavric, B. (1977). Anatoxin- a, a toxic alkaloid from *Anabaena flos-aquae* NRC-44h. *Can. J. Chem.* **55**, 1367-1371. doi:10.1139/v77-189
Dias, F., Antunes, J. T., Ribeiro, T., Azevedo, J., Vasconcelos, V. and Leão, P. N. (2017). Cyanobacterial allelochemicals but not cyanobacterial cells markedly reduce microbial community diversity. *Front. Microbiol.* **8**, 1495. doi:10.3389/fmicb.2017.01495
Ding, W.-X., Shen, H.-M. and Ong, C.-N. (2000). Critical role of reactive oxygen species and mitochondrial permeability transition in microcystin-induced rapid apoptosis in rat hepatocytes. *Hepatology* **32**, 547-555. doi:10.1053/jhep.2000.16183
Echenique-Subiabre, I., Dalle, C., Duval, C., Heath, M. W., Couté, A., Wood, S. A., Humbert, J.-F. and Quiblier, C. (2016). Application of a spectrofluorimetric tool (bbe BenthoTorch) for monitoring potentially toxic benthic cyanobacteria in rivers. *Water Res.* **101**, 341-350. doi:10.1016/j.watres.2016.05.081
Falconer, I. R. and Yeung, D. S. K. (1992). Cytoskeletal changes in hepatocytes induced by *Microcystis* toxins and their relation to hyperphosphorylation of cell proteins. *Chem. Biol. Interact.* **81**, 181-196. doi:10.1016/0009-2797(92)90033-H
Gaylarde, C. C., Gaylarde, P. M., Copp, J. and Neilan, B. (2004). Polyphasic detection of cyanobacteria in terrestrial biofilms. *Biofouling* **20**, 71-79. doi:10.1080/08927010410001681237
Geitler, L. (1932). Cyanophyceae. In: *Kryptogamen-Flora von Deutschland, Österreich und der Schweiz. Ed. 2*. (Rabenhorst, L. Eds) Vol. 14, pp. 673-1196, i-[vi]. Leipzig: Akademische Verlagsgesellschaft.
Gerçe, B., Schwartz, T., Voigt, M., Rühle, S., Kirchen, S., Putz, A., Proksch, P., Obst, U., Syldatk, C. and Hausmann, R. (2009). Morphological, bacterial, and secondary metabolite changes of *Aplysina aerophoba* upon long-term maintenance under artificial conditions. *Microb. Ecol.* **58**, 865. doi:10.1007/s00248-009-9560-6
Giovannoni, S. J., Turner, S., Olsen, G. J., Barns, S., Lane, D. J. and Pace, N. R. (1988). Evolutionary relationships among cyanobacteria and green chloroplasts. *J. Bacteriol.* **170**, 3584-3592. doi:10.1128/jb.170.8.3584-3592.1988
Gross, M. (2004). Emergency services: a bird's eye perspective on the many different functions of stress proteins. *Curr. Protein Pept. Sci.* **5**, 213-223. doi:10.2174/1389203043379684
Gugger, M., Lenoir, S., Berger, C., Ledreux, A., Druart, J.-C., Humbert, J.-F., Guette, C. and Bernard, C. (2005). First report in a river in France of the benthic cyanobacterium *Phormidium favosum* producing anatoxin-a associated with dog neurotoxicosis. *Toxicon* **45**, 919-928. doi:10.1016/j.toxicon.2005.02.031
Gutierrez, P. M.Jr (2016). Antimitotic activity of *Carica papaya* leaf extract in the *in vitro* development of the sea urchin, *Tripneustes gratilla* embryo. *Int. Res. J. Biological Sci.* **5**, 12-17. doi:10.12692/14.6.219-231
Hughes, E. O., Gorham, P. R. and Zehnder, A. (1958). Toxicity of a unialgal culture of *Microcystis* aeruginosa. *Can. J. Microbiol.* **4**, 225-236. doi:10.1139/m58-024
Jüttner, F., Todorova, A. K., Walch, N. and von Philipsborn, W. (2001). Nostocyclamide M: a cyanobacterial cyclic peptide with allelopathic activity from *Nostoc* 31. *Phytochemistry* **57**, 613-619. doi:10.1016/S0031-9422(00)00470-2
Kannan, K. and Jain, S. K. (2000). Oxidative stress and apoptosis. *Pathophysiology* **7**, 153-163. doi:10.1016/S0928-4680(00)00053-5
Kouzminov, A., Ruck, J. and Wood, S. A. (2007). New Zealand risk management approach for toxic cyanobacteria in drinking water. *Aust. N. Z. J. Public Health* **31**, 275-281. doi:10.1111/j.1467-842X.2007.00061.x
Kulik, M. M. (1995). The potential for using cyanobacteria (blue-green algae) and algae in the biological control of plant pathogenic bacteria and fungi. *Eur. J. Plant Pathol.* **101**, 585-599. doi:10.1007/BF01874863
Leite, J. C., Junior, C. G., Silva, F. P., Sousa, S. C., Vasconcellos, M. L. and Marques-Santos, L. F. (2012). Antimitotic activity on sea urchin embryonic cells of seven antiparasitic Morita-Baylis-Hillman adducts: a potential new class of anticancer drugs. *Med. Chem.* **8**, 1003-1011. doi:10.2174/157340612804075070
Manivasagan, P., Bharathiraja, S., Santha Moorthy, M., Mondal, S., Seo, H., Dae Lee, K. and Oh, J. (2017). Marine natural pigments as potential sources for therapeutic applications. *Crit. Rev. Biotechnol.* **38**, 745-761. doi:10.1080/07388551.2017.1398713
Mazzella, L., Buia, M.-C., Gambi, M. C., Lorenti, M., Russo, G. F., Scipione, M. B. and Zupo, V. (1991). Plant-animal trophic relationships in the *Posidonia oceanica* ecosystem of the Mediterranean Sea: a review. In *Plant-Animal Interactions in Marine Benthos* (ed. J. F. Keegan), pp. 165-188. London.
Moore, R. E., Patterson, G. M. L. and Carmichael, W. W. (1988). New pharmaceuticals from cultured blue-green algae. *Biomed. importance Mar. Org.* **13**, 143-150.
Pagliara, P. and Caroppo, C. (2010). A *Leptolyngbya* species isolated from the sponge *Petrosia ficiformis* as potential source of novel compounds. *Rapp. Comm. Int. Mer Médit* **39**, 392.
Pagliara, P. and Caroppo, C. (2011). Cytotoxic and antimitotic activities in aqueous extracts of eight cyanobacterial strains isolated from the marine sponge *Petrosia ficiformis*. *Toxicon* **57**, 889-896. doi:10.1016/j.toxicon.2011.03.006
Pfeiffer, C. and Palińska, K. A. (2002). Characterisation of marine *Phormidium* isolates - Conformity between molecular and ecophysiological results. *J. Plant Physiol.* **159**, 591-598. doi:10.1078/0176-1617-0637
Pietsch, C., Wiegand, C., Amé, M. V., Nicklisch, A., Wunderlin, D. and Pflugmacher, S. (2001). The effects of a cyanobacterial crude extract on different aquatic organisms: evidence for cyanobacterial toxin modulating factors. *Environ. Toxicol.* **16**, 535-542. doi:10.1002/tox.10014
Plavšić, M., Terzic, S., Ahel, M. and Van Den Berg, C. M. G. (2004). Folic acid in coastal waters of the Adriatic Sea. *Mar. Freshw. Res.* **53**, 1245-1252. doi:10.1071/MF02044
Preston, B. L., Snell, T. W. and Dusenbery, D. B. (1999). The effects of sublethal pentachlorophenol exposure on predation risk in freshwater rotifer species. *Aquat. Toxicol.* **47**, 93-105. doi:10.1016/S0166-445X(99)00012-0
Preston, B. L. and Snell, T. W. (2001). Full life-cycle toxicity assessment using rotifer resting egg production: implications for ecological risk assessment. *Environ. Pollut.* **114**, 399-406. doi:10.1016/S0269-7491(00)00232-3
Raniello, R., Iannicelli, M. M., Nappo, M., Avila, C. and Zupo, V. (2007). Production of *Cocconeis neothumensis* (Bacillariophyceae) biomass in batch cultures and bioreactors for biotechnological applications: light and nutrient requirements. *J. Appl. Phycol.* **19**, 383-391. doi:10.1007/s10811-006-9145-4
Ribeiro, T., Lemos, F., Preto, M., Azevedo, J., Sousa, M. L., Leão, P. N., Campos, A., Linder, S., Vitorino, R., Vasconcelos, V. et al. (2017). Cytotoxicity of portoamides in human cancer cells and analysis of the molecular mechanisms of action. *PLoS ONE* **12**, 1-18. doi:10.1371/journal.pone.0188817
Rippka, R., Deruelles, J., Waterbury, J. B., Herdman, M. and Stanier, R. Y. (1979). Generic assignments, strain histories and properties of pure cultures of cyanobacteria. *Microbiology* **111**, 1-61. doi:10.1099/00221287-111-1-1
Romano, G., Russo, G. F., Buttino, I., Ianora, A. and Miralto, A. (2003). A marine diatom-derived aldehyde induces apoptosis in copepod and sea urchin embryos. *J. Exp. Biol.* **206**, 3487-3494. doi:10.1242/jeb.00580
Ruocco, N., Mutalipassi, M., Pollio, A., Costantini, S., Costantini, M. and Zupo, V. (2019). First evidence of *Halomicronema metazoicum* (Cyanobacteria) free-living on *Posidonia oceanica* leaves. *PLoS ONE* **13**, e0204954. doi:10.1371/journal.pone.0204954
Shimizu, Y. (2003). Microalgal metabolites. *Curr. Opin. Microbiol.* **6**, 236-243. doi:10.1016/S1369-5274(03)00064-X

Shurin, J. B. and Dodson, S. I. (1997). Sublethal toxic effects of cyanobacteria and nonylphenol on environmental sex determination and development in *Daphnia*. *Environ. Toxicol. Chem.* **16**, 1269-1276. doi:10.1002/etc.5620160624

Sivonen, K. and Börner, T. (2008). Bioactive compounds produced by cyanobacteria. In *The Cyanobacteria: Molecular Biology, Genomics and Evolution* (eds A. Herrero and E. Flores), pp. 159-197. Norfolk: Caister Academic Press.

Snell, T. W. and Carmona, M. J. (1995). Comparative toxicant sensitivity of sexual and asexual reproduction in the rotifer *Brachionus calyciflorus*. *Environ. Toxicol. Chem.* **14**, 415-420. doi:10.1002/etc.5620140310

Suga, K., Mark Welch, D., Tanaka, Y., Sakakura, Y. and Hagiwara, A. (2007). Analysis of expressed sequence tags of the cyclically parthenogenetic rotifer *Brachionus plicatilis*. *PLoS ONE* **2**, e671. doi:10.1371/journal.pone.0000671

Tan, S., Sagara, Y., Liu, Y., Maher, P. and Schubert, D. (1998). The regulation of reactive oxygen species production during programmed cell death. *J. Cell Biol.* **141**, 1423-1432. doi:10.1083/jcb.141.6.1423

Taylor, M. W., Radax, R., Steger, D. and Wagner, M. (2007). Sponge-associated microorganisms: evolution, ecology, and biotechnological potential. *Microbiol. Mol. Biol. Rev.* **71**, 295-347. doi:10.1128/MMBR.00040-06

Teneva, I., Dzhambazov, B., Koleva, L., Mladenov, R. and Schirmer, K. (2005). Toxic potential of five freshwater *Phormidium* species (Cyanoprokaryota). *Toxicon* **45**, 711-725. doi:10.1016/j.toxicon.2005.01.018

Thompson, C. B. (1995). Apoptosis in the pathogenesis and treatment of disease. *Sci. New Ser.* **26712519**, 1456-1462.

Usher, K. M., Fromont, J., Sutton, D. C. and Toze, S. (2004). The biogeography and phylogeny of unicellular cyanobacterial symbionts in sponges from Australia and the Mediterranean. *Microb. Ecol.* **48**, 167-177. doi:10.1007/s00248-003-1062-3

Whitton, B. A. (1992). Diversity, ecology, and taxonomy of the cyanobacteria. In *Photosynthetic Prokaryotes*, pp. 1-51. Springer.

Wood, S. A., Puddick, J., Fleming, R. and Heussner, A. H. (2017). Detection of anatoxin-producing *Phormidium* in a New Zealand farm pond and an associated dog death. *New Zeal. J. Bot.* **55**, 36-46. doi:10.1080/0028825X.2016.1231122

Yi, D., Liu, X., Zhang, F., Wang, J., Zhao, Y., Sun, D., Ren, J. and Zhang, H. (2011). Oxdative stress on sertoli cells of rats induced by microcystin-LR. *Life Sci. J.* **8**, 249-253.

Zhang, H.-Z., Zhang, F.-Q., Li, C.-F., Yi, D., Fu, X.-L. and Cui, L.-X. (2011). A cyanobacterial toxin, microcystin-LR, induces apoptosis of Sertoli cells by changing the expression levels of apoptosis-related proteins. *Tohoku J. Exp. Med.* **224**, 235-242. doi:10.1620/tjem.224.235

Zupo, V., Mutalipassi, M., Ruocco, N., Glaviano, F., Pollio, A., Langellotti, A. L., Romano, G. and Costantini, M. (2019). Distribution of toxigenic *Halomicronema* spp. in adjacent environments in the Island of Ischia: comparison of strains from thermal waters and free living in *Posidonia oceanica* meadows. *Toxins* **11**, 99. doi:10.3390/toxins11020099